ATOLL ISLAND FRESHWATER RESOURCES: MODELING, ANALYSIS, AND OPTIMIZATION

by

Corey D. Wallace
Ryan T. Bailey
John W. Jenson

WATER AND ENVIRONMENTAL RESEARCH INSTITUTE
OF THE WESTERN PACIFIC
UNIVERSITY OF GUAM

Technical Report No. 155

May 2015

Atoll Island Freshwater Resources: Modeling, Analysis, and Optimization

by

Corey D. Wallace
Ryan T. Bailey
John W. Jenson

Department of Civil & Environmental Engineering, Colorado State University, Fort Collins, CO, United States 80523

Technical Report No. 155
May 2015

Acknowledgements: The work reported herein was funded by the Department of Civil and Environmental Engineering, Colorado State University, and by the Department of Interior via the Water Resources Research Institute Program of the U.S. Geological Survey (Grant no. G11AP20074) administered through the Water and Environmental Research Institute of the Western Pacific at the University of Guam (USGS 104(b). We also acknowledge the World Climate Research Programme's Working Group on Coupled Modelling, which is responsible for CMIP, and thank the climate modeling groups for producing and making available their model output. Our appreciation is also extended to Timothy Gates, Jeffrey Niemann, and Michael Ronayne of Colorado State University for their guidance, insight, and support.

ABSTRACT

Atolls consist of ring-shaped structures of small islets of varying sizes that encircle a shallow central lagoon. Freshwater supply on atoll islands is very fragile, consisting exclusively of rainwater harvested from rainwater catchment systems and groundwater extracted from the freshwater lens. Optimal water management necessitates accurate estimation of the current and future quantity of available freshwater; of principle concern is the quantity of water to be expected in the coming decades under the influence of changing rainfall patterns. In this thesis, current and future quantities of daily captured rainwater and available groundwater are investigated using a modeling approach, with a daily water balance used for rainwater catchment systems and a numerical groundwater flow model used for the groundwater system. The conjunctive use of rainwater and groundwater in a sustainable framework is also explored. Models are tested against observed data, with sensitivity analysis then performed to investigate the governing system factors on available volume of rainwater and groundwater. Future quantities are estimated for the 2010-2050 time period using climate data obtained from general circulation models contributing to the CMIP5 framework.

Rainwater catchment system sensitivity and optimization analyses are carried out for a specific atoll island in Micronesia (Nikahlap, Pakein Atoll, Pohnpei State) to not only isolate parameters influential to system performance but also to identify easily amendable system shortcomings. Results from the simulations show that daily per capita water demand, catchment area, and transmission efficiency govern the volume of stored rainwater. Using simulated future climate data, household-scale design curves are developed to assist island residents in sizing their rainwater catchment systems to satisfy specified rates of reliability. Using the design curves it was determined, for example, that an average household of 4 with a rooftop catchment area of 40 m^2 will require a storage cistern of approximately 1000 L to ensure adequate water supply 90% of the time.

The three-dimensional, density-dependent groundwater flow and transport model SEAWAT is used to simulate the dynamics of the freshwater lens within the atoll geologic system. Of the eight Micronesian atoll islands modeled, five are located in eastern Pohnpei State and three are in western Yap State. Using observed values of lens thickness available for four of the islands modeled, the geologic characteristics of the upper Holocene aquifer were calibrated for both leeward and windward islands. The orientation of the islands in relation to the direction of the prevailing winds has a significant influence on the quantity of available freshwater; islands located on the leeward and windward sides of atolls have a hydraulic conductivity of 25 m day^{-1} and 200 m day^{-1}, respectively. Sensitivity analysis is performed to identify which geologic and climatic variables have the greatest effect on the available volume of extractable groundwater. Results from steady-state simulations show that hydraulic conductivity, the depth to contact between the upper and lower aquifers, and depth of annual recharge govern the volume of the lens. Using future simulated climate data, the size of the freshwater lens is modeled from 2010-2050. Results indicate that, with the exception of islands of extremely narrow width, lens depletion will be infrequent, occurring less than 10% of the time.

When the volume of captured rainwater is depleted, extractable groundwater from the freshwater lens remains the only viable source of freshwater. It is during periods of low rainfall that conjunctive use of captured rainwater and groundwater can meet island community water demand. The concurrent use of rainwater catchment and the groundwater models allows for estimation of the total available volume of freshwater on islands of various size and atoll

orientation for the 2010-2050 study period. Results indicate that when the supply of captured rainwater has been depleted, there will still be an available volume of extractable fresh groundwater nearly 99% of the time. The general nature of these methods makes them further applicable to regions outside of the FSM, and may provide water resources managers with information to more effectively manage community water supply.

TABLE OF CONTENTS

LIST OF TABLES

LIST OF FIGURES

ATOLL ISLANDS

Atoll Island Formation and Geology

Atoll islands, with unique geologic characteristics and a fragile water supply, have long been the focus of scientific interest. Though atolls number more than 175 spread across the Pacific Ocean, the total island land area amounts to only 1800 km^2 (Dickinson, 2009). Most atolls consist of small islets of varying sizes that encircle a shallow central lagoon (Neuendorf, Mehl Jr., & Jackson, 2005). Atoll islets vary in width depending on the size of the carbonate reef platforms upon which they are situated, and do not typically reach more than 2 or 3 meters above sea-level. The freshwater lens that forms in the subsurface of the sandy upper aquifer, the formation of which will be discussed in detail in this chapter, is not only highly dependent on rainfall, but is also limited in width and depth by the size of the island. For this reason, larger atolls of widths greater than 500 meters are typically selected for permanent human settlement (Spennemann, 2006). The central lagoons are also highly variable in both size and depth, though a majority of these are limited in size to less than 1000 km^2. There are several atoll nations scattered across both the Pacific and Indian Oceans, including the Maldives, the Marshall Islands, the Gilbert Islands, and the Federated States of Micronesia (FSM).

Atolls are situated upon carbonate platforms built atop subsided volcanic edifices (Darwin, 1842). As sea levels subsided in the early Holocene era, erosion of these carbonate reef platforms provided a suitable environment for the deposition of sand and other fine sediments. As a result, the subsurface geology of the islets consists of a Holocene aquifer resting upon an older, Pleistocene limestone foundation (Dickinson, 2004; Presley, 2005; Dickinson, 2009). A majority of sediment that composes the Holocene layer is unconsolidated sand and gravel that has been deposited unconformably. The contact between these two distinct layers typically occurs between 15 and 25 meters below the surface of the islands (Wheatcraft and Buddemeier, 1981); (Hamlin and Anthony, 1987). This dual-aquifer system allows for the development of a freshwater region beneath the islands, which floats atop seawater within the aquifer in the shape of a lens (Spennemann, 2006). Upon reaching the contact between the finer sediment of the Holocene aquifer and the highly conductive karstic Pleistocene limestone, the lens is truncated as rapid mixing with seawater occurs. This geologic formation is shown in Figure 1. Constant rainwater infiltration is also needed to sustain a lens of any considerable volume.

The trade winds that blow across the Pacific are driven by high pressure in the Eastern Pacific and lower pressure in the west. This process not only allows for ocean upwelling, but also drives climate patterns across the region. Consequently, larger islets are located on the leeward side of the lagoon, sheltered from the constant barrage of waves caused by the trade winds. Windward islands tend to have much higher hydraulic conductivity as fine sediment is washed away by the waves, ultimately resulting in a thinner lens with a relatively small volume of freshwater as compared to leeward islands (Bailey et al.,2010). As a result, island populations are more commonly situated on larger leeward islands where adequate fresh groundwater supply can be found. An example of islet distribution around the central lagoon is shown in Figure 1. The permeability of the sediment and flat landscape prevents the occurrence of streams or other surface water bodies, limiting atoll island freshwater supply to groundwater and water captured using rainwater harvesting systems (Spennemann, 2006).

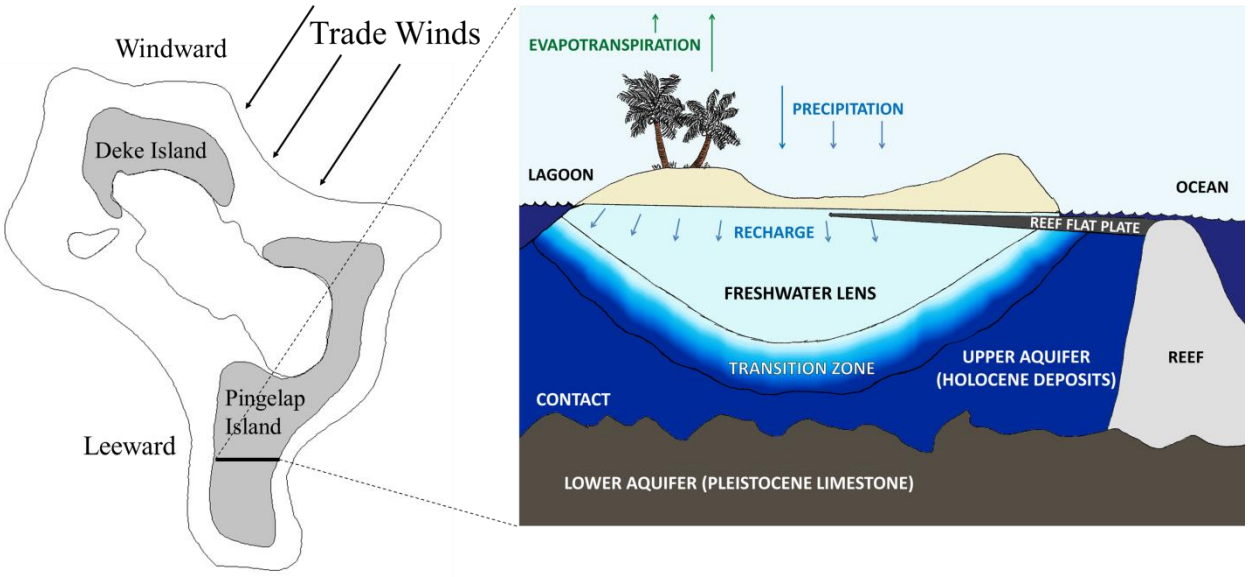

Figure 1. (Left) Location of windward and leeward islands in relation to the direction of the trade winds. (Right) Cross-sectional schematic of the atoll geologic structure, with the freshwater lens forming in the upper Holocene aquifer and limited in extent by contact with the lower Pleistocene aquifer.

Sources of Freshwater

Atoll island communities utilize a combination of groundwater extracted from the freshwater lens and rainwater captured using rainwater harvesting systems. The extremely fragile state of their freshwater resources has limited their demand almost exclusively to domestic uses, though some limited agriculture and the raising of livestock is practiced on larger islands. Crops grown on atoll islands are not sold commercially, but rather, are traditionally grown for subsistence. These usually include coconuts, swamp taro, breadfruit, and pandanus, all of which compete directly with island communities for freshwater (White et al., 2007). It is estimated that coconut palms extract 400-750 mm per year per tree from the freshwater lens (Falkland, 1994). Coconuts, which are abundant on nearly all atoll islets, are a significant source of water for island residents. Animals raised by the communities are limited to chickens and pigs, which are watered using either rain or groundwater. Small populations of feral pigs are present on some larger islands; however they do not compete excessively for freshwater and are thus often allowed to run wild.

Groundwater is most commonly extracted from the freshwater lens using hand-dug wells typically 2 to 3 meters deep and reaching approximately 1 meter below the shallow water table (White and Falkland, 2010). Using buckets or hand-pumps, island residents draw water for domestic uses, most commonly showering, bathing, and washing laundry (Taboroši and Martin, 2011). On larger islands with higher population, sometimes deeper, drilled boreholes are used to meet the increased demand. The fragile nature of the freshwater lens necessitates that pumping by island communities have minimal effect on the thickness of the lens. The sustainable yield is different for each island based on its geologic characteristics and regional climate conditions, with significantly lower yield volume available during major drought.

Sustainable yield has been defined as the quantity of water that can be extracted from the freshwater lens over a long period without producing an undesirable result (Todd, 1959). Though several factors influence the sustainable yield of the lens, including the recharge to the groundwater and storage within the groundwater reservoir, excessive groundwater pumping can also have adverse effects by reducing the natural discharge of the lens to the ocean and

expediting a reduction in the thickness of freshwater (Mather, 1975; Anthony, 1996). To mitigate the effects of both drought and domestic pumping, water resource management practices should be implemented.

As a primary source of water for atoll island communities, the freshwater lens must be carefully managed to ensure adequate supply. In addition to island communities relying on the lens to sustain them, the island ecosystems are also dependent on it for sustenance. Of the high levels of precipitation that percolate into the subsurface to replenish the lens, it is estimated that as low as 20% may be exploitable (Terry and Falkland, 2010). To properly manage water supply drawn from these fragile lenses, not only must water-usage efficiency of island communities be increased, but also human disturbances should be controlled effectively.

Rainwater catchment systems are used extensively worldwide as an alternate source of freshwater for island communities, used almost exclusively for drinking, cooking, and dishwashing, with groundwater being a secondary, emergency supply for such activities (Taboroši and Martin, 2011). Each system consists of a rooftop catchment area, a gutter system to deliver captured rainwater from the roof to a storage reservoir, and a cistern designed to store and protect rainwater that is collected.

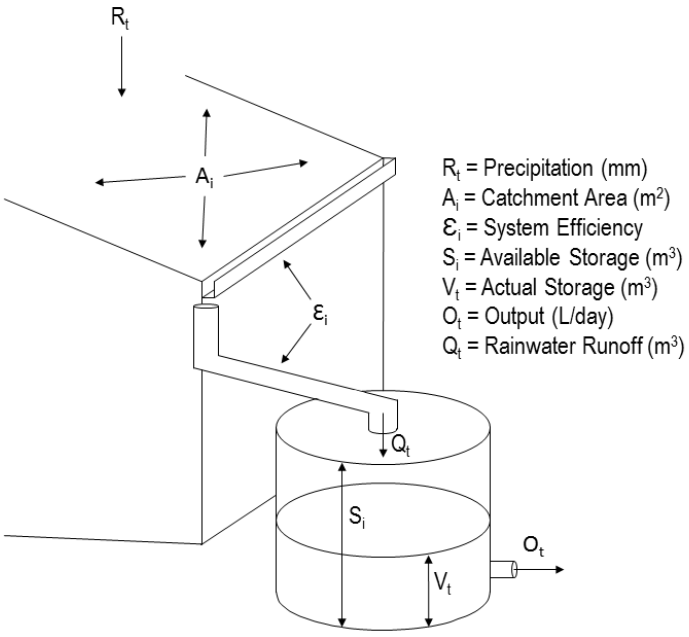

Figure 2. Schematic of a typical rainwater catchment system showing the rooftop catchment area, gutter system for water transmission, and cistern for storing captured rainwater for later use

A desired characteristic of water harvested from these systems is increased water quality as compared to freshwater extracted from hand-dug wells. Groundwater, though typically still of adequate quality for human consumption, tends to have higher chloride concentration and can potentially be contaminated by human waste from poorly installed septic tanks, animal waste, or agricultural runoff (Presley, 2005). Water quality from rainwater harvesting systems must be closely monitored, however, as factors including roof geometry, roof material, location of the roof, rainfall events, and concentration of substances in the atmosphere can all influence the

quality of harvested rainwater (Kwaadsteniet et al., 2013). Potential contamination can also occur through the capture of animal feces or plant matter in the runoff, coupled with long residence time in the storage tanks. For this reason, following periods of heavy drought, it is often necessary for island residents to thoroughly clean the catchment systems' rooftop catchment areas and storage tanks to avoid contamination.

During rainfall events, not all of the rain that falls within the guttered area of the roof is transferred to the storage tank. Rather, each catchment system has a distinct catchment efficiency, defined as the depth of rainfall caught as a percentage of that which ends up in the storage cistern. This efficiency is determined by a combination of factors to be discussed in detail later in chapter 3 of this thesis, but is most significantly influenced by the condition of the gutter system. Typically, catchment efficiency increases with the quantity of rain that falls during a given event (Rowe, 2011). Due to scarcity, water is usually treated as a common-pool resource within atoll island communities; rainwater catchment systems may be installed on large community buildings. Though inadequate supply is often accepted as inevitable on most of the smaller islands, water resource management plays a crucial role in prolonging atoll freshwater resources.

More recently, communities on larger islands have requested improvements in their water infrastructure, including a desire for the installation of showers, flush toilets, and laundry facilities (Anthony, 1996). These amenities, though they will increase the quality of life for residents, will also further increase the usage of water, necessitating more careful management of freshwater resources. In order to manage the supply of water on atolls most effectively, water resource managers need to quantify not only how much freshwater is available in the freshwater lens at any given time, but also a prediction of how the supply may fluctuate under future climate conditions.

Threats to Atoll Freshwater

The low-lying nature of the atoll islands exposes the freshwater supply to immediate threats such as wave-overwash events caused by storm surges, drought, human degradation, and long-term threats such sea-level rise. Storm surge is a temporary rise in sea level usually associated with tropical cyclones, during which powerful winds drive waves against the atoll coastlines and sometimes either partially or entirely inundate the width of the islands for a given period of time (Terry and Falkland, 2010) (Chui and Terry, 2012). A majority of atoll islands contain a central depression, which dips below the shallow water table, creating a permanent, shallow standing pool of water within which residents typically cultivate taro root. Though ideal for this practice, this shallow depression can also result in greater lens salinization following wave-overwash events, during which seawater that has entered the depression contributes salt to the shallow groundwater until it is diluted with rainwater. Storm surges usually occur only during adverse weather conditions, though tsunamis can have a similar effect on the islands. Numerical modeling studies have been conducted to understand the behavior of the seawater that infiltrates through the subsurface as a result of these events. A saline plume forms following a wave-overwash, migrating downward before leaving the aquifer through the permeable basement limestone (Terry and Falkland, 2010; Chui and Terry, 2012; Chui and Terry, 2013; Bailey and Jenson, 2013). Until the lens is replenished, a process which can take up to 12 months, island residents have extremely limited access to potable fresh groundwater supply and must seek other freshwater resources.

The other significant threat posed to small atoll water supply is drought induced by El Nino Southern Oscillation (ENSO) events. During ENSO events there is a sustained warming of the central and eastern Pacific Ocean, which results in ocean current and wind-direction reversals, extreme variations in rainfall patterns, elevated tides, and severe drought (Falkland, 1994). As the occurrence of rainfall on Pacific atolls is strongly correlated to variations in sea-surface temperature, following an El Nino event, infrequent rainfall is later followed by periods of high rainfall (White et al., 1999). It is during these periods of intermittent or no rainfall that atoll community water supply can dwindle and deplete. A drastic reduction in recharge to the subsurface reduces the lens' ability to maintain a zone of low chloride concentration. When sustained over a long period the thickness of the lens is greatly reduced and the volume of extractable freshwater is exhausted (Peterson, 1990).

A major drought in early 1998 marked one of the worst ENSO induced droughts in recorded history, with hundreds of islands in the western and central Pacific experiencing inadequate water supply. A time series of daily rainfall depth for the western Pacific is shown in Figure 3, with a significant drought seen in early 1998 which lasted several months. To sustain island communities during this period, water was imported from the larger volcanic islands that were not as heavily affected by the sporadic rainfall (Bailey et al., 2013). Fortunately, following ENSO drought periods, high levels of rainfall actively replenish the lens and reestablish an equilibrium state. The process of refreshing the lens takes time, however, with even as long as 1.5 years needed to fully recover (Bailey et al., 2009).

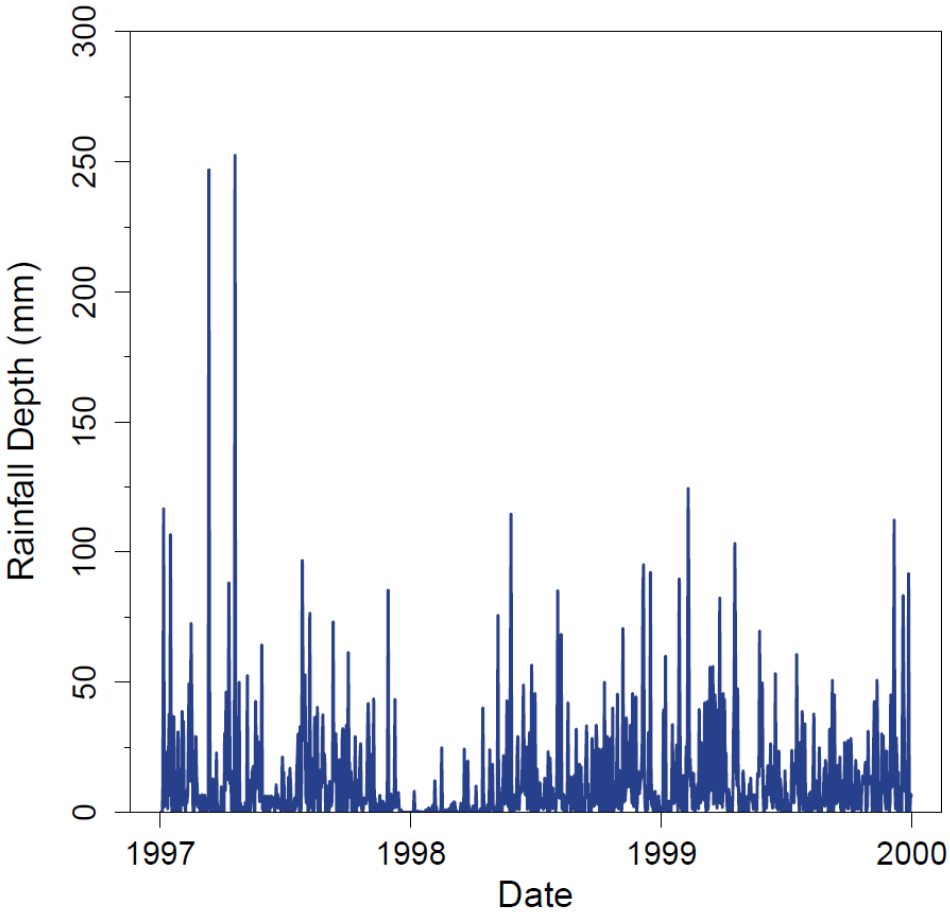

Figure 3. Time series of daily rainfall depth from 1997-1999. Extreme drought in early 1998 is considered one of the most severe droughts in recent Micronesian history

Human factors that contribute to lens degradation include the inappropriate application of pesticides or fertilizers to crops, fecal contamination from improper waste disposal, and over-exploitation of the lens through excess pumping. The high permeability of the island sediment allows for rapid infiltration and mixing of contaminants, such as pesticides and fertilizer, into the shallow water table. These issues lead to the conclusion that not only must water quantity be closely managed, but also that water quality protection measures should be followed. Other behavior that can have adverse effects on the water quality in the lens is that of over-pumping, leading to saline intrusion. In a majority of wells, the depth to water is less than 2 meters, allowing for extraction from the freshwater lens without the installation of drilled wells (Taboroši and Martin, 2011). If water is extracted from the hand-dug wells too quickly, seawater begins to intrude into the freshwater lens from below, a process known as upconing. Excess upconing can salinize the lens, preventing groundwater supply until infiltrating rainwater can once again flush out the salt from the subsurface.

Sea-level rise is a long-term threat to atoll island water supply. During the twentieth century, global sea level rose at an average of 1.8 mm/yr (Douglas, 1997), with accelerated rates as high as 4 mm/yr observed during the first decade of the present century, attributed mainly to large-scale climate change (Beckley et al, 2007). At this rate, a number of studies have predicted a sea-level rise of between 0.5 and 1.0 meter by the year 2100 (Raper and Braithwaite, 2006;

Rahmstorf, 2007; Meier et al., 2007; Pfeffer et al., 2008; Dickinson, 2009). An increase of this magnitude could drastically reduce the widths of atoll islands throughout the Indian and Pacific Oceans, reducing the available volume of extractable freshwater contained within the freshwater lens. It is therefore essential that conjunctive use of groundwater and collected rainwater be employed to bolster the supply of freshwater available to island communities when extractable volume from the lens dwindles.

Atoll Island Groundwater Modeling

To assist in water resource management on small atoll islands, and to further understand the dynamics of lens development and sustainability, attempts to quantify atoll groundwater have employed both numerical and analytical techniques. Using the Dupuit assumption of exclusively horizontal flow, a number of authors have approximated the position of the freshwater/seawater interface at the base of the lens using analytical solutions to the groundwater flow equation (Henry, 1964); (Fetter, Jr., 1972); (Collins & Gelbar, 1971); (Shamir & Dagan, 1971); (Chapman, 1985). Though the approximations made during these studies generally produce valid results, errors occur at the immediate boundary of the islands, where the Dupuit assumption is invalidated due to a significant upward component of flow. The method also does not account for the sharp truncation of the lens between the upper Holocene and lower Pleistocene aquifer units. These investigations have also employed the Ghyben-Herzberg approximation, which assumes a sharp interface between fresh and saline groundwater, across which there is assumed to be no flow (Hubbert, 1940); (Henry, 1964); (Glover, 1964); (Bear & Dagan, 1964); (Rumer, Jr. & Shiau, 1968). These early techniques to quantify freshwater volume have since been improved with further knowledge of the atoll hydrogeologic structure. In reality, the transition between the fresh and saline water is not sharp, but rather a broad transition zone of brackish water (Underwood, 1990). On most atolls, relatively small groundwater fluxes result in a relatively thick transition zone and thinner freshwater lens (Peterson, 1990).

Numerical modeling of atoll groundwater began in 1974 with the work of Lam (Lam, 1974), who assumed a single homogeneous, isotropic aquifer and uniformly horizontal flow; this practice was continued for several years (Lloyd, Miles, Chessman, & Bugg, 1980); (Falkland A. C., 1983). Working on Enjebi Island, Enewetak Atoll in the Marshall Islands, Buddemeier and Holladay (1977) were the first to discuss the dual-aquifer system of atoll islands, consisting of a less-permeable Holocene layer and an underlying, high-permeability karstic limestone Pleistocene layer. Building upon the work of Buddemeier and Holladay (1977), Herman and Wheatcraft (1984) modeled the atoll hydrogeologic system with a dual-aquifer structure. The extreme permeability of the underlying karstic Pleistocene aquifer effectively truncates the lens, limiting its depth to the contact between the two aquifers. Since its development by Voss (1984) a number of investigators have utilized SUTRA, a USGS finite-element based code used to simulate saturated-unsaturated flow. Using SUTRA, variable-density groundwater-flow dynamics have been modeled at an atoll scale (Hogan, 1988); (Underwood, 1990); (Griggs & Peterson, 1993); (Bailey R. T., Jenson, Rubinstein, & Olsen, 2008). Bailey et al. (2009) compared modeling results with published observations of atoll island lens thicknesses, with results indicating a hydraulic conductivity of approximately 50 m/d for leeward islands and approximately 400 m/d for windward islands.

Though several studies have approximated the thickness of the freshwater lens beneath atoll islands of varying widths, it is often desirable to calculate the volume of available freshwater to determine the sustainable yield of the lens. A few studies have modeled the

freshwater lens dynamics in 3-D. Lee (2003) employed TOUGH2, a general-purpose numerical simulator for multiphase fluid and heat flow in fracture-porous media, to determine the effects of various controls on the size of the freshwater lens and the thickness of the transition zone. Using SEAWAT (Langevin, Shoemaker, & Guo, 2003), a MODFLOW/MT3DMS-based code designed to simulate three-dimensional variable-density groundwater flow coupled with multi-species solute transport, Comte et al. (2014) simulated the evolution of groundwater salinity for Grande Glorieuse, a low-lying coral island in the Western Indian Ocean. By assessing model results against field observations, the sensitivity of the freshwater lens to vegetation and climate alterations was determined. No extensive three-dimensional modeling efforts have focused on small atoll islands in the Pacific Ocean.

Using two-dimensional modeling results, (Bailey R. T., Jenson, Rubinstein, & Olsen, 2008) developed an algebraic model to analytically approximate the thickness of freshwater beneath atoll islands as a function of the width of various cross-sections. Given the inherent variability of atoll island geology, the algebraic model performed well, though periodic numerical validation is necessary given the lens' transient nature. The model was later extended to the estimation of groundwater volume by estimating the freshwater lens thickness at various cross-sections across the island surface and interpolating between the sections (Bailey, Khalil, & Chatikavanij, 2014).

Several modeling efforts have been undertaken to understand the effects of sea-level rise and cyclone-driven inundation on atoll islands, and to estimate the resulting annual decrease in available freshwater (Terry & Chui, 2012); (Dickinson, 2009). By analyzing a generic two-dimensional atoll island, it was found that a long-term increase in sea level of 40 centimeters would result in salinization of the islands' central depression and lead to a substantial reduction in lens thickness. A rise in sea level can further aggravate the effects of wave overwash, with potential inundation across the already diminished island width resulting in an even more delicate state of groundwater resources.

Summary of Objectives

The objective of this thesis is to analyze the current state of atoll island freshwater resources within the Federated States of Micronesia in the western Pacific and provide an estimate of how supply may fluctuate under future climate conditions. The Federated States of Micronesia consists of 32 low-lying atolls and four larger volcanic "high islands" scattered across four states; it has a population of just over 100,000, with a majority of citizens residing on the high islands. The freshwater resources of the atoll islands are extremely fragile due to their unique geologic structure and isolated location. Average annual precipitation varies across Micronesia from 3.5 meters to over 5 meters, with rainfall depth increasing from west to east. General circulation models (GCMs) are used to provide future climate scenarios for freshwater volume simulation and analysis. Analysis is performed for both rainwater catchment systems and the freshwater lens. This was accomplished through:

- Investigation and identification of top-performing GCMs for use in estimation of future fluctuation in groundwater and rainwater supply (Chapter 2);
- Analysis of rainwater catchment systems (RWCS) performance and design optimization to maximize freshwater supply, with specific application to Nikahlap Island in the eastern FSM (Chapter 3);

- Using water balance modeling to create RWCS design curves using future estimated rainfall rates, to assist island communities in sizing systems for varying rates of reliability (Chapter 4);
- Development and calibration of three-dimensional groundwater flow and solute transport models to investigate the response of the freshwater lens to a variety of environmental parameters (Chapter 5);
- Estimation of future freshwater lens volume using top-performing GCMs for both the eastern and western FSM regions (Chapter 6); and
- Examination of the potential for conjunctive use of captured rainwater and groundwater, using future estimated climate data (Chapter 7).

Chapter 3 is a reprint of a paper published in 2014 in the Journal of the American Water Resources Association entitled "Sustainable Rainwater Catchment Systems for Micronesian Atoll Communities" (Wallace and Bailey, 2014).

CMIP5 DATASET DOWNSCALING AND ANALYSIS

Introduction

To manage water supply most effectively, successful water resources management requires an estimation of water supply fluctuation under transient climate conditions. To provide this estimate, models of future climate can be used to estimate how conditions may change under uncertain environmental forcings, such as emission-driven carbon cycle change. The Model Intercomparison Project Phase 5 (CMIP5) is a set of coordinated climate model experiments organized by the World Climate Research Programme. The organization consists of more than 20 climate modeling groups, each of which performs a standard set of general circulation model (GCM) simulations (Taylor, Stouffer, & Meehl, 2012). The overall goals of the program are to first, evaluate how realistic these standard models are in simulating the recent past, and to then use the models to provide projections of future climate change (Meehl, et al., 2009). On a more detailed scale, this will also increase understanding of factors responsible for differences in climate projections, including cloud cover and the carbon cycle (Taylor, Stouffer, & Meehl, 2012). The models developed to simulate global climate patterns all respond differently to similar forcing scenarios, necessitating statistical analysis to determine which models replicate historical climate patterns most accurately.

Various scenarios used by the CMIP5 global climate models represent different amounts of radiative forcing, which is a measurement of the capacity of CO_2 to affect the atmospheric energy balance, thereby contributing to climate change (Houghton et al., 2001); (Meehl et al., 1996). Some models prevent the response of the ocean to changes in greenhouse gas (GHG) concentration in order to isolate more rapid responses from cloud and land surfaces, while others use a regression approach to estimate the sensitivity of the climate to global mean temperature change. Contrasting emission scenarios are considered, represented by differences in how the increase and impact of CO_2 is gauged. Carbon cycle feedback experiments involve fluctuating ozone GHG concentrations, with each emission scenario focused on a different representative concentration pathway (RCP). RCPs are labeled according to each scenario's target radiative forcing at year 2100 (Taylor, Stouffer, & Meehl, 2012).

The high emissions scenario is represented by RCP8.5, in which radiative forcing reaches 8.5 W/m^2 at year 2100. RCP6.0 is also a high emissions scenario, but the radiative forcing in this case stabilizes at 6 W/m^2 after 2100. Moderate climate change mitigation is represented by RCP4.5, in which GHG emissions are somewhat restrained and the radiative forcing stabilizes at 4.5 W/m^2 at year 2100. Extreme climate change mitigation, characterized by drastic policy and lifestyle change to decrease the volume of GHG emissions, is represented by RCP2.6, in which radiative forcing peaks at 2.6 W/m^2 near 2100 (Taylor, Stouffer, & Meehl, 2012). All climate models for the RCP scenarios are run from 2006-2100, the intent of which is to understand the anthropogenic influence on climate change by exploring the impacts of various mitigation scenarios. They also help to provide an estimate of climate change and implications for sea-level and carbon cycle changes.

Description of the various climate models and corresponding modeling centers is shown in Table 1. We acknowledge the World Climate Research Programme's Working Group on Coupled Modelling, which is responsible for CMIP, and we thank the climate modeling groups (listed in Table 1 of this paper) for producing and making available their model output. For CMIP the U.S. Department of Energy's Program for Climate Model Diagnosis and

Intercomparison provides coordinating support and led development of software infrastructure in partnership with the Global Organization for Earth System Science Portals.

The remainder of this chapter is organized as follows: downscaling of monthly precipitation and temperature values derived from CMIP5 GCMs is performed to allow for comparison with historical climate data. Multi-criteria statistical analysis is then performed on downscaled GCM datasets to determine which datasets most accurately predict the not only the mean of historical precipitation and temperature data, but also which adequately represent historical climate patterns.

Table 1. CMIP5 climate modeling centers and the names of their corresponding models

Modeling Center (or Group)	ID	Institute ID	Model Name
Commonwealth Scientific and Industrial Research Organization (CSIRO) and Bureau of Meteorology (BOM), Australia	1	CSIRO-BOM	ACCESS1.0
	2		ACCESS1.3
Beijing Climate Center, China Meteorological Administration	3	BCC	BCC-CSM1.1
	4		BCC-CSM1.1(m)
Instituto Nacional de Pesquisas Espaciais (National Institute for Space Research)	5	INPE	BESM OA 2.3
College of Global Change and Earth System Science, Beijing Normal University	6	GCESS	BNU-ESM
Canadian Centre for Climate Modelling and Analysis	7	CCCMA	CanESM2
	8		CanCM4
	9		CanAM4
University of Miami - RSMAS	10	RSMAS	CCSM4(RSMAS)*
National Center for Atmospheric Research	11	NCAR	CCSM4
Community Earth System Model Contributors	12	NSF-DOE-NCAR	CESM1(BGC)
	13		CESM1(CAM5)
	14		CESM1(CAM5.1,FV2)
	15		CESM1(FASTCHEM)
	16		CESM1(WACCM)
Center for Ocean-Land-Atmosphere Studies and National Centers for Environmental Prediction	17	COLA and NCEP	CFSv2-2011
Centro Euro-Mediterraneo per I Cambiamenti Climatici	18	CMCC	CMCC-CESM
	19		CMCC-CM
	20		CMCC-CMS
Centre National de Recherches Météorologiques / Centre Européen de Recherche et Formation Avancée en Calcul Scientifique	21	CNRM-CERFACS	CNRM-CM5
	22		CNRM-CM5-2
Commonwealth Scientific and Industrial Research Organization in collaboration with Queensland Climate Change Centre of Excellence	23	CSIRO-QCCCE	CSIRO-Mk3.6.0
EC-EARTH consortium	24	EC-EARTH	EC-EARTH
LASG, Institute of Atmospheric Physics, Chinese Academy of Sciences and CESS,Tsinghua University	25	LASG-CESS	FGOALS-g2
LASG, Institute of Atmospheric Physics, Chinese Academy of Sciences	26	LASG-IAP	FGOALS-gl
	27		FGOALS-s2
The First Institute of Oceanography, SOA, China	28	FIO	FIO-ESM
NASA Global Modeling and Assimilation Office	29	NASA GMAO	GEOS-5
NOAA Geophysical Fluid Dynamics Laboratory	30	NOAA GFDL	GFDL-CM2.1
	31		GFDL-CM3
	32		GFDL-ESM2G
	33		GFDL-ESM2M
	34		GFDL-HIRAM-C180
	35		GFDL-HIRAM-C360
NASA Goddard Institute for Space Studies	36	NASA GISS	GISS-E2-H
	37		GISS-E2-H-CC
	38		GISS-E2-R
	39		GISS-E2-R-CC
National Institute of Meteorological Research/Korea Meteorological Administration	40	NIMR/KMA	HadGEM2-AO
Met Office Hadley Centre (additional HadGEM2-ES realizations contributed by Instituto Nacional de Pesquisas Espaciais)	41	MOHC (additional realizations by INPE)	HadCM3
	42		HadGEM2-CC
	43		HadGEM2-ES
	44		HadGEM2-A
Institute for Numerical Mathematics	45	INM	INM-CM4
Institut Pierre-Simon Laplace	46	IPSL	IPSL-CM5A-LR
	47		IPSL-CM5A-MR
	48		IPSL-CM5B-LR
Japan Agency for Marine-Earth Science and Technology, Atmosphere and Ocean Research Institute (The University of Tokyo), and National Institute for Environmental Studies	49	MIROC	MIROC-ESM
	50		MIROC-ESM-CHEM
Atmosphere and Ocean Research Institute (The University of Tokyo), National Institute for Environmental Studies, and Japan Agency for Marine-Earth Science and Technology	51	MIROC	MIROC4h
	52		MIROC5
Max-Planck-Institut für Meteorologie (Max Planck Institute for Meteorology)	53	MPI-M	MPI-ESM-MR
	54		MPI-ESM-LR
	55		MPI-ESM-P
Meteorological Research Institute	56	MRI	MRI-AGCM3.2H
	57		MRI-AGCM3.2S
	58		MRI-CGCM3
	59		MRI-ESM1
Nonhydrostatic Icosahedral Atmospheric Model Group	60	NICAM	NICAM.09
Norwegian Climate Centre	61	NCC	NorESM1-M
	62		NorESM1-ME

Methods

To give a detailed estimate of how the supply of available freshwater on atoll islands will change under future climate conditions, daily precipitation data is required; however, CMIP5 GCM output is on a monthly time-scale. Climate variability across Micronesia necessitated the extraction of separate datasets for both eastern and western Micronesia. Average annual rainfall in Yap State (western Micronesia) is approximately 2-3 meters whereas in Pohnpei State (eastern Micronesia) rainfall totals amount to between 3.5-4.5 meters per year. Temperature remains fairly constant across Micronesia; however, separate datasets were also extracted for use in downscaling. Cells of 7.5° longitude and 2.5° latitude were used for extraction, representing the smallest available cell size for CMIP model output. Model data was extracted from 1850-2080, limited in some cases by the amount of output available in certain models. Temporal downscaling was implemented to discretize stress periods and allow for more accurate statistical comparison between model results and observed climate data. By considering daily amounts of precipitation a chain-dependent process, a Markov chain algorithm was used to temporally downscale the precipitation data.

The Markov chain method gives a better approximation to the number of rainy days than a binomial process (Gabriel & Neumann, 1962); (Caskey Jr., 1963); (Todorovic & Woolhiser, 1975). Good statistical representation of wet-day probability is essential to the accurate representation of a climate's precipitation. A Markov chain algorithm is a bivariate stochastic process that utilizes transitional probabilities. The algorithm is expressed by

$$X_t|X_{t-1} \sim Markov(\boldsymbol{P}, p_1)$$

where $\boldsymbol{P}$ is the transitional probability matrix whose elements p_{ij} are defined by

$$p_{ij} = \Pr(X_t = i|X_{t-1} = j) \qquad i,j = \text{wet or dry}$$

and p_1 is the probability distribution vector of the wet and dry classifications (Srikanthan & McMahon, 2001).

Using historical data, one of two values is assigned to each day: 0 if the day is dry and 1 if the day is wet. To determine the classification of each day, the precipitation of that day is compared to a predetermined threshold value (T); the calculated median of average precipitation of each month across all years of data was used as the threshold for this study. If the average precipitation of a given month is greater than the median value, it is classified as wet. Conversely, if the average precipitation of that month is less than the median, it is classified as dry. This classification method is performed for the *n*-day period under consideration, typically as far back as the historical data is available. The total number of rainy days in the study period can then be determined by summing the values assigned to each day.

The amount of precipitation that can statistically occur on each day (*n*) depends on whether the previous day (*n*-1) was wet or dry. The statistical model for days with nonzero precipitation is most commonly a gamma distribution. For this reason, varying precipitation gamma distributions are referenced depending on the classification of each day, making it a first-order process that relies solely on the wet-dry classification of the previous day. The amount of daily precipitation (p) is expressed as an exponentially distributed random variable by

$$H(p) = 1 - e^{-\lambda(p-T)}$$

More detailed explanation of the Markov chain process can be found in (Todorovic & Woolhiser, 1975) and (Srikanthan & McMahon, 2001). Spatial downscaling is not required for either region under consideration as the grid size of the extracted CMIP5 GCMs is relatively small, corresponding to 7.5° longitude and 2.5° latitude. This small cell size represents a single data station so there are no conflicting climate datasets which must be downscaled. Historical data from Yap and Pohnpei States in Micronesia is available from 1952-2006, the daily values of which were classified as wet or dry using the Markov chain algorithm. These values were compared to the average monthly output from the CMIP5 GCMs, with each day within the CMIP5 datasets stochastically assigned a precipitation depth based upon both the historical Markov classification of each day and the average monthly precipitation value of each given month.

Generally, general circulation models tend to overestimate the frequency and underestimate the intensity of daily precipitation, often failing to accurately reproduce the statistics seen in historical records (Mearns, Giiorgi, McDaniel, & Shields, 1995); (Walsh & McGregor, 1995); (Walsh & McGregor, 1997); (Bates, Charles, & Hughes, 1998); (Charles & Bates, 1999). The performance of GCMs varies spatially; models that work well in one region may be inadequate in others. Methods for verification of weather forecasts are controversial. A number of arbitrary scores may indicate a "best" forecast, when in reality the dataset may prove less accurate.

For this study, a multi-score method is utilized to assess the performance of the various CMIP5 GCMs for both Yap and Pohnpei States. Following methodology outlined by Fu et al. (Fu, Liu, Charles, Xu, & Yao, 2013), the Brier score and Significance score were used concurrently to compare and evaluate the GCM probability density function of daily CMIP5 climate variable. The probability density function was created for historical data, the bins from which were applied to CMIP5 climate data to produce similar PDF plots for each model. Probability density function comparison allows for not only analysis of the ability of GCM to reproduce the mean and standard deviation of historical precipitation values, but also its capacity at replicating historical climate patterns (Perkins, Pitman, Holbrook, & McAneney, 2007).

The Brier verification score (BS) is commonly used to compare the quality of weather forecasts. Developed by Glenn Brier (Brier, 1950) it has a minimum value of zero for perfect forecasting and a maximum value of 2 for the worst possible forecasting. The method includes the measurement of the mean squared difference between the predicted probability of an outcome and the actual outcome, reporting the accuracy of probabilistic predictions. The algorithm is expressed by

$$BS = \frac{1}{n}\sum_{i=1}^{n}(P_{mi} - P_{oi})^2$$

where P_{mi} is the modeled i^{th} probability value of each bin and P_{oi} is the observed i^{th} probability value of each bin, and n is the number of bins. For this analysis, the number of bins was fixed at 100. Knowledge of a good relationship between forecasted and observed climate data is insufficient to indicate how well the forecast represents historical values; the frequency with which forecasted are made following historical climate patterns is also necessary. Probability density functions are used to indicate the likelihood of the GCM output to adequately reflect historical data. The size of the dataset has an effect on the quality of the Brier score analysis, with larger sets generally producing a lower, more accurate BS. Analysis of downscaled climate

data significantly increases the ensemble size of the dataset, providing a larger number of data points for a more accurate estimate of the BS for each CMIP5 GCM.

The Significance score (S_{score}) is used to evaluate how well climate forecasts capture the attributes of historical data. It is much more difficult for a model to replicate a PDF, indicative of overall climate patterns, than it is to simulate the mean and standard deviation of historical data. Mean analysis can hide biases or systematic errors because they do not allow for comparison of the entire data distribution. S_{score} analysis requires high quality observed data at a suitable temporal resolution (Peterson et al., 1998); (Griffiths et al., 2005). It used probability density functions to demonstrate forecasts' capability to simulate values that are rare and may be more common in the future. Significant overlap between the new modeled distribution and the observed data indicates higher accuracy and better replication of historical climate patterns. S_{score} analysis calculates the cumulative minimum value of each binned value for two distributions, quantifying the overlap between the two PDFs. This common, overlapping area is expressed as

$$S_{score} = \sum_{i=1}^{n} Minimum(P_{mi}, P_{oi})$$

where, similar to the BS analysis, P_{mi} is the modeled i^{th} probability value of each bin and P_{oi} is the observed i^{th} probability value of each bin, and n is the number of bins. If the forecasted PDF reflects historical values poorly it will have a score close to zero, signifying little overlap. Higher values of the S_{score} indicate better performing GCMs.

The normalized root mean square error (NRMSE) and relative error statistics were also calculated to give an indication of whether each GCM dataset adequately estimated the historical mean precipitation. Though calculated, it is not a governing statistic in CMIP5 GCM selection for reasons discussed previously. The long term monthly mean and standard deviation of precipitation values were first compared using the relative error statistic, quantifying the similarity between modeled and observed values. The relative error is the absolute error divided by the magnitude of the exact value. This statistic is only valid on a ratio scale, which is a scale that has a true zero. Since precipitation has a true zero (i.e. days with no rainfall) the statistic is valid for this analysis. The NRMSE represents the standard deviation of the difference between predicted and observed values, divided by the range of observed values of the variable being analyzed. It is used to compare the similarity of two time series by considering both mean and standard deviation (Randall, 2007). In general, statistically "best" performing models for NRMSE and relative error were not able to correctly replicate the PDF distribution of historical data over the same period.

For this study, CMIP5 GCMs were evaluated for their capability of accurately reproducing historical trends for both eastern (Pohnpei) and western (Yap) Micronesia. The number of GCM datasets extracted represents all available models for the selected RCP scenario. Separate analysis was performed for both regions of Micronesia due to fluctuations in climate patterns observed even across small distances. Results for Pohnpei and Yap States will be analyzed and discussed individually, with internal discussion on the different RCP scenarios considered. Each of the four forcing scenarios (i.e. RCP2.6, RCP4.5, RCP6.0, and RCP8.5) was analyzed for both regions to determine which models performed best.

Results

Top Performing GCMs for Pohnpei State

The CMIP5 GCM output for Pohnpei State is first analyzed. Table 2 shows the monthly mean, monthly standard deviation, NRMSE, relative error, BS, and S_{score} for each of the GCMs analyzed for Pohnpei under the RCP 2.6 forcing scenario.

Table 2. Monthly mean and standard deviation, normalized root mean square error, relative error, Brier Score, and Significance Scores for each of the climate models under the RCP2.6 forcing scenario

GCMs	Mean (mm)	St Dev	NRMSE	RE (%)	BS	S_{score}
3	13.3	25.2	0.30	3.55	0.015	55.3
4	13.2	22.0	0.51	2.29	0.003	79.2
6	13.3	22.0	0.28	3.49	0.002	83.0
7	13.2	20.0	0.28	2.35	0.010	70.9
11	13.2	21.2	0.30	2.92	0.016	61.8
13	13.2	21.1	0.30	2.77	0.011	69.0
21	13.3	21.1	0.34	3.33	0.002	83.7
23	13.3	22.4	0.30	3.12	0.006	73.1
24	13.2	21.7	0.30	2.57	0.004	78.8
27	13.3	20.7	0.30	3.17	0.003	83.3
28	13.1	20.3	0.51	1.52	0.003	82.2
31	13.4	22.9	0.30	3.84	0.002	83.3
32	13.2	22.0	0.27	1.75	0.003	78.1
33	13.3	22.1	0.51	2.98	0.004	75.8
36	13.1	21.7	0.51	1.52	0.003	82.3
38	13.3	21.0	0.51	3.43	0.002	83.4
40	12.9	23.7	0.33	-0.48	0.011	61.0
43	13.3	22.5	0.33	2.65	0.008	66.5
47	13.2	21.9	0.33	2.21	0.006	75.0
52	13.4	20.8	0.33	3.64	0.008	73.4
49	13.3	21.4	0.33	3.31	0.005	77.7
54	13.0	22.8	0.33	1.24	0.003	81.2
53	13.4	24.1	0.33	4.61	0.004	76.9
58	13.2	21.6	0.33	2.34	0.002	81.6
61	13.2	21.5	0.28	2.39	0.003	82.6
62	13.2	21.8	0.33	1.85	0.003	82.5

Considering the results of the BS and S_{score} analyses, CNRM-CM5 (GCM 21) is the best performing model for Pohnpei State, and bcc-csm1-1 (GCM 3) is the worst performing model. BS values ranged from 0.002 to 0.015, where a smaller value indicates a better fit to historical data. S_{score} values ranged from 55.3% to 83.7%, where models with a higher score show more overlap with the historical climate patterns. The S_{score} quantifies the overlap between the GCM PDFs and the PDF produced by observed values of precipitation. The top three datasets selected for modeling under the RCP2.6 scenario for Pohnpei State are CNRM-CM5 (GCM 21), GISS-E2-R (GCM 38), and GFDL-CM3 (GCM 31). These models produced BS values of 0.0023, 0.0024, and 0.0025, respectively. Their S_{score} values were 83.7%, 83.4%, and 83.3%, respectively. The relative error results indicate that HadGEM-AO (GCM 40) and MPI-ESM-LR (GCM 54) performed relatively well, while MPI-ESM-MR (GCM 53) and GFDL-CM3 (GCM 31) showed fairly high relative error values of 4.61% and 3.84%, respectively. These results exemplify the need for GCM analysis using probability density functions. One of the top three performing models according to the BS and S_{score} analyses was determined to be one of the poorest fits to historical data by the NRMSE and relative error analyses. Likewise, GCMs

indicated to be good fits to historical data by NRMSE and relative error analysis had some of the worst BS and S_{score} values.

Figure 4a, Figure 4b, and Figure 4c show a comparison between the historical climate data PDF and those produced by the three top-performing modeled datasets CNRM-CM5 (GCM 21), GISS-E2-R (GCM 38) and GFDL-CM3 (GCM 31), respectively. For comparison, Figure 4d shows the PDF analysis of the worst performing model for Pohnpei State for the RCP2.6 scenario, bcc-csm1-1 (GCM 3). Analysis showed an overlap of only 55.3% with the historical data, which is strongly evident in the PDF comparison.

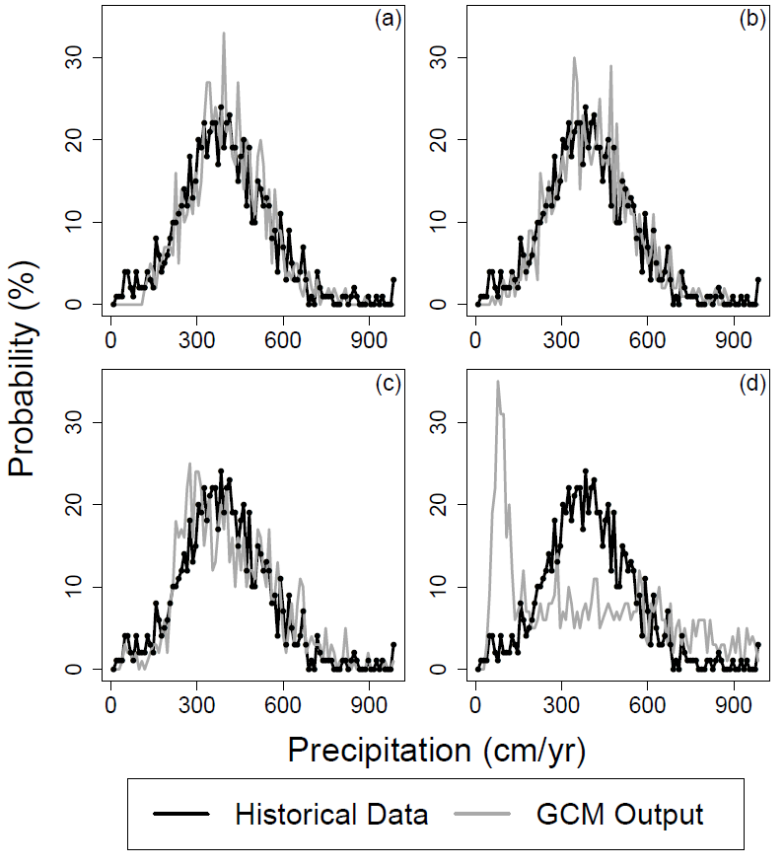

Figure 4. PDF comparison of the top three performing GCMs for the RCP2.6 forcing scenario with historical data in Pohnpei State. The best performing climate models were (a) CNRM-CM5, (b) GISS-E2-R, and (c) GFDL-CM3, while the worst performing was (d) bcc-csm1-1

Table A2 in Appendix I shows the statistical analysis results for each of the GCMs considered under the RCP4.5 scenario. RCP4.5 is considered a medium mitigation scenario because it identifies a concentration pathway relative to pre-industrial conditions. BS values ranged from 0.002 to 0.018, indicating that GFDL-CM3 (GCM 31) performed best and that bcc-csm1-1 (GCM 3) performed worst. S_{score} values ranged from 53.0% to 85.7%, with GFDL-CM3 (GCM 31) showing the most overlap with historical data and ACCESS-1-3 (GCM 2) showing the least amount of overlap. In this case, the lowest performing GCM as indicated by the BS did not match the lowest performing GCM as indicated by the S_{score} analysis. Though the values do not correlate as expected, the scores deviate by only a few one-hundredths of a percent. BS and S_{score} values for the top performing modeled datasets do correlate, however, indicating a good

statistical fit to the historical data. Figure 5 displays the probability density functions of the three top-performing CMIP GCM datasets for the RCP4.5 forcing scenario.

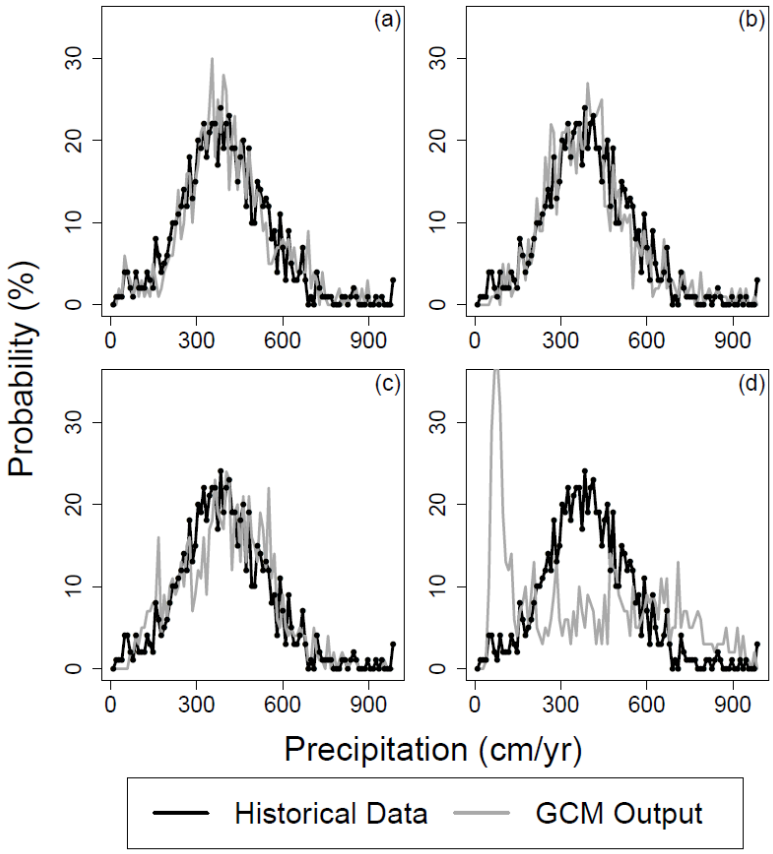

Figure 5. PDF comparison of RCP4.5 GCM performance against historical climate data in Pohnpei State. The best performing GCMs for this forcing scenario were (a) GFDL-CM3, (b) CCSM4, and (c) GISS-E2-R-p1; the worst performing was (d) ACCESS1-1

Figure 5a shows the PDF comparison of GFDL-CM3 (GCM 31), with overlapped the historical data by 85.7% It is noted that this GCM was also one of the top performing GCMs for the RCP2.6 scenario as well, indicating that this GCM dataset seems to be relatively accurate at climate pattern prediction for Pohnpei State. Figure 5b and Figure 5c show the PDF results for the other two selected top-performing datasets, in which CCSM4 (GCM 11) showed an overlap with historical data of 85.2% and GISS-E2-R-p1 (GCM 38a) an overlap of 83.9%. Figure 5d displays the PDF comparison between ACCESS-1-1 (GCM 2) and the historical data. ACCESS-1-3 is determined to be the worst performing GCM for the RCP4.5 forcing scenario, with an overlap of 53.0%.

Table A3 in Appendix I displays the comparison statistics for each GCM under the RCP6.0 forcing scenario. BS values ranged from 0.001 to 0.015, indicating that GISS-E2-R (GCM 38) fit the historical data best and that bcc-csm1-1 (GCM 3) showed the worst performance. S_{score} values ranged from 56.5% to 86.2%, with results agreeing with the BS for the best and worst performing GCMs. GISS-E2-R (GCM 38) was determined to accurately reproduce historical climate conditions while bcc-csm1-1 (GCM 3) did a poor job. The results of the PDF comparisons for the RCP6.0 forcing scenario are displayed in Figure 6.

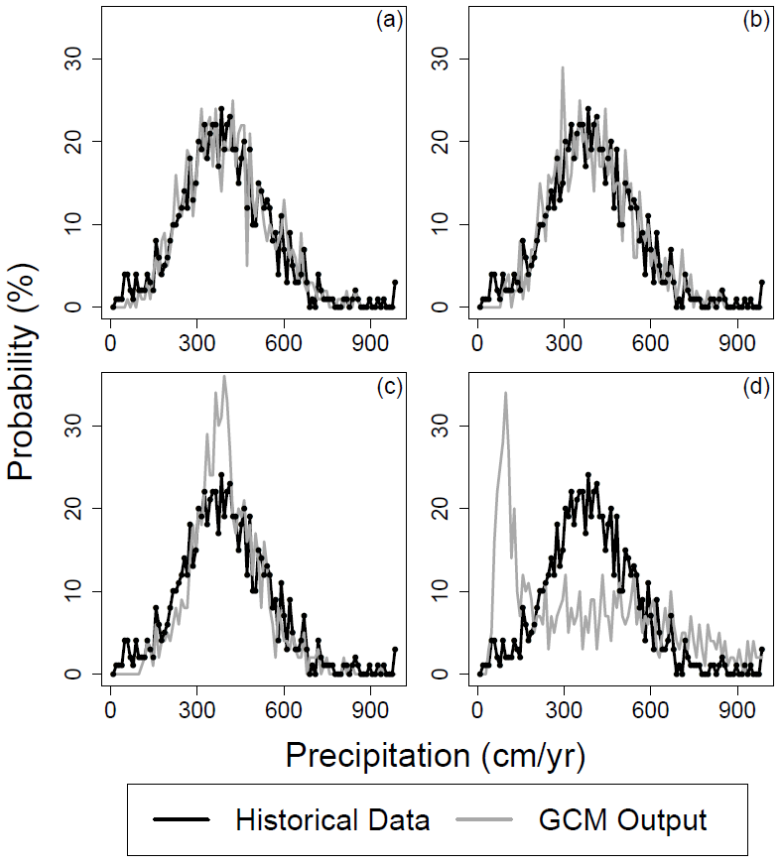

Figure 6. PDF comparison of GCM output to historical climate data for the RCP6.0 forcing scenario in Pohnpei State. The best performing GCMs for this scenario were (a) GISS-E2-R, (b) GISS-E2-H, and (c) FIO-ESM. The worst performing was (d) bcc-csm1-1

Figure 6a shows results of PDF comparison between GISS-E2-R (GCM 38) and observed precipitation values in Pohnpei State, indicating that it was able to accurately replicate historical climate patterns 86.2% of the time. The other two top-performing GCMs are GISS-E2-H (GCM 36) and FIO-ESM (GCM 28), with overlapping percentages of 84.3% and 83.4%, respectively. The results for the worst-performing GCM, bcc-csm1-1 (GCM 3), are shown in Figure 6d for contrast. The overall shape of the precipitation distribution is highly dissimilar to that seen in the historical data. The model shows only a 56.5% overlap with observed values, indicating its inadequate capability at replicating observed climate patterns.

Results from the analyses of the RCP8.5 forcing scenario are shown in

Table A4 in Appendix I. BS values ranged from 0.002 to 0.016, with NorESM1-ME (GCM 62) showing the best results and HadGEM2-AO (GCM 40) performing most poorly. S_{score} values ranged from 53.9% to 86.8%, with agreement between the results of the BS and S_{score} analyses. NorESM1-ME (GCM 62) most accurately reproduced the observed historical data and HadGEM2-AO (GCM 40) showed the worst performance of the GCMs analyzed.

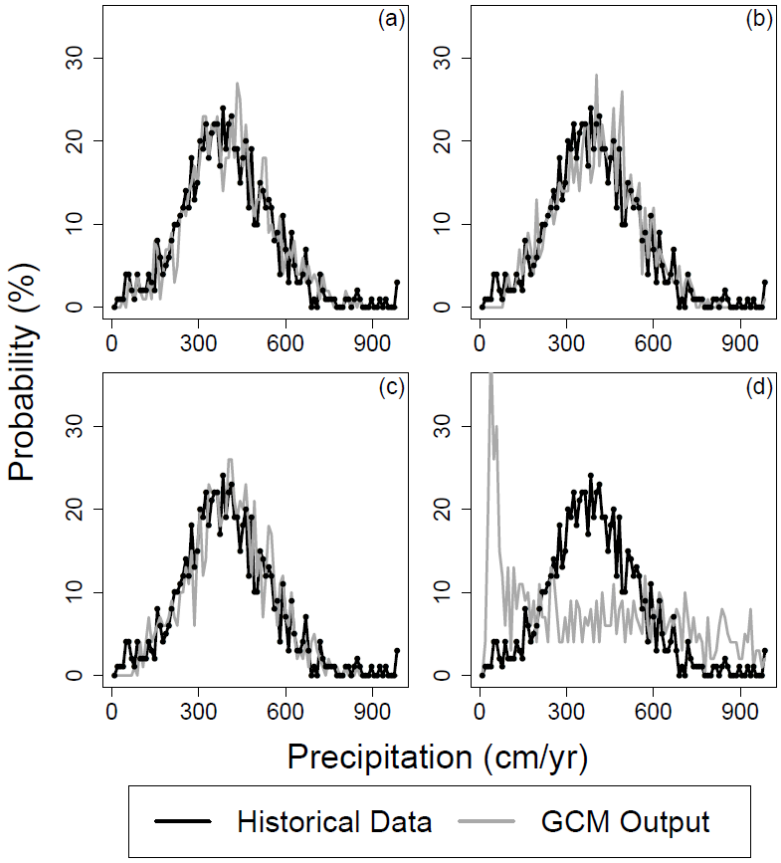

Figure 7. PDF comparison between GCM output and historical data in Pohnpei State. The three best and one lowest performing GCMs for this scenario were (a) NorESM1-ME, (b) GISS-E2-R-p2, (c) GISS-E2-R-p1, and (d) HadGEM2-AO

Figure 7 displays the PDF analyses of the three CMIP datasets ranked as replicating the historical data most accurately and also the GCM which ranked lowest. The results of the NorESM1-ME (GCM 62) comparison are displayed in Figure 7a, which show an overlap of 86.8% with historical data. This represents the highest overlap of any GCM output analyzed for Pohnpei State. GISS-E2-R-p2 (GCM 38b) and GISS-E2-R-p1 (GCM 38a) overlapped the historical data by 86.6% and 86.4%, respectively. The model that fit the historical data worst, HadGEM2-AO (GCM 40), overlapped the observed values by 53.9%; this is shown in Figure 7d.

Top Performing GCMs for Yap State

The results for the GMC analysis of Yap State are now presented and discussed.

Table A5 in Appendix I shows the statistical analysis results of RCP2.6. BS values ranged from 0.003 to 0.043, with GISS-E2-H (GCM 36) most accurately replicating historical values and CSIRO-Mk3-6-0 (GCM 23) performing worst. S_{score} values ranged from 41.0% to 83.3%, with all ranks agreeing with those indicated by the BS analysis. The three top-performing GCMs for the RCP2.6 forcing scenario in Yap State are GISS-E2-H (GCM 36), GFDL-ESM2M (GCM 33), and NorESM1-ME (GCM 62). Figure 8 shows the results of the probability distribution function comparisons of the three best performing GCMs and of the worst performing.

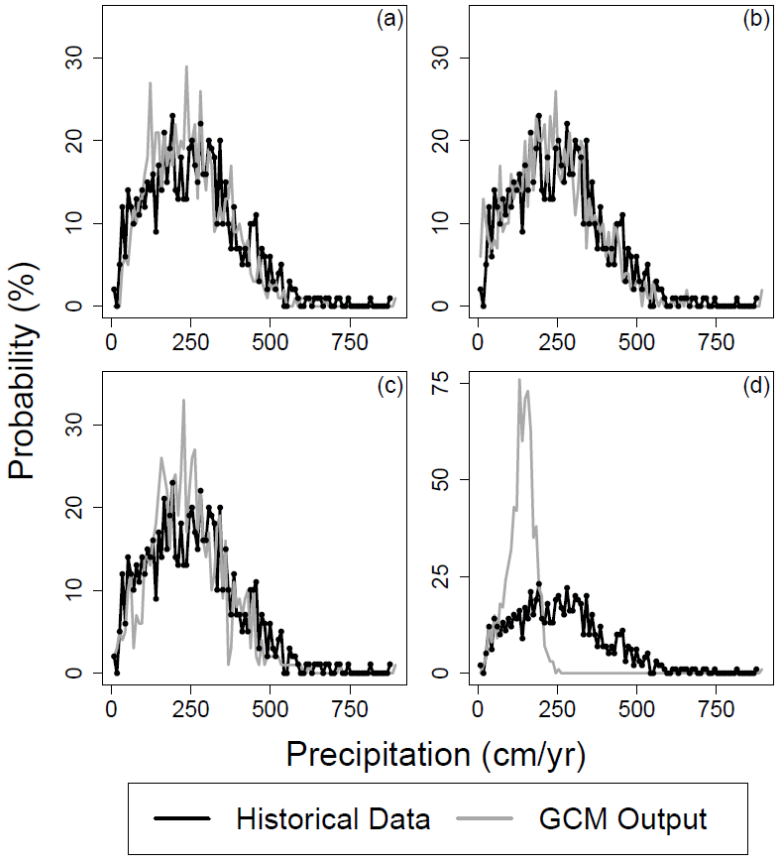

Figure 8. PDF comparison of the three best and one lowest performing GCMs for RCP2.6 against historical data in Yap State. The best performing models were (a) GISS-E2-H, (b) GFDL-ESM2M, and (c) NorESM1-ME; the lowest performing was CSIRO-Mk3-6-0

Figure 8a displays the PDF produced by the GISS-E2-H (GCM 36) climate model compared to the PDF of the historical values. The modeled climate data overlapped the observed values by 83.3%. Figure 8b and Figure 8c correspond to GFDL-ESM2M (GCM 33) and NorESM1-ME (GCM 62), which showed S_{score} values of 82.2% and 81.9%, respectively. Figure 8d shows the PDF comparison of the lowest performing GCM, CSIRO-Mk3-6-0 (GCM 23), which overlapped the observed data by 41.0%.

The results of the statistical analysis performed for the RCP4.5 forcing scenario are shown in

Table A6 in Appendix I. BS values ranged from 0.002 to 0.017, indicating that GISS-E2-H-p1 (GCM 36a) performed the best and that bcc-csm1-1 (GCM 3) had the lowest ranked performance. S_{score} values ranged from 62.2% to 84.4%, reinforcing the results of the BS analysis by indicating that GISS-E2-H-p1 (GCM 36a) overlapped the historical data most and that bcc-csm1-1 (GCM 3) showed the worst performance. A visual representation of the PDF analyses performed on the GCMs is shown in Figure 9.

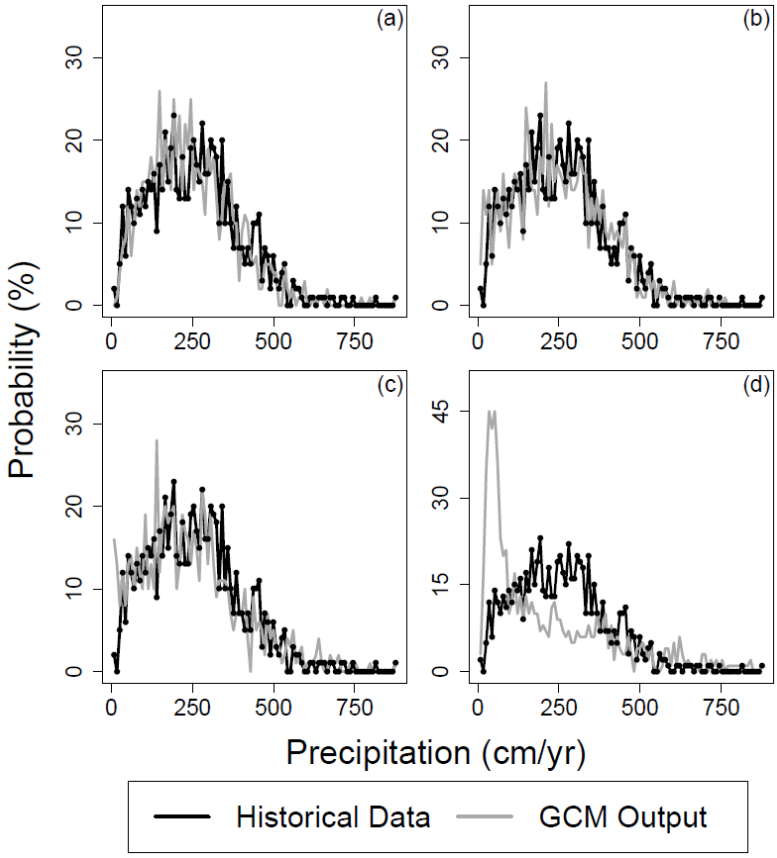

Figure 9. PDF comparison of (a) GISS-E2-H-p1, (b) GFDL-ESM2M, (c) FGOALS_g2, and (d) bcc-csm1-1 in Yap State for the RCP4.5 forcing scenario

Figure 9a shows the PDF comparison of the highest performing GCM, GISS-E2-H-p1 (GCM 36a), to the historical data, with an overlap of 84.4%. Figure 9b and Figure 9c display the PDF comparisons of the new two GCMs determined to be the highest performing. GFDL-ESM2M (GCM 33) showed an overlap with historical data of 84.3% while FGOALS_g2 (GCM 25) had an overlap of 83.4% The lowest performing GCM for the RCP4.5 forcing scenario was bcc-csm1-1 (GCM 3), shown in Figure 9d, which overlapped the historical distribution by 62.2%.

Table A7 in Appendix I shows the statistical analysis results for the RCP6.0 forcing scenario. BS values for this scenario ranged from 0.003 to 0.028, with the lowest scoring (and therefore best performing) GCM determined to be MRI-CGCM3 (GCM 58). S_{score} values ranged from 46.4% to 80.2%, indicating that the worst performing GCM for this analysis was CSIRO-Mk3-6-0. Figure 10 shows the results of the PDF comparison for three of the best performing GCMs and for the worst performing.

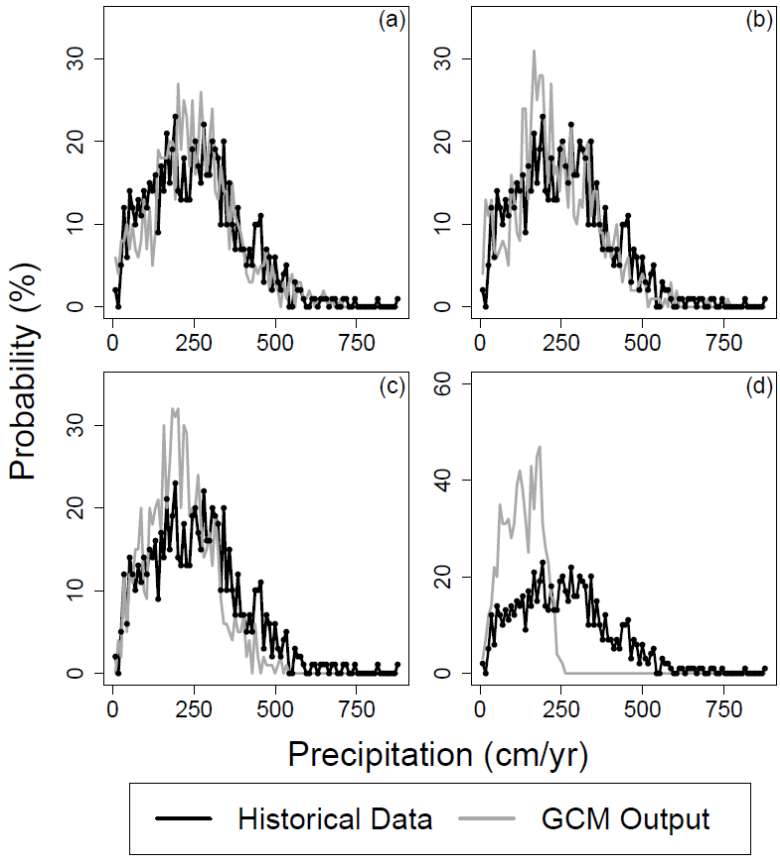

Figure 10. PDF comparison between GCM output and historical data for the RCP6.0 forcing scenario in Yap State. Top performing GCMs are (a) MRI-CGCM3, (b) GFDL-ESM2M, and (c) GISS-E2-R while the lowest performing was (d) CSIRO-Mk3-6-0

The top performing GCM as determined by the PDF analysis was MRI-CGCM3 (GCM 58), which received a BS value of 0.003 and an S_{score} value of 80.2%. This analysis is shown in Figure 10a. The other highest performing GCMs for this forcing scenario are GFDL-ESM2M (GCM 33) and GISS-E2-R (GCM 38). GFDL-ESM2M (GCM 33) received a BS value of 0.004 and overlapped the historical data by 79.3% GISS-E2-R (GCM 38) had a BS of 0.005 and showed an overlap with the observed values of 77.7%. The overall worst performing GCM for this scenario was CSIRO-Mk3-6-0 (GCM 23), with a BS value of 0.025 and an S_{score} of 46.4%.

The results of the statistical analysis of the GCMs under the RCP8.5 forcing scenario are shown in Table A8 in Appendix I. BS values ranged from 0.002 to 0.039, with GISS-E2-H-p2 (GCM 36b) performing the best and CSIRO-Mk3-6-0 (GCM 23) showing the poorest performance. S_{score} values ranged from 42.1% to 83.9%. For this forcing scenario, the BS analysis agreed with the results of the S_{score} analysis in ranking the best and worst performing GCMs. Figure 11 shows the results of the PDF comparisons between the GCMs and the observed data.

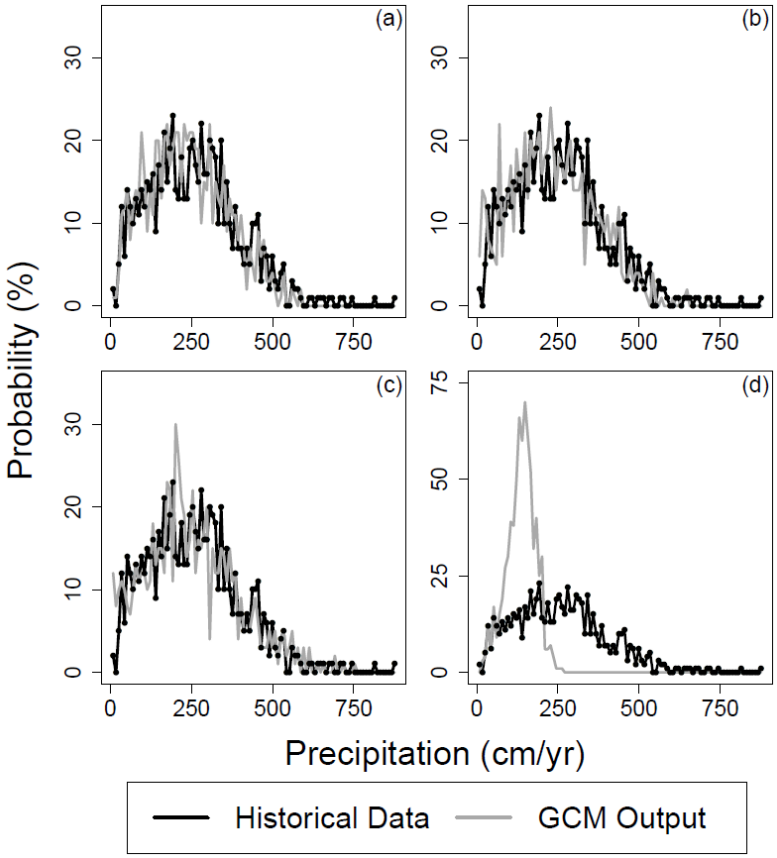

Figure 11. PDF comparison between GCM output and historical data for the RCP8.5 forcing scenario in Yap State. The best performing models were (a) GISS-E2-H-p2, (b) GFDL-ESM2M, and (c) MRI-CGCM3; the worst performing GCM was (d) CSIRO-Mk3-6-0

GISS-E2-H-p2 (GCM 36b) is shown in Figure 11a, with an overlap of 83.9% with the historical data. Figure 11b and Figure 11c show the PDF comparisons of GFDL-ESM2M (GCM 33) and MRI-CGCM3 (GCM 58), respectively. GFDL-ESM2M (GCM 33) overlapped the historical data by 82.5% and MRI-CGCM3 (GCM 58) showed an overlap with the observed values of 82.2%. The worst performing GCM for this forcing scenario was CSIRO-Mk3-6-0 (GCM 23), with a BS of 0.039 and an S_{score} of 42.1%.

Discussions and Conclusion

Climate data was derived from various GCMs from the Coupled Model Intercomparison Project Phase 5 World Climate Research Programme. More than 20 climate modeling groups from research stations around the world provide estimated future climate data under varying climate change scenarios. The scenarios focused on in this study are those that include various representative concentration pathways (RCP), which represent different emissions scenarios. RCP forcing scenarios range from conditions which estimate little to no increase in either the emission rate or concentration of greenhouse gas in the atmosphere, to conditions which represent extremely high emission rates and significant increase in atmospheric greenhouse gas concentration. The overall goal of the CMIP5 climate modeling is to provide an estimate of the anthropogenic influence on climate change, and what implications it could have for sea-level and carbon cycle changes.

A Markov chain algorithm was used to downscale monthly climate data extracted from the CMIP5 website. Various climate models from modeling groups around the world were downscaled to provide climate data at a daily temporal discretization for use in groundwater and rainwater catchment models. By considering precipitation a chain-dependent process, wherein the probability of rainfall on a given day relies on whether rainfall occurred on the previous day, historical climate data from 1952 through 2012 was used to classify each day as either wet or dry. Once downscaled, each climate model was ranked based on its ability to estimate not only the mean and standard deviation of the historical data, but also on its capacity to replicated observed climate patterns. The top three best-performing GCMs have been selected for each of the four representative concentration pathways for both Yap and Pohnpei States. The top models will be used in both three-dimensional atoll groundwater models developed using USGS's SEAWAT and in the RWCS water balance to be discussed later in this paper. A summary of the top models, with their respective Brier scores and Significance scores, is shown in Table 3.

Table 3. Summary of three top performing models in Pohnpei and Yap States with their corresponding Brier and Significance scores

Region	RCP	GCM	BS	S_{score}
Pohnpei	2.6	CNRM-CM5	0.0023	83.7
		GISS-E2-R	0.0024	83.4
		GFDL-CM3	0.0025	83.3
	4.5	GFDL-CM3	0.0016	85.7
		CCSM4	0.0019	85.2
		GISS-E2-R-p1	0.0021	83.9
	6.0	GISS-E2-R	0.0015	86.2
		GISS-E2-H	0.0019	84.3
		FIO-ESM	0.0028	83.4
	8.5	NorESM1-ME	0.0016	86.8
		GISS-E2-R-p2	0.0018	86.6
		GISS-E2-R-p1	0.0016	86.4
Yap	2.6	GISS-E2-H	0.0029	83.3
		GFDL-ESM2M	0.0028	82.2
		NorESM1-ME	0.0035	81.9
	4.5	GISS-E2-H-p1	0.0022	84.4
		GFDL-ESMSM	0.0026	84.3
		FGOALS_g2	0.0029	83.4
	6.0	MRI-CGCM3	0.0032	80.2
		GFDL-ESM2M	0.0037	79.3
		GISS-E2-R	0.0052	77.7
	8.5	GISS-E2-H-p2	0.0024	83.9
		GFDL-ESM2M	0.0027	82.5
		MRI-CGCM3	0.0033	82.2

The lowest performing models were also determined, mostly for comparison with the top-models to exemplify the results of the Brier and Significance score analyses. Almost all of the lowest performing GCMs showed significant left skew, regardless of region or forcing scenario being considered. It is noted that, while the GCMs with the worst performance had relatively low overlap with the historical climate data probability distribution function, all of the models showed reasonable values for the estimated mean and standard deviation of precipitation values. It was frequently observed that models indicated by the Brier and Significance score tests as being top performers did not show the best statistical match when analyzed by the NRMSE

and relative error tests. As discussed previously, mean and standard deviation analyses may indicate the ability of each GCM to correctly model the magnitude of historical climate data, but give no indication of their capability in matching climate patterns.

There are also several cases when the GCM rankings indicated by the Brier score analysis did not agree with those produced by the Significance score analysis. This is exemplified by the analysis of the RCP6.0 forcing scenario for Yap State. The lowest scoring GCM according to the Brier score analysis was CCSM4 (GCM 11). Though these results do not agree with the results of the Significance score, the disagreement is statistically small. Significance score analysis will remain the governing statistical parameter for determination of the performance of GCMs as it identifies not only the capability of each GCM to estimate the mean and standard deviation of the historical dataset, but also to replicate the observed climate patterns. Using a combination of the Brier and Significance analyses to determine the top-performing GCMs for each region under the four forcing scenarios allowed for analysis of not only the ability of each GCM to replicate magnitude, but also climate patterns of the historical data.

SUSTAINABLE RAINWATER CATCHMENT SYSTEMS FOR MICRONESIAN ATOLL COMMUNITIES[1]

Introduction

Rainwater Catchment Systems (RWCS) are used extensively worldwide by communities and individual household units as a means to store fresh water when surface water or groundwater is not readily available, not easily accessible, or has been contaminated and requires expensive treatment methods (Gould & Nissen-Petersen, 1999). Typically comprised of a roof of impermeable material acting as the catchment area, a gutter system to deliver collected runoff water from the roof, and a cistern or storage tank to store the rainwater, RWCS have been increasingly used in the last three decades to harvest rainwater due to recent development of low-cost designs, problems with surface water and groundwater such as salinity, chemical contamination (Gould & Nissen-Petersen, 1999), diminishing urban water supplies (Farreny, et al., 2011); (DeBusk & Hunt, 2013), an emphasis on rural development, and as a means for stormwater control and supplying supplemental water in urban settings (Basinger, Montalto, & Lall, 2010); (Steffen, Jensen, Pomeroy, & Burian, 2013). Dependence on collected rainwater to fulfill domestic water needs ranges from occasional and intermittent use, where rainwater supplements water derived from surface water and groundwater, to almost exclusive reliance, such as in southeast Asia (Özdemir, et al., 2011), central China, the Australian outback, eastern and southern Africa (Mwenge Kahinda, Taigbenu, & Boroto, 2007); (Baguma, Loiskandl, & Jung, 2010); (Opare, 2012), small oceanic islands and low-elevation atolls (Krishna, 1989); (Han & Ki, 2010), and Bermuda, where roof-top rainwater harvesting is mandated by law for all buildings (Rowe, 2011).

Despite the frequent use of RWCS and their implementation in regions worldwide, two fundamental problems prevent the consistent and sustainable use of RWCS. First, inadequate storage can occur during periods of low rainfall, with stored volumes of rainfall subject to depletion if consistent daily precipitation does not occur. This inadequacy is particularly acute for regions that experience a pronounced wet season and dry season, such as southeast Asia (Han & Ki, 2010); (Özdemir, et al., 2011) and in the islands of the Pacific Ocean, where the storage accumulated during the wet season at times may not be sufficient to sustain domestic water supply during the dry season (Taboroši & Martin, 2011). Small oceanic islands such as atoll islands are particularly vulnerable due to their lack of surface water resources and the fragile nature of their fresh groundwater lens (Kim, et al., 2003), especially during times of El Niño-induced drought (White & Falkland, 2010); (Bailey, Jenson, & Taborosi, 2013). Second, sustainability is impeded by potential contamination and degradation of the collected rainwater due to animal feces and plant matter captured in the runoff, microbial contamination, and

[1] As published in the Journal of the American Water Resources Association, Corey D. Wallace, Ryan T. Bailey Used with permission, from Journal of the American Water Resources Association:1-15 (2014).

possible long residence time in storage tanks (Sung, et al., 2010). Water quality surveys of rain catchment supplies have been conducted in regions worldwide (Uba & Aghogho, 2000); (Lye, 2002); (Sung, et al., 2010); (Ahmed, Gardner, & Toze, 2011), with many studies reporting significant presence of pathogens (Crabtree, Ruskin, Shaw, & Rose, 1996); (Simmons, Hope, Lewis, Whitmore, & Gao, 2001); ((RMI), 2005); (Sung, et al., 2010) whereas others report relatively high-quality water, such as in Micronesia (Dillaha & Zolan, 1985); (Detay, Alessandrello, Come, & Groom, 1989), although recent studies have not been conducted.

To analyze RWCS performance, numerous studies in many regions of the world have used a water balance modeling approach (Jenkins, Pearson, Moore, Sun, & Valentine, 1978) to perform a quantitative assessment of volumes captured and stored by RWCS at hourly, daily, or monthly time steps. The model has been used to assess potential for and benefits of implementing RWCS in regions worldwide (Fewkes, 1999); (Villarreal & Dixon, 2005); (Basinger, Montalto, & Lall, 2010); (Han & Ki, 2010); (Rowe, 2011); (Steffen, Jensen, Pomeroy, & Burian, 2013), as well as investigating the sensitivity of model parameters for optimum design (Mun & Han, 2012). Input to the system consists of the depth of precipitation for each time step multiplied by the available catchment area and transmission efficiency, giving net runoff volume from the roof transferred to the storage tank. Output from the system consists of water extracted to meet user demands.

Due to rainfall input and demand output often occurring during a single time step, the resulting change in storage calculation sometimes can depend on the assumed sequence of events (rainfall input, possible tank overflow, demand output). Jenkins et al. (1978) established two principal algorithms to calculate change in storage based on the assumed sequence: the "Yield-after-Spillage" (YAS) operating method, in which water demand is subtracted from the stored water after any excess water is allowed to spill via overflow, and the "Yield-before-Spillage" (YBS), in which the water demand is subtracted before the spillage check is performed. Fewkes (1999) determined that the YAS algorithm provides a more conservative approximation of system performance regardless of the model time step when compared to the YBS method, since the overflow water is not available for consumption. Hence, the YAS algorithm has been used principally in RWCS studies (Villarreal & Dixon, 2005); (Basinger, Montalto, & Lall, 2010); (Palla, Sansalone, Gnecco, & Lanza, 2011); (Mun & Han, 2012), although the YBS algorithm has been used in regions where peak water demand is known to occur during the mornings hours of the day, and hence typically before rainfall input and potential tank spillage (Chui, Liaw, & Cheng, 2009); (Steffen, Jensen, Pomeroy, & Burian, 2013). Typically, daily time steps are used since they provide enhanced temporal resolution relative to monthly time steps but not a significant difference relative to hourly time steps (Fewkes, 1999). The use of daily time steps, and hence tracking day-to-day volume fluctuations and depletions, is particularly important when a community relies solely on captured rainwater.

System efficiency, a function of the degree of roof material imperviousness, roof and gutter leaks, and surface depressions, typically is given a value between 70% and 95% (Han & Ki, 2010) (Rowe, 2011); (Farreny, et al., 2011) and treated deterministically. Lower values are assigned to leaky systems, whereas higher values are given to well-sealed systems that are properly maintained. Previous studies have focused on individual household RWCS without regard to the temporally-varying total collected volume for a given community or village. Furthermore, no studies have quantitatively assessed the performance of RWCS for small Pacific islands, for which rainwater is often the only viable source of fresh water for the island community and for which a baseline assessment and recommendations for optimal RWCS design is vital to sustain community well-being.

In this study, a quantitative analysis is provided for RWCS of atoll islands in the Federated States of Micronesia (FSM) in the western Pacific to assess baseline conditions and to provide strategies for implementing sustainable systems. Analysis is performed for the 1997-1999 time period, during which an intense El Niño event and associated major drought were experienced in the geographic region of the FSM and during which rainwater supplies became depleted (Taboroši & Martin, 2011). Using the YAS water balance algorithm of Jenkins et al. (1978) and daily measured rainfall depths for the FSM, analysis is performed for the island of Nikahlap on Pakein Atoll, located northwest of Pohnpei in the eastern region of the FSM, for which individual RWCS features and dimensions have been documented (Taboroši & Martin, 2011). To assess island-wide sustainability, analysis is performed at the village scale, with each of the household and public RWCS taken into account in the overall assessment. Also, to provide a general assessment of island RWCS across the geographical extent of the FSM, and since lower magnitudes of precipitation typically are experienced in the western portion of the FSM, analysis also is performed for a generic island located in the western FSM with RWCS infrastructure identical to that of the Nikahlap community.

Specific objectives include: (1) the estimation of probable daily baseline conditions of rainwater storage volume during 1997-1999, taking into account system uncertainty, (2) the identification of specific RWCS parameters that govern total collected water volume and the number of consecutive days of insufficient water supply, referred to as *NCDI*, (3) the determination of whether sufficient water supply can be sustained during times of drought via RWCS design optimization using available infrastructure, and (4) the provision of general guidelines for atoll island RWCS in the FSM to prepare for future climate conditions. Although a short analysis period, due to the major 1998 drought, the 1997-1999 period analyzed in this study represents a worst-case scenario in terms of RWCS performance and one that can be used to investigate and recommend methods of optimization. A similar procedure was adopted by Rowe (2011) for RWCS analysis and tank sizing in Bermuda. As the FSM government seeks to make each atoll island community sustainable in regards to water resources, particularly during even the most severe droughts, such an analysis is crucial.

Following an overview of the geography, people, and climate of the FSM and placing current RWCS practices within a general water resources context, methods and results will be presented and discussed, followed by a discussion of general design and maintenance requirements to enhance the possibility of sustaining quantity and quality of RWCS water for FSM atoll islands. Due to the representative nature of Nikahlap Island in relation to other FSM atoll island communities in terms of population and rainwater harvesting infrastructure, it is expected that analysis results will apply generally to other atoll islands within the FSM. Additionally, as many nations in the Pacific and Indian Ocean basins are comprised principally or solely of small islands similar to the ones assessed in this study, results can provide water resource managers and policy makers from these nations with important guidance in designing and maintaining individual and communal RWCS.

Study Area

Geography, People, and Climate of the FSM

The Federated States of Micronesia (FSM) is a geographically insular nation spread across a geographic area of more than 2 million km^2 of the western Pacific Ocean (Figure 12), and is comprised of four volcanic “high islands” (Yap, Chuuk, Pohnpei, and Kosrae) and 32 atolls, with each atoll consisting of several small carbonate islets (i.e., atoll islands) and coral reefs

surrounding a shallow lagoon. The FSM has a total population of approximately 108,000, with a negative growth rate of -0.38% observed in recent years that is projected to continue (Micronesia, 2002).

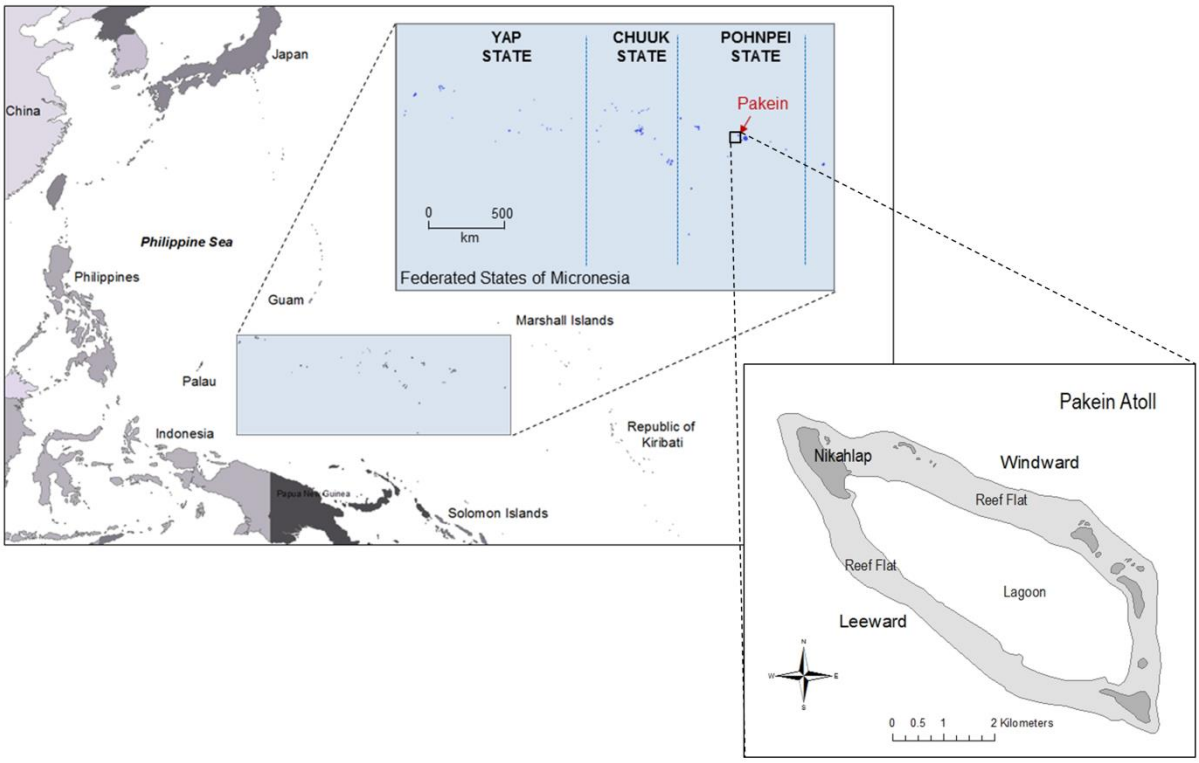

Figure 12. Map of the Western Pacific Region with a Magnified Map of the Federated States of Micronesia, showing the Boundaries among the States of Yap, Chuuk, and Pohnpei. A magnified map of Pakein Atoll in Pohnpei State is also shown, with Nikahlap Island being the islet of interest in rainwater catchment systems analysis

Whereas the high islands have moderate land surface areas (100-350 km^2), the low atoll islands have extremely small land surface areas (< 1 km^2) and low elevations (< 2-3 m), and consequently support populations, with only 4.5% of the total FSM population residing on the 32 atolls. Typically, population per atoll island is a few hundred or less (Micronesia, 2002). For example, average population per atoll, with atoll residents spread throughout one or more atoll islands, is 385 for the atolls in Yap State and 418 for atolls in Pohnpei State. Atoll inhabitants subsist by cultivating coconuts, swamp taro, breadfruit, and pandanus (Falkland A. , Water Resource Management, 2002), although agriculture must be monitored closely so as not to excessively compete with domestic fresh water use.

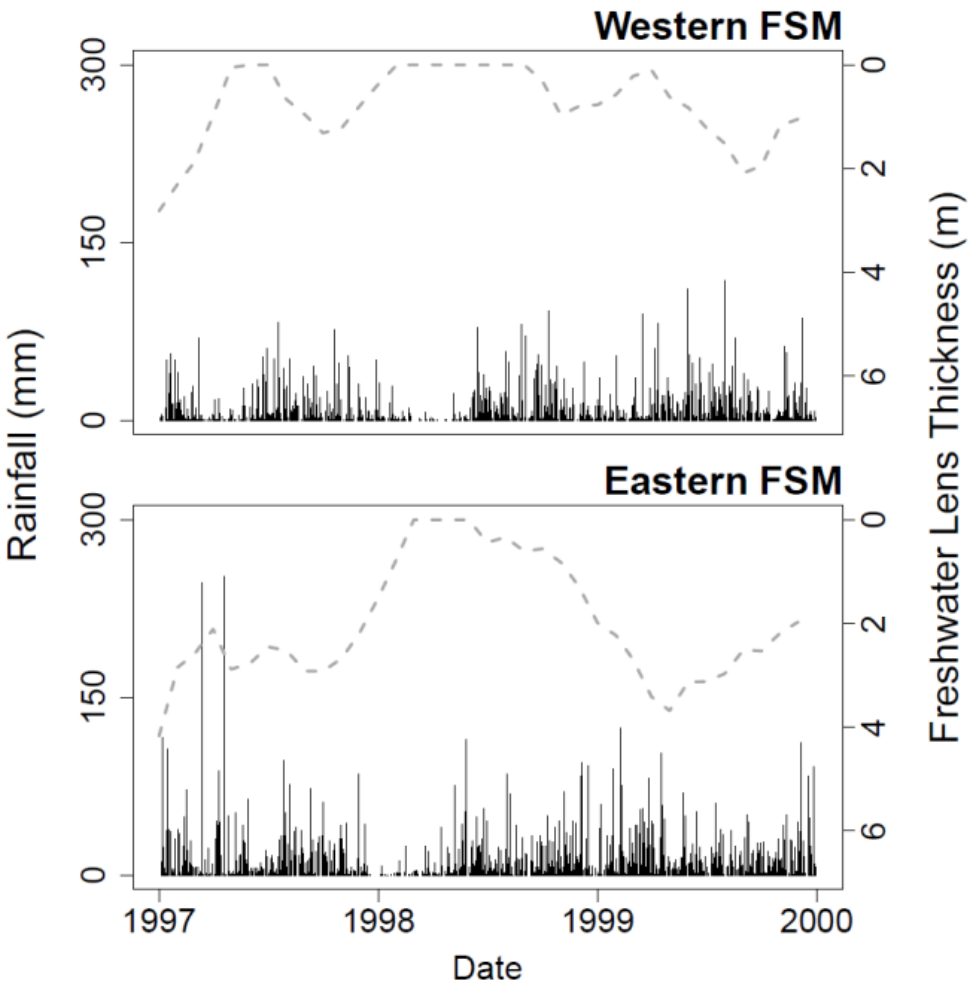

Figure 13. Time Series Plot Displaying the Historical Rainfall Data for Western and Eastern Federated States of Micronesia (FSM) from January 1, 1997 to December 31, 1999. Also shown is the estimated groundwater freshwater lens thickness over the same period for an island with a width of 400 m, as estimated by Bailey *et al*. (2013). The lens thickness is reflective of rainfall patterns, with fresh groundwater depletion during periods of drought (first months of 1998).

Average temperatures throughout the region range from 26 to 27 °C (79 to 81 °F) with a relative humidity over 80%. North-east trade winds yield frequent heavy rainfall, with average annual rainfall depths for the Yap, Chuuk, Pohnpei, and Kosrae regions of approximately 3.0 m, 3.4 m, 4.8 m, and 5.2 m, respectively, exhibiting the general increase in average annual depth from the western to the eastern regions of the FSM, with the western islands of the Yap and Chuuk regions experiencing a more prolonged dry season (Lander & Khosrowpanah, 2004). The region also experiences seasonal El Niño events, during which warm ocean water currents that develop off the west coast of South America induce climatic changes across the Pacific Ocean, typically resulting in drought conditions during the winter and spring months of the event. Drought duration can be lengthened during severe El Niño events, with reduced rainfall in late autumn extending into the spring and summer of the following year. For example, during the extreme El Niño-induced drought of 1998, the annual total rainfall for Pohnpei State for 1998 is the lowest on record during the period of 1953 through 2001 (Lander & Khosrowpanah, 2004), and the 16.2 mm of rainfall for January is the lowest monthly total on record. Similar reductions in rainfall during the initial months of 1998 were experienced throughout the FSM. Figure 13

shows daily rainfall depths (mm) for the western (Yap) and eastern (Pohnpei) FSM regions during 1997-1999, displaying the drought during the first months of 1998.

3.2.2 Water Use and Water Resources of FSM Atoll Island Communities

Due to small land surface, low elevations, geographic remoteness, and expected changes in climate, atoll island communities are some of the most vulnerable worldwide in terms of freshwater scarcity and depletion of water resources (Nurse, R., & Suarez, 2998); (Carpenter, Stubbs, & Overmars, 2002); (White, et al., 2007). Fresh water in Micronesian atoll islands communities is used only for cooking, drinking, rinsing, laundry, and dishwashing, with ocean water and groundwater use for bathing (Stephenson, 1984); (MacCracken, Jenson, Heitz, Rubinstein, & Mylroie, 2007); (Bailey R. T., Jenson, Rubinstein, & Olsen, 2008). Hence, although not measured directly, daily per capita usage likely is within the minimum suggested range of 20 to 50 L/day suggested by the United Nations (UN) World Water Assessment Program (WWAP) to fulfill basic needs for drinking, cooking, and cleaning. Fresh water sources for atoll islands within the FSM are representative of small islands throughout the Pacific and Indian Oceans, and include collected rainwater and groundwater (White & Falkland, 2010), with the high permeability of atoll island soil precluding the development of streams or surface water reservoirs.

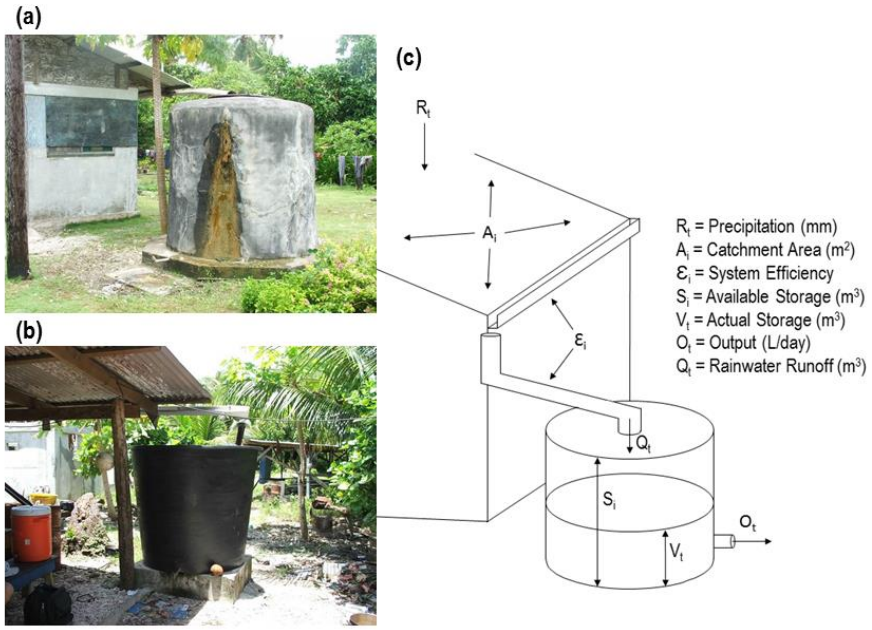

Figure 14. Examples of Currently Used Household RWCS in the Federated States of Micronesia. (a) Shows a RWCS on Ulithi Atoll that employs a ferro-concrete tank in a state of minor disrepair; (b) shows a RWCS on Ulithi Atoll that employs a fiberglass tank; and (c) is a RWCS schematic detailing the various parts of a functioning RWCS, including the roof catchment area, water transmission system, and storage tank.

Due to the small land surface area, low elevation, and thin soil zone of atoll islands, the fresh groundwater lens is naturally fragile in terms of fresh water quantity and quality (White, et al., 2007); (White & Falkland, 2010), and hence island residents rely principally on rainwater collected from RWCS for fresh water needs. RWCS in the FSM (see Figure 14a and Figure 14b for examples) are composed primarily of galvanized corrugated metal for the roof, and reinforced concrete, steel, or fiberglass for the storage tank, with screens and wire meshes often

used over the tank inlet to filter out large particles or debris from runoff. The guttering systems used to collect and transport flow to a cistern are primarily made of galvanized metal, but can be fashioned from plastic pipe and bamboo depending on the resources available (Dillaha & Zolan, 1985). RWCS are uniquely designed for multiple structures within a community, including individual house units, schools, and community buildings. Water stored in larger systems, such as those attached to schools or community buildings, often can be shared by multiple families or distributed to the community. RWCS in Micronesia have been reported to provide relatively high-quality water in recent decades (Dillaha & Zolan, 1985); (Detay, Alessandrello, Come, & Groom, 1989), although using rusted roofs and metal tanks reduces water quality (Detay, Alessandrello, Come, & Groom, 1989) and can impart a metallic taste to water, as reported by island residents (Taboroši & Collazo, 2011).

During normal climatic periods, RWCS on atoll islands within the FSM are able to provide adequate water supply to the community. During periods of drought, however, such as during the first months of 1998 (see Figure 13), collected rainwater volumes can quickly become depleted. Fresh groundwater volumes also were depleted during the 1998 drought for the majority of atoll islands, with an estimated 99 out of 105 islands of the FSM having experienced complete groundwater depletion during the peak of the 1998 drought (Bailey, Jenson, & Taborosi, 2013). For example, Figure 13 shows the time series of groundwater lens thickness for typical atoll islands (400-m width) for both the western and eastern FSM regions, as estimated by Bailey et al. (2013), with thickness depleting to zero during the 1998 drought. With both rainwater and groundwater depleted, many communities on atoll islands in the FSM required water to be brought by ship from neighboring high islands such as Pohnpei until normal rainfall patterns resumed to allow for adequate storage by the RWCS (Taboroši & Collazo, 2011); (Taboroši & Martin, 2011).

Nikahlap Island, Pakein Atoll, Pohnpei State

Pakein Atoll is a small coral atoll in the eastern part of the Caroline Islands, located approximately 30 km northeast of within the state of Pohnpei (see Figure 12), and consists of 16 small islets with a total land area of 1.2 km^2. The lagoon has a spatial area of 11.2 km^2 and a maximum depth of 55 m. The vast majority of the residents live on Nikahlap Island, located on the western side of Pakein Atoll, with 90 people and 12 households. Similar to other atoll island communities in the FSM, residents live a subsistence lifestyle, engaging in taro farming, agroforestry, copra harvesting, and fishing (Taboroši & Martin, 2011). There are no technology-related demands for water, and water for drinking, cooking, washing dishes, and washing clothes is obtained from RWCS. A recent survey of the water usage patterns within the Nikahlap island community (Taboroši & Martin, 2011) documented the community's RWCS infrastructure, with details of the 8 RWCS including existing and unused storage capacity (m^3), cistern material, and existing and potential guttered roof area (m^2) presented in Table 4. Though not described in Table 4, four concrete tanks and one fiberglass tank with a total available volume of approximately 30 m^3 are currently unused.

Table 4. Detailed description of existing rain catchment system infrastructure on Nikahlap Island, Pakein Atoll, Pohnpei State, Federated States of Micronesia. Values acquired from the case study by Taboroši and Martin (2011).

RWCS Number	Use	Existing Storage *S* m^3	Unused Storage *S* m^3	Cistern Material	Catchment Area *A* m^2	Potential Area *A* m^2
1	daily	7.19	13.25	PVC	16	192
2	sporadic	2.65	5.68	Fiberglass	4	24
3	daily	5.68	3.79	Concrete	20	40
4	daily	0.95	--	Stainless Steel	12	24
5	daily	2.65	--	Fiberglass	17.5	35
6	daily	5.68	--	Concrete	10	30
7	daily	0.21	--	PVC	20	40
8	daily	0.21	5.68	PVC	3	3

Rainfall is approximately 4.5 m/yr, with a slight reduction in monthly rainfall occurring from January to March, and hence under normal climatic patterns the community's collection of RWCS is able to sustain adequate water supply. However, during times of major drought, stored rainwater supply can become depleted. For example, during the 1998 drought, fresh water supplies from RWCS were depleted completely, with water sent by the FSM Government via a ship (Taboroši & Martin, 2011) to relieve the water stress in the community. Fresh water was pumped, via a long PVC pipe, from the ship to the island to fill the RWCS tanks. Due to the low population, subsistence lifestyle, water usage patterns, reliance on RWCS to supply fresh water needs, and the constant threat of drought, the community on Nikahlap Island is highly representative of the majority of atoll island communities throughout the FSM.

Methods

RWCS Storage Volume Calculations

Time-dependent volume of stored rainwater by a RWCS is calculated in this study using the water balance algorithm of Jenkins et al. (1978), accounting for depth of rainfall, guttered roof catchment area, available storage volume, daily water use from the storage tank, and the system efficiency, with the latter defined as the percentage of potential total rainwater volume that is retained during transport from the roof to the storage tank. When implemented at the community scale, with multiple individual RWCS employed for households and community buildings, the water balance algorithm is given as follows to calculate the end-of-time step volume of stored rainwater for a succession of time steps:

$$V_t = \sum_{i=1}^{n} \max\left\{V_{t_i-1} + \min\left[\left(A_i P_t \varepsilon_i\right), \left(S_i - V_{t_i-1}\right)\right] - O_{t_i}, 0\right\} \qquad (1)$$

where V_t is the volume of rainwater stored at the end of the current time step t [L^3]; n is the number of individual RWCS for the island community; V_{t_i-1} is the volume of rainwater for the i^{th} RWCS at the previous time step [L^3]; A_i is the size of the rooftop catchment area for the i^{th} RWCS [L^2], corresponding to the portion of the roof that is guttered; P_t is the depth of precipitation at time step t [L], and is assumed to be uniform for the community; ε_i is the system efficiency for the i^{th} RWCS, defined as the percentage of rain caught by the roof that reaches the storage tank, included to represent the water that is lost during transmission from the roof to the tank; S_i is the capacity of the storage tank for the i^{th} RWCS [L^3]; and O_{t_i} is the total water demand of the i^{th} RWCS for time step t [L^3]. System parameters are as shown in the physical context of a typical RWCS in Figure 14C.

The volume of rainwater stored at the end of the current time step is calculated via Equation (1) by adding the volume of collected runoff $Q_{t_i} = A_i P_t$, multiplied by the system efficiency ε, and subtracting the daily output usage. However, stored rainwater volumes V_{t_i} cannot exceed the volume S_i of the storage tank, and hence the actual volume added during a given time step may be less than the potential volume of $A_i P_t \varepsilon_i$, depending on the difference between S_i and V_{t_i} for the time step. Because the minimum value between $A_i P_t \varepsilon_i$ and $\left(S_i - V_{t_i-1}\right)$ is selected before the water demand O_{t_i} is subtracted, the algorithm in Equation (1) represents the YAS algorithm, and hence a conservative approach in terms of end-of-day stored volumes. This distinction becomes particularly important when tanks are frequently at or near full capacity, which can occur in regions of high rainfall rates such as the FSM. Furthermore, total time step output O_{t_i} cannot be more than the available stored volume.

Model Application to FSM Atoll Island Communities

The water balance algorithm of Equation (1) is applied using a daily time step to the community on Nikahlap Island, Pakein Atoll in the state of Pohnpei, FSM, and to a generic island in the western FSM region containing identical RWCS infrastructure as Nikahlap. Both applications are for the 1997-1999 period. Daily time steps are used due to the importance of monitoring day-to-day storage volume fluctuations, since the community relies solely on rainwater for domestic water needs. The individual RWCS (n = 8) that comprise the community system (Table 1) include observed guttered rooftop catchment area A and storage capacity S. Average efficiency ε (ranging from 0.5 to 0.9) is assigned according to observations of the gutter system in Taboroši and Martin (2011), and daily water usage O depends on the number of residents using the RWCS and the per capita daily usage. Daily precipitation depth P_t is shown in Figure 13 for the eastern (Pakein Atoll) and western FSM regions, with the eastern rainfall patterns applied to Nikahlap and the western rainfall patterns applied to the generic western island, hence encompassing the range of climatic conditions expected in the FSM. Although only three years of historical rainfall data are used, the time period corresponds to one of the strongest drought events recorded in the FSM (Lander & Khosrowpanah, 2004), hence providing a critical test for the system of RWCS and a means to identify optimal RWCS infrastructure for future sustainability.

Analysis of the Nikahlap community RWCS and the western FSM island RWCS consists of (i) a baseline assessment to indicate the likely daily stored rainwater volumes during the 1997-1999 period, (ii) a sensitivity analysis to determine the influence of each system parameter on RWCS performance, and (iii) an optimization analysis to determine if sufficient water supply can potentially be maintained for atoll island RWCS during drought periods in the FSM using existing material (i.e., existing unused roof area and storage tanks). For the baseline assessment, the water balance algorithm results are tested against observed RWCS performance on Nikahlap, i.e., depletion of the RWCS tanks occurs during the months of the 1998 drought period (Taboroši & Martin, 2011).

Table 5. Baseline Conditions for Nikahlap Island and a generic western FSM island. Storage capacity and catchment area for each RWCS (see Table 1) are held constant to reflect the currently-used RWCS infrastructure. The number of consecutive days with insufficient water storage (NCDI) and the total volume collected during 1997-1999 (m^3) are used as system metrics for each scenario. Wasted water (m^3), i.e., rainwater volume that cannot be collected due to the limited storage capacity of the RWC, also is reported for each scenario.

Scenario	Efficiency	Daily Per Capita Use (L/day)	# Days Insufficient Water	*NCDI*	End of Day Volume (m^3)	Wasted Water (m^3)
Nikahlap (Eastern FSM)						
1	0.5	15	832	157	1126	86
2	0.6	15	765	157	1494	113
3	0.7	15	498	126	2712	207
4	0.8	15	465	126	3250	185
5	0.9	15	412	126	3807	192
6	0.5	30	1081	591	163	92
7	0.6	30	1075	398	244	85
8	0.7	30	1063	298	317	123
9	0.8	30	1024	224	602	97
10	0.9	30	991	190	789	147
11	0.5	45	1091	984	62	34
12	0.6	45	1088	983	140	44
13	0.7	45	1088	983	137	61
14	0.8	45	1089	983	177	128
15	0.9	45	1083	983	239	129
Western FSM						
1	0.5	15	987	210	499	60
2	0.6	15	1023	211	346	68
3	0.7	15	920	166	682	62
4	0.8	15	747	165	1357	95
5	0.9	15	596	165	2274	115
6	0.5	30	1086	875	151	29
7	0.6	30	1088	875	141	40
8	0.7	30	1077	606	228	50
9	0.8	30	1075	410	235	59
10	0.9	30	1072	329	274	69
11	0.5	45	1093	1092	27	35
12	0.6	45	1093	1092	41	36
13	0.7	45	1092	877	69	46
14	0.8	45	1092	877	64	62
15	0.9	45	1091	877	113	64

In recognition that values of ε and O are uncertain, with O dependent on the daily per capita usage during 1997-1999, and assuming that population (90 persons) and individual RWCS dimensions (A and S; see Table 4) are known and constant during 1997-1999, 15 scenarios using a range of values for ε (0.5 to 0.9) and daily per capita usage rate (15 to 45 L/day) are used in the baseline assessment, as shown in Table 5. In an attempt to account for uncertainty in system efficiency, the value of ε assigned to each of the 8 individual RWCS is determined using random number generation to produce values within a standard deviation of 0.1 from the mean value shown in Table 5. The range of daily per capita usage is slightly lower than the range suggested by the UN WWAP to indicate the minimalist water usage patterns observed on FSM atoll islands. For the sensitivity analysis, each RWCS parameter (A, S, ε and daily per capita water usage) is treated as uncertain, with each value modified in 12.5% increments above and below the median value while holding constant all other parameter values. Daily per capita usage was varied from 10 to 50 L/day, ε varied from 0.5 to 0.9, total community A from 244 m^2 to 488 m^2, and total community S from 30.9 to 61.8 m^3, with A and S based on potential dimensions of each of the 8 existing RWCS of Nikahlap (see Table 4). For the optimization analysis, total potential

community A (488 m^2) and S (61.8 m^3) are used, with ε and daily per capita usage treated as uncertain parameters, similar to the baseline assessment.

For all analysis scenarios, RWCS performance as indicated by the model is measured using three metrics: total cumulative end-of-day stored volumes, calculated by summing the end-of-day volumes simulated by Equation (1); the number of days during the 3-year period with insufficient water, and the number of consecutive days with insufficient water (*NCDI*), with insufficient water defined as water volumes below the required daily per capita water usage volume for the island population. For the sensitivity analysis, *NCDI* is used as the metric for analysis of parameter influence. The volume of rainwater "wasted" or spilled by the RWCS, i.e., the difference between the potential collected rainwater volume on a given day and that limited by the storage tank capacity is also assessed for each scenario. For each scenario, it is assumed that the storage tanks initially contained a volume of collected rainwater equal to half of their overall storage capacity. For the sensitivity analysis, the value of ε for each RWCS was assigned the mean value rather than modifying each value about the standard deviation, as done in the baseline and optimization analyses.

Results and Discussion

Baseline Conditions: 1997-1999

Table 5 shows the results of the baseline analysis for both Nikahlap and for the generic western FSM island. For Nikahlap, *NCDI* ranges from 126 to 984 for the 15 scenarios, and for the western island, the number ranges from 165 to 1092. It should be noted that for many of these days, water storage is still available, but at a lower volume than the 20 L/day per capita rate suggested by the UN WWAP. Total end-of-day stored volume of rainwater ranges from 62 m^3 to 3807 m^3 for Nikahlap and from 27 m^3 to 2274 m^3 for the western FSM island. The low volumes correspond to Scenario 11, which has the highest per capita daily usage rate and the lowest value of ε, whereas the high volumes correspond to Scenario 5, with the lowest per capita daily usage rate and the highest value of ε.

An expected trend is the increase in *NCDI* and the decrease in total stored water as the daily per capita usage rate increases. For example, for Scenarios 5, 10, and 15 for Nikahlap, which apply a systematic increase of 15 L/day in the daily per capita usage rate at a constant system efficiency of 0.9, *NCDI* is 126, 190, and 983 days, respectively, and the total stored water is 192 m^3, 147 m^3, and 129 m^3, respectively. Also, when daily per capita usage rates are held constant and ε is increased, *NCDI* decreases and the end-of-day total volume storage increases. It is interesting to note, however, that upon reaching 70% system efficiency for the scenarios using a daily per capita usage rate of 15 L/day (Scenarios 3, 4, and 5), *NCDI* does not decrease below 126 days for Nikahlap and 165 days for the western island, indicating that increases in roof catchment area and storage tank capacity are required to provide additional stored volumes. This result is further emphasized by the calculated volumes of wasted water (last column of Table 5), which provides an indication of the amount of additional water that could be collected if roof catchment area and storage tank size were adequate to store the total depth of daily rainfall.

The ability for the RWCS of Nikahlap and of the western island to provide water storage to the island community is further demonstrated in Figure 15, which shows the time series of simulated daily end-of-day stored water volumes for selected scenarios from the baseline assessment. The time series for the "best-case" storage conditions during 1997-1999 (Scenario

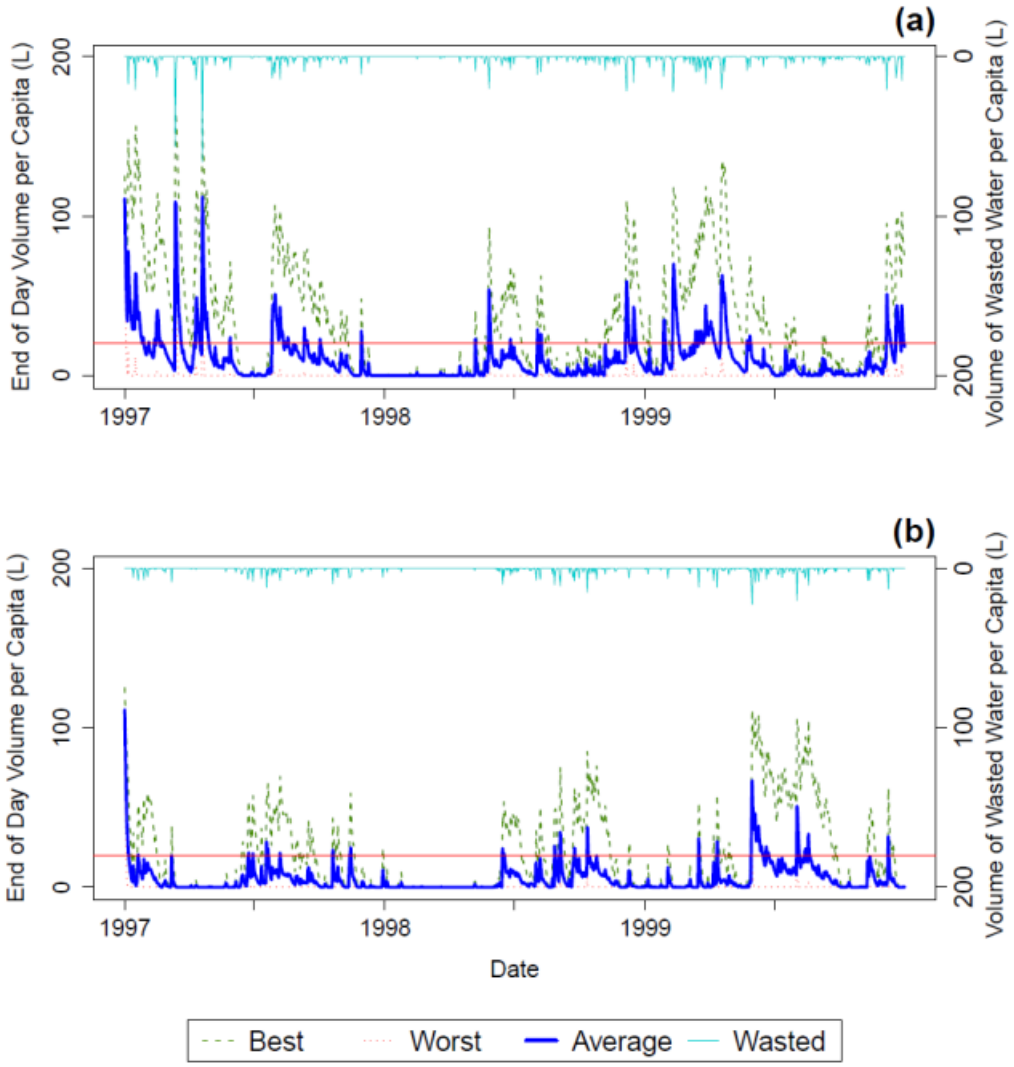

Figure 15. Time Series of Simulated Daily Total Volume of Stored Water for (a) Nikahlap Island and (b) for a Generic Western Federated States of Micronesia Island, under Baseline Conditions. The blue line indicates the average of all baseline scenarios, with the "best" (Scenario 5) and "worst" (Scenario 11) case scenarios also shown to provide a range of uncertainty in simulated values. The volume of wasted water is inversely plotted to show the relationship between the periods with a large volume of stored rainwater and the associated volume of wasted water, indicating that storage tank capacity was surpassed and potential captured water was lost. The red line on the figure indicates the United Nations water use standard of 20 l/day per capita.

5), the "worst-case" condition (Scenario 11), and the average of the end-of-day stored water volumes for Scenario 1-15 are shown, providing an indication of the mean and uncertainty in the results. The minimum UN daily per capita usage guideline of 20 L/day also is shown, to indicate the time periods during which insufficient water supply is stored. Due to the higher rate of rainfall in the eastern FSM region, daily storage values for Nikahlap are on average higher than for the western island. Both the eastern (Nikahlap) and western island RWCS show similar patterns in the end-of-day volume of stored water, with rapid increases occurring on days of high rainfall and gradual depletion of stored volumes during periods of low rainfall. In general, results agree with the experience of the island communities during the 1998 drought, i.e., that the

catchment systems did not collect and store sufficient volumes of water to meet domestic needs (Taboroši and Martin, 2011).

Besides providing total volumes for the community, it is also of interest to analyze the performance of each individual RWCS during 1997-1999 to identify potential changes for system enhancement. Figure 16 shows a time series of end-of-day storage volume for six of the 8 individual RWCS for Scenario 8 (median RWCS parameter values $\varepsilon = 0.7$ and daily per capita usage rate of 30 L/day). Results for RWCS 7 and 8 are omitted due to negligible storage tank size ($S = 0.21$ m^3; see Table 4) and resulting negligible collected volumes as compared to the other six RWCS. As with the total volumes shown in Figure 15, the RWCS in the eastern region have more stored water due to higher rates of rainfall. Overall, RWCS 1, 2, and 5 store the largest volumes of water due to their relatively large storage capacities and associated catchment areas, while the storage tank of RWCS 4 often is filled to its capacity of 0.95 m^3, indicating that the end-of-day stored water volume is limited by the size of the storage tank rather than the depth of rainfall, system efficiency ε, or roof catchment area. This can be seen for both Nikahlap

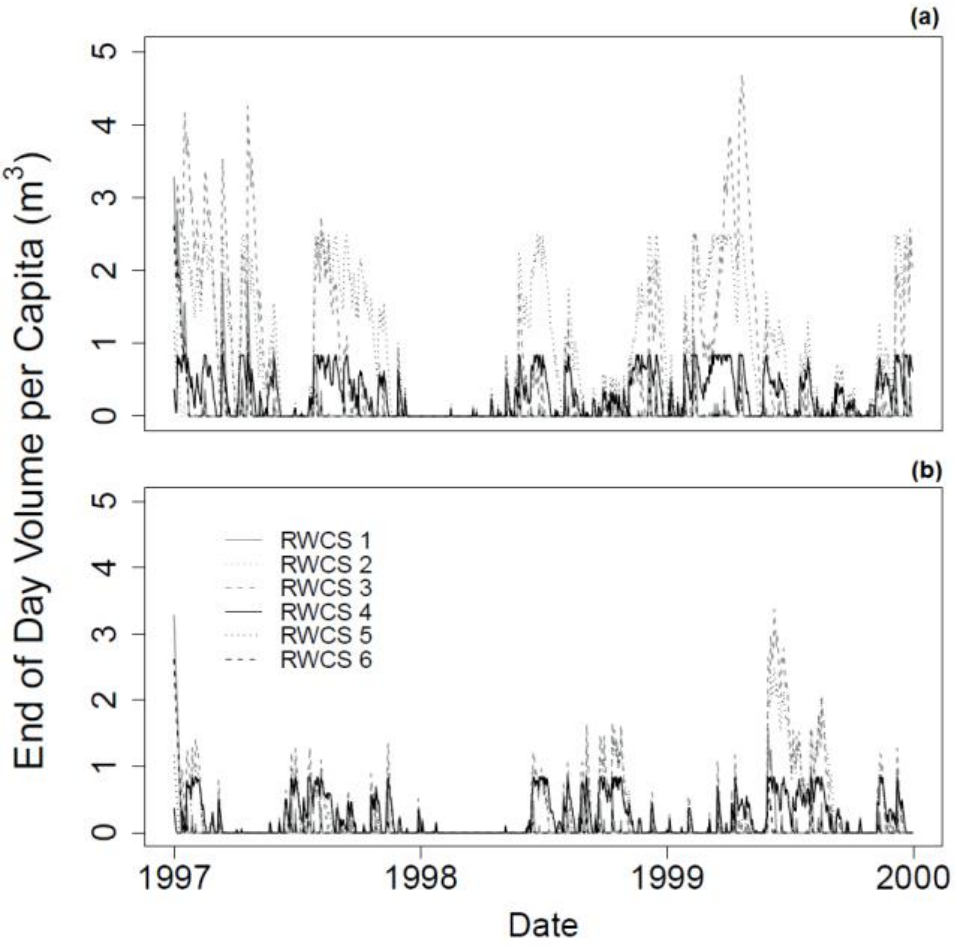

Figure 16. Time Series of Simulated Daily Volume of Stored Water in Six Different Rainwater Catchment System (RWCS) Cisterns (see Table 1) for (a) Nikahlap Island and (b) a Generic Island in the Western Federated States of Micronesia, under Baseline Conditions. Catchment systems 7 and 8 are excluded due to eligible daily water volumes compared to RW CS 1-6. Results correspond to median RWCS parameter values, i.e., system efficiency is equal to 70% and daily per capita use is 30 l/day (see Table 5).

(Figure 16a) and for the western island (Figure 16b). The potential for RWCS enhancement by implementing unused storage volume is explored in the next two sections.

Sensitivity Analysis

Table 6 shows the results of the sensitivity analysis for Nikahlap and for the western FSM atoll island.

Table 6. Sensitivity analysis of the RWCS for Nikahlap Island and a generic western FSM island. The shaded values indicate the perturbed parameter for each scenario, with all other parameters held constant at their median value. As with Baseline conditions reported in Table 5, system metrics include the consecutive days of insufficient water and the total volume collected during 1997-1999

Scenario	Efficiency	Daily Per Capita Use (L/day)	Storage Capacity (m^3)	Catchment Area (m^2)	# Days Insufficient Water	*NCDI*	End of Day Volume (m^3)	Wasted Water (m^3)
Nikahlap (Eastern FSM)								
1	0.7	30	46.3	244	164	115	1241	366
2	0.7	30	46.3	305	136	109	1589	684
3	0.7	30	46.3	366	120	44	1962	1055
4	0.7	30	46.3	427	115	43	2280	1484
5	0.7	30	46.3	488	104	43	2482	1943
6	0.7	30	30.9	366	157	52	1202	1157
7	0.7	30	39	366	128	48	1581	1099
8	0.7	30	46.3	366	120	44	1962	1055
9	0.7	30	54.1	366	115	38	2349	1026
10	0.7	30	61.8	366	110	34	2736	1001
11	0.5	30	46.3	366	157	113	1350	450
12	0.6	30	46.3	366	133	108	1641	734
13	0.7	30	46.3	366	120	44	1962	1055
14	0.8	30	46.3	366	116	43	2247	1421
15	0.9	30	46.3	366	107	43	2430	1809
16	0.7	10	46.3	366	0	0	3624	2284
17	0.7	20	46.3	366	81	30	2823	1553
18	0.7	30	46.3	366	120	44	1962	1055
19	0.7	40	46.3	366	185	118	1361	764
20	0.7	50	46.3	366	375	126	926	552
Western FSM								
1	0.7	30	46.3	244	174	121	1238	301
2	0.7	30	46.3	305	143	99	1474	503
3	0.7	30	46.3	366	119	61	1696	734
4	0.7	30	46.3	427	97	56	1925	998
5	0.7	30	46.3	488	84	53	2127	1285
6	0.7	30	30.9	366	165	80	1088	805
7	0.7	30	38.6	366	140	68	1394	766
8	0.7	30	46.3	366	119	61	1696	734
9	0.7	30	54.1	366	98	54	1996	710
10	0.7	30	61.8	366	79	48	2303	692
11	0.5	30	46.3	366	162	113	1312	357
12	0.6	30	46.3	366	138	97	1505	533
13	0.7	30	46.3	366	119	61	1696	734
14	0.8	30	46.3	366	104	57	1897	958
15	0.9	30	46.3	366	85	53	2072	1201
16	0.7	10	46.3	366	0	0	3477	1491
17	0.7	20	46.3	366	52	26	2407	999
18	0.7	30	46.3	366	119	61	1696	734
19	0.7	40	46.3	366	183	122	1321	573
20	0.7	50	46.3	366	306	153	1036	449

The shaded values indicate the perturbed parameter for each scenario, with all other parameters held constant at their median value. For both Nikahlap and the western island, the parameter with the strongest influence on total end-of-day stored volume is daily per capita usage rate. For Nikahlap, a decrease of 75% (3624 m^3 to 926 m^3) in stored volume occurs when the rate is

increased from 10 L/day to 50 L/day (Scenarios 16-20), compared with an increase of 50% (1241 m^3 to 2482 m^3), 56% (1202 m^3 to 2736 m^3), and 44% (1351 m^3 to 2430 m^3) when *A*, *S*, and ε increase from the minimum to maximum parameter value. Similar levels of decrease and increase occur for *NCDI* as well. By increasing *A*, *S*, and ε, *NCDI* decreases to 43 days, 34 days, and 43 days, respectively. If only 10 L/day is used and *A*, *S*, and ε are kept at median values (Scenario 16), no days during 1997-1999 have an insufficient volume of stored water. Thus, although not ideal, island communities can ration their water to ensure their supply is not depleted during periods of extreme water stress.

The relative influence of each parameter on *NCDI* is demonstrated in Figure 17, which shows the change in *NCDI* for both Nikahlap (Figure 17A) and the western island (Figure 17b) given a factor increase or decrease in each parameter value. As seen also in Table 6, an increase in daily per capita usage rate causes an increase in *NCDI*, whereas an increase in *A*, *S*, and ε yield a decrease in *NCDI* and therefore more favorable storage conditions. As evidenced by the steeper slope, the daily per capita usage rate has the strongest influence on *NCDI*, followed by *A* and ε, although the effect of the latter two is greatly reduced as their values increase from the median value. The storage capacity *S* has a relatively small influence on the system regardless of whether it is increased or decreased from the median value, suggesting that the other RWCS parameters should be targeted to provide optimal storage conditions, which is explored in the following section.

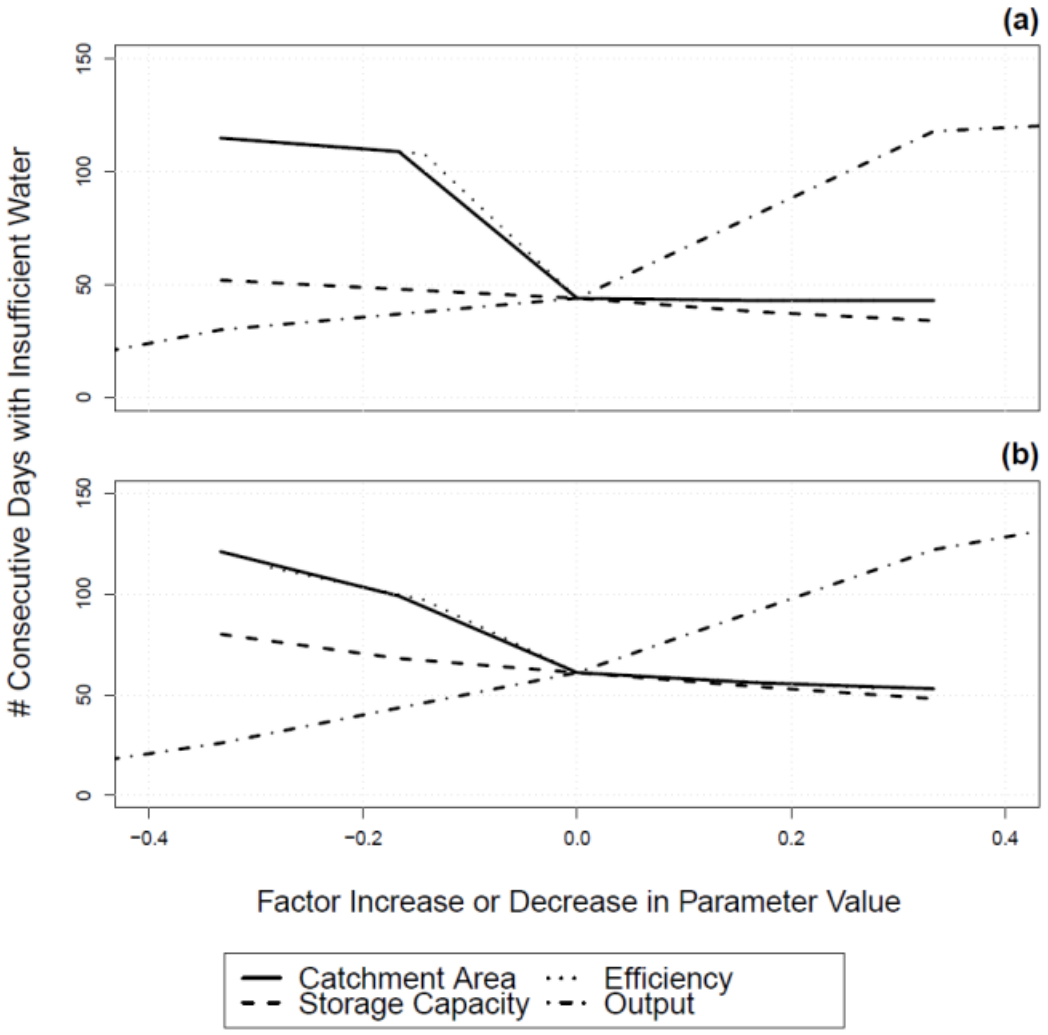

Figure 17. Sensitivity Analysis of the Rainwater Catchment Systems (RWCS) for (a) Nikahlap Island and (b) a Generic Western FSM Island, Showing the Change in the Number of Consecutive Days with Insufficient Water Supply Given a Factor Increase or Decrease in the Value of Each RWCS Parameter. The slope of the line designates its influence on the system output, with a steeper line indicating a higher significance level.

3.4.3 Optimization Analysis

Table 7 shows optimization results for both regions, using the available storage tank capacity and roof catchment area for the 8 RWCS (see Table 4) across the ranges of system efficiency (0.5 to 0.9) and daily per capita usage rate (15 L/day to 45 L/day). For Nikahlap, *NCDI* reaches zero for all scenarios that have a usage rate of 15 L/day except for Scenario 1, which has a mean RWCS efficiency of 50%. If usage rate is increased to 30 L/day, *NCDI* ranges from 81 to 100 – the value of *NCDI* does not decrease according to the increase in system efficiency because of the randomized values of efficiency used for each RWCS, and if the rate is increased to 45 L/day, *NCDI* ranges from 114 to 162. In the western FSM, where precipitation values on average are lower, the lowest value of *NCDI* achieved is 8 days, for the scenario of maximum system efficiency (90%) and minimum daily per capita demand (15 L/day) (Scenario 5). For usage rates of 30 L/day and 45 L/day, the lowest value of *NCDI* achieved, i.e. with a system efficiency of 90%, is 113 days and 244 days, respectively.

Results are further demonstrated using a time series of total end-of-day storage volumes, shown in Figure 18. Similar to the baseline assessment (Figure 15), the best-case condition (Scenario 5), worst-case condition (Scenario 11), and average of all scenarios are shown, providing the mean and range of uncertainty in the simulations. Large end-of-day volumes of water are able to be stored for both Nikahlap and the western FSM island, with per capita water storage decreasing below the minimum UN standard only during the peak of the 1998 drought for the average of the scenarios, and no days of insufficient water occurring for the best-case condition for Nikahlap.

Table 7. Optimization results of the RWCS for the Nikahlap Island RWCS and a generic western FSM RWCS, using the optimal (i.e., potential) storage capacity (61.8 m^3) and roof catchment area (488 m^2), as indicated in Table 1. These values represent the maximum amount both could assume given only minor adjustments (i.e., adding gutter length, pipe fittings, etc.) to the existing RWCS. System efficiency was adjusted in equal increments between 0.5 and 0.9 and the daily per capita water demand was fluctuated between 15 and 45 L/day.

Scenario	Efficiency	Output	# Days Insufficient Water	*NCDI*	End of Day Volume (m^3)	Wasted Water (m^3)
Nikahlap (Eastern FSM)						
1	0.5	15	12	11	4358	1709
2	0.6	15	0	0	4515	2360
3	0.7	15	0	0	4732	2842
4	0.8	15	0	0	4778	3402
5	0.9	15	0	0	4780	3489
6	0.5	30	105	99	2863	1251
7	0.6	30	106	100	2613	1228
8	0.7	30	85	81	3525	2159
9	0.8	30	87	83	3629	2191
10	0.9	30	81	77	3846	2593
11	0.5	45	164	158	1582	704
12	0.6	45	168	162	2058	723
13	0.7	45	135	133	2054	1205
14	0.8	45	121	116	2656	1720
15	0.9	45	120	114	2660	1851
Western FSM						
16	0.5	15	49	48	3892	995
17	0.6	15	45	44	3921	1142
18	0.7	15	28	26	4312	1818
19	0.8	15	23	22	4460	2065
20	0.9	15	9	8	4506	2359
21	0.5	30	170	165	2128	547
22	0.6	30	147	142	2439	868
23	0.7	30	146	141	2677	991
24	0.8	30	140	136	2865	1165
25	0.9	30	120	113	3078	1480
26	0.5	45	480	454	813	183
27	0.6	45	402	384	1117	290
28	0.7	45	324	310	1451	504
29	0.8	45	281	265	1882	743
30	0.9	45	257	244	1823	837

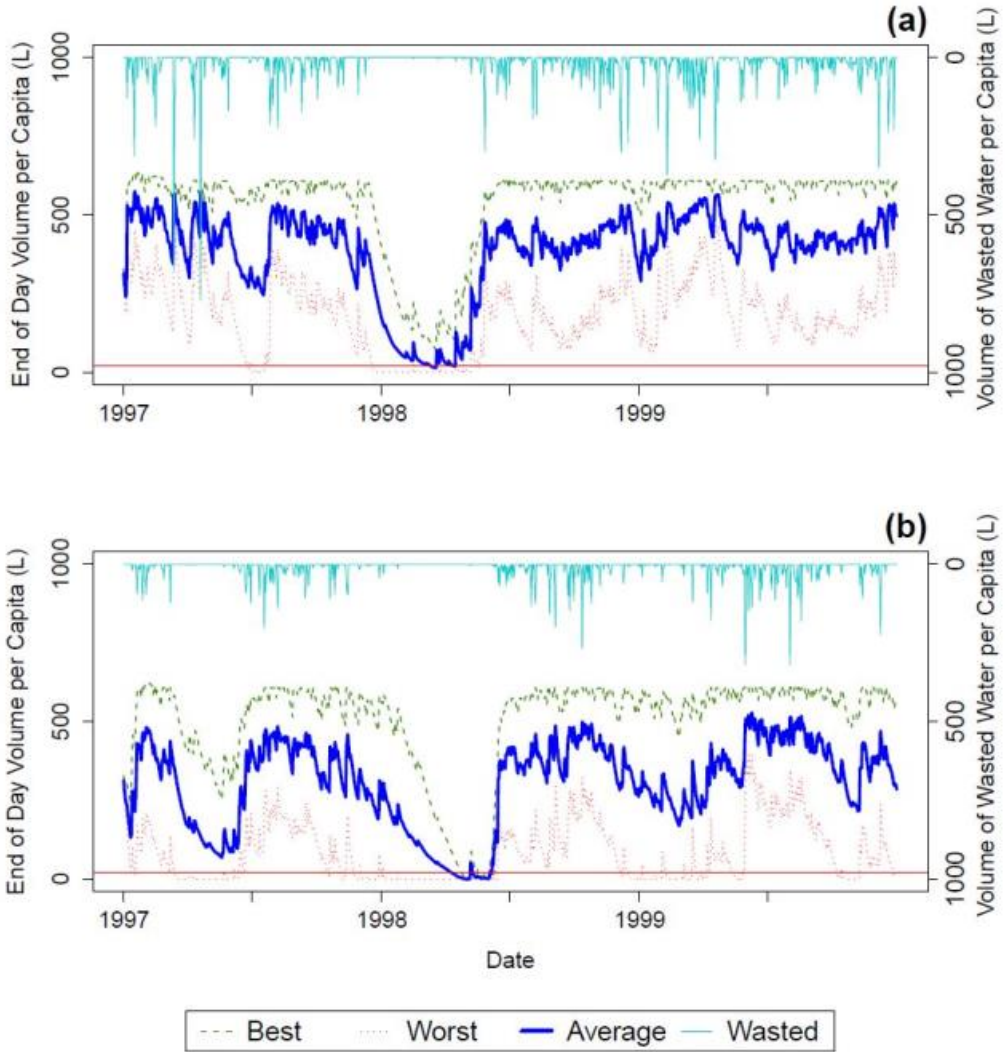

Figure 18. Time Series of the Simulated Daily Total Volume of Water Stored in All Rainwater Catchment Systems for (a) Nikahlap Island and for (b) a Generic Western FSM Island, under Optimized Conditions (i.e., using potential roof catchment area and existing storage tank volumes). The volume of wasted water is also plotted to highlight the inverse relationship between it and the volume of water stored. The red line represents the United Nations water use standard of 20 l/day per capita.

Overall, enhanced storage by the community system of RWCS can be seen through a comparison with the time series results for the baseline assessment (Figure 15). Due to full use of potential roof catchment area and storage tank capacity, the total end-of-day stored rainwater plateaus during the latter months of 1997 and throughout much of 1999, indicating that storage tanks are full. From the sensitivity analysis results, the enhanced system behavior is due likely to an increased roof catchment area rather than increased storage capacity. In general, results demonstrate that, if available roof catchment area and unused storage tanks are integrated into the 8 RWCS, adequate daily volumes of rainwater likely could be achieved even during the intense drought of 1998 if rationing (15 L/day) is adopted by the island community.

RWCS Sustainability for Atoll Islands

As reported by Dillaha and Zolan (1985), Taboroši and Martin (2011), and Taboroši and Collazo (2011), RWCS are often under-utilized in the FSM due to unused roof catchment area,

and abandoned and unused tanks. Taboroši and Martin (2011) noted that most of the unused storage tanks are made of concrete that are in disrepair and often lacking a cover. This is a relatively inexpensive repair that can greatly increase the storage potential of the collective RWCS. Furthermore, catchment area can be enhanced by extending gutters and using both sides of the roof. As demonstrated in this study through the optimization analysis, including the unused infrastructure components likely could allow water supply to be sustained during intense drought events with the adoption of slight rationing (daily per capita usage rate = 15 L/day).

Aside from sustaining sufficient water supply, maintaining acceptable water quality also is of primary concern for RWCS (Dillaha & Zolan, 1985); (Lye, 2009); (Ahmed, Gardner, & Toze, 2011). Maintenance procedures include preventative measures, cleaning operations, and water treatment. A screen or mesh can be placed over the intake pipe to the storage tanks to prevent debris or animal feces from entering the system and causing water contamination, and a first-flush diverter can be used to prevent the contaminants carried by the first wave of roof and gutter runoff water during a rainfall event from entering the storage tank. Also, to eliminate direct sunlight from reaching the stored water and subsequent acceleration of microbial growth and associated water quality degradation, a tight top cover should be placed on the storage tank. Finally, to prevent disturbance of stored water and sediment re-suspension, a U-shaped inlet design can be implemented on the transporter pipe if the inlet pipe to the storage tank is placed within the storage tank to a certain distance along the depth of the tank (Han & Ki, 2010).

It is also recommended that cleaning of roof catchments, storage tanks, screens and gutters should occur following heavy storm events when flows are elevated and at the start of the dry season or wet season when flow patterns change. Treatment options include using chlorine to periodically clean the inside of the storage tanks to kill any bacteria and boiling water prior to drinking (Özdemir, et al., 2011). As suggested by Lye (2009), RWCS can be a valuable asset to provide water supply if they are properly designed and well-maintained. Periodic testing of water quality should also be performed for coliform bacteria and fecal coliform bacteria concentrations, such as the sampling performed by Dillaha and Zolan (1985) and Detay et al. (1989) in the FSM.

Conclusion

This study applied a water balance model to rooftop rainwater catchment systems (RWCS) in atoll island communities in the Federated States of Micronesia to first, assess stored water volumes during a period of drought; second, identify the RWCS parameters that govern these volumes; and third, and determine if available sufficient volumes of water could by sustained during a major drought if all potential island community infrastructure is applied to the catchment systems. The water balance model accounts for roof catchment area, storage tank size, daily per capita water demand, system efficiency, and historical daily depths of rainfall, and was applied to the series of 8 RWCS on Nikahlap Island, Pakein Atoll, Pohnpei State in the eastern FSM region for the 1997-1999 time period. A similar assessment was performed using historical rainfall depths from the western FSM region, to provide a general analysis for the western FSM atoll islands.

Results, corroborated by the experience of FSM atoll island communities during the 1998 drought, indicate that water volumes become depleted shortly after the onset of the drought. For Nikahlap Island, it is estimated that adequate water volumes during the drought could have been maintained if (1) all available roof area and storage tank capacity were implemented into the individual RWCS, with these areas and capacities specified from field data (Taboroši & Martin,

2011), (2) the island residents resorted to minimal levels of rationing, i.e., 15 L/day per capita, rather than the United Nations' minimum recommended of 20 L/day, and (3) the RWCS were maintained to provide medium (60%) to high degrees (90%) of system efficiency. For the western FSM atoll islands, more rationing would be required due to the overall lower amount of rainfall received as compared to the eastern FSM region. It should be noted that this study does not account for a change in per capita daily usage (i.e., rationing) during times of drought. Additional work is required to understand and quantify rationing trends and behavior during periods of low rainfall, and to implement results into a similar RWCS water balance study.

A sensitivity analysis, which focused on the influence of RWCS parameters on the total end-of-day captured volumes of rainwater as well as the number of consecutive days of insufficient water, indicated that daily per capita water usage rate has the strongest influence, followed by roof catchment area and system efficiency. As water rationing is non-ideal in regards to public health and well-being, it is suggested that atoll island communities focus on expanding the area of roofs attributing to rainfall catchment and providing regularly-scheduled maintenance on RWCS gutter and pipe systems to maximize system efficiency. Overall, study results can provide atoll island water resource managers and government officials with valuable data for consideration in water security measures.

DEVELOPMENT OF RAINWATER CATCHMENT SYSTEM DESIGN CURVES USING SIMULATED FUTURE CLIMATE DATA

Introduction

Rainwater Catchment Systems around the World

Rainwater harvesting is the practice of capturing storm runoff using a catchment area, usually a rooftop, and storing it for later use. Typical systems consist of a guttered catchment area, a conveyance system to deliver captured rainwater from the catchment area, and a storage cistern designed to store rainwater for later use. Rainwater catchment systems (RWCS) are used around the world to supplement water supply in regions with insufficient groundwater or surface water sources, or in areas with high water demand. Wide-scale system installation has been hindered by a lack of experience and the absence of successful demonstrative sites. Catchment system suppliers typically use a 'rule-of-thumb' approach to system design, resulting in unrealistic payback periods or lack of accuracy and detail in system size (Roebuck & Ashley, 2006); (Ward, Memon, & Butler, 2010).

Catchment systems are used intermittently around the United States, with regional restrictions placed upon their installation in areas with rigid water rights laws. In Raleigh, North Carolina, RWCS were installed by a large portion of the population in response to severe drought in 2007, when restrictions were placed on the amount of potable water that could be extracted from the public water supply (Jones & Hunt, 2010). It was found that, while the installation of standard 55 gallon barrels as storage cisterns was capable of meeting domestic water demand, the stored volume was incapable of adequately supply water for even a single irrigation event. It was reported that, while designing household-scale RWCS, the establishment of a basic recommendation for size and configuration was difficult due to the conflicting goals of reliable water supply and minimized system cost. Guo and Baetz (Guo & Baetz, 2007) found that for successful design, system performance must be simulated and evaluated over a long period.

RWCS are also being installed in Ireland to keep pace with their growing demand for water, which is one of the highest in Europe. Catchment systems have the potential to supply 94% of domestic water supply to Irish households (Li, Boyle, & Reynolds, 2010). In Bermuda RWCS are mandated for all buildings, providing the primary source of freshwater for domestic supply (Rowe, 2011). Captured rainwater supply is supplemented by groundwater and treated seawater. Typically, 80% of roofs are guttered for rainwater collection in an attempt to maximize catchment area. Communities in the south-eastern portion of England have the lowest water resource per capita in the UK, necessitating the use of RWCS.

A majority of developing countries are located in water-scarce regions characterized by erratic rainfall and high risk of drought (Helmreich & Horn, 2008). Jordan is ranked one of the world's 10 most water-stressed countries (Abdulla & Al-Shareef, 2009), wherein only 3.5% of the population currently uses captured rainwater as a primary source of drinking water, though new homes are required to install RWCS. Collected rainwater quality is a bigger concern than the design in this region, in which air pollution necessitates the use of first-flush systems and slow-sand filtration prior to consumption. Rural regions in central Namibia use rainwater captured from both rooftop and ground catchment areas to supply communities with water. Here, domestic supply averages 39 L/day per capita (Sturm, Zimmermann, Schutz, Urban, & Hartung, 2009). The use of domestic RWCS is growing in Ghana, where water supply shortages during the dry season and a lack of infrastructural facilities necessitate alternative sources of freshwater (Opare, 2012). RWCS are relatively affordable as compared to other alternatives for deriving

freshwater in water-scarce areas, such as reverse osmosis or other more advanced water quality treatments. In Namibia, the materials for an average RWCS with a ferro-concrete cistern cost just under 500 USD (Sturm, Zimmermann, Schutz, Urban, & Hartung, 2009). The low cost of RWCS installation as compared to other sources of water or water treatment technologies makes it a viable method for water shortage problems even in developing countries.

Optimal RWCS Design

Optimized RWCS design can maximize the volume of stored rainwater available during times of water scarcity by increasing system efficiency. Systems are designed to meet community needs based on the daily per capita rate of water use and the regional depth of annual rainfall. Higher levels of community demand necessitate the design of systems capable of capturing a larger volume of rainwater and storing it. The depth of rainfall to be collected is a governing parameter as well, with both the catchment area and storage cistern needing to be sized to capture and hold an expected volume of water. Improper system design can have adverse consequences. If RWCS are under-designed, the catchment area may be incapable of collecting a sufficient volume of rainwater to fill the storage cistern. Conversely, under-design of cisterns can limit the volume of rainwater stored, shortening the period over which there is available freshwater supply. Over-design of systems can have undesired effects on the quality of captured rainwater. A catchment system area designed too large for the regional rainfall depth can contribute to water quality degradation, as captured rainwater is not capable of adequately flushing the catchment area of pollutants (Evans, Coombes, & Dunstan, 2006). Storage cisterns that exceed the necessary dimensions can lead to stagnation of captured rainwater as communities are not able to use the water in pace.

In terms of system design, catchment area size and cistern storage capacity are the parameters that can be adjusted. The depth of annual rainfall cannot be changed, but the demand of the community can be altered during periods of water stress to prolong the period over which captured rainwater can be used. A commonly used tool is a system design curve, which relates the catchment area size and storage capacity of an optimized system for different levels of reliability (Ngigi, 1999). The reliability of system performance can be described in two ways: either as the total actual volume of rainwater supply as compared to water demand, or as the fraction of time during which the demand is fully met (Liaw & Chiang, 2014). On a typical design curve, a RWCS is sized by selecting either a desired catchment area or storage capacity and then determining the corresponding parameter value for a given rate of reliability.

Systems with higher reliability rates tend to require higher values of both catchment area and storage capacity, providing adequate water supply a higher percentage of the time. Liaw and Chiang (2014) developed regional RWCS design curves for Northern Taiwan using long-term historical data. All new construction is required to implement domestic RWCS to supplement public water supply. Using historical data as a case study, the simulated performance of systems designed using the design curves and the performance of actual systems showed high correlation. In Kenya, RWCS design curves are used to size systems at a 70% level of reliability (Ngigi, 1999).

Application to Micronesian Atoll Communities

Rainwater harvesting has important implications for ensuring adequate water supply for Micronesian atoll communities. Annual rainfall across Micronesia varies, but ranges from 3-6 meters per year moving west to east. These high levels of rainfall are conducive to the collection

of rainwater for domestic use. Periodic droughts occur throughout Micronesia, usually triggered by ENSO events which alter ocean temperatures. These events, though sporadic, can result in extreme drought sustained for up to several months. It is during these dry periods that freshwater supply on atoll islands can deplete, necessitating the import of water from surrounding larger islands to sustain communities if an alternate source of freshwater, such as that collecting using RWCS, is not available.

RWCS are the principle source of potable water in Micronesia (Dillaha & Zolan, 1985), used primarily as a source of water for cooking and drinking. On small atoll islands, groundwater can be brackish, and of unacceptable quality for anything aside from bathing or washing clothes. Rainwater harvesting is also practices on the larger volcanic islands where surface water sources are more plentiful due to the convenience of having a water source near the home. A large portion of RWCS in Micronesia are in disrepair, and do not capture the maximum potential volume of rainwater from precipitation events. Many of the issues with existing RWCS are related to either broken or unused storage cisterns or leaky gutter systems that result in the loss of a large portion of water collected on the roof (Taboroši & Martin, 2011). Water quality of captured rainwater is not a large concern in Micronesia. The air quality throughout the country, which if in poor condition can contribute to degraded water quality, is relatively pristine, attributed to the absence of larger manufacturing industries and the use of automobiles limited to the larger volcanic islands. Frequent rainfall events of significant depth usually prevent the collection of animal feces and plant debris on rooftops. During the dry season or intermittent drought periods, rooftops must be cleaned, however, to prevent water quality issues from arising.

Methods

To assist with optimal RWCS design in Micronesia, household-scale system design curves are created in this thesis to size systems according to varying rates of reliability, which in this case is defined as the fraction of time in which demand is fully met. An average per capita water usage rate of 30 L/d was used to simulate average system performance in Micronesia, with an assumed household population of 4. This water usage rate is above the UN recommended provision of 20 L/day per capita, making the design conservative. RWCS can be designed at the community level, wherein the combined catchment areas and storage capacities of all building equipped with systems are considered, or on a household-scale where each dwelling is considered separately. This report focuses on the design of household-scale systems to allow each system to achieve the desired reliability rate.

On a community scale, a group of systems that may be considered on average to be highly reliable may still contain systems that fall below that reliability. By creating system design curves that each individual system can use to size catchment area and storage capacity, a higher overall rate of reliability can be achieved. The use of long-term climate data is required for the development of system design curves. Downscaled CMIP5 GCM climate datasets from the period 2010-2050 were used to estimate the required size of systems under various climate change scenarios. GCMs used correspond to those statistically evaluated in Chapter 2, with the top 8 that most accurately replicated historical conditions used to represent future climate conditions. Due to the high level of dependence island communities place on RWCS performance, design curves are developed for the 90%, 95%, and 99% reliability scenarios. System design at 100% reliability is difficult to achieve without over-sizing system catchment area or storage capacity. The stochastic nature of rainfall makes it highly variable and difficult to design a statistically “optimal” system for rainwater catchment. Eastern (Pohnpei) and Western

(Yap) regions of Micronesia are considered due to the climate variability across Micronesia. Annual average rainfall in Yap State amounts to 2.5-3 meters, while in Pohnpei State annual totals amount to around 4 meters (Lander & Khosrowpanah, 2004). Because the performance and operation of RWCS are dependent on rainfall depth, separate design curves are made for both regions to capture the effect of climate variability.

Household-scale design curves are developed using the water balance algorithm developed by Jenkins et al. (1978), discussed in detail in Chapter 3. The algorithm considers the depth of rainfall, size of rooftop catchment, available storage volume, conveyance efficiency, and daily volume of water extracted from the system. When used with daily rainfall data, the volume of captured rainwater can be tracked for each day, and the number of days with volume inadequate to meet demand recorded. System reliability was determined by summing the number of days with inadequate water supply and comparing it to the total number of days in the study period; GCM datasets extended from 2010-2050. Supply was considered inadequate when the volume of captured rainwater reached zero. Systems with 90% reliability had inadequate stored volume on approximately 1500 days of the study period, those with 95% reliability approximately 750 days, and those with 99% reliability approximately 150 days. These relatively high rates of system reliability were chosen for development of design curves because of the dependence placed upon RWCS by island communities.

When the freshwater lens beneath atoll islands becomes brackish and eventually depletes during periods of drought, residents rely on captured rainwater to sustain themselves until the lens is replenished by rainfall. If the systems designed for these islands do not have a high rate of reliability, water may need to be imported at great cost from larger islands. While it is not expected that island communities will design their RWCS to be 99% reliable, the design curves provide a reference as to what dimensions they should plan for when designing to ensure adequate water supply during dry periods.

Results

Four household-scale RWCS design curves were developed for both eastern and western Micronesia, corresponding to the four representative concentration pathway (RCP) scenarios discussed in Chapter 2. Figure 19 shows the design curves for eastern (Pohnpei) Micronesia, with the darker, thicker lines representing the design curve created by averaged output from the 8 top-performing GCMs as determined by the multi-score assessment conducted in Chapter 2.

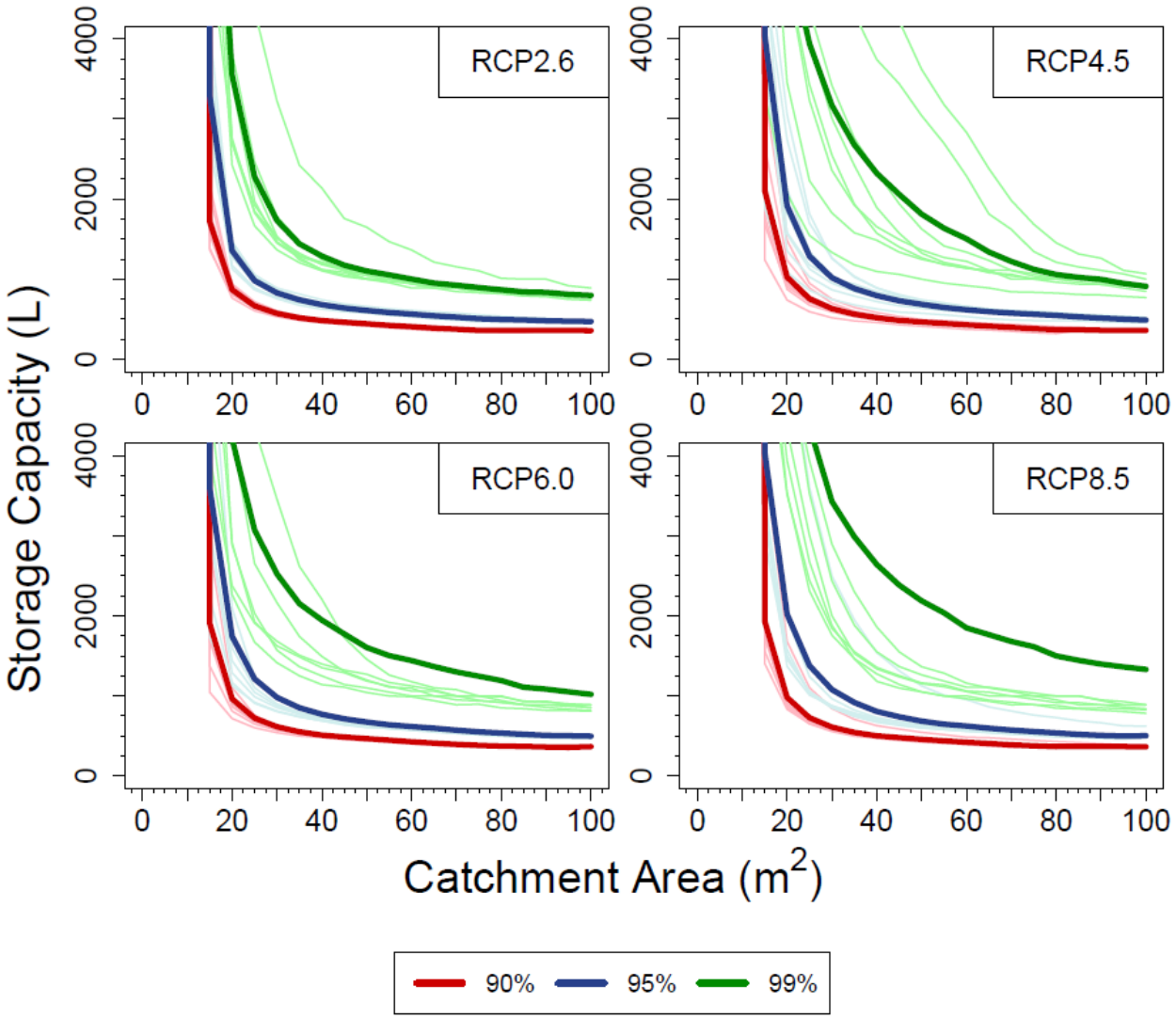

Figure 19. Household-scale RWCS design curves for Pohnpei State developed at the 90% (red), 95% (blue) and 99% (green) levels of reliability. Thicker, darker curves represent the average of the design curves created by the output of the top 8 regional GCMs (shown in lighter colors)

The individual design curves created from the output of GCM are also shown in lighter colors on the plot. While there is some overlap between the various system reliability rates, generally the design curves corresponding to systems of lower reliability are shifted down and to the left of those of higher system reliability. For this reason, it is typically easier for communities to design systems that provide lower rates of reliability because both the catchment area and storage capacity can be designed smaller. For all four forcing scenarios the 99th percentile reliability curve is shifted significantly right and up from that of the 90% reliability. In some cases, nearly double the storage capacity is required for 99% reliability as for 90% reliability. The design curves for the RCP2.6 climate scenario are relatively clustered, showing lower variability between the three system reliability rates that any other RCP scenario.

All RCP scenarios show a minimum design catchment area around 12 m^2 before increasing asymptotically with storage capacity. The 99% reliability design curves require catchment area to meet or exceed 20 m^2, though this value is for the average of all scenarios. As

seen in the lighter lines that indicated individual model output, the design curves for 90% reliability are relatively clustered while those for 99% reliability are further spaced. The higher required system dimensions indicate a potential decrease in annual rainfall as predicted by the RCP8.5 forcing scenario. The minimum storage capacity observed in all of the RCP scenarios is approximately 350 liters, below which any increase in catchment area cannot achieve the reliability levels indicated by the design curves.

Figure 20 shows the design curves developed for the four RCP scenarios in Yap State. The positions of the curves are relatively similar for each of the RCP scenarios, with curves shifting up and to the right with increasing storage capacity.

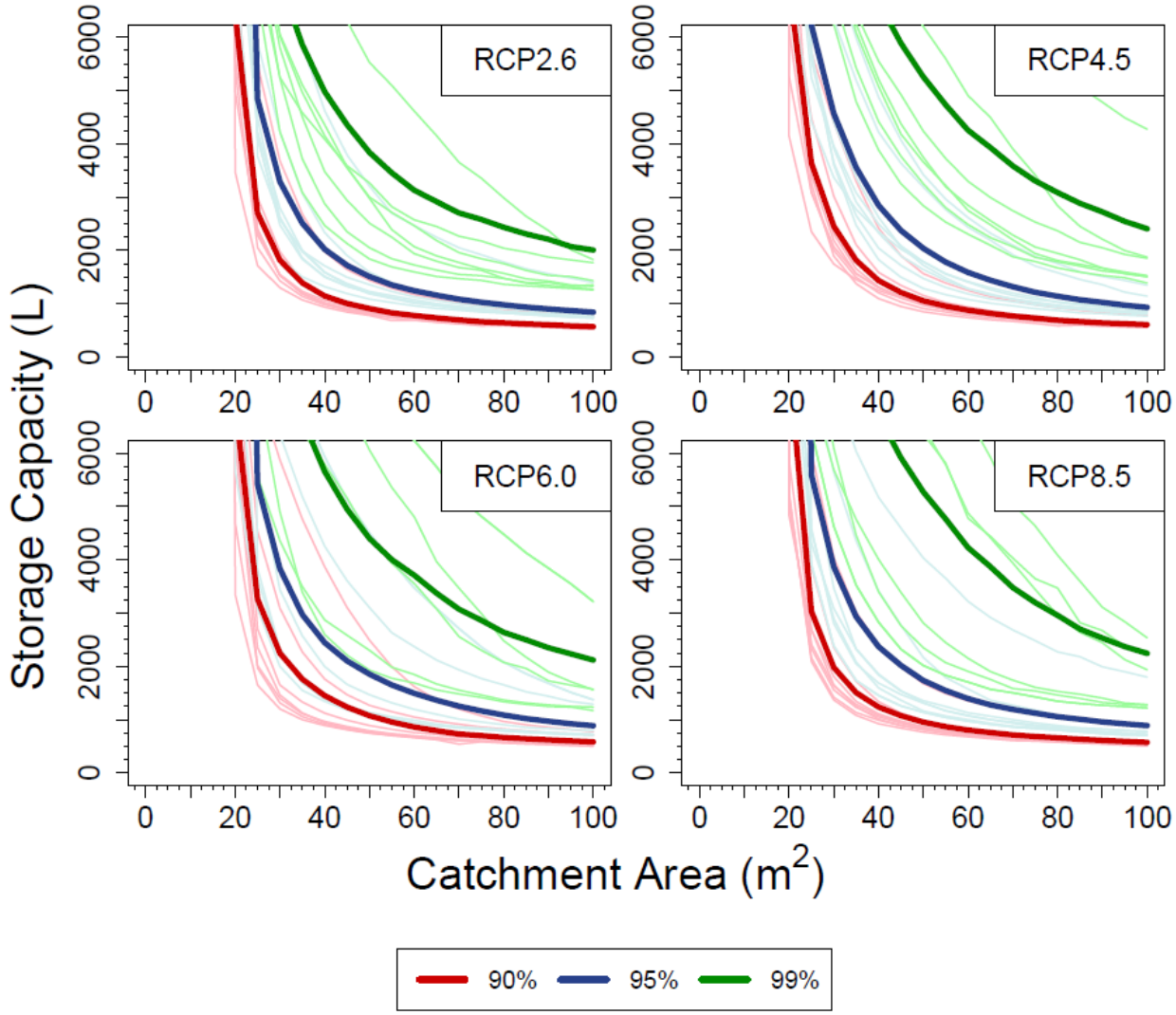

Figure 20. Household-scale RWCS design curves for Yap State developed at the 90% (red), 95% (blue) and 99% (green) levels of reliability.

This trend indicates that each RCP forcing scenario shows very similar climate change effects, allowing system design to remain conservative. Each design curve appears to level off near a storage capacity of 500 liters, after which any further increase in catchment area has no effect on the reliability of the system. The 90% and 95% reliability curves of each GCM for RCP2.6 are

highly clustered, indicated agreement between the GCM output and the performance of the system. The individual 99% reliability curves for all of the RCP scenarios show high variability, though the average curve still lies in approximately the same location for each.

Because captured rainwater plays such a large role in supplying atoll island communities with freshwater, further investigation was performed to determine how large RWCS would need to be designed to consistently meet household demand for the entire 2010-2050 study period. Figure 21 shows the system designed curves for Yap State developed to consistently supply each household with 120 liters per day, an adequate volume for a household of 4 people each with a daily water demand of 30 liters per capita. As indicated by the design curves for each of the RCP forcing scenarios, systems designed to supply a daily average of 120 liters would be larger in size than those previously considered. The minimum catchment area size indicated on the curves is approximately 25 m^2, below which the system would not be able supply the desired volume of captured rainwater regardless of an increase in storage capacity. Based on the knowledge of the existing RWCS present on atolls in Micronesia, as discussed in Chapter 3, the system size required for this volume of rainwater supply is feasible, but requires further development of RWCS infrastructure. However, in designing systems to satisfy a daily demand of 120 liters, adequate water supply can be ensured for a majority of the study period.

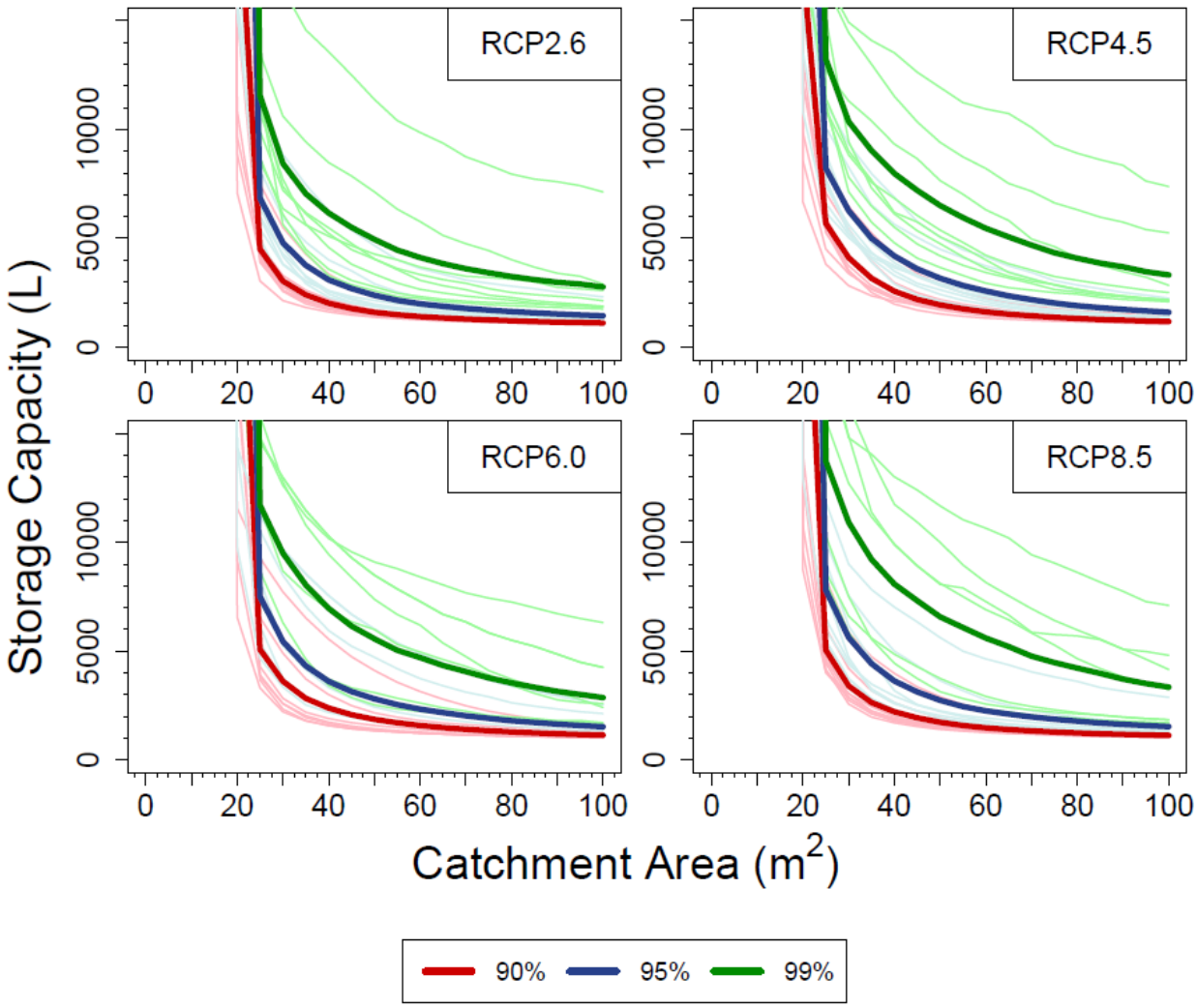

Figure 21. RWCS design curves for sizing systems designed to supply an average household with a consistent daily volume of 120 liters, in which case the system would be highly reliable.

Discussions and Conclusion

The design curves developed for eastern and western Micronesia are intended to assist island communities in designing household-scale RWCS with reliability rates high enough to ensure adequate water supply during drought periods. The lowest reliability rate considered was 90% due to the high level of dependence atoll communities place on RWCS to supply them with potable water. The household-scale RWCS design curves developed further the reliability of the community system by ensuring each individual system is designed to be sustainable during drought, rather than optimizing a group of systems as a whole wherein some dwellings may still have inadequate design. In general, the spacing of the design curves for the various reliability rates increased with each consecutive RCP forcing scenario. Under the RCP2.6 scenario, which represents extreme climate change mitigation via reduction of greenhouse gas emissions, each of the reliability scenario curves are grouped relatively tightly. In contrast, curves developed under the RCP8.5 scenario, characterized by high emissions, are more spaced out. This difference in spacing most likely indicates more erratic rainfall patterns as predicted by the selected GCMs, making it more difficult for systems to achieve 99% reliability. In both Pohnpei and Yap States,

there are marked similarities between the design curves for the RCP2.6 and RCP6.0 forcing scenarios. Though the design curves produced by the individual GCMs show different degrees of scatter, the locations of the average curves are comparable.

Due to the variability in rainfall between eastern and western Micronesia, the design curves developed for both regions are on a drastically different scale. Those developed for Yap State require almost double the storage capacity than those for Pohnpei State for the same size catchment area. The minimum required size of catchment area is 20 m^2 in Yap State, below which the systems are incapable of achieving above 90% reliability regardless of any increase in storage capacity; the minimum catchment area required in Pohnpei State is approximately 12 m^2. Conversely, a minimum storage capacity of about 350 liters in Pohnpei State and 500 liters in Yap State are required to achieve high reliability rates. The difference in the required size of systems is due to the lower annual rainfall in Yap State, where rainfall totals amount to just under 3 meters as compared to the 4 meters seen in Pohnpei. By utilizing the system design curves, island communities can ensure that each household RWCS achieves a desired rate of reliability. Not only will this provide an alternate source of drinking water aside from groundwater extraction, but will also help prolong adequate water supply during drought periods.

THREE-DIMENSIONAL GROUNDWATER MODEL DEVELOPMENT AND CALIBRATION

Introduction

Atoll Geologic Structure

Atoll island groundwater systems are extremely fragile and must be closely monitored and managed to ensure adequate supply for island communities. Atoll aquifers consist of an upper Holocene-age layer and a lower Pleistocene-age layer. The Holocene layer consists of sand and other fine sediment unconformably deposited as sea levels rose near the end of the Pleistocene Age. This layer is typically 15-25 meters thick and has a hydraulic conductivity relatively low as compared to the underlying Pleistocene layer. The Pleistocene layer is composed of karstic limestone, formed from the eroded remnants of submerged reefs that formed atop volcanic platforms. The hydraulic conductivity of the Holocene aquifer has been estimated to be 1 to 2 orders of magnitude less than that of the Pleistocene aquifer (Hunt & Peterson, 1980); (Woodroffe & Falkland, 1997); (Bailey, Jenson, & Olsen, 2009). The unique geologic composition of atoll islands was first characterized as a dual-aquifer system by Ayers and Vacher (Ayers & Vacher, 1986). Before their research, atoll groundwater systems were modeled as a single layer aquifer, leading to inaccuracies in the estimation of groundwater development and freshwater thickness.

A freshwater lens forms beneath atoll islands as rainwater infiltrates the unsaturated zone and recharges the aquifer. The upper Holocene aquifer has a hydraulic conductivity and geologic characteristics suitable for the lens' development. The thickness and volume of the freshwater lens is dependent exclusively on rainwater recharge to flush seawater from the subsurface and create a zone of low chloride concentration. As freshwater infiltrates it flushes out seawater that has intruded in to the upper aquifer, effectively creating a region of freshwater that "sits" atop the higher-density seawater. As rainwater infiltrates the subsurface, its weight and relatively low density pushes seawater contained within the Holocene deposits out through the basement Pleistocene limestone. Because the development of the lens is highly dependent on recharge from infiltrating rainwater, a relatively constant depth of rainfall is required to sustain a lens of considerable thickness and volume. Seawater intrusion occurs as the higher density seawater mixes with the freshwater in the subsurface. Without continual recharge, the lens will thin and eventually deplete. The overall size of the freshwater lens also depends upon the geometry of the island beneath which it forms. Islands with smaller widths will have a much smaller freshwater lens as there is not as much surface area beneath which the lens can develop.

At the contact between the Holocene and Pleistocene aquifers, rapid mixing occurs due to the extremely high permeability of the underlying karstic limestone. This contact between the two aquifers truncates the lens, limiting its thickness and ultimately its volume to the depth of the Holocene deposits. On smaller atolls where the freshwater lens is more limited by the width of the islet, the limiting nature of this geologic feature is not seen. Larger atolls where the freshwater lens is able to reach the contact without being limited by the width of the islet experience lens truncation as the freshwater attempts to reach below the Holocene layer. For this reason, atolls have a finite volume of available freshwater regardless of their size, limited by the depth to contact between the two aquifers. The low-lying elevation and relatively flat topography of atoll islets prevents the formation of surface water sources. High permeability sediments found in the Holocene aquifer induce instantaneous infiltration of all rainwater not captured by

rainwater harvesting systems directly into the subsurface. For this reason, atoll communities shave limited access to freshwater, which is derived mainly from hand-dug wells and RWCS.

Previous Modeling Efforts

Past modeling efforts have focused on estimating the thickness of the freshwater lens using historical data. Early efforts used the Dupuit assumption of exclusively horizontal flow to analytically approximate the thickness of the freshwater lens by calculating the position of the freshwater/seawater interface at the base of the lens. Other initial analytical efforts assumed a sharp interface between the fresh and saline groundwater, known as the Ghyben-Herzberg approximation. In reality, the interface between fresh and saline water is a broad transition zone of brackish water. Two-dimensional modeling has been performed to numerically estimate the thickness of the freshwater lens at a distinct cross-section of specified width. Lam (Lam, 1974) assumed a single homogeneous, isotropic aquifer with horizontal flow. This assumption was later disproved by the discovery of the atoll dual-aquifer system. In 1984, Voss developed SUTRA, a USGS finite-element based code used to simulate the variable-density flow dynamics for both saturated and unsaturated flow. Bailey et al. (2008) used SUTRA to model Micronesian atoll islands of varying widths to estimate the thickness of the freshwater lens. Using observed values of freshwater lens thickness for various islands, they estimated the hydraulic conductivity of windward islands to be approximately 400 m/d and that of leeward islands to be approximately 50 m/d.

Three-dimensional modeling has also been performed to simulate groundwater flow dynamics. Lee (2003) determined the effects of various controls on the size of the freshwater lens using TOUGH2, while Comte et al. (2014) simulated the groundwater flow system beneath Grande Glorieuse Island in the western Indian Ocean. No three-dimensional modeling efforts have focused on the groundwater flow dynamics beneath atoll islands in Micronesia. The objectives of this study are to develop three-dimensional models for various representative islands throughout Micronesia, and to calibrate the models using observed values of freshwater lens thickness. Sensitivity analysis will also be performed on the island models, with the intent of determining which factors have the greatest influence on the development and size of the freshwater lens. Factors to be investigated include the hydraulic conductivity, depth to contact between the upper Holocene and lower Pleistocene aquifers, the annual lens recharge rate, and the coconut root extraction rate.

Methods

Island Selection

SEAWAT, a finite-difference based code developed by the USGS, couples MODFLOW and MT3DMS to simulate three-dimensional, variable-density, saturated groundwater flow. For this study, the sole MT3DMS specie considered in the groundwater flow system was chloride, the concentration of which governs the size of the freshwater lens. Three-dimensional models were created for eight different islands: five in Pohnpei State and three in Yap State. Islands selected were those designated as most representative of those throughout Micronesia. Models were created for Yap and Pohnpei States to attempt to quantify the differences in lens volume caused by the differences in precipitation rates across Micronesia. Yap State has an average annual rainfall of 2.5-3.5 meters while the total for Pohnpei State is closer to 3.5-4.5 meters.

The islands of Fassarai, Mangejang, and Mogmog were selected for Yap State. Ulithi Atoll, the location of the three islands modeled in Yap State is not in the trade wind realm.

Rather, it is in the typhoon circulatory region, in which typhoons can occur during any month of the year. The islands on the atoll are noted for their flatness and lowness, making them subject to relatively frequent wave-overwash events and gradual sea-level rise. Fassarai is located on the windward side of Ulithi atoll, subject to the barraging of waves induced by tropical typhoons. It is approximately 2000 meters in length and has an average width of about 200 meters, with an overall surface area of approximately 350,000 m^2. It's relatively small width allows it to be modeled as an infinite-strip island, which are island that are assumed to be infinite in length due to the significant difference between the width and length of the island. This sort of approximation is used mainly in two-dimensional modeling, where the volume of the freshwater lens can be approximated if the cross-sectional width of the island is assumed relatively constant and an island length can be determined. Fassarai was modeled to elaborate upon the algebraic model volume approximations made by other modeling efforts using analytical estimation (Bailey R. T., Jenson, Rubinstein, & Olsen, 2008).

Mangejang is a roughly circular island also located on the windward side of Ulithi Atoll; it is about 400 meters wide, with a surface area of approximately 115,000 m^2. It was chosen because of its fairly representative size and circular shape, which is most conducive to the formation of a freshwater lens. Because Mangejang is a windward island, its hydraulic conductivity will be much higher than if it were located on the leeward side of the atoll, resulting in a lens thickness lower than other islands of similar size located on the leeward side. It is modeled to further understanding of the dynamics of the freshwater lens as it forms beneath circular islands.

Mogmog is an irregularly shaped, windward atoll islet; it has a width of approximately 450 meters and is one of four inhabited islands on Ulithi Atoll. The other two islands modeled on Ulithi Atoll are not inhabited, but were chosen for their geologic characteristics. Mogmog has a population of about two-hundred, with thirty-five households and forty families (Sueo, 2003). Modeling efforts seek not only to understand the development of the freshwater lens beneath an irregularly shaped island, but also to estimate the freshwater volume beneath the island for use by island residents.

The islands of Deke, Pingelap, Kahlap, Ngatik, and Nikahlap were selected from Pohnpei State. Deke Island is located on the windward side of Pingelap Atoll. It has a width of about 560 meters and an overall surface area of approximately 620,000 m^2. Deke is currently uninhabited, mainly due to the low volume of freshwater available within the lens, as reported by residents of Pingelap Atoll. Pingelap Island is also located on Pingelap Atoll, but it is on the leeward side, sheltered from the waves induced by the trade winds. Its relatively large size and location on the atoll has allowed for permanent settlement, hosting approximately 250 residents who have made home on the island. Pingelap has an average width of about 550 meters and a surface area of about 1.34M m^2. The island itself stretches towards the windward side of the atoll, but the area modeled represents only the area over which permanent settlement has been established. It is over this area that a majority of the freshwater lens develops, as the northern portion of the island grows narrow in width (250 meters) and is not able to support a lens of relatively considerable volume. The Pingelap and Deke Island models can be used to study the differences in lens development between leeward and windward islands on a relatively small atoll. Higher rainfall than that seen in Yap State also provides the opportunity for the more rapid development of larger freshwater lenses.

Kahlap Island is located on Mwoakilloa Atoll in Pohnpei State. It was selected for its leeward position on the atoll, and for its unique shape. Similar to Fassarai, Kahlap can be viewed

as an infinite strip islands due to its high length to width ratio. Kahlap has a length of about 2200 meters and an average width just over 200 meters; the total surface area of the island is about 600,000 m^2. This island was selected to further study the lens dynamics beneath infinite strip islands, and to compare the development and volume to Fassarai in Yap State. It is expected that, though both Fassarai and Kahlap have similar lengths and widths, Kahlap will show a greater freshwater lens volume due to the higher rainfall rates recorded in Pohnpei State.

Ngatik Island is located on the leeward side of Sapwuahfik Atoll, 150 kilometers southwest of the capitol island of Pohnpei. The island has a width of about 700 meters and a surface area just over 800,000 m^2. It is the only inhabited island on Sapwuahfik Atoll, supporting about 600 people who live along the perimeter of the island (Anthony, 1996). Ngatik was chosen for its close proximity to the island of Pohnpei, and also for its representative shape and island community population.

The last island chosen for this study is Nikahlap Island, located on Pakein Atoll. Nikahlap is on the leeward side of the atoll, sheltered from trade wind-induced waves, and has a width of approximately 550 meters and a surface area just under 650,000 m^2. The island was selected not only for its location and geometry, but also because of the information previously collected by Taboroši and Martin (2011) about the RWCS present on the island. Not only will the model results quantify the volume of freshwater available in the lens, but they can be used to couple the groundwater and captured rainwater volumes to prevent the island community from experiencing the issue of inadequate freshwater supply. This case study is presented and discussed in detail in Chapter 6.

Model Development

After the islands were selected, a grid and input files were developed for each model. Using Google Earth, each of the islands was traced to create a polygon, which was then exported and converted for us in ArcGIS. Using the tools available in ArcGIS, the geometry of each island was precisely measured and superfluous vertices were removed. The USGS pre-processing program ModelMuse was used to develop the mesh for each island model. ModelMuse is a graphical user interface for MODFLOW-2005 and MT3DMS, which also allows for the creation of SEAWAT input files. A model mesh was developed by overlaying the island shapefiles derived from Google Earth with a grid of calculated width and height. The size of the grid and the dimensions of each grid cell were determined analytically by measuring the width and height of each island under consideration and dividing the measurements by a desired cell size.

The cell size was determined on a model-by-model basis, with the objective of minimizing the cell size as much as possible to retain accuracy while still allowing the model to run efficiently. Once imported into ModelMuse, the boundaries of the island shapefiles were traced to denote the models' active and inactive cells. An example of a mesh created for Pingelap Island on Pingelap Atoll is shown in Figure 22. Figure 22a shows a screen capture of the island as viewed through Google Earth, Figure 22b is a plan view of the top layer of model mesh constructed with ModelMuse, and Figure 22c shows the three-dimensional representation of model output viewed through USGS' ModelViewer.

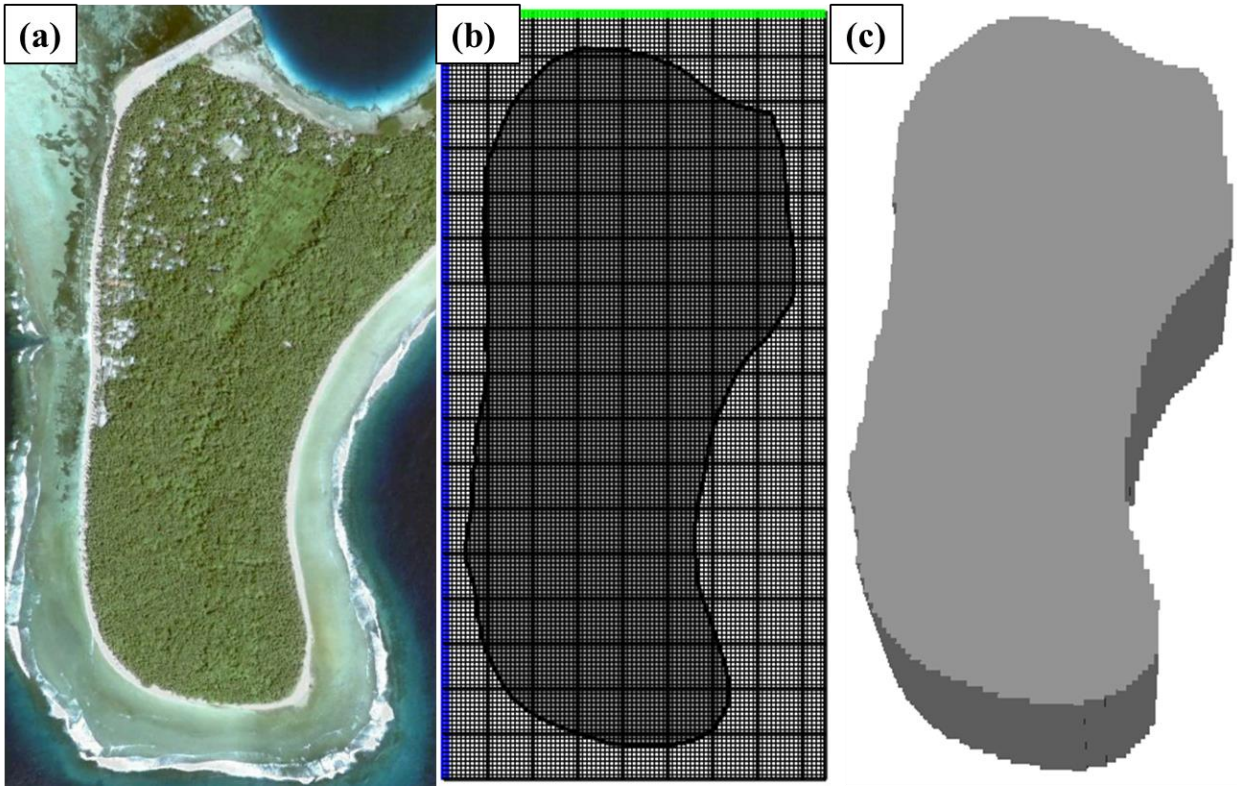

Figure 22. Mesh development for Pingelap Island in Pohnpei State. (a) shows a Google Earth screenshot of the island. (b) shows the layout of the finite-difference mesh developed using the USGS developed program ModelMuse. (c) shows the three-dimensional representation of the island as viewed through ModelViewer

Similar figures illustrating the process mesh development for the other 7 Micronesian atoll islands are located in Appendix II.

Using hydraulic conductivity values estimated by Bailey et al. (2008), leeward islands were initially assumed to have a hydraulic conductivity of 50 m/d and windward islands were initially assigned a hydraulic conductivity value of 400 m/d. These values were later adjusted during model calibration. The upper aquifer of the atoll geologic system was assumed to be isotropic and homogeneous, an assumption made by other modelers due to the gradual, even deposition of sediments which compose the Holocene aquifer. Due to the relatively small island surface area, recharge was applied uniformly to each grid cell across each model. The value of the recharge to the lens was determined by analyzing historical recharge trends. Using historical precipitation data and observed values of lens recharge volume, it was calculated that lens recharge amounts to approximately 63% of the rainfall depth in Pohnpei State and approximately 54% of the rainfall depth in Yap State. This method allowed for the calculation of lens recharge for each time step using the historical climate data extracted for both regions.

The specific yield of the upper Holocene aquifer, which determines the volume of available extractable freshwater, was set at 0.32 (Morris & Johnson, 1967). The specific storage of the aquifer was also specified at 7.5×10^{-4}, a value determined by (Batu, 1998). These parameters, though considered during the calibration exercises, showed little influence on the development of freshwater lens when adjusted. For this reason, they remained at their reported values for the duration of the study.

Coconut palms have long been known to transpire large volumes of water from the freshwater lens. Often, roots from large palm trees can reach 2-3 meters below the topographic

surface of the island (Falkland A. C., 1994). Coconut roots extract 400-750 mm per year per tree in areas with 100% tree cover. Typically, trees are spaced about 8 meters apart (Falkland A. C., 1994). Wells implemented in the model simulated the extraction of water from the lens due to coconut palm transpiration. A value of 700 mm per tree per year was used to give a conservative estimate of the volume extracted from the freshwater lens.

The higher the extraction rate of each coconut tree, the more recharge required each day to sustain the lens thickness and volume. In models with square cells of 10 meters per side, it was assumed that one coconut tree per cell would be present to extract water. Cells in models of this size were given a pumping rate equivalent to the volume one tree would extract from the lens. In smaller models (i.e. those will cells of 5 meters on each side) it was assumed that coconut trees would span two cells instead of being solely contained in one. These cells were given a pumping rate equivalent to half of what a single coconut tree would transpire each data. Atoll island boundary cells were represented by constant-head cells with constant concentration equal to that of seawater. This established the lateral boundaries of the freshwater lens and simulated the saline intrusion that occurs over time if constant rainwater infiltration is not available to recharge the lens. The constant head value given to these cells simulates an increase in pressure with depth and the groundwater flow dynamics associated with such. These cells were also assigned a constant concentration to simulate the contact with seawater.

Steady-state runs were first conducted to establish a baseline condition for the freshwater lens thickness and volume. The steady-state runs used average annual precipitation depths to represent average climate conditions for each region, operating on a daily time step. In Pohnpei State, each steady-state model was subjected to an annual precipitation depth of 4 meters. Historical recharge amounts to about 63% in eastern Micronesia, so each model in this region was given approximately 2.4 meters of recharge annually. In Yap State the average annual precipitation is about 3 meters. Using the observed recharge percentage of a little over 50%, each model received 1.5 meters of recharge annually. Recharge values were applied uniformly over the island surface, with a constant nonzero daily rate used which amounted to the calculated annual recharge total for each region. The model grid and three-dimensional representation of each island are shown in Figures B1-B7 in Appendix II, along with a description of each model mesh shown in Table 8.

Table 8. Description of SEAWAT model meshes developed for 8 Micronesian atoll islands, detailing the number of rows, columns, and layers as well as the size of each grid cell

Island	No. of Rows	No. of Columns	No. of Layers	Grid Size (m)
Deke	105	140	29	10
Pingelap	170	85	29	10
Kahlap	210	140	29	10
Ngatik	100	180	29	10
Nikahlap	150	120	29	10
Fassarai	212	140	29	10
Mangejang	100	108	29	5
Mogmog	115	230	29	5

Model Calibration

Once the initial runs had been performed to establish a preliminary lens thickness, each model was calibrated using observed values of lens thickness. The first island model calibrated was Pingelap Island on the leeward side of Pingelap Atoll. The objective of the calibration was

to have model output match observed lens thickness for Pingelap Island as reported by Ayers and Vacher (1986). The initial hydraulic conductivity used as 50 m/d, as reported by Bailey et al. (2009). The hydraulic conductivity was adjusted until the freshwater lens size estimated by the three-dimensional model matched the observed lens thickness. The model was then further calibrated using data recorded by Anthony (Anthony, 1996); during which the baseline model was given transient recharge values calculated using the historical rainfall.

The historical climate data was given as monthly precipitation totals from January 1986 to December 1989, shown in Table 9.

Table 9. Historical monthly average precipitation depth on Pingelap Island from 1986-1989 used in model calibration (Anthony, Hydrogeology and ground-water resources of Pingelap Island, Pingelap Atoll, State of Pohnpei, Federated States of Micronesia, 1996)

	Jan.	**Feb.**	**Mar.**	**Apr.**	**May**	**Jun**	**July**	**Aug.**	**Sept.**	**Oct.**	**Nov.**	**Dec.**	**Annual**
1985	M	M	M	M	M	M	M	M	M	M	12.33	17.79	M
1986	13.28	9.71	24.05	7.41	17.75	12.94	7.52	8.83	11.36	11.94	22.09	18.80	165.68
1987	10.18	6.19	24.71	7.98	6.90	10.3	19.82	19.06	13.12	8.16	16.59	10.19	153.20
1988	14.49	8.13	8.40	6.08	14.37	19.86	14.05	16.05	14.68	16.12	9.90	12.90	155.03
1989	11.02	10.26	15.54	20.65	17.33	10.44	15.99	14.45	9.56	11.97	15.08	21.03	173.32
1990	6.59	3.29	4.95	12.05	--	--	--	--	--	--	--	--	--
Mean	11.11	7.52	15.53	10.83	14.09	13.39	14.35	14.60	12.18	12.05	15.92	15.73	161.81
N	5	5	5	5	4	4	4	4	4	4	5	5	4

Each monthly total was evenly divided by the number of days in the given month so that each day during the calibration period received a nonzero value for recharge. Over this same period, the thickness of the freshwater lens was measured using several observation wells located across Pingelap Island. Model calibration was based on the location where the freshwater lens was observed to be thickest; this occurred at the center of the island, as expected given the general curvature of the lens. Hydraulic conductivity values of the upper Holocene aquifer were adjusted until the model output reasonably matched the observed values of lens thickness. Other parameters, such as the porosity of the soil, were altered with little effect. It was therefore determined that, of the properties of the soil that could be adjusted, hydraulic conductivity was the most influential to model output. A summary of the calibrated model parameters is shown in Table 10.

Given the similar geologic nature and soil characteristics of Micronesian atolls, the calibrated value of hydraulic conductivity obtained from the Pingelap Island case study was assigned to other leeward island models in both Pohnpei and Yap States. Using observed value of lens thickness for three other islands, the calibrated hydraulic conductivity value obtained for Pingelap Island was tested further. An observed lens thickness was recorded for Ngatik Island on Sapwuahfik Atoll, a leeward island with characteristics similar to those found on Pingelap. The calibrated hydraulic conductivity value was applied to the Ngatik Island model, which was then run using the constant average daily value for recharge. The lens thickness produced was compared with the observed value. If the model output did not match observed conditions, the hydraulic conductivity was slightly altered and the model rerun. If this was the case, the Pingelap model was also rerun using the new value for hydraulic conductivity to ensure agreement across all islands. This iterative process was carried out until an adequate, calibrated value for hydraulic conductivity was obtained.

Table 10. Summary of calibrated model parameters for leeward islands established during three-dimensional model development

Parameter [units]	Value	Source
General aquifer properties		
Compressibility of porous matrix [m^2/N]	1 x 10^{-9}	(Freeze & Cherry, 1979)
Specific yield [m^3 m^{-3}]	0.32	(Morris & Johnson, 1967)
Coconut Root Extraction [mm/yr]	700	(Falkland, 1994)
Upper Holocene aquifer		
Porosity [m^3 m^{-3}]	0.2	(Anthony, 1987)
Upper deposits thickness [m]	10	(Hamlin & Anthony, 1987)
Upper deposits horizontal K [m/d]	25	
Upper deposits vertical K [m/d]	5	
Lower deposits thickness [m]	10	
Lower deposits horizontal K [m/d]	30	
Lower deposits vertical K [m/d]	7	
Lower Pleistocene aquifer		
Porosity [m3 m-3]	0.3	(Swartz, 1962)
Thickness [m]	35	
Horizontal K [m/d]	5000	(Oberdorfer, Hogan, & Buddemeier, 1990)
Vertical K [m/d]	1000	(Oberdorfer, Hogan, & Buddemeier, 1990)

Observed lens thickness values were also available for Kahlap Island on Mwoakilloa Atoll and Deke Island on Pingelap Atoll (Anthony, 1996), seen in Table 11.Table 11 Both of these islands are located on the windward side of the atolls, meaning they are expected to have a much higher hydraulic conductivity value that that found for leeward islands. The initial hydraulic conductivity value used for windward islands was that estimated by Bailey et al. (2009) of 400 m/d. Model output was compared to observed values of lens thickness, and the hydraulic conductivity altered slightly for each consecutive model run until the results correlated with historical values of lens thickness.

Sensitivity Analysis

Sensitivity analysis was performed on each island model to determine the influence of various parameters on lens development and size. The four parameters selected for analysis were the hydraulic conductivity, depth to contact between the Holocene and Pleistocene aquifers, the annual recharge rate, and the rate of coconut root extraction from the freshwater lens. The hydraulic conductivity was chosen as a potentially influential parameter following model calibration, during which a small change in its value could have a large effect on the size of the freshwater lens. The depth to contact between the upper Holocene deposits and the lower Pleistocene limestone was recognized as being potentially important because it acts as a truncation point, beyond which the lens cannot develop. It was assumed that islands with a shallow contact point would show significantly lower freshwater lens volume as it is truncated prematurely.

The annual recharge rate was selected for analysis due to the fragile state of the freshwater lens and its reliance on recharge from rainwater infiltration. The rate of coconut root extraction was recognized as potentially having a heavy influence on the size of the freshwater lens because of the close proximity of coconut roots to the freshwater. Coconut palm roots reach 2-3 meters below the topographic surface of the atolls, often extending directly into the freshwater lens. As the roots extract water and the coconut palms transpire, they compete directly for freshwater contained within the lens. Higher rates of coconut root extraction could therefor spur higher competition with island communities for available freshwater.

A range of value was selected for each of the parameters to observed changes in the size of the lens; the range selected was intended to represent the maximum and minimum extremes of each parameter. For the analysis, a median value was chosen for each of the parameters investigated. This allowed for slight adjustment of the parameter being analyzed to observe the response of the groundwater system without a response triggered by the other parameters.

Hydraulic conductivity was varied from 10 m/d to 500 m/d, with a value of 35 m/d used when not being analyzed. The depth to contact was varied from 10 meters to 40 meters, with a value of 25 meters used when not being analyzed. Though the observed depth to the contact within the atoll dual-aquifer system typically ranges from 15-25 meters below sea level (Wheatcraft & Buddemeier, 1981); (Hamlin & Anthony, 1987), the model was run using higher values to determine whether a larger lens could develop. The average annual rainfall depth was adjusted from 0.5 meters to 4 meters, and given a value of 2 meters when not the parameter under consideration. The rate of coconut root extraction varied from 400 mm/yr to 800 mm/yr, with a value of 600 mm/yr used when not being analyzed. Further sensitivity analysis was run for Deke Island, the intent of which was to determine what effect various rates of coconut root extraction could have on the development of the lens under transient climate conditions.

Using the climate data for Pingelap Atoll recorded by Anthony (1992), the Deke Island model was run at five increasing rates of coconut root extraction: 400 mm/yr, 500 mm/yr, 600 mm/yr, 700 mm/yr, and 800 mm/yr. If coconut root extraction rate has a significant influence on the development and size of the freshwater lens, each increasing extraction rate would result in a large difference in the thickness and volume of the lens under the same transient climate conditions.

Islands analyzed were Pingelap, Nikahlap, Deke, Mangejang, and Fassarai. The islands were chosen for their geometric characteristics, known to have an effect on the development of the freshwater lens. Large islands like Pingelap and Nikahlap have larger surface areas, providing a larger space beneath which the freshwater lens can develop. Deke and Mangejang were chosen because they are somewhat smaller than Pingelap and Nikahlap, but still have considerable surface area. They are also relatively round in shape, a geometry which can more easily be extrapolated to other islands. Fassarai Island was chosen because it is viewed as an infinite-strip island, the lens dynamics of which are much different than that of rounder islands.

Results

Model Calibration

The first model calibrated, Pingelap Island, used an initial hydraulic conductivity value of 50 m/d. This run did not include coconut root extraction as simulate by the Well package. Hydraulic conductivity was first calibrated without this parameter in an attempt to narrow the value down while still allowing for efficient runtime. This hydraulic conductivity value was reported by Bailey et al. (2008) as the value at which a two-dimensional model of the atoll groundwater system most accurately reproduced observed lens thickness values. For the three-dimensional model this initial value for hydraulic conductivity was too high, not allowing the lens to reach the freshwater thickness of 16 meters reported by Ayers and Vacher (1986). For this scenario, the freshwater lens reached a maximum thickness of 11.53 meters. At this point the lens was partially truncated by the contact between the Holocene and Pleistocene aquifers. The depth to contact was therefore lowered from 15 meters to 20 meters. Following further calibration it was found that a hydraulic conductivity of 35 m/d resulted in a modeled lens thickness of 15.6 meters, accurately replicating the observed lens thickness. The limit of the

freshwater lens is assumed to be when the chloride concentration in the lens exceeds 0.89 g/kg. Seawater has a chloride concentration of 35 g/kg, with everything between it and freshwater composing the transition zone of brackish water.

Further calibration was performed on Pingelap Island using the historical monthly precipitation totals and lens thickness measurements made by Anthony (1996) for the period from 1986-1989. During this period, the thickness of the freshwater lens at its deepest point was measured to be 15 meters; this was the target value of the modeled thickness of freshwater for this scenario. For these simulations, coconut root extraction was included as a model parameter to further calibrate the hydraulic conductivity. As coconut palms transpire, it was predicted that a lower value for hydraulic conductivity would be necessary to allow the freshwater region to grow larger to account for root extraction. Using the previously calibrated hydraulic conductivity of 35 m/d, the average lens thickness modeled over the four year period as 12.98 meters. This lower value indicated that the rate at which coconut roots were extracting water has an effect on the development and overall size of the freshwater lens. A lower hydraulic conductivity was used in an attempt to mitigate this effect and once again match observed lens thickness values. A hydraulic conductivity of 25 m/d was used, resulting in an average lens thickness of 14.7 meters, a value close to the thickness measured by Anthony (1996). A time series of the fluctuation in the thickness of the freshwater lens is shown in Figure 23; also plotted is the average depth of

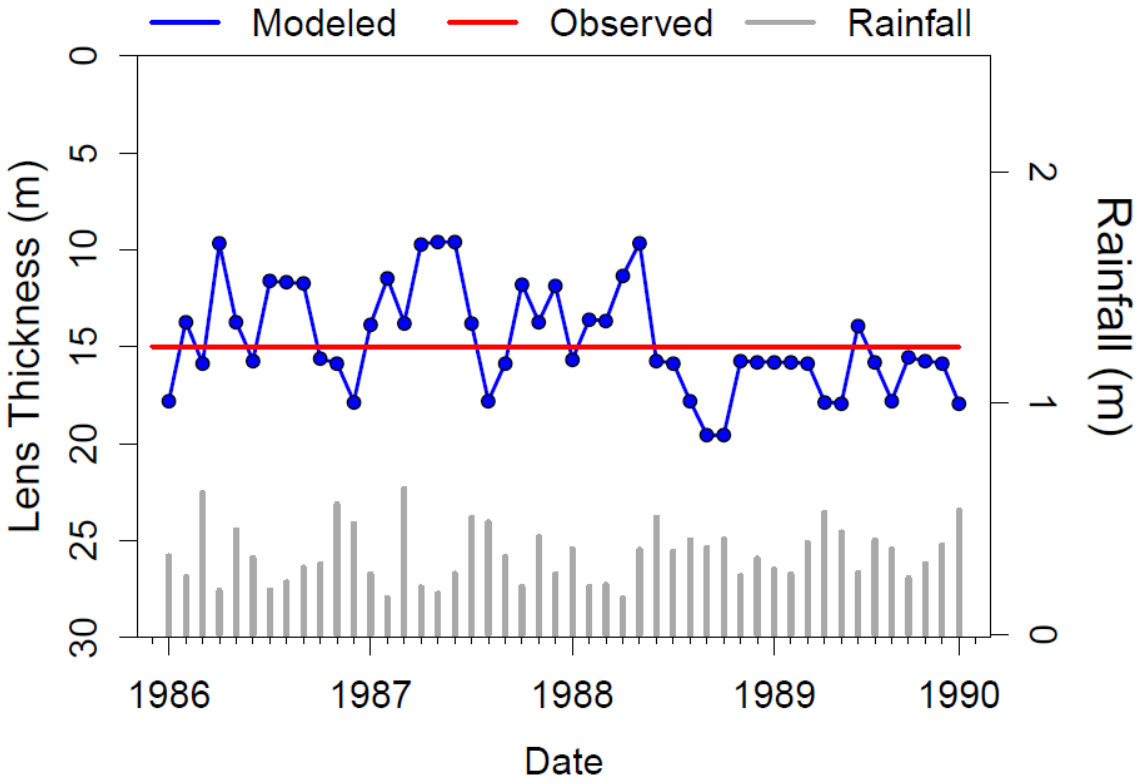

Figure 23. Calibration results of Pingelap Island in Pohnpei State. The blue line is the model output using the historical climate data provided by Anthony (1994), the monthly depth of which is represented by the gray bars. The average observed lens thickness for the period is shown in red.

rainfall for each month during the period, indicating the presence of high or low levels of rainfall, and the observed value of lens thickness for reference.

Following the calibration of Pingelap Island, other leeward islands were calibrated. The similar geologic setting in which the atoll islands across Micronesia formed led to the assumption that each model would use similar values of hydraulic conductivity. These model runs served as validation of the calibrated value for hydraulic conductivity. The other leeward island with an observed value for lens thickness was Ngatik Island on Sapwuahfik Atoll; Ngatik has an average lens thickness of 20 meters (Anthony, 1996). Using the previously calibrated hydraulic conductivity value of 25 m/d, the simulated lens thickness of Ngatik Island was 19.6 meters, shown in Figure 24. This close match to historical data verifies the calibrated hydraulic conductivity value for leeward islands.

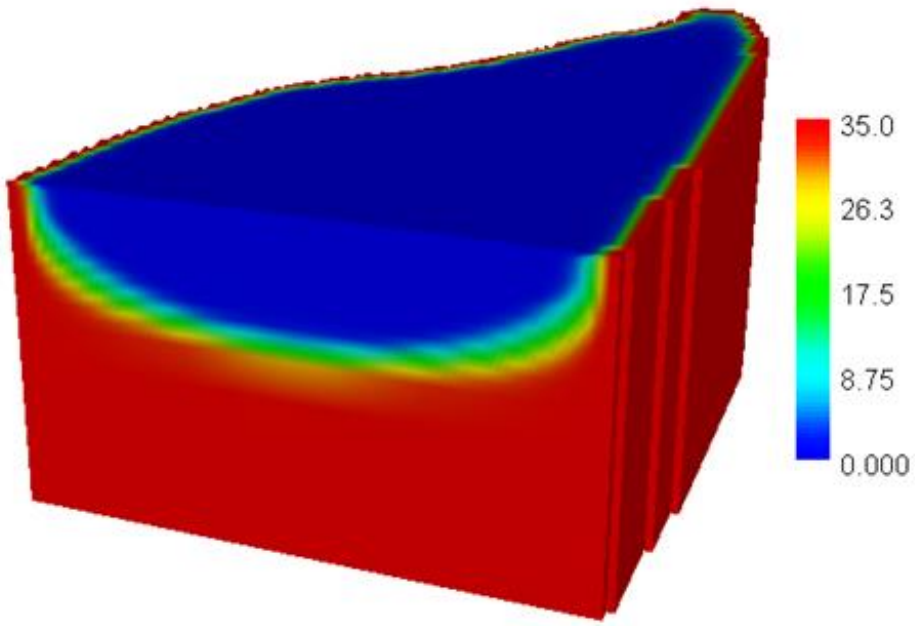

Figure 24. Cross-sectional view of the steady state model run of Ngatik Island. A calibrated hydraulic conductivity value of 25 m/d was found to produce a maximum lens thickness of 19.6 meters. Red indicates seawater salt concentration of 35 g/kg and blue indicates freshwater concentration of salt near 0 g/kg. A transitional zone is seen between the freshwater and seawater regions, with truncation occurring at a depth of 20 meters as the lens meets the contact between the Holocene and Pleistocene aquifers

Observed lens thickness values were then used to calibrate the hydraulic conductivity of windward islands, whose position on the atoll results in a higher hydraulic conductivity than that seen on leeward islands. The initial models were again run in the absence of coconut root extraction to allow the lens to develop while establishing a probable range of conductivity values. The first windward island considered was Deke Island on Pingelap Atoll. An initial hydraulic conductivity of 400 m/d was used following the findings of Bailey et al. (2008); this resulted in a lens thickness of 2.7 meters, well below the reported value of 4 meters. In an attempt to steer the model output towards the observed value of lens thickness, the hydraulic conductivity was lowered to encourage development of a larger freshwater zone.

It was determined that, in the absence of coconut palms, a hydraulic conductivity of 300 m/d was most accurate, yielding a freshwater lens thickness of 3.7 meters. Following these initial runs, coconut root extraction was introduced to further calibrate the hydraulic conductivity.

Using an extraction rate of 700 mm/yr, it was determined that a hydraulic conductivity of 200 m/d most accurately replicated the historical conditions on Deke Island, yielding a lens thickness of 3.72 meters. Figure 25 shows the location of both Pingelap and Deke Islands on Pingelap Atoll with their corresponding calibrated lens thickness.

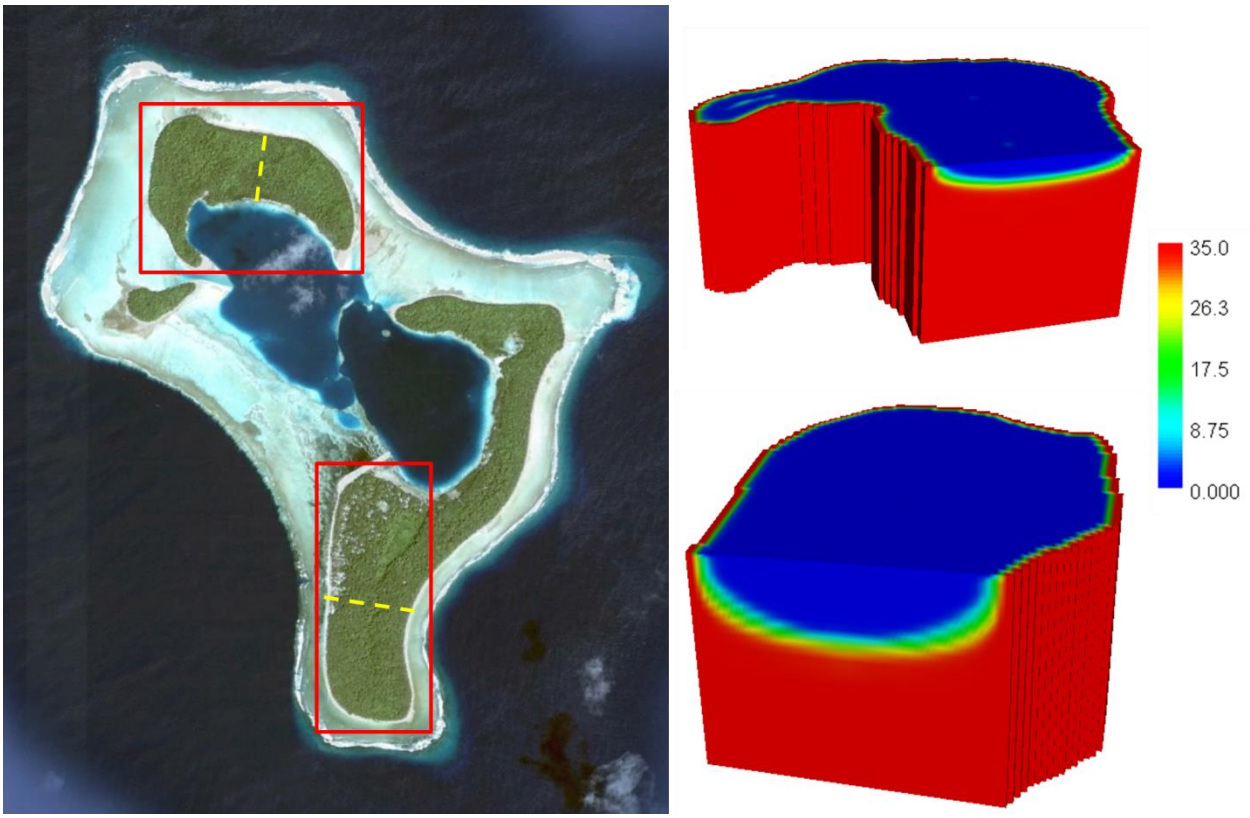

Figure 25. Cross-sectional views of the three-dimensional model output for Deke (above) and Pingelap (below) Islands on Pingelap Atoll (left). The calibrated hydraulic conductivity of Pingelap Atoll is 25 m/d, producing a lens thickness of 14.7 meters. The lens thickness of Deke Island was modeled at 3.72 meters using a hydraulic conductivity of 200 m/d.

The next windward island with observed freshwater lens thickness was Kahlap Island on Mwoakilloa Atoll. As done previously, the initial model was run in the absence of coconut root extraction to determine whether the calibrated hydraulic conductivity value for Deke Island was also appropriate for Kahlap Island. The first value of hydraulic conductivity used was 300 m/d, resulting in a lens thickness of 2.2 meters, almost one-third of the reported thickness of 6 meters. The hydraulic conductivity was again lowered to encourage development of a thicker freshwater lens. Using a hydraulic conductivity of 100 m/d, the model output a lens thickness of 5.64 meters. This calibrated hydraulic conductivity value of 100 m/d was also found to accurately replicate the observed thickness following the introduction of coconut palm transpiration.

After calibration, it was determined that islets located on the leeward side of atolls have hydraulic conductivity of 25 m/d while those located on the windward side have a hydraulic conductivity between 100 and 200 m/d. Using these calibrated values of hydraulic conductivity, each model was run using the average annual precipitation depth until they reached equilibrium; the results of these model runs are shown in Table 11.

Table 11. Calibrated model results for each of the 8 islands modeled. When available, the observed lens thickness for each island is provided as reference to the calibrated lens thickness and volume estimates. The location of each island on the atoll is also provided, with windward islands having a hydraulic conductivity of 25 m/d and leeward islands of 200 m/d.

Island	Atoll	Location on Atoll	Width (m)	Observed Lens Thickness (m)	Modeled Lens Thickness (m)	Modeled Lens Volume (m^3)
Deke	Pingelap	Windward	400	4	3.72	193,200
Pingelap	Pingelap	Leeward	750	16	15.55	1,421,560
Kahlap	Mwoakilloa	Windward	425	6	5.64	235,649
Ngatik	Sapwuahfik	Leeward	900	20	19.59	1,780,091
Nikahlap	Pakein	Leeward	550	--	13.67	1,131,384
Fassarai	Ulithi	Windward	200	--	0.27	1868
Mangejang	Ulithi	Windward	400	--	6.98	103,847
Mogmog	Ulithi	Windward	450	--	2.98	4208

The freshwater lens beneath Deke Island reached 3.72 meters in thickness, and contained just under 200,000 m^3. Pingelap's freshwater lens reached 15.55 meters in thickness and contained 1.4M m^3. The freshwater lens of Kahlap Island grew to be 5.64 meters thick and contained about 240,000 m^3. Ngatik Island, another leeward island, had a lens 19.59 meters thick and containing about 1.8M m^3. Nikahlap Island's lens grew to 13.67 meters thick and contained 1.13M m^3. The three islands on Ulithi Atoll, Fassarai, Mangejang, and Mogmog, has lens thicknesses of 0.27 meters, 6.98 meters, and 2.98 meters, respectively, and lens volumes of 1868 m^3, 104,000 m^3, and 4208 m^3, respectively. Visual representations of the calibrated lens thickness for all other islands are shown in Figures B8-B12 in Appendix II. Table 10 shows the calibrated model parameters.

Sensitivity Analysis

Sensitivity analysis was first performed for hydraulic conductivity; results from the analysis are shown in Table 12.

Table 12. Sensitivity analysis results showing the response of both the lens thickness and lens volume to incremental changes in hydraulic conductivity. Lens thickness values are reported in meters and lens volume in cubic meters.

Hydraulic Conductivity (m/day)		10	20	50	100	200	350	500
Mangejang	Thickness (m)	9.32	8.42	6.98	4.68	2.65	0.22	0.11
	Volume (m^3)	148992.5	137588.2	105135.3	65147.7	27873.8	1919.8	14.0
Fassarai	Thickness (m)	4.14	3.59	2.21	1.70	1.19	0.29	0.14
	Volume (m^3)	38455.2	23097.3	23246.8	25168.9	10827.3	2494.7	137.1
Nikahlap	Thickness (m)	15.63	15.55	13.62	9.46	7.00	4.69	3.63
	Volume (m^3)	1359075.4	1273722.7	1037038.7	751804.5	459852.2	236257.5	103821.2
Pingelap	Thickness (m)	17.60	17.56	13.49	8.44	6.22	4.68	2.68
	Volume (m^3)	1448916.3	1587191.9	1198567.9	813377.7	564176.0	344157.9	174681.8
Deke	Thickness (m)	10.82	11.55	10.78	7.74	5.19	2.70	1.69
	Volume (m^3)	361249.9	574523.3	661839.3	476898.8	285498.0	140595.4	60564.9

Hydraulic conductivity values ranged from 10 m/d to 500 m/d, with the intent to bracket all potential values and indicate how the lens thickness and volume changes with each. At a hydraulic conductivity of 10 m/d the maximum values of both lens thickness and volume were observed for all islands. In most cases an increase in hydraulic conductivity corresponded to a linear decrease in lens thickness. On the larger islands (Pingelap and Nikahlap) the decrease was more logarithmic, showing rapid decline initially and then slowly trailing off at higher values of hydraulic conductivity. The relationship between hydraulic conductivity and lens thickness/volume is shown in Figure 26.

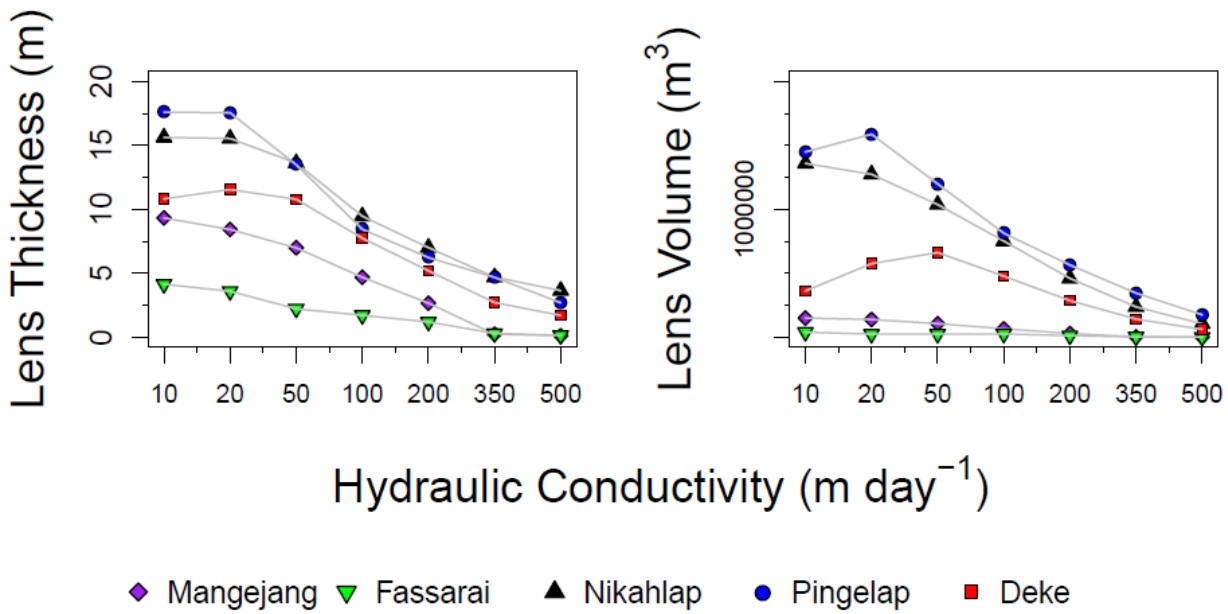

Figure 26. Relationship between lens thickness (top) and lens volume (bottom) to increasing values of hydraulic conductivity. Results show that hydraulic conductivity has a relatively strong influence on the development and size of the lens.

The effect on larger islands was more drastic for freshwater volume, with a steep, negative linear relationship observed as hydraulic conductivity increased. Smaller islands had a much shallower slope, with Fassarai showing almost no change in lens volume as hydraulic conductivity changed.

The next parameter considered during the sensitivity analysis was the depth to contact between the Holocene and Pleistocene aquifers; the results from the analysis are shown in Table A9 in Appendix I. The depth to contact limits the size of the freshwater lens, especially on larger atolls because it prevents the region of low chloride concentration from fully developing. The depth to contact was varied between 10 meters and 350 meters, though on most atolls this depth does not typically extend below 25 meters. Deeper contact was modeled to allow the lens to fully develop without being truncated to determine its potential size for each island. Using a contact depth of 10 meters, all islands showed the minimum value for lens thickness and volume. The development of the lens was truncated by the contact, severely limiting its size.

At contact depths of 20 meters and above, no considerable increase was observed in the lens thickness of any of the islands. The lens volume reached its maximum value at a depth to contact of 50 meters on all island but Nikahlap and Pingelap. Fassarai maintained a freshwater lens volume of approximately 20,000 m^3, Mangejang a volume of 120,000 m^3, and deke a volume of 800,000 m^3. The freshwater lens of Nikahlap and Pingelap Islands continued to increase in volume for each increasing depth to contact, though the increases in volume were relatively low as compared to lower values of depth to contact. The maximum value modeled for the lens volume beneath Nikahlap Island was about 1.15M m^3 while Pingelap showed a volume of approximately 1.4M m^3. The response of the modeled lens thickness and volume to contact depth are shown in Figure 27.

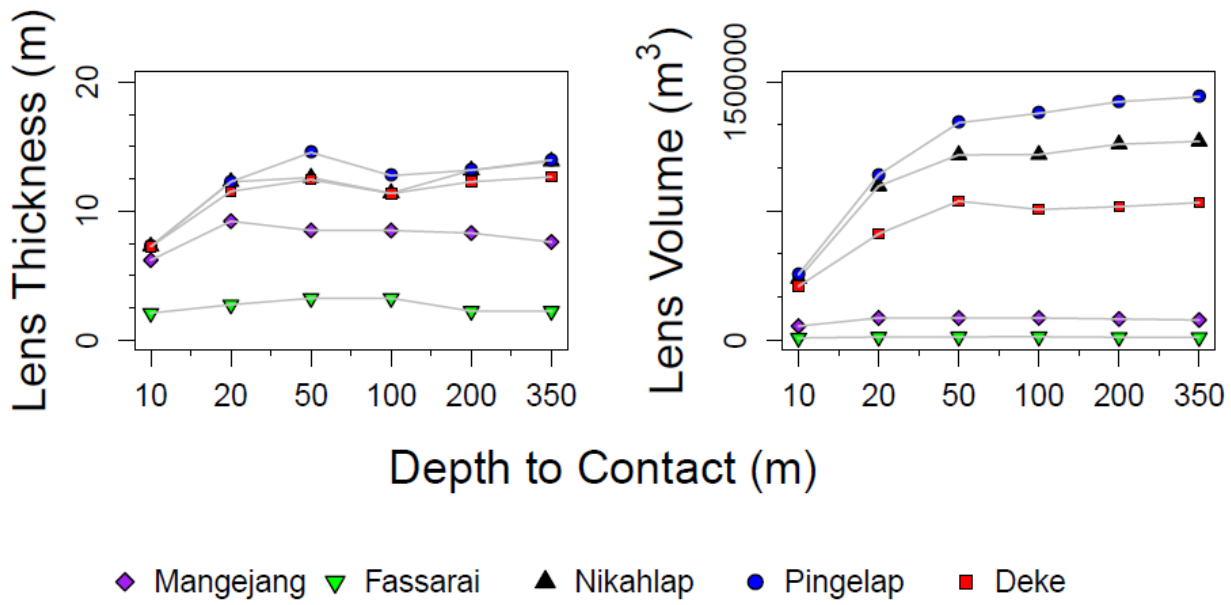

Figure 27. Reaction of the freshwater lens thickness (top) and volume (bottom) to increasing depth of contact between the upper Holocene and lower Pleistocene aquifers. Results indicate a strong influence until the contact falls below the natural size of the lens, after which time little influence is seen.

Total annual recharge depth was the next parameter investigated, the results from which are shown in Table A10 in Appendix I. The depth of recharge was varied from 0.5 m/yr to 4 m/yr, showing a strong influence on the thickness of the lens, as shown in Figure 28. The smaller islands of Fassarai and Mangejang showed a linear increase in lens thickness as the recharge depth increased. The other, larger islands showed a logarithmic increase in lens thickness with increasing recharge depth, with rapid increase at lower depths which then trailed off at higher depths. A similarly strong influence is seen on the lens volume, also shown in Figure 28. As seen previously, the smaller islands of Fassarai and Mangejang experienced a linear increase in lens volume as the recharge depth increased. Deke Island showed an increase in lens volume for all recharge depths between 0.5-1.5 meters, but then maintained a constant volume for all greater recharge depths. This indicates that the lens was truncated by the depth to contact and limited in size by the island geometry. The large islands of Pingelap and Nikahlap again showed a logarithmic increase in lens volume as the recharge depth was increased.

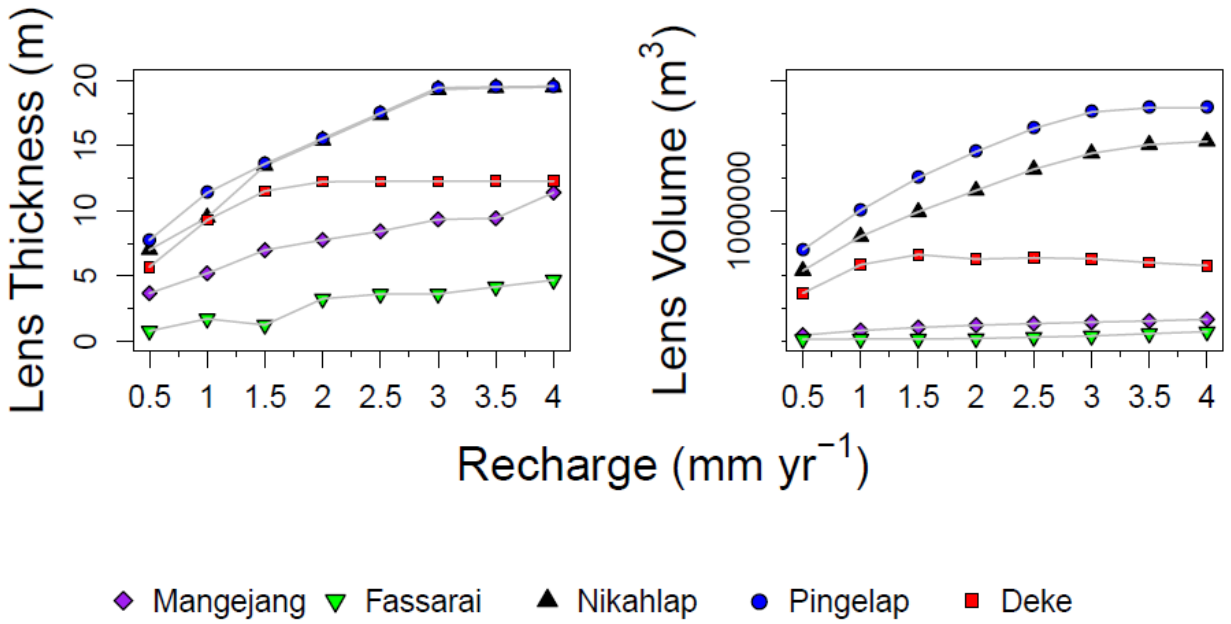

Figure 28. Time series of the fluctuations in lens thickness (top) and volume (bottom) to changes in the depth of annual lens recharge. The steep slope of the lines indicate a strong relationship, though for smaller islands like Mangejang and Fassarai it is less influential

The final parameter analyzed for its influence on the development of the freshwater lens was the rate of coconut root extraction. Rates of coconut root extraction were varied from 400 mm/yr to 800 mm/yr; this range was decided upon using data collected by Falkland (1994). The results of the analysis are shown in Table A11 in Appendix I. In almost all cases, the rate of coconut root extraction had an insignificant effect on both the freshwater lens thickness and volume. The smaller islands of Fassarai, Mangejang, and Deke showed virtually no decrease in either lens thickness or volume across the range of values for coconut root extraction. The larger islands of Pingelap and Nikahlap showed a shallow linear decrease in lens volume as coconut root extraction increased, but almost no change in lens thickness was observed. The results for the responses of the freshwater lens thickness and volume are shown in Figure 29.

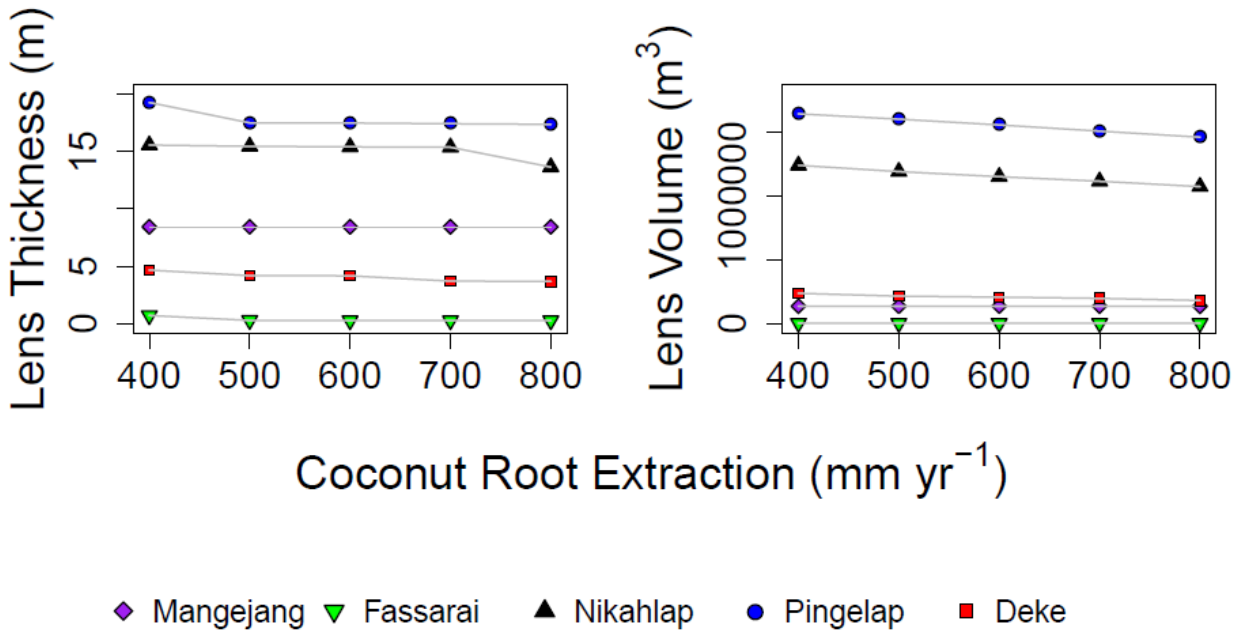

Figure 29. Response of the freshwater lens thickness (top) and volume (bottom) to varying depths of annual coconut root extraction. Results show a minimal influence as compared to the other parameters analyzed.

The results of this analysis indicate that while hydraulic conductivity and recharge depth both have an extreme influence on the thickness and volume of the freshwater lens, the same cannot be said of the depth to contact and the coconut root extraction rate. The depth to contact between the two aquifers had a limited effect on the size of the lens, showing more influence at shallower depths. As the contact became very deep, its influence was no long felt as the lens beneath each island was able to fully develop without truncation. The rate of coconut root extraction had almost no influence on any of the five islands analyzed. The calibrated models use a coconut extraction rate of 700 mm/yr, as suggested by the research conducted by Falkland (1994). The results of the transient sensitivity analysis performed on Deke Island are shown in Figure 30. The clustering of the results and highly similar modeled lens thickness for each extraction rate scenario reinforce the conclusion that coconut root extraction plays a minor role in the development and size of the freshwater lens.

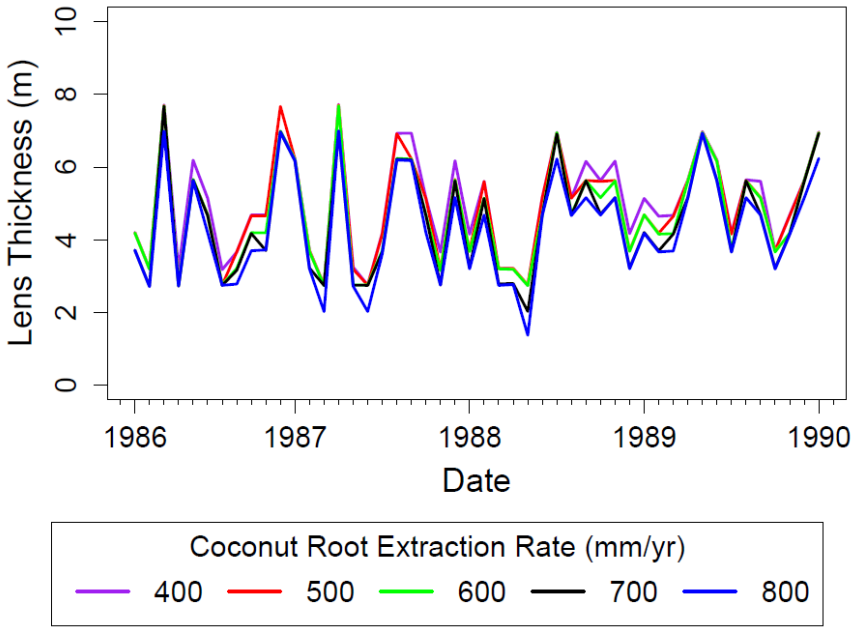

Figure 30. Sensitivity analysis results showing fluctuation in lens thickness on Deke Island for various depths of coconut root extraction, modeled to determine if its effect was more influential during transient-state simulation. Results indicate that the depth of annual extraction has almost no influence on the thickness or volume of the lens, with very little change observed between the different extraction rates.

Discussions and Conclusion

Three-dimensional models were developed using the USGS code SEAWAT to simulate the groundwater flow dynamics beneath Micronesian atoll islands. Islands selected for this study were Pingelap and Deke Islands on Pingelap Atoll, Kahlap Island on Mwoakilloa Atoll, Ngatik Island on Sapwuahfik Atoll, Nikahlap Island on Pakein Atoll, and Mangejang, Fassarai, and Mogmog Islands located on Ulithi Atoll. Islands were selected in both eastern (Pohnpei) and western (Yap) regions of Micronesia to capture the effects of climate variability on the development of the freshwater lens beneath the islands. Calibration was performed for islands with observed values of lens thickness to ensure model output accurately replicated historical values. It was determined that, at a coconut root extraction rate of 700 mm/yr, leeward islands generally have a hydraulic conductivity of 25 m/d and windward islands have a hydraulic conductivity of 200 m/d.

During calibration, it was found that a hydraulic conductivity value of 100 m/d was necessary for Kahlap Island to reach a lens thickness and volume similar to that observed. This apparent discrepancy in the calibrated value of hydraulic conductivity of windward islands is caused by the geometry of Kahlap Island. Similar to Fassarai Island, Kahlap Island can be viewed as an infinite strip island due to its extremely low width to length ratio. These sorts of islands have extremely low values of lens thickness and volume as compared to larger, rounder islands. The lens thickness recorded by (Anthony, Vacher, & Quinn, 2007) was just for the northern part of Kahlap, where a large average island width is seen. Because the three-dimensional model developed for Kahlap Island envelops the entire island's geometry, a lower hydraulic conductivity value was necessary to compensate for the narrower infinite-strip section of the island further south.

A sensitivity analysis was performed to investigate the influence of various parameters on the development and size of the freshwater lens. Parameters analyzed include the hydraulic

conductivity, depth to contact between the upper Holocene and lower Pleistocene aquifers, the annual depth of recharge, and the coconut root extraction rate. It was found that the hydraulic conductivity and annual recharge depth both played a major role in the development and size of the freshwater lens. These results had already been inferred by other modeling groups when analyzing the atoll islands two-dimensionally. The depth to contact, while it can have a major influence on the development of the freshwater lens if too shallow, has no effect on the lens once it passes the maximum potential depth of that lens. This maximum potential depth is island specific, and depends mainly on the geometry and surface area of that island.

The rate of coconut root extraction had almost no influence on any of the islands modeled, indicating that coconut palms do not compete as excessively for freshwater as previously thought. Further modeling work was to be performed to investigate the effect of coconut palm density and clustering on islands, but following the results of this sensitivity analysis it was determined that further work was redundant. It is noted that values for the thickness and volume of the freshwater lens as determined by the sensitivity analysis are not indicative of the actual values for each island. The modeled values are instead a relative measurement of the influence of each parameter on the lens size and development, having been obtained using standardized parameter values which did not necessarily represent the geologic or climate characteristics of either region.

ESTIMATION OF FUTURE FRESHWATER LENS VOLUME USING SIMULATED CLIMATE DATA

Introduction

The freshwater supply on atoll islands is very fragile, consisting solely of groundwater and captured rainwater. Optimization of RWCS using system design curves is a viable method to help ensure adequate water supply during drought periods. Systems designed at high rates of reliability are expected to supply enough freshwater to sustain communities a majority of the time. Typically, the larger the system the higher volume of water it can yield during the same rainfall event as compared to a smaller system designed for fewer people. Despite the design of system at high rates of reliability, when community use of captured rainwater outpaces the length of drought periods, the volume of available freshwater is depleted. It is during such times that groundwater is turned to as the remaining primary source of freshwater before it must be imported from the surrounding larger islands.

During drought periods, the lens beneath atoll islands drastically thins, usually becoming slightly brackish. Though the water quality is not as high as when there is plentiful rainfall to replenish the lens, it is still of adequate quality for human consumption until such time as precipitation rates increase. Lens recovery following such events usually takes time as well, requiring high volumes of recharge to flush seawater out of the aquifer and reestablish a region of low chloride concentration. In some cases, this process can take up to several years to fully restore the lens to previous conditions (Bailey, Jenson, & Olsen, 2009). When water must be imported from the larger surrounding volcanic islands, it is done so at great expense. Water was imported to atolls across Micronesia following a major drought in 1998, considered by many to be the worst drought in Micronesian history. Though water imported was pumped from ships to storage tanks located in island villages, heavy water rationing was required to extend the time over which the freshwater could be used

To prolong community use of fresh groundwater, water management practices must be implemented to ration out the remaining supply. Effective island water resources management involves knowledge of not only the daily per capita usage of island residents, but also an estimate of the sustainable yield of the freshwater lens as it fluctuates through time. Sustainable yield is the quantity of water that can be extracted from the freshwater lens over a long period without having adverse effects on the quality of water in the aquifer (Todd, 1959). Water quality degradation can occur if the pumping rate by island communities is too high, resulting in upconing of seawater and salinization of the freshwater region. To assist with successful freshwater resources management, numerical groundwater estimation of the volume of the freshwater lens is performed using simulated future climate data.

Methods

Model Input

Using the three-dimensional flow and transport model SEAWAT, models were created to numerically estimate the volume of freshwater beneath atoll islands. Calibrated models for several atoll islets located in Pohnpei and Yap States were developed, as discussed in Chapter 5. These models, due to their representative sizes and locations, serve not only to directly compute the volume of freshwater beneath the islands, but also provide a reference as to what volume can be expected beneath other similar atoll islets. Some of the islands modeled are circular, showing lens development patterns characteristic of generic islands throughout Micronesia. The long,

skinny islands chosen are typical of "infinite-strip" islands recognized in literature as being simpler to model two-dimensionally. By choosing this type of island for use in three-dimensional model development, thickness and volume estimates produced by other two dimensional modeling efforts can be compared. In Pohnpei State in eastern Micronesia, islands modeled include Deke, Pingelap, Kahlap, Ngatik, and Nikahlap; in Yap State in western Micronesia, Fassarai, Mangejang, and Mogmog Islands were modeled. In depth discussion of the development and calibration of these models can be seen in Chapter 5. Calibration results indicate that windward islands have a hydraulic conductivity of 25 m/d while leeward islands have a higher value of hydraulic conductivity of approximately 200 m/d.

Future simulated climate data was extracted from the CMIP5 database for four representative concentration pathway (RCP) forcing scenarios. Each RCP scenario represents a different greenhouse gas emission rate and mitigation strategy. Due to computation and time constraints, only the RCP2.6 and RCP8.5 forcing scenarios were chosen to estimate future atoll groundwater supply. RCP2.6 is a low emission, high mitigation scenario in which atmospheric greenhouse gas concentrations are expected to either maintain their current level or decline by the year 2050. Contrarily, RCP8.5 is a high emission scenario in which no mitigation strategies are implemented and greenhouse gas emissions drastically increase. The use of these two scenarios effectively brackets the other RCP pathways, representing low and high emissions scenarios between which the RCP4.5 and RCP6.0 forcing scenarios statistically fall. The top three CMIP5 GCMs were chosen for use in the future SEAWAT model runs, extending from 2010 to 2050. The top three chosen show variability between various GCM outputs while still maintaining the ability to accurately replicate historical climate patterns.

Soil Water Balance Calculation

The depth of recharge to the freshwater lens was calculated for each day of the study period using a soil water balance. The evapotranspiration for each day was first estimated by the Penman-Monteith equation, using simulated future values of relative humidity and net incoming solar radiation extracted from CMIP5 and daily values of wind speed obtained from historical averages. Using historical wind speed data obtained for both Yap and Pohnpei States, the wind speed for each day of the year from 1952-2006 was averaged to give a single value for each. This daily average wind speed was then extrapolated into the future, assuming a negligible deviation in wind patterns from the calculated average. A soil water balance was set up to estimate the volume of recharge to the freshwater lens for each day of the 2010-2050 study period. After establishing an operating range of soil moisture, the depth of soil moisture deficit was tracked for each day using the simulated values of precipitation and evapotranspiration. Excess water which entered the aquifer after the soil moisture deficit had been filled contributed to recharge of the lens. This method was used to determine recharge to the lens in place of the average values used during model calibration because it was unsure how recharge rates may fluctuate with changing future climate conditions.

During model development, steady-state model runs estimated recharge in Pohnpei State as 63% of rainfall and in Yap State as 54% of rainfall. In both RCP forcing scenarios considered, average recharge in Pohnpei state calculated using the soil water balance method amounted to approximately 71% and in Yap State to 59%. Had the average historically-based recharge patterns been used, recharge to the freshwater lens would have been underestimated.

Once the recharge for the study period had been determined, the daily values within each month were summed to obtain a monthly total, which was then evenly redistributed to each day.

It was determined during early model runs that, given daily values of recharge, rapid fluctuations in depth were not captured by model output, and did therefore not accurately represent the behavior of the lens. By equally distributing the total depth within a month to each of its days, the model was able to adapt to changes in recharge depth and allow the lens to react. The model was also operated on an hourly time-step to allow the lens more time to reach a steady-state for each day of applied recharge.

Results

Lens Thickness and Volume for the RCP2.6 Forcing Scenario

The results of the future models runs are presented to give a detailed overview of how changing climate conditions may affect the thickness and volume of the freshwater lens. The first forcing scenario presented is RCP2.6, which represents the lowest increase in atmospheric greenhouse gas concentrations by 2050. The statistically top-performing models for Pohnpei State are CNRM-CM5, GISS-E2-R, and GFDL-CM3. To give a visual representation of the magnitude and fluctuation of lens thickness and volume, a time series for the RCP2.6 forcing scenario over the period 2010-2050 for Nikahlap Island is shown in Figure 31. Though each of the GCMs show extreme drought at different time, it is observed that output from GFDL-CM3 shows a much more consistent depth of recharge to the freshwater lens. This results in lens thickness that is more consistently near the average, with a smaller standard deviation. Time series of fluctuation in lens thickness and volume of the other islands in Pohnpei State are shown in Appendix II.

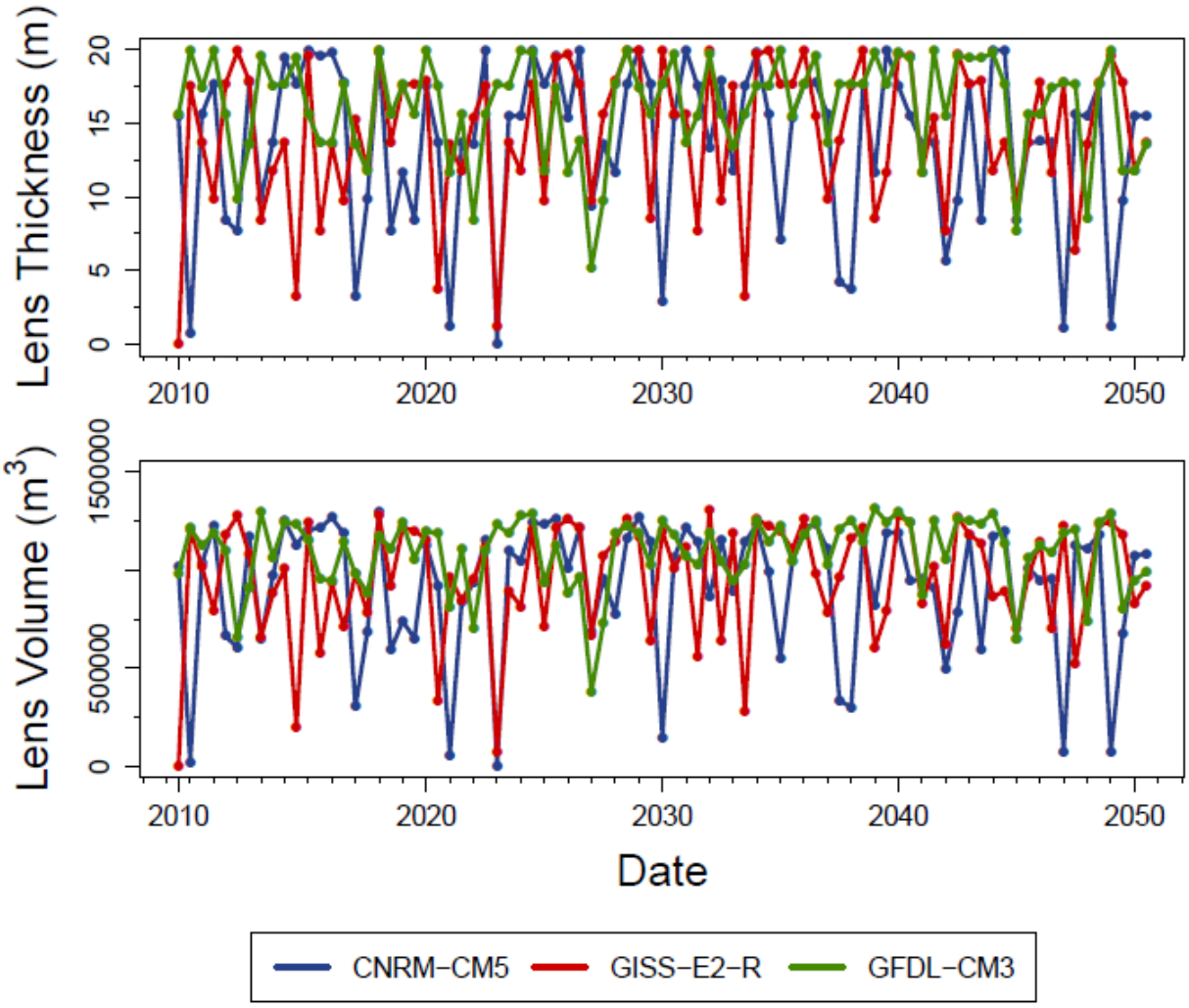

Figure 31. Time series of the fluctuation in lens thickness (top) and volume (bottom) during the study period from 2010-2050. More frequent drought is observed to occur in the CNRM-CM5 and GISS-E2-R output, though the average lens thickness and volume is approximately the same for all three climate models.

The time series fluctuation in lens thickness and volume for Mangejang Island in Yap State are shown in Figure 32. As observed in the time series for Nikahlap Island, each GCM evoked a different response to the lens based on its modeled frequency and magnitude of drought and heavy rainfall events. Lens thickness values are much lower for Mangejang Island, averaging around 7 meters as opposed to the much higher lens thicknesses observed for leeward islands in Pohnpei State. This is attributed both to its windward location on Ulithi Atoll, resulting in a much higher hydraulic conductivity, and the lower rainfall depth in Yap State.

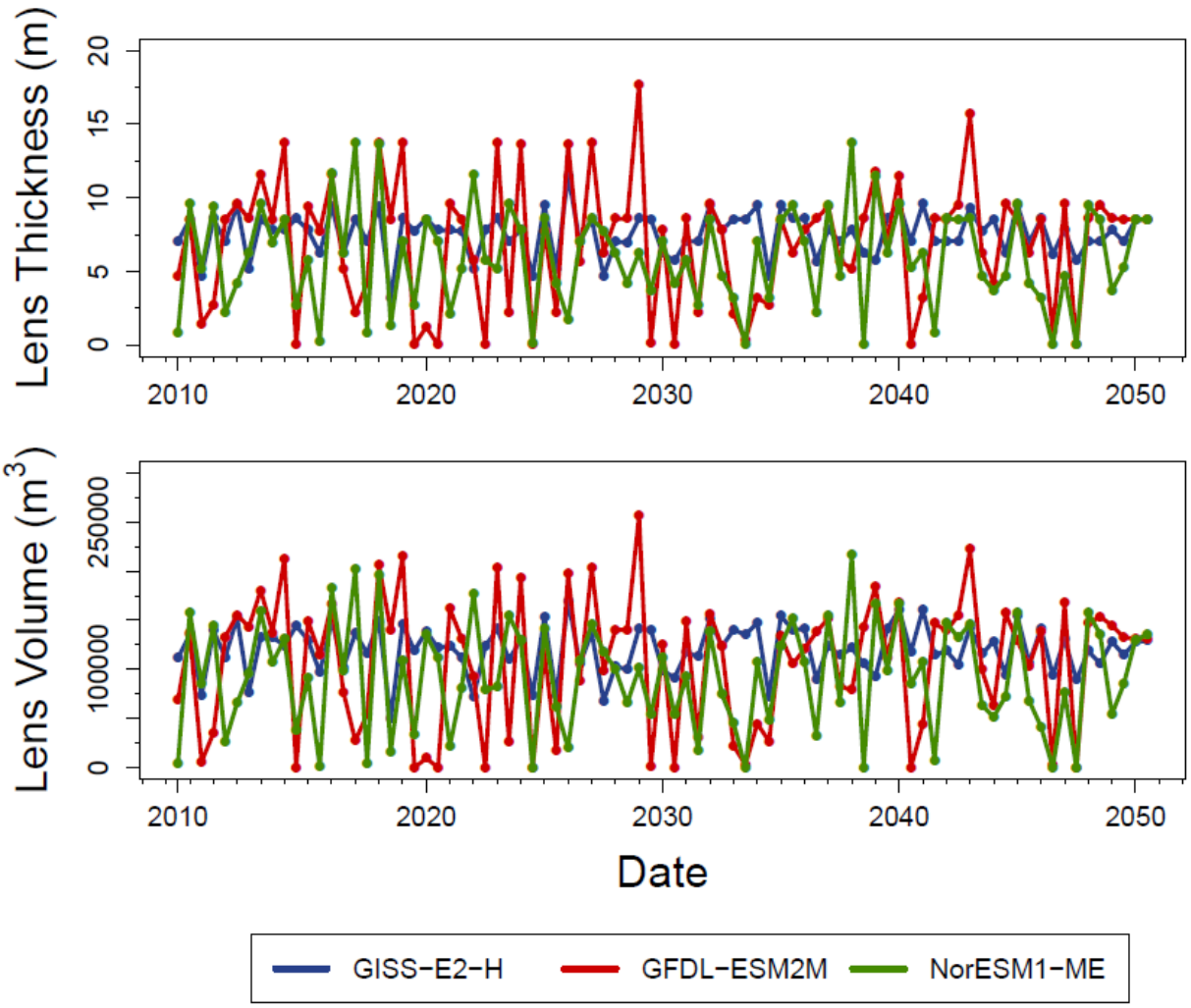

Figure 32. Time series of the changes in lens thickness and volume for Mangejang Island in Yap State from 2010-2050. Output from GFDL-ESM2M indicates more frequent periods of heavy rainfall, while that from NorESM1-ME shows more frequent drought.

The time series plots for Fassarai and Mogmog Islands in Yap State can be found in Appendix II. Figure 33 shows the frequency histograms of the lens thickness for Deke Island produced by output from the three GCMs.

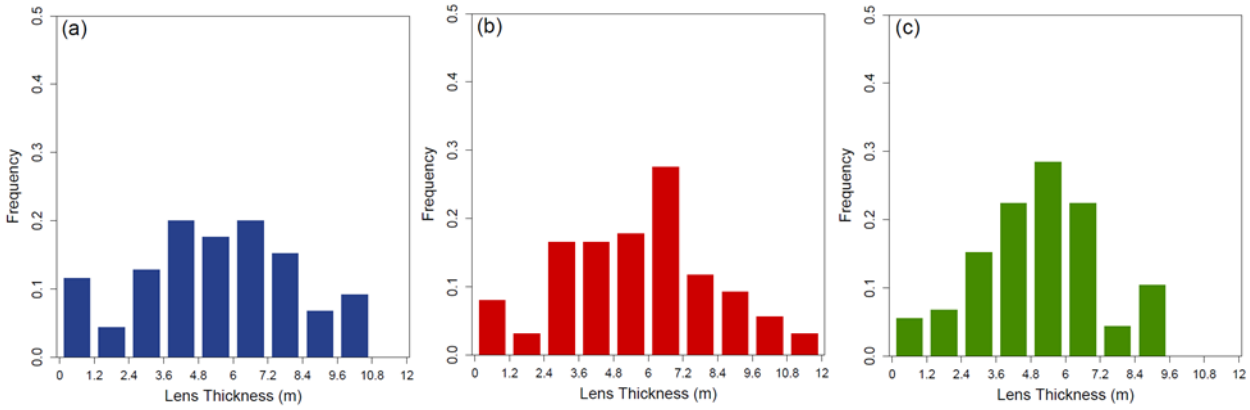

Figure 33. Frequency distribution of the lens thickness of Deke Island for the RCP2.6 forcing scenario. The distributions are relatively normally distributed, the lens depletion generally seen between 5-10% of the time.

Figure 33a corresponds to the lens thickness produced by CNRM-CM. Lens thickness values are mostly clustered towards the center of the range of values, hovering between 2.4 and 8.4 meters a majority of the time. For just over 10% of the 2010-2050 period, the lens thins to less than 1.2 meters, indicating that the freshwater volume is largely depleted. Nearly 20% of the study period showed a lens thickness between 6 and 7.2 meters. The lens thickness values for GISS-E2-R are shown in Figure 33b. This GCM resulting in similar results to that of CNRM-CM4 in that a majority of the time the lens had a thickness between 2.4 and 8.4 meters. However, close to 8% of the study period showed a lens thickness of less than 1.2 meters. It was from the output of this GCM that the deepest freshwater lens of all three of the GCM simulations was observed, reaching 12 meters in thickness. The values for lens thickness produced by output from GFDL-CM3 are much more normally distributed, as shown in Figure 33c. More than 80% of lens thickness value fell between 2.4 and 7.2 meters. This indicates that, based on this climate model output, the lens will maintain a minimal volume of freshwater a majority of the time. Only 4% of the values fell below 1.2 meters in thickness.

The frequency histograms of lens thickness for Kahlap Island are shown in Figure 34. As seen in Figure 34a, which corresponds to lens thickness values produced by CNRM-CM5, the values are right skewed, with a lens thickness over 6 meters seen over 60% of the time.

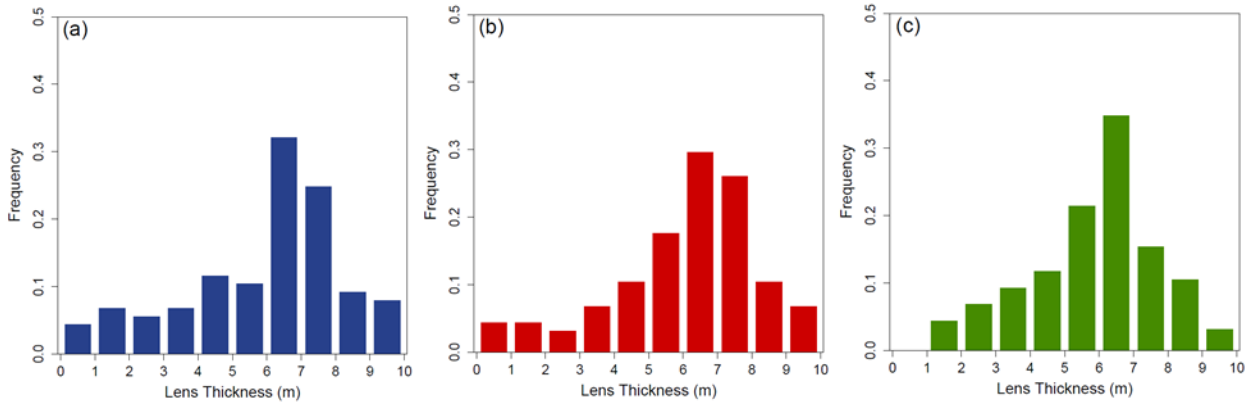

Figure 34. Lens thickness frequency distributions of the top three GCMs for Kahlap Island in Pohnpei State. Results from all three models indicate that a lens thickness betwen 6 and 7 meters is most common.

Other lower values of lens thickness showed statistical uniformity in their frequency, with lens thickness values below 1 meter seen only 3% of the time. Lens thickness values for GISS-E2-R

are displayed in Figure 34b, which also shows a heavy right skew of values. Values of lens thickness below 4 meters were only modeled 12% of the time. For a majority of the study period, lens thickness values fluctuated between 6 and 8 meters. Similar results are seen in Figure 34c, which shows the lens thickness frequency histogram for GFDM-CM3. For this climate dataset, lens thickness fluctuated between 6 and 7 meters for nearly 40% of the study period.

Figure 35 shows the lens thickness frequency histograms for Pingelap Island. In Figure 35a and Figure 35b, which show results from CNRM-CM5 and GISS-E2-R, more than 30% of lens thickness values fell between 18 and 20 meters.

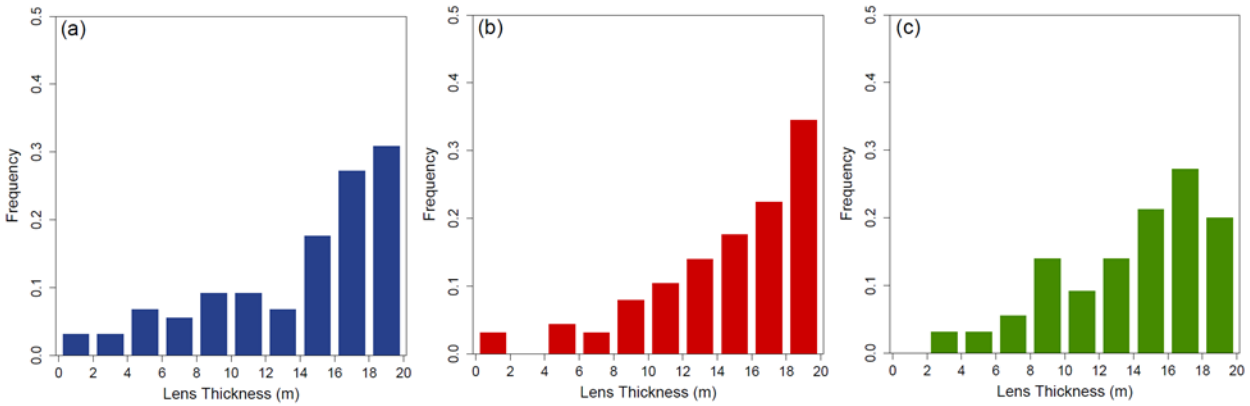

Figure 35. Frequency distributions of the lens thickness for the top three GCMs for the RCP2.6 forcing scenario on Pingelap Island. The distributions are heavily right-skewed, indicating that for a majority of the study period the lens was at its maximum volume.

This indicates that there was sufficient rainfall to fully replenish the lens and flush out seawater. Lens thickness values truncate at 20 meters as the lens encountered the contact between the upper Holocene and lower Pleistocene aquifers. Only a small portion of the time did the lens thickness reach below 2 meters, indicating that the freshwater had been depleted. Figure 35c, which corresponds to GFDL-CM3, shows a slightly different distribution. Though still right skewed, more than 60% of the time the lens was more than 14 meters thick. As compared to the other two GCMs, a larger portion of the study period showed a lens of lower thickness. Despite its reduced freshwater volume the lens under this GCM output never depleted, and maintained at least 2 meters of thickness for the entire study period.

Patterns of lens thickness for Nikahlap Island are fairly similar to those seen for Pingelap Island, the frequency distributions of which are shown in Figure 36.

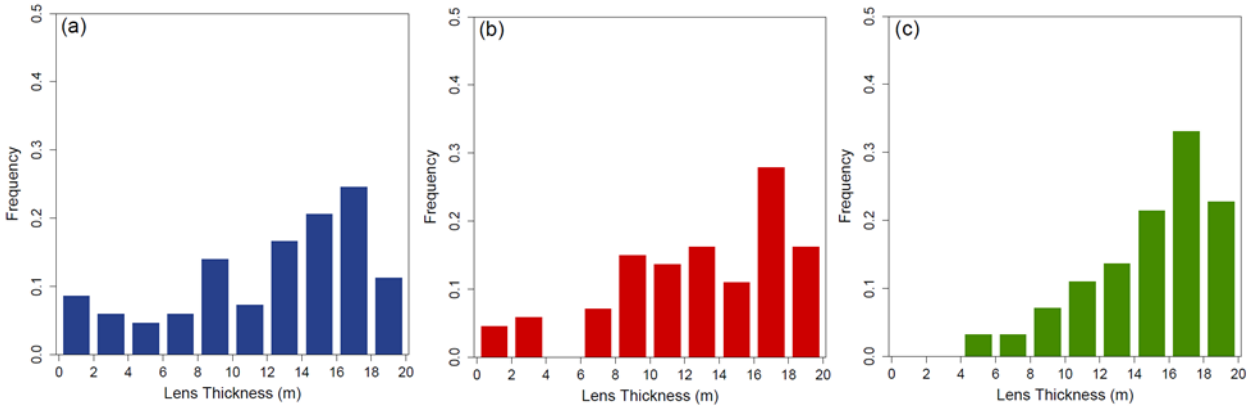

Figure 36. Lens thickness frequency distributions for Nikahlap Island under the RCP 2.6 forcing scenario. Similar to those seen for Pingelap Island, the distributions are right-skewed, though there is more frequent lens depletion seen in output from CNRM-CM5 (a).

Each of the lens reactions to the GCM output show a right skew, with larger values of lens thickness seen a greater portion of the study period. Figure 36a corresponds to output from CNRM-CM5. Though it is relatively uniform as compared to output from the other two GCMs, a lens thickness above 14 meters is seen over 50% of the time. Output from this climate dataset also caused the lens to thin below 2 meters for nearly 10% of the study period. The frequency histogram of lens thickness produced by output from GISS-E2-R is shown in Figure 36b, in which is seen that for nearly 30% of the study period the lens was between 16 and 18 meters thick. Figure 36c shows the greatest right skew, with over 70% of lens thickness values above 14 meters.

The frequency histograms of lens thickness for Ngatik Island show perhaps the greatest amount of skew of any island modeled under the RCP2.6 forcing scenario, results from which are shown in Figure 37.

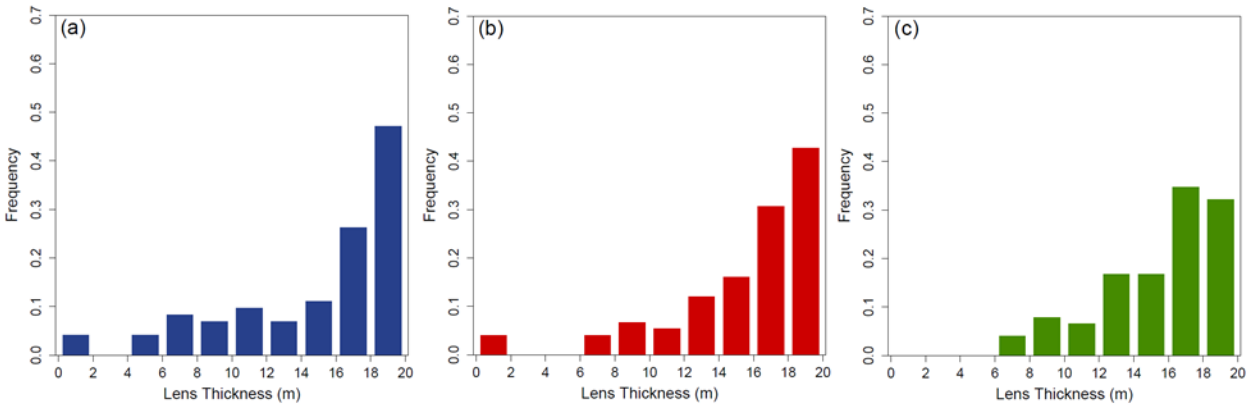

Figure 37. Frequency distributions of lens thickness for the top three GCMs for Ngatik Island. Right-skew indicates that the lens was near its maximum volume for a large portion of the study period.

The lens thickness from all three of the GCM outputs exceeded 16 meters at least 70% of the time. This indicates that drought in the region did not significantly affect the thickness of the lens. The freshwater lens beneath Nikahlap Island, frequency histograms for which are displayed in Figure 36, reacted differently to GCM output. For CNRM-CM5, lens thickness for nearly 5% of the study period was below 2 meters, indicating that the freshwater had become largely salinized. A similar trend is seen from the output of GISS-E2-R, in which about 4% of the time a

lens thickness below 2 meters was modeled. Results were much different for GFDL-CM3, however, with the lens never thinning past 6 meters and a lens thickness above 14 meters seen a majority of the time.

The lens thickness frequency distributions for Yap State are highly dissimilar to those produced by GCM output for Pohnpei State. Figure 38 shows the frequency histograms for Mangejang Island; all three of the GCMs produced very different frequency distributions.

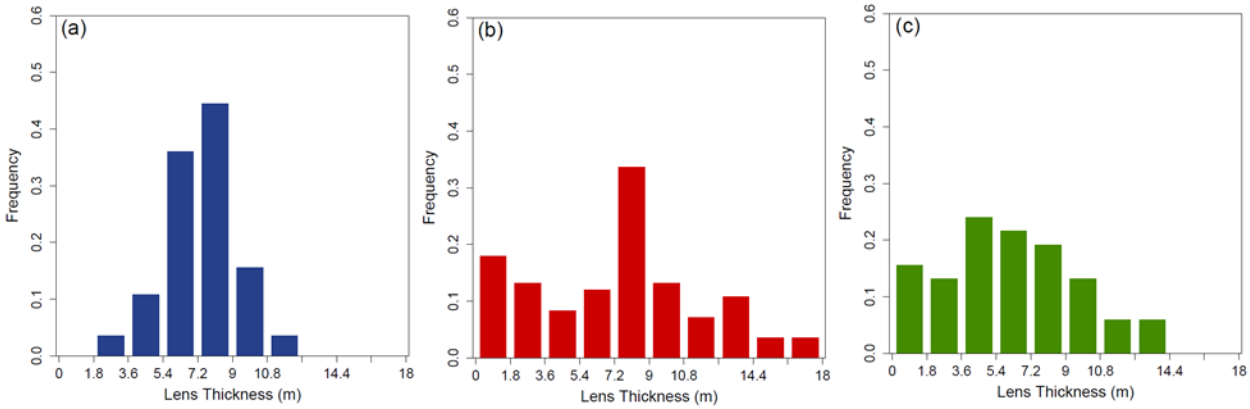

Figure 38. Lens thickness frequency distribution for the top three GCMs for Mangejang Island in Yap State. The distribution for GISS-E2-H (a) is uniformly distributed, while those for (b) GFDL-ESM2M and (c) NorESM1-ME are more uniform with frequent lens depletion.

Figure 38a shows the reaction of the lens to output from GISS-E2-H, which produced a normally distributed frequency with lens thickness maintained between 5.4 and 9 meters nearly 80% of the study period. Output from GFDL-ESM2M incited a much different reaction from the lens, showing a complete freshwater depletion nearly 20% of the time. During this same period, however, lens thickness remained between 7.2 and 9 meters almost 40% of the time. The frequency distribution from NorESM1-ME again showed a dissimilar distribution to the other two outputs, being somewhat left skewed with a lens thickness between 3.6 and 9 meters modeled nearly 60% of the study period. Lens depletion was quite common under this scenario as well, modeled just over 15% of the time.

Figure 39 shows the frequency distributions of lens thickness for Fassarai Island in Yap State. Due to the extremely narrow island geometry, land surface area beneath which the lens can develop is limited. For all three of the top-performing GCMs for Yap State, a lens thickness below 0.3 meters was seen for 60-80% of the study period. This is also due to the windward location of Fassarai Island on Ulithi Atoll, resulting in a higher hydraulic conductivity value and lower overall lens volume.

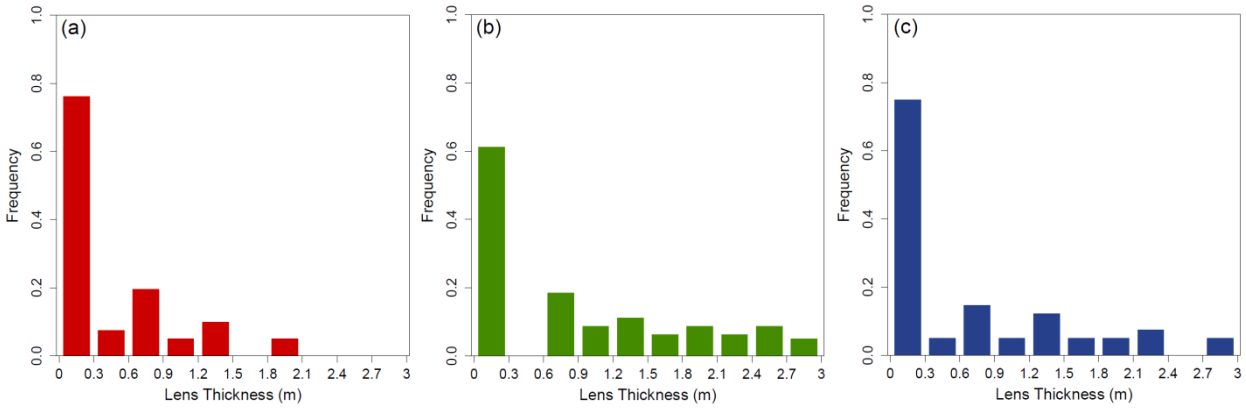

Figure 39. Lens thickness frequency distributions for Fassarai Island in Yap State for the RCP2.6 forcing scenario. The top-performing GCMs for Yap State were (a) GISS-E2-H, (b) GFDL-ESM2M, and (c) NorESM1-ME.

The lens thickness frequency distributions for Mogmog Island are shown in Figure 40. As observed for the other two islands modeled in Yap State, lens depletion is rather common, occurring for over 20% of the study period for the distributions in Figure 40b and Figure 40c. While the lens depletes relatively frequently, it often has a thickness and volume much greater than that seen for Fassarai Island, due mostly to the semi-circular geometry and relatively. low length to width ratio. The geometries of each island can be seen in Appendix II.

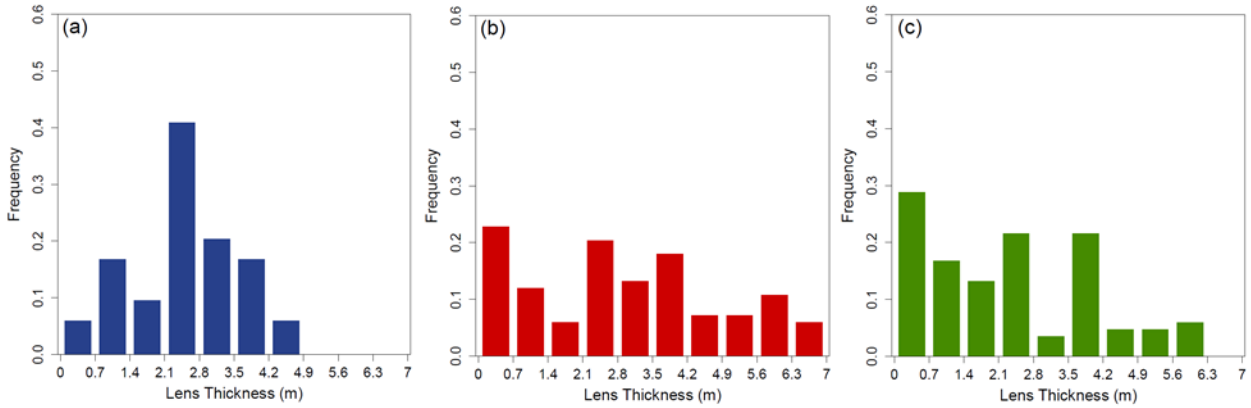

Figure 40. Lens thickness frequency distributions for Mogmog Island in Yap State for the RCP2.6 forcing scenario. The top-performing GCMs for Yap State were (a) GISS-E2-H, (b) GFDL-ESM2M, and (c) NorESM1-ME. Though distribution (a) is uniformly distributed with an average lens thickness between 2.1 and 2.8 meters, the distributions shown in (b) and (c) are left skewed, with lens depletion seen over 20% of the time.

Table 13 shows the average lens thickness for each GCM over the study period in the RCP2.6 scenario, and the corresponding standard deviation as an indicator of how frequently the lens was depleted or reached the contact between the dual aquifers.

Table 13. Average and standard deviation of lens thickness on each of the islands modeled for the top three GCMs in the RCP2.6 forcing scenario. Those with a higher standard deviation indicate more frequent prediction of drought and wet periods.

	GCM	Deke	Pingelap	Kahlap	Ngatik	Nikahlap	GCM	Fassarai	Mangejang	Mogmog
Average	**CNRM-CM5**	5.44	15.42	6.05	16.98	13.75	**GISS-E2-H**	0.43	7.57	2.53
Std. Dev.		2.70	4.84	2.20	4.30	5.53		0.38	1.46	1.06
Average	**GISS-E2-R**	5.73	15.95	6.32	17.33	14.34	**GFDL-ESM2M**	0.74	6.98	2.80
Std. Dev.		2.50	4.18	1.95	3.51	4.93		0.83	4.28	2.03
Average	**GFDL-CM3**	5.09	15.12	5.95	16.88	16.21	**NorESM1-ME**	0.49	5.97	2.09
Std. Dev.		1.95	4.02	1.75	3.14	3.37		0.63	3.40	1.72

Standard deviation values tend to be higher in larger islands with a thicker freshwater lens, as seen for Pingelap, Ngatik, and Nikahlap. From the results it is observed that standard deviation values for lens thickness produced by CNRM-CM5 are much higher than those of the GFDL-CM3. This is consistent with the frequency histograms produced for Pohnpei State, in which the output from CNRM-CM5 more regularly resulted in lens depletion. In the results from Yap State, the standard deviation values of the reaction of the lens to output from GFDL-ESM2M are much higher than those seen using GISS-E2-H. As observed in the frequency histograms produced for Yap State, GISS-E2-H showed a normal distribution of lens thickness while GFDL-ESM2M was more uniformly distributed.

Lens Thickness and Volume for the RCP8.5 Forcing Scenario

Results from the RCP8.5 forcing scenario are now presented, providing a comparison to the results of the RCP2.6 output and bracketing the spectrum of statistically plausible results produced by the RCP4.5 and RCP6.0 scenarios. Figure 41 shows the variation in lens thickness and volume for Nikahlap Island under the RCP8.5 scenario.

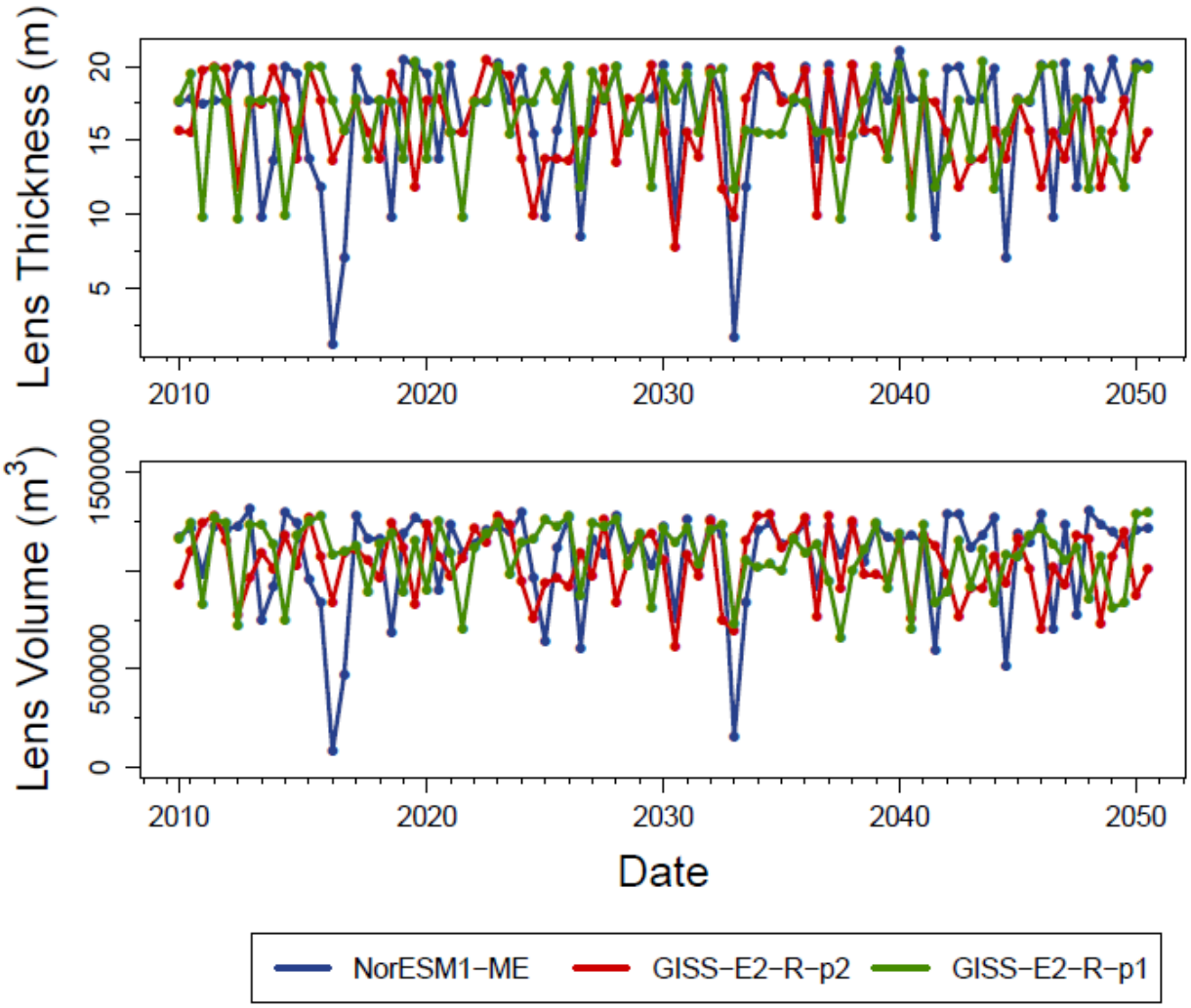

Figure 41. Time series of the fluctuation in lens thickness (top) and volume (bottom) for Nikahlap Island under the RCP8.5 forcing scenario. All three climate datasets show infrequent drought, indicated by the relatively low deviation from the average values of thickness and volume.

It is noted that, though the NorESM1-ME GCM showed intermittent periods of heavy drought, lens thickness values show drastically lower fluctuation than those seen during the RCP2.6 scenario. Conversely, fluctuations in lens thickness and volume under the RCP8.5 forcing scenario in Yap State were similar to those seen during the RCP2.6 forcing scenario; the modeled fluctuations in lens thickness and volume for Mangejang Island in Yap State are shown in Figure 42.

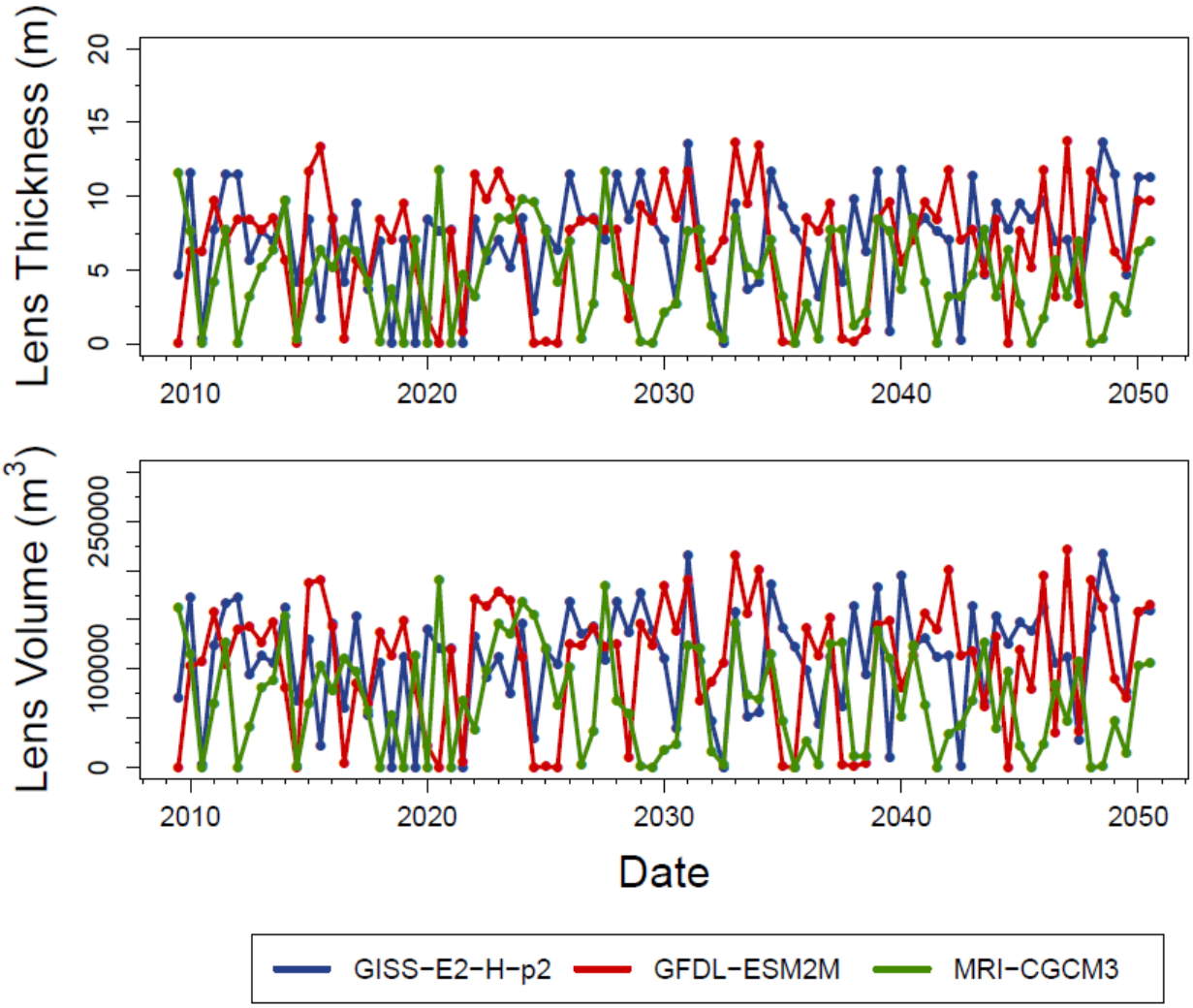

Figure 42. Time series of changes in lens thickness and volume during the RCP8.5 forcing scenario on Mangejang Island in Yap State. Results indicate that climate patterns predicted by RCP8.5 are similar to those forecasted by RCP2.6.

Due to both the lower annual rainfall depth seen in Yap State and the windward location of Mangejang Island on Ulithi Atoll, lens depletion was seen periodically throughout the 2010-2050 study period. Time series showing the fluctuation in lens thickness and volume for the other islands in Pohnpei and Yap States are seen in Figures B19-B24 in Appendix II. The lens thickness frequency distributions of the output from the top three GCMs on Deke Island are shown in Figure 43.

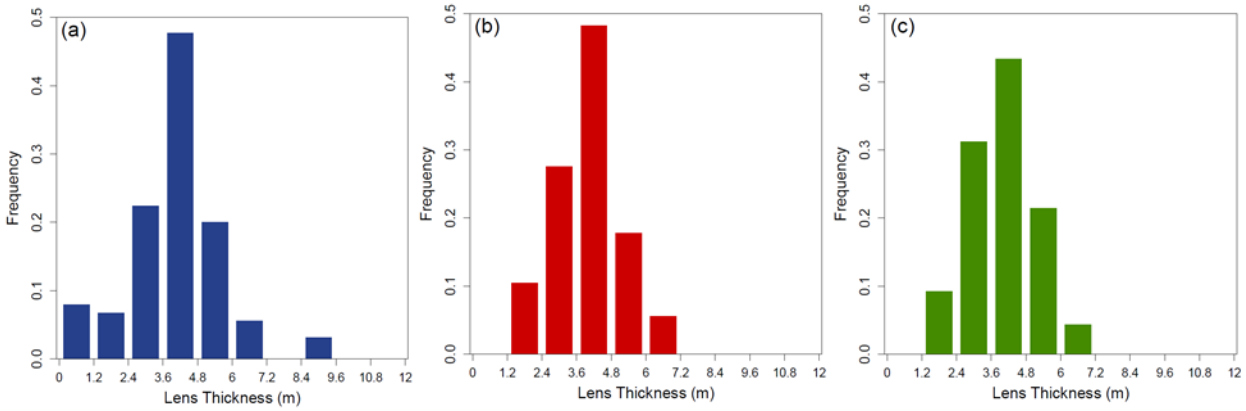

Figure 43. Lens thickness frequency distributions for Deke Island in Pohnpei State for the RCP8.5 forcing scenario. Output from the top three GCMs is shown: (a) NorESM1-ME, (b) GISS-E2-R-p2, and (c) GISS-E2-R-p1

The distribution of the lens thickness for each of the GCMs is normally distributed, with values between 3.6 and 4.8 meters seen over 40% of the time in each. NorESM1-ME was the only GCM to show lens depletion, which occurred for nearly 10% of the study period. The frequency distributions for Kahlap Island, shown in Figure 44, are also normally distributed, with a lens thickness between 7.5 and 9 meters seen for nearly 50% of the study period for each of the GCMs modeled. Lens depletion was again seen from output of NorESM1-ME, which forecasted exhaustion of the freshwater region for nearly 5% of the time. As compared to the lens thickness frequency diagrams corresponding to the RCP2.6 forcing scenario, lens depletion is relatively infrequent and the average lens thickness is high a majority of the time.

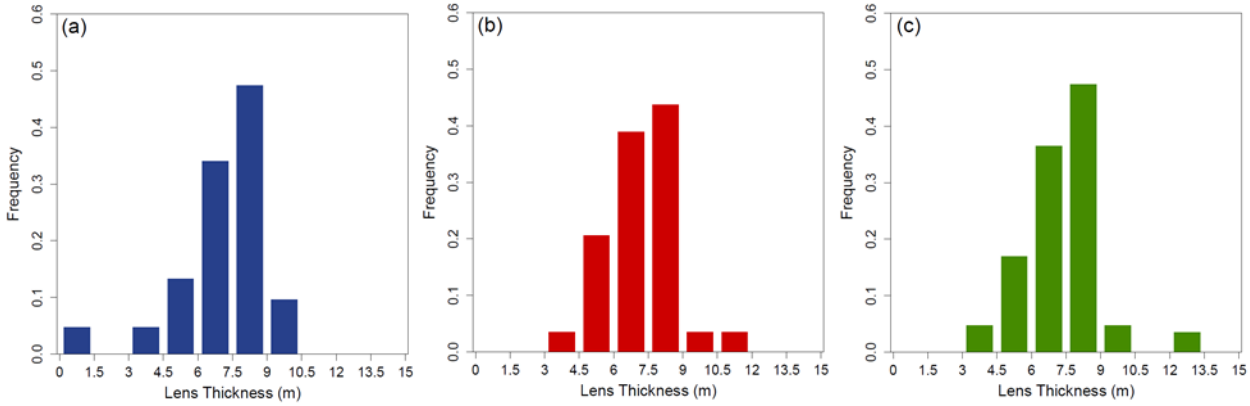

Figure 44. Lens thickness frequency distributions for Kahlap Island in Pohnpei State. The top performing GCMs for the RCP8.5 forcing scenario were (a) NorESM1-ME, (b) GISS-E2-R-p2, and (c) GISS-E2-R-p1

The lens thickness frequency distributions for Nikahlap Island are shown in Figure 45. As compared to the frequency distributions for the RCP2.6 forcing scenario, the lens thickness for the GCM outputs are highly right skewed. This indicates that the lens was thicker a higher portion of the time, and that less frequent aquifer salinization occurred.

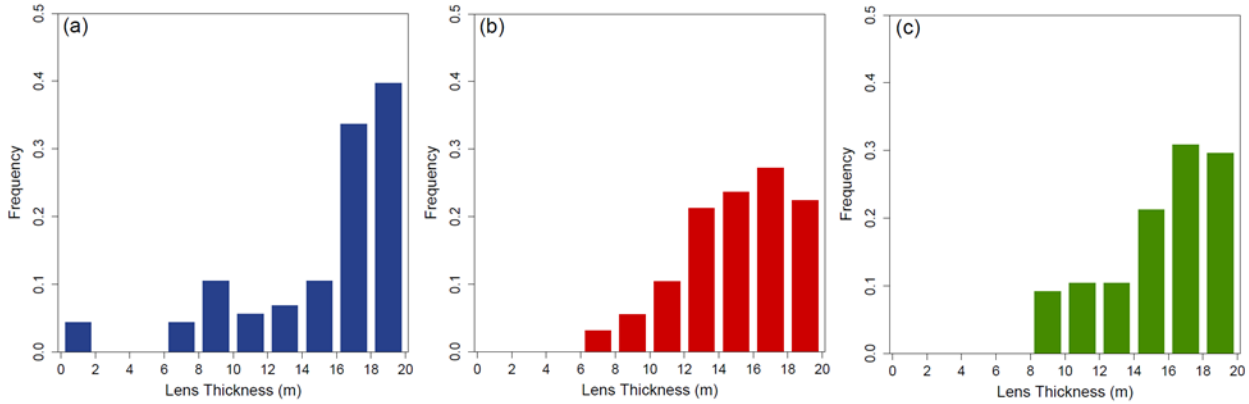

Figure 45. Lens thickness frequency distribution for Nikahlap Island under the RCP8.5 forcing scenario. The distributions show heavy right-skew, similar to those seen under the RCP2.6 forcing scenario, with lens depletion seen only for NorESM1-ME output

Figure 46 shows the frequency distributions of the lens thickness for Pingelap Island. The results from each GCM output are similar to those for Nikahlap Island, showing heavy right skew, and indicating that for a majority of the study period the lens had a high freshwater volume. The lens thickness did not generally deplete to levels lower than those sustainable for community living, with values above 4 meters of thickness seen in each case.

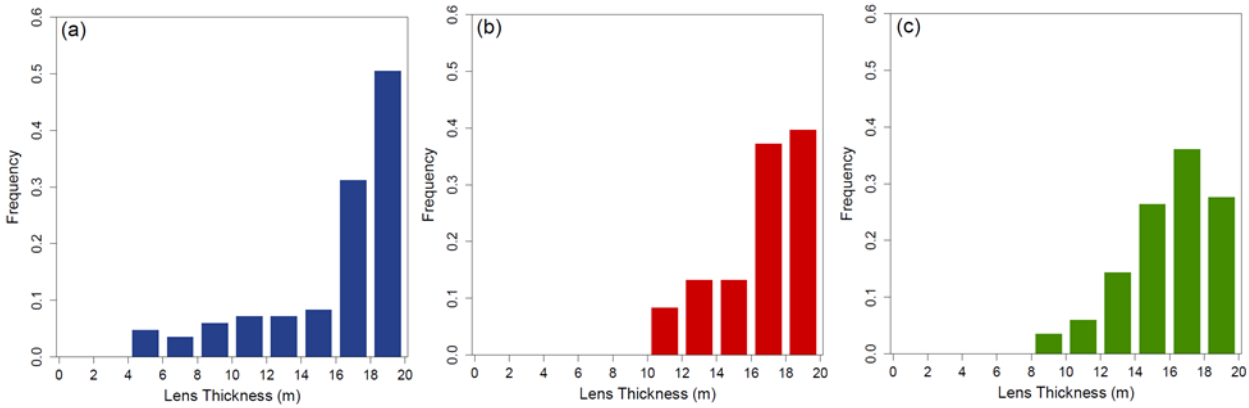

Figure 46. Lens thickness frequency distributions for the top three climate datasets for Pingelap Island. Heavy right-skew is observed, with the lens thinning to no less than 4 meters for any of the GCM outputs

The absence of lens depletion, aside from the influence of the island size in the development of a large freshwater zone, indicates that droughts were less frequent during the RCP8.5 forcing scenario than they were for the RCP2.6 scenario. Figure 46a shows the results from NorESM1-ME, during which over 75% of the study period had a lens thickness of over 16 meters. The skew is not as heavy in Figure 46b and Figure 46c, which correspond to output from GISS-E2-R-p2 and GISS-E2-R-p1, respectively. However, for both of the latter then lens never depleted below 6 meters throughout the 2010-2050 study period.

Figure 47 shows the lens thickness frequency distribution for Ngatik Island for the RCP8.5 forcing scenario. The distributions for each of the top-performing GCMs show heavy right skew, with a lens thickness over 18 meters seen nearly 70% of the time for NorESM1-ME.

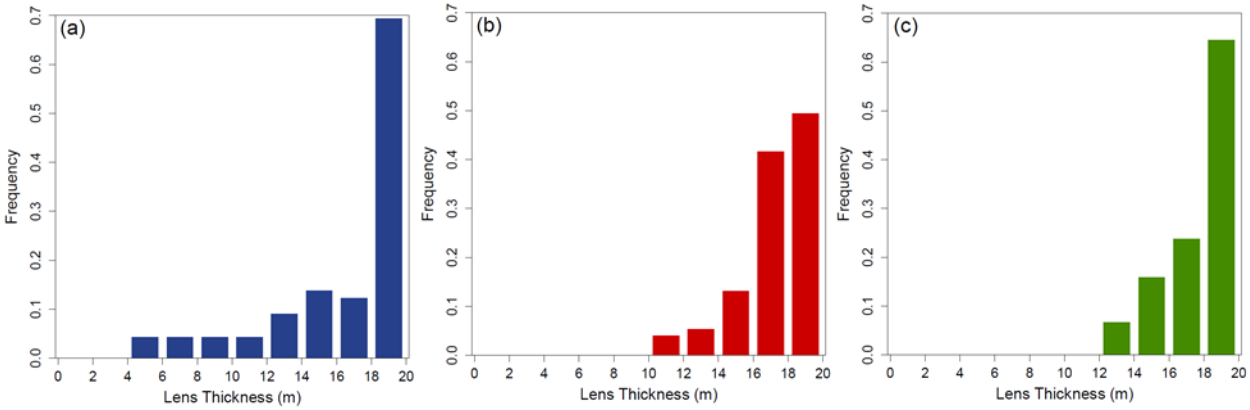

Figure 47. Lens thickness frequency distributions for the top three climate datasets for Ngatik Island. Heavy right-skew is observed, with the lens thinning to no less than 4 meters for any of the GCM outputs. The top-performing GCMs for this forcing scenario were (a) NorESM1-ME, (b) GISS-E2-R-p2, and (c) GISS-E2-R-p1

Lens thickness values less than 4 meters were not seen at any point during the 2010-2050 study period, indicating that the fresh groundwater resources of Ngatik Island remained intact even during drought periods. This is attributed mainly to the size and leeward location of Ngatik Island on Mwoakilloa Atoll.

The lens thickness for Mangejang Island in Yap State, shown in Figure 48, shows dissimilar distributions amongst the top three GCMs. For GISS-E2-H-p2 and GFDM-ESM2M the lens was between 7.5 and 9 meters thick for nearly 30% of the study period, while for MRI-CGCM3 the lens thickness fluctuates regularly between 3 and 9 meters. Lens depletion is prevalent for each of the datasets, however, with MRI-CGCM3 showing freshwater lens thickness below 1.5 meters for nearly 25% of the study period.

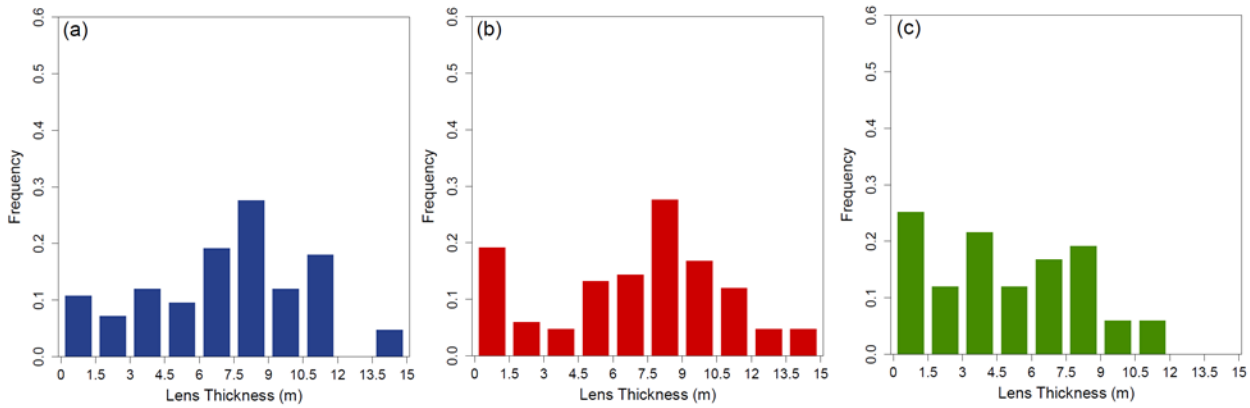

Figure 48. Lens thickness frequency distributions for Mangejang Island in Yap State. The top three GCMs for the RCP8.5 forcing scenario were (a) GISS-E2-H-p2, (b) GFDM-ESM2M, and (c) MRI-CGCM3.

Figure 49 shows the lens thickness frequency distribution for the three top-performing GCMs for Fassarai Island. Lens depletion is very frequent, with lens thickness values below 1.5 meters seen for over 50% of the study period for each GCM. Higher lens thickness values of up to 15 meters are observed, but for only 5% of the study period. A lower volume of fresh groundwater is seen for Fassarai Island not only because of its windward location on Ulithi Atoll, but also for its extremely high length to width ratio, which effectively limits the development of a lens of any considerable thickness or volume.

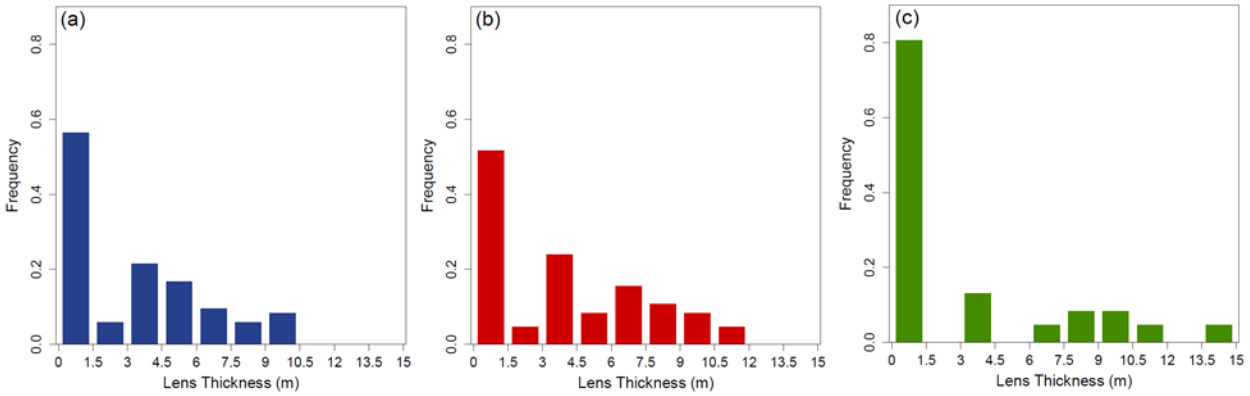

Figure 49. Lens thickness frequency distributions for Fassarai Island in Yap State. The top three GCMs for the RCP8.5 forcing scenario were (a) GISS-E2-H-p2, (b) GFDM-ESM2M, and (c) MRI-CGCM3.

The frequency distributions of lens thickness for the top three GCMs for Mogmog Island in Yap State are shown in Figure 50. The distributions of lens thickness are much more uniform as compared to those of Fassarai Island, though frequent lens depletion is still modeled.

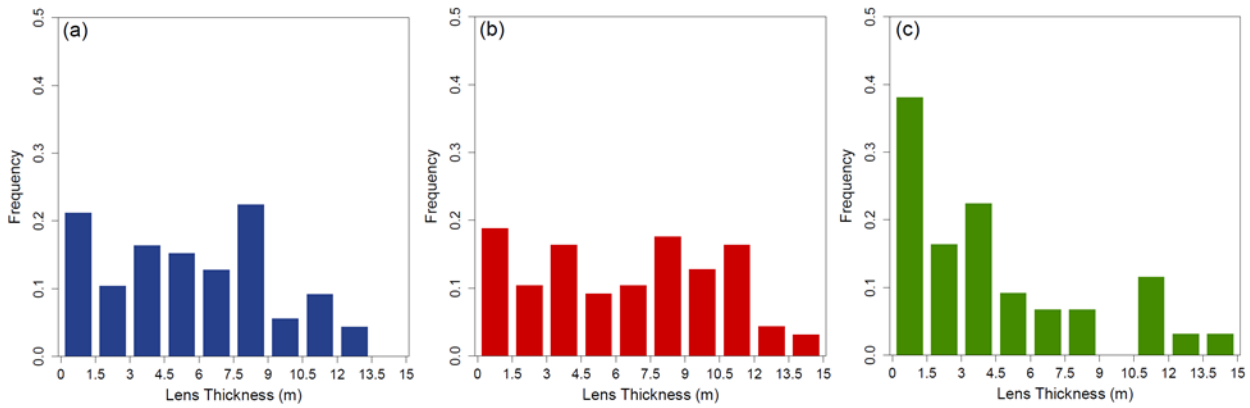

Figure 50. Lens thickness frequency distributions for Mogmog Island in Yap State. The top three GCMs for the RCP8.5 forcing scenario were (a) GISS-E2-H-p2, (b) GFDM-ESM2M, and (c) MRI-CGCM3. The lens thickness values are relatively uniformly distributed, though lens depletion is still rather common.

Figure 50c, which corresponds to output from MRI-CGCM3, shows a lens thickness less than 1.5 meters for nearly 40% of the study period.

The average and standard deviation of the lens thickness values for each GCM for the RCP8.5 forcing scenario are shown in Table 14. Generally, the average lens thickness found on each of the islands is larger than that seen under the RCP2.6 forcing scenario, results from which are shown in Table 13. It is also noted that the standard deviation values for the RCP8.5 forcing scenario are lower, indicating less extreme fluctuations in climate patterns. This agrees with the frequency distribution analysis performed for each island, which showed that the RCP2.6 forcing scenario often resulted in more frequent lens depletion than the RCP8.5 forcing scenario. These results indicate that groundwater supply in both regions of Micronesia is more stable under the RCP8.5 forcing scenario than under the RCP2.6.

Table 14. Average and standard deviations of lens thickness for each of the island models for the RCP8.5 forcing scenario. Smaller values of standard deviation indicate less frequent drought and more consistent lens thickness than under the RCP2.6 forcing scenario.

	GCM	Deke	Pingelap	Kahlap	Ngatik	Nikahlap	GCM	Fassarai	Mangejang	Mogmog
Average	**NorESM1-ME**	6.81	17.50	7.12	18.82	16.66	**GISS-E2-H-p2**	0.71	7.12	2.89
Std. Dev.		2.01	3.68	1.54	3.05	4.31		0.72	3.40	1.97
Average	**GISS-E2-R-p2**	6.60	17.56	7.03		16.66	**GFDL-ESM2M**	0.87	6.82	3.28
Std. Dev.		1.86	2.52	1.24		4.31		0.83	3.87	2.17
Average	**GISS-E2-R-p1**	6.66	17.00	7.09		16.66	**MRI-CGCM3**	0.53	4.53	1.99
Std. Dev.		1.77	2.41	1.36		4.31		0.84	3.25	2.00

Discussions and Conclusion

The future volume of the freshwater lens has important implications on the sustainability of adequate living conditions on atoll islands. If the freshwater lens becomes consistently too thin to support groundwater extraction, or if annual recharge becomes insufficient to promptly replenish the lens following wave-overwash events, it may be incapable of supporting community life. Using the results for freshwater lens thickness and volume under the various GCM datasets, island communities can more effectively prepare for future conditions and determine the best management strategies to ensure adequate freshwater supply as climate conditions change. Results indicated that, based on the output of some climate models, lens depletion was rather common, and persisted in some cases for more than 10% of the 2010-2050 study period. It is during these periods of low freshwater lens volume that island communities must have effective water resource management strategies to ensure adequate water supply.

On larger islands, where the freshwater lens has a greater surface area beneath which to develop, lens depletion is less common. In many cases the largest islands modeled (Pingelap, Nikahlap, and Ngatik) showed a maximum lens thickness of 20 meters a large portion of the time. While lens depletion did occur based on output from some of the GCM datasets, it was fairly infrequent, and usually did not last for more than a couple of months before the lens was replenished. Smaller islands, especially those on the windward side of atolls, experienced frequent lens depletion. In some cases, such as that of Fassarai Island, the island geometry is not conducive to the formation of large lenses. Lens thickness on the island never reached more than a few meters, and was frequently salinized during periods of lower rainfall. Generally, the hydraulic conductivity of windward islands is too high to support a lens of any considerable thickness. Lens thickness on these islands frequently dipped below 2 meters, with extractable groundwater available only in extremely limited volumes. The effects of this are observed historically, as island communities almost never establish permanent settlements on these islands.

To bracket the potential reaction of the lens to different climate change scenarios, the RCP2.6 and RCP8.5 forcing scenarios were used to model lens volume. These scenarios correspond to the two extreme ends of climate change scenarios, RCP2.6 representing a minimal increase in the concentration of atmospheric greenhouse gas and RCP8.5 representing a maximum increase. Despite their extreme differences in terms of their implication on the increase of global temperatures and potential change in precipitation depths, both scenarios produced fairly similar results. Though both showed periods of both extreme drought and heavy rainfall, the results from neither infer that atoll islands will become uninhabitable by the year 2050. That said, island communities will need to implement water resources management techniques to ensure themselves adequate water during the predicted drought periods. By not

relying solely on groundwater as a resource for freshwater supply, island communities will be able to sustain their way of life.

Results presented in both the frequency distributions of the various islands and the time series plots of lens thickness and volume indicate that, generally, lens thickness is consistently higher under the RCP8.5 forcing scenario. Not only is there less deviation around the average value of lens thickness, but less frequent droughts occur, inhibiting depletion of the freshwater volume of the lens. Generally, drought periods forecasted by the RCP2.6 forcing scenario are more frequent and less intense, while those predicted by the RCP8.5 forcing scenario are sporadic and relatively extreme. The results imply that under the RCP8.5 forcing scenario, the volume of the freshwater lens in the coming decades will be consistently larger and more capable of supporting island communities.

It is interesting to note that these implications coincide with the climate scenario under which there is an extreme increase in the atmospheric concentration of greenhouse gas and little use of climate change mitigation strategies. It is unsure which of the climate scenarios modeled is more likely to occur, however they give an indication of likely climate patterns in the coming decades. Heavy drought is likely to occur about once each decade based on the previously presented time series plots. During these dry periods, island communities will need to rely on alternate sources of freshwater, such as captured rainwater. By adequately managing freshwater supply and implement drought preparedness strategies, the lifestyles of atoll island communities can likely be sustained.

CONJUNCTIVE USE OF GROUNDWATER AND CAPTURED RAINWATER

Introduction

Freshwater supply on atoll islands consists of both groundwater and captured rainwater. Groundwater is manually extracted from the freshwater lens using hand-dug wells which penetrate the water table 1 to 2 meters. Though the rate at which water is extracted is relatively slow as compared to other methods which utilize electric pumps to draw larger volumes, seawater upconing and temporary salinization of the aquifer can still occur if excessive volumes are drawn too quickly. The freshwater lens is also extremely fragile due to its dependence on constant recharge from precipitation to maintain a region of low chloride concentration. During drought periods, not only does the lens deplete as a result of community extraction, but also thins as freshwater mixes with seawater at the transitional boundary. Lens depletion as a result of periods with low precipitation can require up to 1.5 years to fully restore the lens to its prior thickness and volume (Bailey & Jenson, 2013). Wave over-wash events are also a threat to the freshwater contained in the lens, with seawater inundation across the surface of the atoll causing salt to permeate the lens through the unsaturated zone.

RWCS, though less perceptible to damage from wave inundation, hold a relatively small volume as compared to the freshwater lens. When precipitation is available on a regular basis to flush and recharge the systems, a majority of community water demand can be satisfied by properly designed systems. During drought periods, both the quantity and quality of captured rainwater diminish. Even systems designed with large storage cisterns to serve a large portion of the community run out of captured rainwater when there is a lack of precipitation to recharge them. When insufficient precipitation is available to flush the system, contaminants such as animal feces and plant debris can collect on rooftop catchment areas, contributing to degraded water quality.

To extend how long the freshwater supply on atoll islands can sustain communities, combined use of captured rainwater and groundwater is necessary. The volume of captured rainwater can be maximized by properly designing systems with a desired rate of reliability. At higher reliability rates, a system can statistically satisfy community water demand over a longer period than those at lower rates. System design curves are an effective design tool to ensure that RWCS perform optimally to collect and store enough water. Groundwater obtained from the lens must be extracted at a sustainable rate to prevent seawater upconing and to protect the integrity of the freshwater region. Each freshwater lens has a sustainable yield based upon the geologic characteristics of the aquifer and the dimensions and location of the island beneath which it is located. For atoll islands in the Maldives, it was estimated that sustainable yield is approximately 35% of the annual recharge (Falkland A. , Addu Atoll, Maldives, 2000). Estimation of the available volume of captured rainwater and extractable groundwater in the coming decades will assist island water resources managers more effectively regulate the community supply of freshwater.

Methods

Rainwater Catchment System Design

A case study is performed for Nikahlap Island on Pakein Atoll in Pohnpei State. It was selected for its leeward location on the atoll capable of supporting a lens of considerable thickness and volume, and for the study performed by Taboroši and Martin (2011) on the current

state of the community RWCS. The volumes of extractable groundwater and captured rainwater are estimated concurrently for the period 2010-2050, and the trends in their combined volumes analyzed. The top performing GCMs for Pohnpei State for both RCP2.6 and RCP8.5 were used to exemplify the application of conjunctive use of rainwater and groundwater. CNRM-CM5 was used for the RCP2.6 scenario and NorESM1-ME for the RCP8.5 scenario. As discussed in Chapter 2, these GCMs had the highest Brier and Significance scores when compared to historical data. This indicates that the models are able to accurately replicate historical climate variability. Because rainwater catchment is tracked on a daily time step, accurate representation of historical climate patterns is important for obtaining good estimation of the end-of-day stored volumes of captured rainwater.

Though information on community-scale RWCS on Nikahlap Island exists, the specific system dimensions may not be characteristic of RWCS available to communities of different sizes. The population of Pakein Atoll is approximately 90 people, with 12 households and several community buildings used to capture rainwater. Atolls of different sized may have more of less buildings depending on the population and the number of public services available. The capacities of community-scale RWCS are affected by the number of roofs available for catchment area and by community water demand. Captured rainwater volume is calculated on a daily time step using downscaled climate data. As seen in Chapter 3, the dimensions of the catchment area and storage tank have a direct influence on the available volume of captured rainwater. Systems in Micronesia need to be designed at a high rate of reliability to ensure adequate freshwater supply during periods of low rainfall. The system for the case study was sized at 90% reliability. This sizing criterion was chosen to provide reduced system cost as opposed to systems of higher rates of reliability while still supplying a conservative volume of captured rainwater. Analysis was performed on a household-scale so it can more easily be extrapolated to community-scale RWCS. This allowed for the application of the RWCS design curves developed in Chapter 4.

Estimation of Freshwater Lens Sustainable Yield

The volume of fresh groundwater present in the lens throughout the study period was modeled using the USGS code SEAWAT, which three-dimensionally simulates groundwater flow and solute transport. The resulting values of freshwater volume were multiplied by the porosity of the upper Holocene aquifer to provide an estimate of the actual freshwater volume. The volume of groundwater that can be extracted by communities via hand-dug wells is less than the total volume of the aquifer. Excessive pumping can cause upconing and salinization of the freshwater lens. Using the estimate of sustainable yield provided by Falkland (2000) as 35% of annual recharge, the percentage of extractable freshwater volume was calculated. Though Micronesia receives almost double the annual precipitation seen in the Maldives, the similar geologic characteristics of atolls in both regions led to the adoption of this as an estimate of sustainable yield. The annual volume of recharge for each year of the study period was calculated and multiplied by 0.35 to provide an estimate of the extractable freshwater. This value was compared to the modeled total freshwater volume of the lens for the same year. The fraction of extractable groundwater was calculated for each of the islands, and then averaged to give a single sustainable yield percentage as a portion of total lens freshwater volume for both windward and leeward islands.

The available freshwater volumes from captured rainwater and extractable groundwater are analyzed concurrently; the volume of extractable freshwater from the lens is often orders of

magnitude greater than the volume acquired from RWCS. To allow for investigation of the trend in available freshwater volume, each source is plotted on its own scale. The modeled volume of freshwater in the lens was output on a bi-annual basis due to hardware capacity restraints. To allow for effective volume comparison with RWCS, daily volumes of available captured rainwater were summed into monthly averages that could then be plotted alongside the groundwater volumes; the excess number of daily data points made comparison difficult. By estimating the volumes of both captured rainwater and extractable groundwater available to island communities, patterns in their available supply are identified. This information can then assist in more efficient water resources management by giving island communities an estimate of how much total freshwater is available and when the importation of water from larger islands may be necessary.

Results

RCP2.6 Forcing Scenario

Generally, the response of the RWCS to changes in precipitation rates is much faster than that of the freshwater lens. This is due primarily to the relatively small volume as compared to the volume of extractable groundwater. As a result, the amount of time required to replenish the volume of captured rainwater is much lower than that for lens to recover following depletion. Figure 51 shows a time series from 2010-2050 of the volume of extractable groundwater plotted against the volume of captured rainwater for the RCP2.6 forcing scenario.

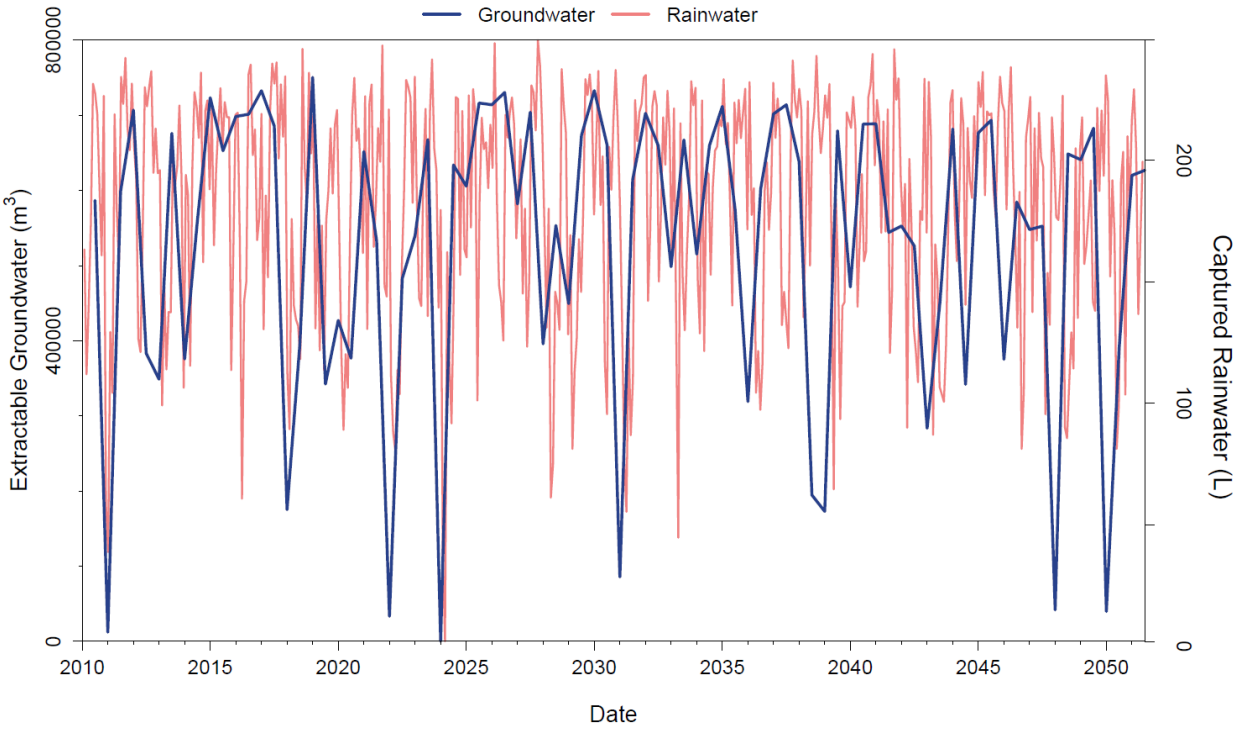

Figure 51. Time series of the fluctuations in extractable groundwater and captured rainwater from 2010-2050. The volume of captured rainwater is observed to deplete more frequently than the groundwater, and to lag behind groundwater depletion by several weeks when periods of heavy drought occur.

Based on the original estimates made by Falkland (2000), the percentage of total freshwater lens volume that can be sustainably extracted for community use was estimated at about 55% of the

total freshwater volume for leeward islands and approximately 10% for windward islands. While fluctuations in the volume of captured rainwater are much more rapid than those seen in the freshwater lens, both curves follow the same general pattern. During periods of low rainfall, the volume of both sources decreases. Depletion of the lens is much more infrequent because of the relatively large volume of freshwater present. Often during light, sporadic drought the volume of captured rainwater decreases drastically while the volume of the freshwater lens maintains a relatively constant level. This is indicative of the extreme response of RWCS volume as compared to that of the freshwater lens. Lens depletion does occur during periods of extreme drought, which seem to occur about once each decade. Concurrent depletion of both the extractable groundwater and captured rainwater represents complete exhaustion of the atoll island freshwater supply. It is noted, however, that depletion of the volume of captured rainwater lags slightly behind that of the freshwater lens. When the volume of the freshwater lens decreases drastically during periods of heavy drought, significant decrease in the volume of captured rainwater does not occur for several weeks or more.

A frequency distribution of the volume of captured rainwater from 2010-2050 under the RCP2.6 forcing scenario is shown in Figure 52. Generally the distribution is right-skewed, showing that for about 60% of the study period there were more than 210 liters of stored rainwater. About 12% of the time, there was less than 30 liters of captured rainwater available. For a standard household of 4 people, a conservative stored volume less than 30 liters is inadequate to fully meet the demand, even if the water is rationed. Based on the frequency distribution of captured rainwater volume, systems optimized at 90% reliability supply inadequate volume to consistently meet this demand. During periods where the stored rainwater in the systems is insufficient satisfy the demands of the household, freshwater supply must be supplemented with extracted groundwater.

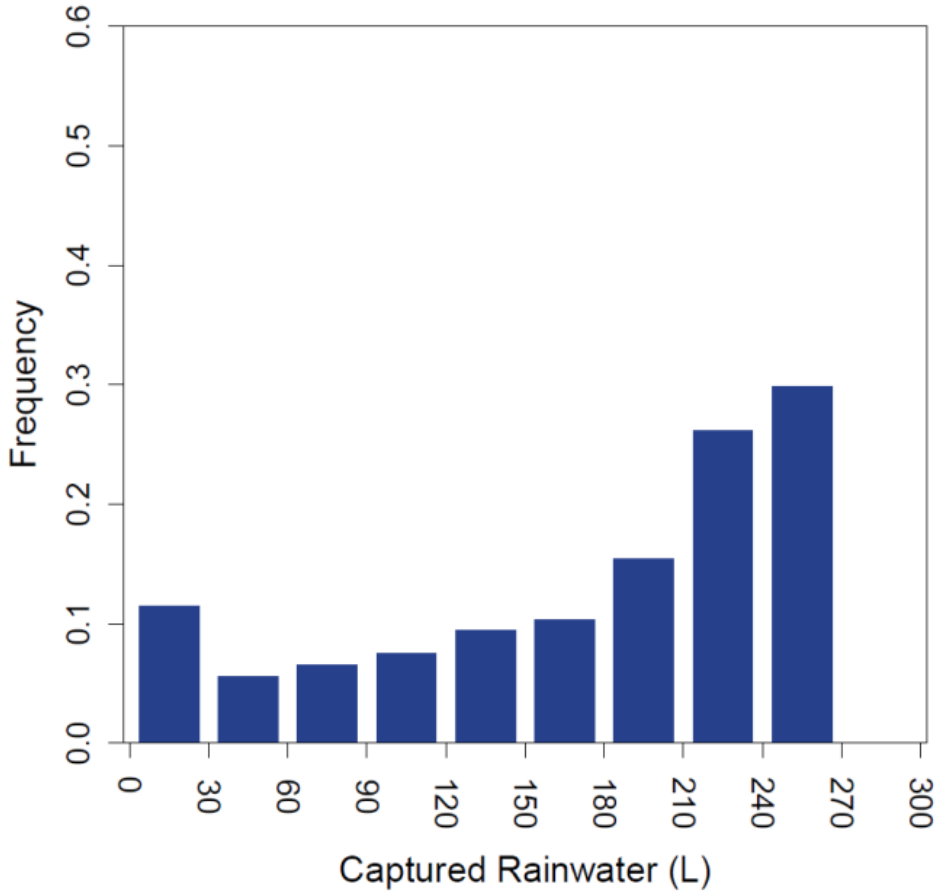

Figure 52. Frequency distribution of the volume of captured rainwater available to fill household water demand for the RCP2.6 forcing scenario. Though for a large portion of the study period the system is filled to capacity, the volume depletes over 10% of the time.

Figure 53 shows the frequency distribution of the volume of remaining extractable groundwater when RWCS volume drops below 30 liters. Because of the rapid fluctuations in the volume of captured rainwater, the lens was not often depleted when captured rainwater supply depletes. Over 50% of the time that there was insufficient rainwater to meet demand, the extractable groundwater volume was still at the high end of the lens' capacity.

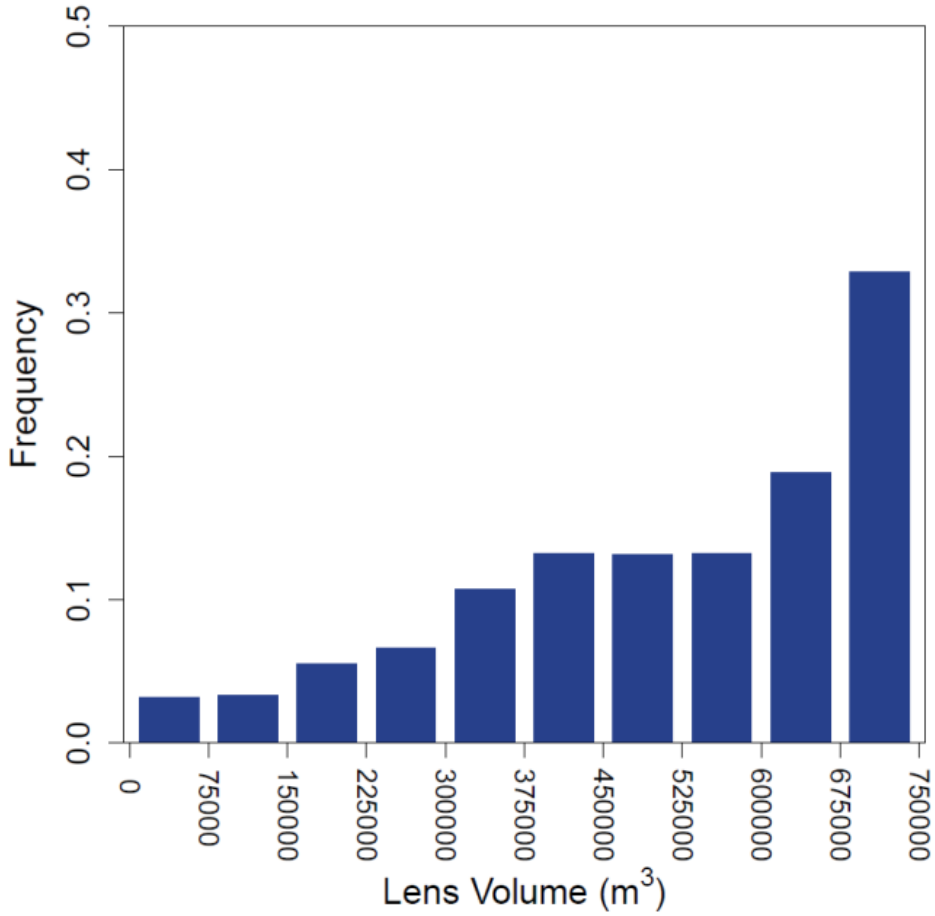

Figure 53. Frequency distribution of the remaining volume of extractable groundwater available when the volume of captured rainwater is depleted for the RCP2.6 forcing scenario. Results indicate that both sources become depleted for less than 1% of the study period from 2010-2050.

Approximately 3% of the time, there was very little remaining extractable freshwater in the lens when the supply of captured rainwater had been depleted. In this case, water would need to be imported from the larger islands to sustain the communities until precipitation can recharge the volumes of both the lens and the RWCS.

RCP8.5 Forcing Scenario

A time series of the volume of captured rainwater and volume of extractable groundwater for the RCP8.5 forcing scenario is shown in Figure 54.

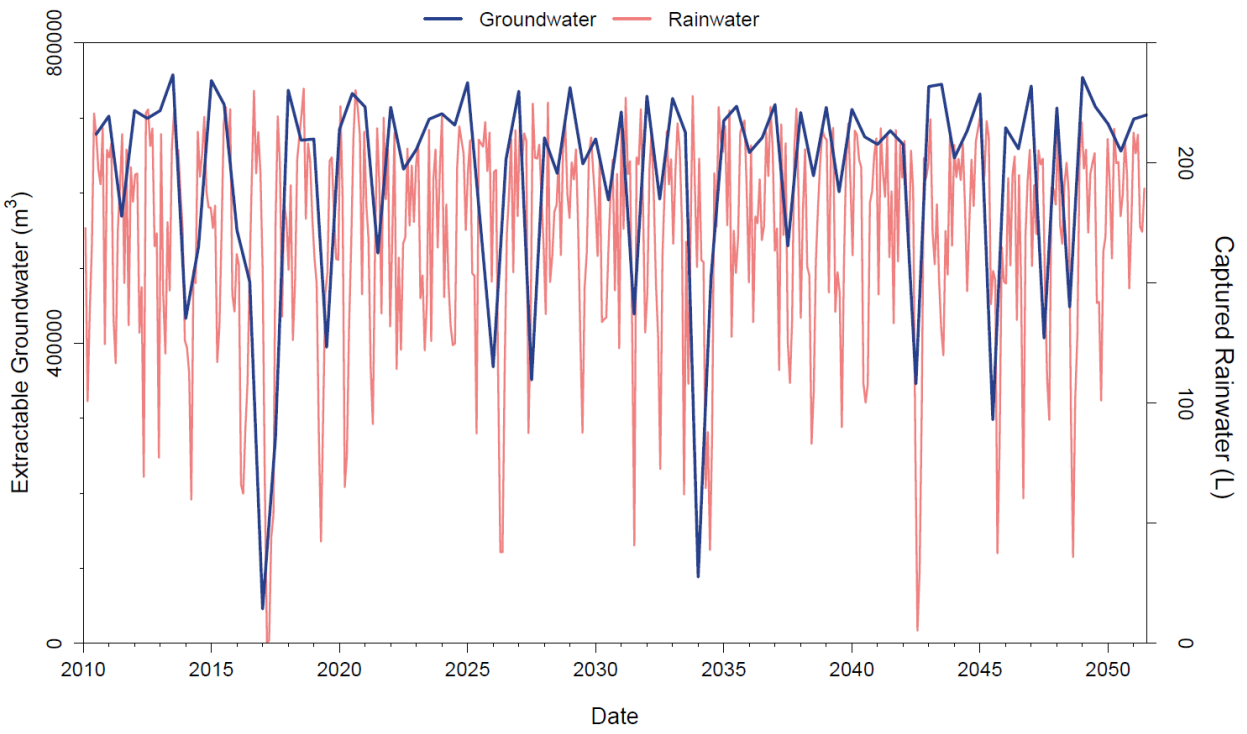

Figure 54. Time series showing the volumes of extractable groundwater and captured rainwater from 2010-2050 for the RCP8.5 forcing scenario. The volume of the lens is much more constant as compared to the fluctuation seen during the RCP2.6 forcing scenario, though drought periods that do occur are more intense. Depletion of captured rainwater supply is again seen to lag slightly behind that of the groundwater.

The trend in the fluctuation of captured rainwater volume is similar to that seen under the RCP2.6 forcing scenario, with frequent and relatively drastic decrease observed during light drought. It is again recognized that depletion of captured rainwater supply lags behind decrease in groundwater volume by several weeks. Generally, the volume available from both resources was higher for the RCP8.5 forcing scenario than for the RCP2.6. This follows the pattern discussed in Chapter 6, where freshwater resources were better developed and maintained during the RCP8.5 scenario.

Figure 55 shows the frequency distribution of the daily volume of captured rainwater for a system with 90% reliability.

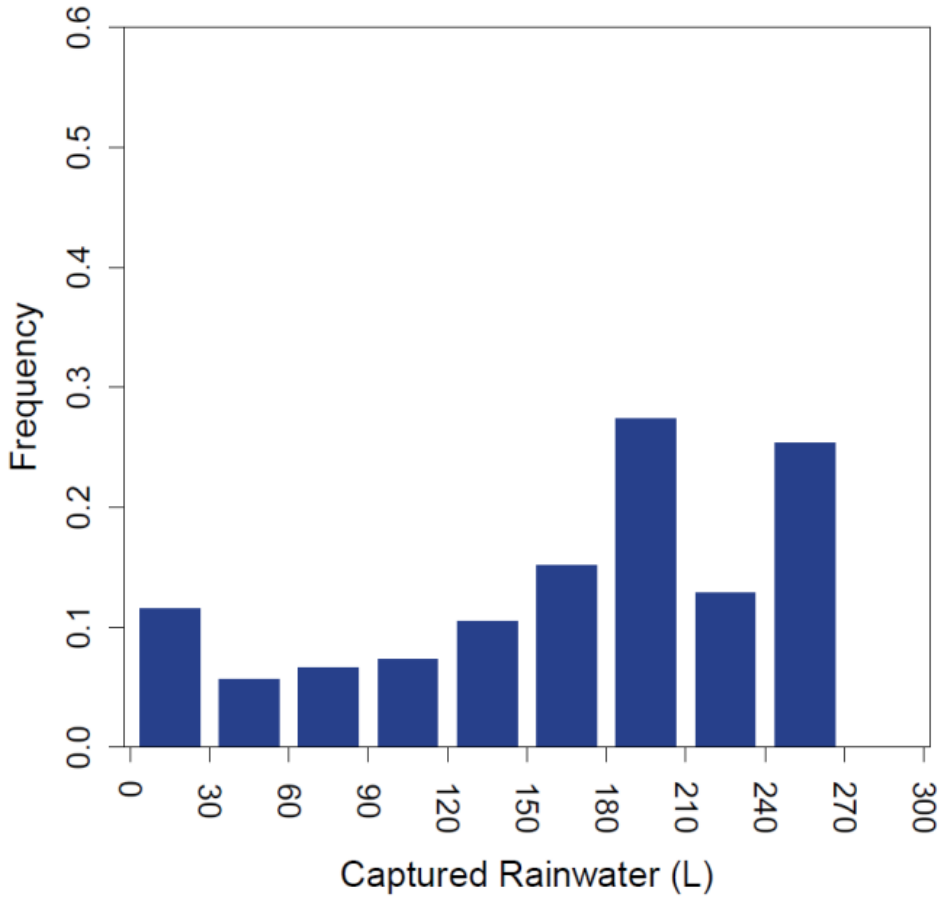

Figure 55. Frequency distribution of the volume of captured rainwater from 2010-2050. Over 60% of the time there is more than 180 liters available for use, though supply depletes nearly 12% of the time.

The distribution is similar to that seen during the RCP2.6 forcing scenario, with the captured rainwater volume showing some right-skew. For over 60% of the study period the available freshwater stored in the system was above 180 liters, a volume sufficient to supply an average household of 4 with a daily demand of 30 liters per capita. This indicates that climate dataset output from the RCP8.5 forcing scenario contained infrequent droughts, allowing the RWCS to reach its storage capacity a majority of the time. The volume in the catchment system was below 30 liters for just over 10% of the study period, indicating that household residents would need to supplement their freshwater supply with groundwater.

To quantify the volume of groundwater available for extraction during periods when the volume of captured rainwater depleted, a frequency distribution of the sustainable lens volume was produced, shown in Figure 56.

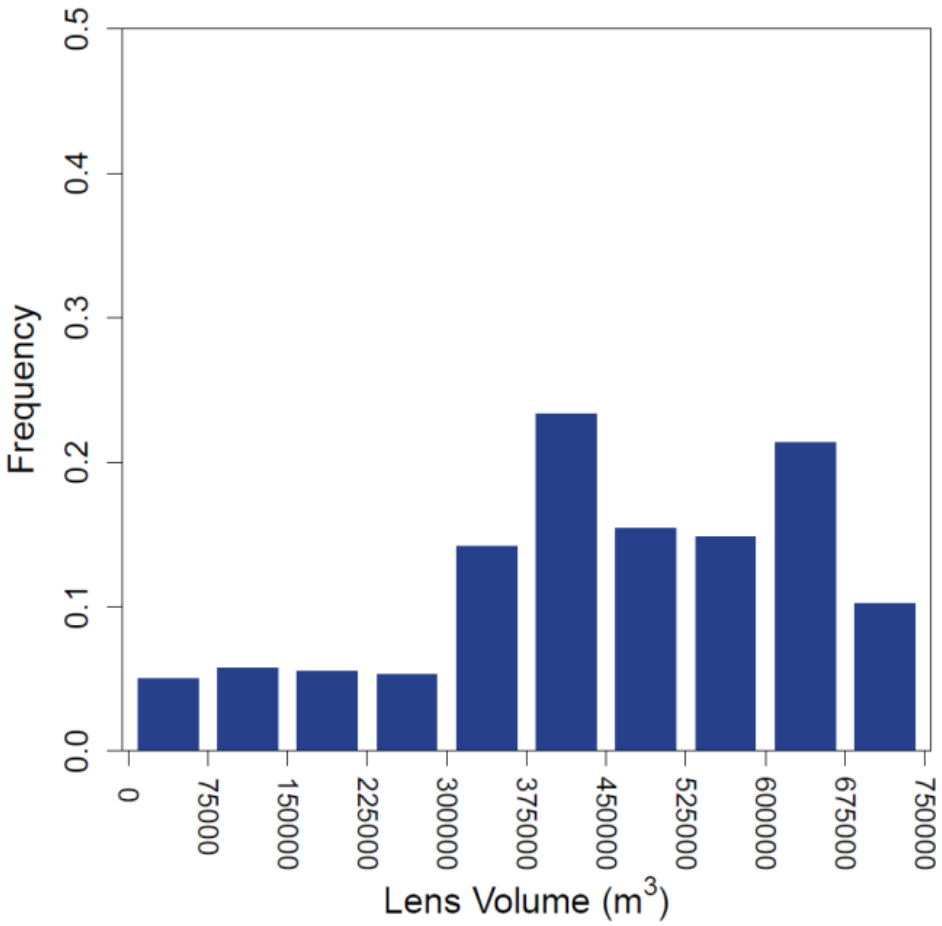

Figure 56. Frequency distribution of the volume of extractable groundwater when the volume of captured rainwater is depleted. Approximately 1% of the study period showed almost complete depletion of extractable groundwater at the same time that captured rainwater supply had been exhausted

The distribution is more uniform than that observed during the RCP2.6 forcing scenario, which indicates that the lens did not have as much extractable freshwater when the volume of captured rainwater was exhausted. Nearly 5% of the time the lens had less than 75,000 m^3 of freshwater available for extraction; this volume is very low and indicates that the lens is near depletion. In total, the lens had less than 300,000 m^3 of available water for about 20% of the study period. This analysis indicates that, though drought periods under the RCP8.5 forcing scenario are less frequent, they are generally of greater magnitude and often result in depletion of both captured rainwater and extractable groundwater.

Discussions and Conclusion

Freshwater resources on Nikahlap Island consist solely of rainwater collected using RWCS and groundwater extracted from hand-dug wells. RWCS, when designed correctly, can provide island residents with a majority of their freshwater demand. RWCS design curves assist in designing systems at different rates of reliability; the household system considered during this study was sized at a reliability rate of 90%. When the volume of captured rainwater is depleted, the freshwater lens is turned to as an alternate source to meet water demand. The sustainable yield of the freshwater lens was determined to be about 55% and 10% of the total freshwater

volume for leeward islands and windward islands, respectively. This estimate is based on the initial estimates made by Falkland (2000) that the sustainable yield is approximately 35% of the annual recharge.

Fluctuation in the volume of captured rainwater was similar for both the RCP2.6 and RCP8.5 forcing scenarios. Because the volume of captured rainwater is relatively small it is quickly depleted, and is therefore highly dependent on consistent rainfall to maintain an adequate supply. The RWCS contained more than 210 liters for over 60% of the time for both forcing scenarios, enough to fully meet the demand of the household residents. However, the system contained less than 30 liters for approximately 12% of the study periods under both forcing scenarios, indicating supply had been depleted. The similarities in the frequency distributions of the volume of captured rainwater for both scenarios indicate the sensitive reaction catchment systems have to rainfall. As both climate models showed high capability in replicating historical climate patterns, the daily variability in rainfall is not statistically different. As a result, the volume of captured rainwater fluctuates about the same under both forcing scenarios.

The behavior of the lens to the different forcing scenarios is dissimilar, however, due to the large-scale climate pattern trends evoked by the different magnitudes of radiative forcing. Frequency distributions of the remaining volume of extractable freshwater when the volume of captured rainwater was depleted were created to quantify how often island residents could rely on the lens as an alternate source. During the RCP2.6 forcing scenario, the lens thickness frequency distribution showed heavy right-skew, with maximum extractable lens volume available over 30% of the time. Also during this scenario, only 3% of the study period showed total lens depletion. The lens thickness frequency distribution for the RCP8.5 forcing scenario was much more uniform, though larger values of lens volume were still more common. There was a higher percentage of the time during which the lens depleted at the same time as the volume of captured rainwater was exhausted, seen nearly 5% of the time.

Based on the contrasting frequency distributions produced by the two forcing scenarios it is concluded that drought periods simulated by the RCP8.5 forcing scenario, though less frequent, tended to be of much higher magnitude that those predicted by the RCP2.6 forcing scenario. Though it is unknown which of the climate forcing scenarios is more likely to occur, general knowledge about what percentage of the time there will be insufficient water supply to support island community life gives island water resources managers the ability to plan accordingly.

In order to successfully use rainwater and groundwater conjunctively to maintain an adequate freshwater supply, island water resources managers need an estimation of how much water they can expect to find on the atoll, especially during drought periods. Based on the results of the case study on Nikahlap Island, a majority of the time when the supply of captured rainwater was depleted there was still an available volume of groundwater for extraction. When both supplies depleted concurrently, water would need to be imported from the larger volcanic islands, though this occurred for less than 1% of the 2010-2050 study period. It is important to mention that, though the case study indicates adequate water supply 99% of the time, the results are dependent on a number of parameters that were used. Amongst those most influential are the assumed daily per capita water demand of the island community and the efficiencies of the RWCS gutter systems, both of which can significantly affect the captured rainwater volume. Extractable groundwater supply is highly dependent on the orientation of the island on the atoll, with leeward islands containing a larger volume of fresh groundwater than windward islands. To

ensure accuracy and to optimize freshwater supply, the methods presented in this chapter should therefore be specifically applied to other islands of interest.

Generally, the freshwater lens is less sensitive to daily fluctuations in precipitation than RWCS. After several days without rainfall, the volume of captured rainwater can be exhausted if water rationing is not practiced; over 60% of the time when the volume is depleted freshwater lens can be used as an alternate source of freshwater without risk of aquifer salinization. These findings can be extrapolated to other atoll islands of different size and location, though the sustainable yield of the atoll aquifer system is dependent on the location of the island on the atoll (leeward or windward) and should be verified on a case-by-case basis. Through knowledge of the total volume available for combined use of captured rainwater and groundwater, island communities can more effectively manage their supply in the future.

CONCLUSIONS AND RECOMMENDATIONS

Atoll Island Freshwater Resources

A number of environmental parameters have a strong influence on the development and sustainability of the atoll island freshwater lens, most notably the hydraulic conductivity, depth of annual recharge, and the depth to contact between the upper and lower aquifers. Results further indicate a hydraulic conductivity of 25 m day^{-1} for leeward islands and 200 m day^{-1} for windward islands. The fragile state of atoll freshwater supply relies heavily on a constant rate of precipitation; during periods of heavy drought depletion of both captured rainwater and extractable groundwater can occur. Future climate data simulated by CMIP5 global climate models predict the occurrence of major drought periods about once each decade. It is during these periods when supply can dwindle that effective water resources management is vital to the sustainability and preservation of atoll island community freshwater supply.

Conjunctive Use of Captured Rainwater and Groundwater

By combining the supply of both captured rainwater and groundwater, atoll communities can prolong their freshwater supply during periods of heavy drought. Proper RWCS sizing, which can be achieved using system design curves, is necessary for optimal collection of rainwater. Though the volume of captured rainwater depletes relatively frequently as a result of fluctuations in rainfall, the concurrent volume of extractable freshwater is enough to fill the remaining freshwater demand a majority of the time. When both sources deplete simultaneously, water importation from the larger volcanic islands is necessary; this is more apt to occur on islands of smaller surface area. As the size, shape, and atoll orientation of each island have an effect on the fresh groundwater volume, specific analysis should be performed for each island of interest, with particular attention paid to the assumed daily per capita water demand and RWCS efficiency.

Application of Methods to Regions Outside of the FSM

The methods presented in this thesis, though uniquely applied to atoll islands throughout the FSM, can be adapted to atoll nations throughout the Pacific and Indian Oceans. Given the potential change in global climate patterns and the similar atoll geologic response, concern over adequate community freshwater supply will continue to grow, and more effective water resources management strategies should be installed to mitigate the effects. RWCS design curves can be developed for systems around the world using water balance modeling, allowing for optimal system sizing and lowered frequency of depletion. Estimation of the fresh groundwater volume gives water resources managers a better approximation of the extractable supply, with the sustainable yield of the atoll aquifer system estimated to be about 55% and 10% of the total freshwater lens volume for leeward islands and windward islands, respectively.

Future Research

This thesis has focused on the potential changes in precipitation rates as simulated by GCMs under varying rates of increase in radiative forcing, and their effect on the freshwater supply of atoll islands. Investigation into the effects that sea-level rise will have on atoll islands would provide an even clearer understanding of the future supply of freshwater. An increase in sea-level could drastically reduce the supply of fresh groundwater should surface area decrease excessively, which can occur at varying rates depending on beach slope. Investigation into atoll

community water rationing should also be conducted to identify other potential strategies for prolonging freshwater supply. These analyses could contribute to more effective atoll island water resources management and may provide an estimate of how long atoll community living can be sustained.

REFERENCES

(RMI), R. o. (2005). *Millennium development goals national progress report.*

Abdulla, F. A., & Al-Shareef, A. W. (2009). Roof rainwater harvesting systems for household water supply in Jordan. *Desalination*, 195-207.

Ahmed, W., Gardner, T., & Toze, S. (2011). Microbiological quality of roof-harvested rainwater and health risks: A review. *Journal of Environmental Quality*, 1-9.

Anthony, S. S. (1987). Hydrogeochemistry of a small limestone-island: Laura, Majuro Atoll, Marshall Islands. *M. S. thesis, Department of Geology and Geophysics, University of Hawaii at Manoa*.

Anthony, S. S. (1996). Hydrogeology and ground-water resources of Kahlap island, Mwoakilloa Atoll, State of Pohnpei, Federated States of Micronesia. *USGS Water Resources Investigation Report 92*.

Anthony, S. S. (1996). Hydrogeology and ground-water resources of Ngatik Island, Sapwuahfik Atoll, State of Pohnpei, Federated States of Micronesia. *USGS Water Resources Investigation Report 92*.

Anthony, S. S. (1996). Hydrogeology and ground-water resources of Pingelap Island, Pingelap Atoll, State of Pohnpei, Federated States of Micronesia. *USGS Water Resources Investigation Report 92*.

Anthony, S. S., Vacher, H. L., & Quinn, T. (2007). Hydrogeology of selected islands of the Federated States of Micronesia. *Geology and Hydrogeology of Carbonate Islands: Developments in Sedimentology*, 693-706.

Ayers, J. F., & Vacher, H. L. (1986). Hydrogeology of an atoll island: A conceptual model from detailed study of a Micronesian example. *Groundwater*, 2-15.

Baguma, D., Loiskandl, & Jung, H. (2010). Water Management, Rainwater Harvesting and Predictive Variables in Rural Households. *Water Resource Managment*, 3333-3348.

Bailey, R. T., & Jenson, J. W. (2013). Effects of Marine Overwash for Atoll Aquifers: Environmental and Human Factors. *Groundwater*.

Bailey, R. T., Jenson, J. W., & Olsen, A. E. (2009). Numerical Modeling of Atoll Island Hydrogeology. *Groundwater*, 184-196.

Bailey, R. T., Jenson, J. W., & Olsen, A. E. (2010). Estimating the Ground Water Resources of Atoll Islands. *Water*, 1-27.

Bailey, R. T., Jenson, J. W., & Taborosi, D. (2013). Estimating the freshwater lens thickness of atoll islands in the Federated States of Micronesia. *Hydrogeology Journal*, 441-457.

Bailey, R. T., Jenson, J. W., Rubinstein, D., & Olsen, A. E. (2008). Groundwater resources of atoll islands: observations, modeling, and management. *Water and Environmental Research Institute of the Pacific (WERI) Technical Report No. 119*.

Bailey, R. T., Khalil, A., & Chatikavanij, V. (2014). Estimating Current and Future Groundwater Resources of the Maldives. *Journal of the American Water Resources Association*, 112-122.

Basinger, M., Montalto, F., & Lall, U. (2010). A rainwater harvesting system reliability model based on nonparametric stochastic rainfall generagor. *Journal of Hydrology*, 105-118.

Bates, B. C., Charles, S. P., & Hughes, J. P. (1998). Stochastic downscaling of numerical climate model simulations. *Environmental Modelling Software*, 325-331.

Batu, V. (1998). *Aquifer Hydraulics: A Comprehensive Guide to Hydrogeologic Data Analysis.* New York: John Wiley & Sons.

Bear, J., & Dagan, G. (1964). Some exact solutions of interface problems bymeans of the hodograph method. *Journal of Geophysical Research*, 1563-1572.

Beckley, B. D., Lemoine, F. G., Luthcke, S. B., Ray, R. D., & Zelensky, N. P. (2007). A reassessment of global and regional mean sea level trends from TOPEX and Jason-1 altimetry based on revised reference frame and orbits. *Geophysical Research Letters*.

Brier, G. W. (1950). Verification of forecasts expressed in terms of probability. *Mon Wea Rev*, 1-3.

Buddemeier, R. W., & Holladay, G. (1977). Atoll hydrology: Island groundwater characteristics and their relationship to diagenesis. *Third International Coral Reef Symposium*, 167-173.

Carpenter, C., Stubbs, J., & Overmars, M. (2002). Proceedings of the Pacific Regional Consultation on Water in Small Island Countries. *Asian Development Bank and South Pacific Applied Geoscience Council*.

Caskey Jr., J. E. (1963). A Markov Chain Model for the Probability of Precipitation Occurence in Intervals of Various Length. *Mon. Wea. Rev*, 298-301.

Chapman, T. G. (1985). The use of water balances for water resources estimation with special reference to small islands. *Australian Development Assistance Bureau Bulletin No. 4*.

Charles, S. P., & Bates, B. C. (1999). A spatiotemporal model for downscaling precipitation occurence and amounts. *Journal of Geophysical Research*, 31657-31669.

Chui, T. F., & Terry, J. P. (2012). Modeling Fresh Water Lens Damage and Recovery on Atolls After Storm-Wave Washover. *Groundwater*, 412-420.

Chui, T. F., & Terry, J. P. (2013). Influence on sea-level rise on freshwater lenses of different atoll island sizes and lens resilience to storm-induced salinization. *Journal of Hydrology*, 18-26.

Chui, Y. R., Liaw, C. H., & Cheng, L. C. (2009). Optimizing Rainwater Harvesting Systems as an Innovative Approach to Saving Energy in Hilly Communities. *Renewable Energy*, 492-498.

Collins, M. A., & Gelbar, L. W. (1971). Seawater intrusion in layered aquifers. *Water Resources Research*, 971-979.

Comte, J.-C., Join, J.-L., Banton, O., & Nicolini, E. (2014). Modelling the response of fresh groundwater to climate and vegetation changes in coral islands. *Hydrogeology Journal*, 1905-1920.

Crabtree, K. D., Ruskin, R. H., Shaw, S. B., & Rose, J. B. (1996). The detection of Cryptosporidiumoocysts and Giardiacysts in cistern water in the U.S. Virgin Islands. *Water Resources*, 208-216.

Darwin, C. (1842). *The Structure and Distribution of Coral Reefs.* London: Smith, Elder and Co.

DeBusk, K. M., & Hunt, W. F. (2013). Characterizing Rainwater Harvesting Performance and Demonstrating Stormwater Management Benefits in the Humd Southeast USA. *Journal of the American Water Resources Association*, 1398-1411.

Detay, M., Alessandrello, E., Come, P., & Groom, I. (1989). Groundwater contamination and pollution in Micronesia. *Journal of Hydrology*, 149-170.

Dickinson, W. R. (2004). Impacts of eustasy and hydro-isostasy on the evolution and landforms of Pacific atolls. *Palaeogeography, Palaeoclimatology, Palaeoecology*, 251-269.

Dickinson, W. R. (2009). Pacific Atoll Living: How Long Already and Until When? *GSA Today*, 4-10.

Dillaha, T. A., & Zolan, W. J. (1985). Rainwater catchment water quality in Micronesia. *Water Resources*, 741-746.

Douglas, B. C. (1997). Global sea level rise: a redetermination. *Surveys in Geophysics*, 279-292.

Evans, C. A., Coombes, P. J., & Dunstan, R. H. (2006). Wind, rain and bacteria: the effect of weather on the microbial composition of roof-harvested rainwater. *Water Research*, 37-44.

Falkland, A. (2000). Addu Atoll, Maldives. *Report on Groundwater Investigations, Regional Development Project, First Phase*.

Falkland, A. (2002). Water Resource Management. *Proceedings of the Pacific Regional Consultation on Water in Small Island Countries.* Suva: Asian Development Bank and South Pacific Applied Geoscience Commission.

Falkland, A. C. (1983). *Christmas Island (Kiritimati) Water Resources Study Vol. 1.* Victoria: Australian Department of Housing and Construction.

Falkland, A. C. (1994). Climate, Hydrology and Water Resources of the Cocos (Keeling) Islands. *National Museum of Natural History Atoll Research Bulletin No. 400*.

Farreny, R., Morales-Pinzon, T., Guisasola, A., Taya, C., Rieradevall, J., & Gabarrell, X. (2011). Roof selection for rainwater harvesting: Quantity and quality assessments in Spain. *Water Research: a journal of the International Water Association*.

Fetter, Jr., C. W. (1972). Position of the saline water interface beneath oceanic islands. *Water Resources Research v. 8*, 1307-1314.

Fewkes, A. (1999). The use of rainwater for WC flushing: the field testing of a collection system. *Building the Environment*, 765-772.

Freeze, R. A., & Cherry, J. A. (1979). *Groundwater.* Englewood Cliffs, New Jersey: Prentice Hall.

Fu, G., Liu, Z., Charles, S. P., Xu, Z., & Yao, Z. (2013). A score-based method for assessing the performance of GCMs: A case study of southeastern Australia. *Journal of Geophysical Research: Atmospheres*, 4154-4167.

Gabriel, K. R., & Neumann, J. (1962). A Markov chain model for daily rainfall occurence at Tel Aviv. *Quarterly Journal of the Royal Meteorological Society*, 90-95.

Glover, R. E. (1964). The pattern of fresh water flow in coastal aquifer. *Sea Water in Coastal Aquifers, USGS Water Supply Paper 1613-C*, 32-35.

Gould, J., & Nissen-Petersen, E. (1999). Rainwater Catchment Systems for Domestic Supply. In *Practical Action.*

Griffiths, G. M., & et al. (2005). Change in mean temperature as a predictor of extreme temperature change in the Asia-Pacific region. *International Journal of Climatology*, 1301-1330.

Griggs, J. E., & Peterson, F. L. (1993). Ground-Water Flow Dynamics and Development Strategies at the Atoll Scale. *Groundwater*, 209-220.

Guo, Y., & Baetz, B. W. (2007). Sizing of rainwater storage units for green building applications. *Journal of Hydrologic Engineering*, 197-205.

Hamlin, S. N., & Anthony, S. S. (1987). Ground-water resources of the Laura area, Majuro Atoll, Marshall Islands. *USGS Water Resources Investigation Report 87-4047*.

Han, M., & Ki, J. (2010). Establishment of sustainable water supply systems in small islands through rainwater harvesting (RWH): case study of Guja-do. *Water Science & Technology (WST)*, 148-153.

Helmreich, B., & Horn, H. (2008). Opportunities in rainwater harvesting. *Desaliniation*.

Henry, H. R. (1964). Interfaces between saltwater and fresh water in coastal aquifers. *Sea Water in Coastal Aquifers, USGS Water Supply Paper 1613-C*, 35-39.

Herman, M. E., & Wheatcraft, S. W. (1984). Groundwater dynamics investigation of Enjebi Island, Enewetak Atoll: An interpretive computer model simulation. *Finite Elements in Water Resources* (pp. 133-142). London: Springer-Verlag.

Hogan, P. (1988). Modeling of freshwater-seawater interaction on Enjebi Island, Enewetak Atoll. *Master's thesis (Geology)*.

Houghton, J. T., & et al. (2001). *Climate Change 2001: The Scientific Basis.* Cambridge: Cambridge University Press.

Hubbert, M. K. (1940). The theory of groundwater motion. *Journal of Geology*, 785-944.

Hunt, J. C., & Peterson, F. L. (1980). Groundwater resources of Kwajalein Island, Marshall Islands. *University of Hawaii, Water Resources Research Center Technical Report No. 126*, 1-91.

Jenkins, D., Pearson, F., Moore, E., Sun, J. K., & Valentine, R. (1978). Feasibility of rainwater collection systems in California. *Contribution No. 173, California Water Resources Center*.

Jones, M. P., & Hunt, W. F. (2010). Performance of rainwater harvesting systems in the southeastern United States. *Resources, Conservation and Recycling*, 623-629.

Kim, Y., Lee, K., Koh, D., Lee, D., Lee, S., Park, W., . . . Woo, G. (2003). Hydrogeochemical and isotropic evidence of groundwater salinization in a coastal aquifer: a case study in Jeju volcan island, Korea. *Journal of Hydrology*, 282-294.

Krishna, J. (1989). Cistern Water Systems in the U.S. Virgin Islands. *Fourth International Conference on Rain Water Cistern Systems*, (pp. 1-11). Manila.

Kwaadsteniet, M. d., H., D. P., van, D. A., Kahn, W., & Cloete, T. E. (2013). Domestic Rainwater Harvesting: Microbial and Chemical Water Quality and Point-of-Use Treatment Systems. *Water Air Soil Pollution*, 1-19.

Lam, R. K. (1974). Atoll permeability calculated from tidal diffusion. *Journal of Geophysical Research v. 79*, 3073-3081.

Lander, M. A., & Khosrowpanah, S. (2004). Rainfall climatology for Pohnpei Islands, Federated States of Micronesia. *Water and Environmental Research Institute of the Western Pacific (WERI) Technical Report NO. 103*.

Langevin, C. D., Shoemaker, W. B., & Guo, W. (2003). *MODFLOW-2000, the U.S. Geological Survey Modular Ground-Water Model-Documentation of the SEAWAT-2000 Version with the Variable-Density Flow Process (VDF).* U.S. Geological Survey.

Lee, A. G. (2003). 3-D Numerical Modeling of Freshwater Lens on Atoll Islands. *TOUGH Symposium*, (pp. 1-7). Berkeley.

Li, Z., Boyle, F., & Reynolds, A. (2010). Rainwater harvesting and greywater treatment systems for domestic appliation in Ireland. *Desalination*, 1-8.

Liaw, C.-H., & Chiang, Y.-C. (2014). Dimensionless Analysis for Designing Domestic Rainwater Harvesting Systems at the Regional Level in Northern Taiwan. *Journal of Water*, 3913-3933.

Lloyd, J. W., Miles, J. C., Chessman, G. R., & Bugg, S. F. (1980). A groundwater resources study of a Pacific Ocean atoll - Tarawa, Gilbert Islands. *Water Resources Bulletin 16, No. 4*, 646-653.

Lye, D. J. (2002). Health risks associated with consumption of untreated water fro household roof catchment systems. *Journal of the American Water Resources Association*, 1301-1306.

Lye, D. J. (2009). Rooftop runoff as a source of contamination: A review. *Science of the Total Environment*, 5429-5434.

MacCracken, R. S., Jenson, J. W., Heitz, L. F., Rubinstein, D. H., & Mylroie, J. E. (2007). Water resources analysis of Fais Island, Federated States of Micronesia. *Water and Environmental Research Institute of the Western Pacific (WERI) Technical Report No. 111*.

Mather, J. D. (1975). Development of the groundwater resources of small limestone islands. *Quarterly Journal of Engineering Geology*, 141-150.

Mearns, L. O., Giiorgi, F., McDaniel, L., & Shields, C. (1995). Analysis of daily variability of precipitation in a nested regional climate model: Comparison with observations and doubled CO2 results. *Global Planet.Change*, 55-78.

Meehl, G. A., Washington, W. M., Erickson III, D. J., Briegleb, B. P., & Jaumann, P. J. (1996). Climate change from increased CO2 and direct and indirect effects of sulfate aerosols. *Geophysical Research Letters 23*, 3755-3758.

Meehl, G., Goddard, L., Murphy, J., Stouffer, R. J., Boer, G., Danabasoglu, G., . . . Stockdale, T. (2009). Decadal Prediction: Can It Be Skillful? *American Meteorological Society*, 1467-1485.

Meier, M. F., Dyurgerov, M. B., Rick, U. K., O'Neel, S., Pfeffer, W. T., Anderson, R. S., & Glazovsky, A. F. (2007). Glaciers dominate eustatic sea-level rise in the 21st century. *Science*, 1064-1067.

Micronesia, F. S. (2002). *FSM Census of Population and Housing.* Palikir, Pohnpei: Government of the Federated States of MIcronesia, Division of Statistics.

Morris, D. A., & Johnson, A. I. (1967). *Summary of Hydrologic and Physical Properties of Rock and Soil Materials, as Analyzed by the Hydrologic Laboratory of the U.S. Geological Survey.* Washington: United States Government Printing Office.

Mun, J. S., & Han, M. Y. (2012). Design and operational parameters of a rooftop rainwater harvesting system: definition, sensitivity and verification. *Journal of Environmental Management*, 147-153.

Mwenge Kahinda, J., Taigbenu, A. E., & Boroto, J. R. (2007). Domestic rainwater harvesting to improve water supply in rural South Africa. *Physics and Chemistry of the Earth*, 15-18.

Neuendorf, K. K., Mehl Jr., J. P., & Jackson, J. A. (2005). *Glossary of Geology.* Berlin: American Geological Institute.

Ngigi, S. N. (1999). Optimization of rainwater catchment systems design parameters in the arid and semiarid lands of Kenya. *9th International Rainwater Conference.*

Nurse, L., R., M., & Suarez, A. (2998). Small Islands States. *The Regional Impacts of Climate Change: An Assessment of Vulnerability*, 333-354.

Oberdorfer, J. A., Hogan, P. J., & Buddemeier, R. W. (1990). Atoll island hydrogeology: Flow and freshwater occurence in a tidally dominated system. *Journal of Hydrology*, 327-340.

Opare, S. (2012). Rainwater harvesting: an option for sustainable rural water supply in Ghana. *GeoJournal*, 695-705.

Özdemir, S., Elliot, M., Brown, J., Nam, P. K., Hien, V. T., & Sobsey, M. D. (2011). Rainwater harvesting practices and attitudes in the Mekong Delta of Vietnam. *Journal of Water, Sanitation, and Hygiene for Development*, 171-177.

Palla, A., Sansalone, J. J., Gnecco, I., & Lanza, L. G. (2011). Storm water infiltration in a monitored green roof for hydrologic water restoration. *Water Sci. Technol.*, 766.

Perkins, S. E., Pitman, A. J., Holbrook, N. J., & McAneney, J. (2007). Evaluation of the AR4 Climate Models' Simulated Daily Maximum Temperature, Minimum Temperature, and Precipitation over Australia Using Probability Density Functions. *Journal of Climate*, 4356-4376.

Peterson, F. L. (1990). *Groundwater Recharge Storage and Development on Small Atoll Islands.* Honolulu: University of Hawaii at Manoa, Honolulu Water Resources Research Center.

Peterson, T. C., & et al. (1998). Homogeneity adjustments of in-situ atmospheric data: A review. *International Journal of Climatology*, 1493-1517.

Pfeffer, W. T., Harper, J. T., & O'Neel, S. (2008). Kinematic constraintes on glacier contributions to 21st century sea-level rise. *Science*, 1340-1343.

Presley, T. K. (2005). Effects of the 1998 Drought on the Freshwater Lens in the Laura Area, Majuro Atoll, Republic of the Marshall Islands. *USGS Scientific Investigations Report 2005-5098*.

Rahmstorf, S. (2007). A semi-empirical approach to projecting future sea-level rise. *Science*, 368-370.

Randall, D. A. (2007). Climate models and their evaluation. In *Climate Change 2007: The Physical Science Basis*. Cambridge: Cambridge University Press.

Raper, S. C., & Braithwaite, R. J. (2006). Low sea-level rise projections from mountain glaciers and icecaps under global warming. *Nature*, 311-313.

Roebuck, R. M., & Ashley, R. M. (2006). Predicting the hydraulic and life-cycle cost performance of rainwater harvesting systems using a computer based modelling tool. *7th International Conference on Urban Drainage and 4th Internation Conference on Water Sensitive Urban Design*, (pp. 2699-2706). Melbourne.

Rowe, M. P. (2011). Rain water harvesting in Bermuda. *Journal of the American Water Resources Association*, 1219-1227.

Rumer, Jr., R. R., & Shiau, J. C. (1968). Salt Water Interface in a Layered Coastal Aquifer. *Water Resources Research*, 1235-1247.

Shamir, U., & Dagan, G. (1971). Motion of the seawater interface in coastal aquifer: A numerical solution. *Water Resources Research*, 644-657.

Simmons, G., Hope, V., Lewis, G., Whitmore, J., & Gao, W. (2001). Contamination of potable roof-collected rainwater in Auckland, New Zealand. *Water Research*, 1518-1524.

Spennemann, D. H. (2006). Freshwater Lens, Settlement Patterns, Resources Use and Connectivity in the Marshall Islands. *Tranforming Cultures eJournal*, 44-63.

Srikanthan, R., & McMahon, T. A. (2001). Stochastic generation of annual, monthly and daily climate data: A review. *Hydrology and Earth System Sciences*, 653-670.

Steffen, J., Jensen, M., Pomeroy, C. A., & Burian, S. J. (2013). Water supply and stormwater management benefits of residential rainwater harvesting in U.S. cities. *Journal of the American Water Resources Association*, 810-824.

Stephenson, R. A. (1984). A Comparison of freshwater use customs on Ulithi Atoll with those of selected other Micronesian islands. *WERI Technical Report No. 51*.

Sturm, M., Zimmermann, M., Schutz, K., Urban, W., & Hartung, H. (2009). Rainwater harvesting as an alternative water source in rural sites in central northern Namibia. *Physics and Chemistry of the Earth*, 776-785.

Sueo, K. (2003). Traditional Culture, Tourism, and Social Change in Mogmog Island, Ulithi Atoll. *Kagoshima University Research Center for the Pacific Islands Occasional Papers 39*, 1-9.

Sung, M., Kan, C. C., Wan, M. W., Yang, C. R., Wang, J. C., Yu, K. C., & Lee, S. Z. (2010). Rainwater harvesting in schools in Taiwan: system characteristics and water quality. *Water Science & Technology*, 1767-1778.

Swartz, J. H. (1962). Some physical constants for the Marshall Island area. *USGS Professional Paper 260-AA*.

Taboroši, D., & Collazo, M. S. (2011). Mwoakilloa Atoll: freshwater resources and their usage, state, and infrastructure. *Island Research & Education Initiative*.

Taboroši, D., & Martin, M. (2011). Pakein Atoll: freshwater resourcesand their usage, state, and infrastructure. *Island Research & Eduation Initiative*.

Taylor, K. E., Stouffer, R. J., & Meehl, G. A. (2012). An Overview of CMIP5 and the experiment design. *Bulletin of the American Meteorological Society 93*, 485-498.

Terry, J. P., & Chui, T. F. (2012). Evaluating the fate of freshwater lenses on atoll islands after eustatic sea-level rise and cyclone-driven inundation; A modelling approach. *Global and Planetary Change*, 76-84.

Terry, J. P., & Falkland, A. C. (2010). Responses of atoll freshwater lenses to storm-surge overwash in the Northern Cook Islands. *Hydrogeology journal*, 749-759.

Terry, J. P., & Falkland, A. C. (2010). Responses of atoll freshwater lenses to storm-surge overwash in the Northern Cook Islands. *Hydrogeology Journal*, 749-759.

Todd, D. K. (1959). *Ground-water Hydrology.* New York: Wiley.

Todorovic, P., & Woolhiser, D. A. (1975). A Stochastic Model of n-Day Precipitation. *Journal of Applied Meteorology*, 17-24.

Uba, B. N., & Aghogho, O. (2000). Rainwater quality from different roof catchments in the Port Harcourt District, Rivers State, Nigeria. *Journal of Water Supply: Res. Techol.*, 281-288.

Underwood, M. R. (1990). Atoll island hydrogeology: Conceptual and numerical models. *Ph.D. Dissertation*. University of Hawaii at Manoa, Honolulu.

Villarreal, E. L., & Dixon, A. (2005). Analysis of a rainwater collection system for domestic water supply in Ringdansen, Norrkoping, Sweden. *Building and Environment*, 1174-1184.

Voss, C. (1984). A finite-element simulation model for saturated-unsaturated, fluid density-dependent ground-water flow with energy transport of chemically-reactive single-species solut transport. *USGS Water Resources Investigation Report 84-4369.*

Wallace, C. D., & Bailey, R. T. (2014). Sustainable Rainwater Catchment Systems for Micronesian Atoll Communities. *Journal of the American Water Resources Association (JAWRA)*, 1-15.

Walsh, K. J., & McGregor, J. L. (1995). January and July climate simulations over the Australian region using a limited-area model. *Climate*, 2387-2403.

Walsh, K. J., & McGregor, J. L. (1997). An assessment of simulations of climate variablity over Australia with a limited area model. *International Journal of Climatology*, 201-223.

Ward, S., Memon, F. A., & Butler, D. (2010). Rainwater harvesting: model-based design evaluation. *Water Science & Technology*, 85-96.

Wheatcraft, S. W., & Buddemeier, R. W. (1981). Atoll island hydrology. *Ground Water*, 311-320.

White, I., & Falkland, T. (2010). Management of freshwater lenses on small Pacific islands. *Hydrogeology Journal*, 227-246.

White, I., Falkland, T., & Scott, D. (1999). Droughts in small coral islands: Case study, South Tarawa, Kiribati. *Technical Documents in Hydrology No. 26*.

White, I., Falkland, T., Perez, P., Dray, A., Metutera, T., Metai, E., & Overmars, M. (2007). Challenges in freshwater management in low coral atolls. *Journal of Cleaner Production*, 1522-1528.

Woodroffe, C. D., & Falkland, A. C. (1997). Geology and hydrogeology of the Cocos (Keeling) Islands. *Geology and Hydrogeology of Carbonate Islands. Developments in Sedimentology 54*, 885-908.

APPENDIX I

Table A1. Thickness in meters for each of the 29 model layers used in each of the eight island models. Due to similarity in atoll geologic structure, the same vertical discretization was used for each model.

Layer	Thickness (m)
1	0.5
2	0.5
3	0.5
4	0.5
5	0.5
6	0.5
7	0.5
8	0.5
9	0.5
10	0.5
11	0.5
12	0.5
13	0.75
14	0.75
15	0.75
16	0.75
17	0.75
18	0.75
19	0.75
20	0.75
21	0.75
22	0.75
23	0.75
24	0.75
25	7
26	7
27	7
28	7
29	7

Table A2. Statistical results of RCP4.5 forcing scenario in Pohnpei State. It is observed that higher NRMSE and RE values are seen in this scenario than in the RCP2.6 forcing scenario

GCMs	Mean (mm)	St Dev	NRMSE	RE (%)	BS	S_{score}
1	13.5	25.2	1.77	4.11	0.014	54.4
2	13.4	25.3	1.30	3.02	0.018	53.0
3	13.1	26.3	0.73	1.71	0.018	53.0
4	13.1	22.2	0.57	1.34	0.006	71.9
6	13.3	23.1	1.48	3.45	0.002	83.6
7	13.1	21.1	0.44	1.03	0.003	81.1
11	13.1	21.5	0.67	1.56	0.002	85.2
12	13.3	21.2	1.10	2.56	0.002	83.3
13	13.2	21.0	1.15	2.67	0.003	79.8
19	13.3	21.6	0.95	2.20	0.004	77.7
20	13.0	21.0	0.11	0.26	0.002	82.1
21	13.3	21.0	1.26	2.92	0.002	82.3
23	13.0	21.6	0.12	0.29	0.003	79.8
24	13.3	21.7	1.25	2.92	0.003	82.9
25	13.2	21.4	0.89	2.08	0.003	79.5
28	13.1	23.2	0.69	1.61	0.004	76.4
31	13.3	22.2	1.15	2.67	0.002	85.7
32	13.3	21.3	1.19	2.78	0.003	79.7
33	13.4	22.1	1.89	4.40	0.004	77.3
36a	13.3	20.9	1.26	2.93	0.002	83.0
36b	13.2	20.8	1.06	2.46	0.002	82.5
36c	13.1	20.5	0.63	1.47	0.002	83.5
37	13.2	21.3	0.88	2.05	0.003	81.0
38a	13.1	20.6	0.42	0.98	0.002	83.9
38b	13.2	21.3	0.93	2.16	0.003	82.3

Table A3. Statistical results of RCP6.0 forcing scenario in Pohnpei State. 20 GCMs were analyzed for this scenario as not as many modeling groups focused on this particular forcing

GCMs	Mean (mm)	St Dev	NRMSE	RE (%)	BS	S_{score}
3	13.3	25.0	1.32	3.08	0.015	56.5
4	13.2	22.2	0.83	1.92	0.004	76.7
11	13.2	21.3	0.93	2.17	0.015	65.3
23	13.3	23.0	1.07	2.49	0.005	75.0
28	13.1	21.0	0.42	0.99	0.003	83.4
31	13.1	22.5	0.70	1.63	0.004	78.5
32	13.0	22.1	0.19	0.45	0.004	76.3
33	13.2	22.5	0.80	1.85	0.004	75.8
36	13.1	22.2	0.41	0.96	0.002	84.3
38	13.1	20.8	0.60	1.39	0.001	86.2
40	13.1	23.9	0.30	0.70	0.011	59.9
43	13.2	22.9	0.91	2.11	0.009	64.1
46	13.3	22.8	1.19	2.77	0.006	74.0
47	13.2	22.8	1.00	2.33	0.006	74.1
52	13.3	21.6	1.22	2.85	0.006	76.4
49	13.3	21.1	1.13	2.64	0.005	79.6
50	13.3	21.8	1.30	3.02	0.005	77.5
58	13.2	21.6	0.86	2.00	0.003	81.5
61	13.1	22.7	0.66	1.53	0.002	83.0
62	13.1	22.1	0.80	1.85	0.003	81.0

Table A4. Statistical results of RCP8.5 forcing scenario in Pohnpei State. 39 GCMs were analyzed for this forcing, which represents a high emissions scenario driven by emissions

GCMs	Mean (mm)	St Dev	NRMSE	RE (%)	BS	S_{score}
1	13.4	24.9	1.61	3.74	0.011	60.4
2	13.4	24.9	1.40	3.26	0.015	56.7
3	13.4	25.2	1.38	3.21	0.015	55.4
6	13.4	22.5	1.49	3.48	0.003	82.1
7	13.2	20.6	0.91	2.13	0.009	70.4
11	13.3	21.1	1.07	2.48	0.009	70.7
12	13.3	22.5	1.30	3.04	0.003	81.7
13	13.2	20.8	1.00	2.33	0.012	67.2
19	13.3	22.2	1.14	2.66	0.004	77.8
20	13.0	21.0	0.33	0.77	0.002	84.0
21	13.2	19.9	0.97	2.25	0.010	67.6
23	13.2	20.5	0.85	1.98	0.006	71.8
24	13.3	21.3	1.39	3.24	0.008	72.5
25	13.4	21.3	1.32	3.08	0.004	78.4
28	13.1	20.7	0.68	1.58	0.003	80.7
31	13.2	22.1	0.73	1.70	0.002	85.2
32	13.1	21.1	0.48	1.13	0.002	82.1
33	13.3	21.5	1.29	2.99	0.003	80.5
36a	13.1	20.7	0.63	1.48	0.002	83.8
36b	13.2	20.7	1.10	2.55	0.002	84.1
36c	13.1	20.2	0.63	1.47	0.002	84.9
38a	13.2	20.3	0.95	2.21	0.002	86.4
38b	13.2	20.7	0.96	2.23	0.002	86.6
38c	13.3	20.3	1.33	3.09	0.003	82.5
40	13.0	24.8	0.09	0.21	0.016	53.9
42	13.0	23.7	0.24	0.56	0.012	58.1
43	13.2	23.5	0.96	2.25	0.011	58.3
45	13.3	20.6	1.05	2.44	0.004	78.9
46	13.3	21.8	1.35	3.15	0.013	64.8
47	13.2	21.7	0.85	1.98	0.007	74.4
48	13.3	23.7	1.05	2.45	0.009	63.5
52	13.3	20.5	1.33	3.10	0.010	69.0
49	13.4	21.6	1.48	3.45	0.004	78.1
50	13.4	21.5	1.46	3.40	0.005	76.9
54	13.1	21.3	0.72	1.67	0.004	79.2
53	13.4	21.9	1.63	3.79	0.002	82.6
58	13.2	21.6	0.90	2.10	0.004	77.2
61	13.1	21.3	0.64	1.50	0.002	83.7
62	13.1	21.7	0.88	2.04	0.002	86.8

Table A5. Statistical results of RCP2.6 forcing scenario in Yap State.

GCMs	Mean (mm)	St Dev	NRMSE	RE (%)	BS	S_{score}
3	8.2	18.4	0.43	-3.37	0.015	67.4
4	8.3	16.8	0.32	-2.47	0.005	76.6
6	8.5	16.0	0.04	-0.33	0.005	77.7
7	8.3	15.0	0.27	-2.10	0.018	58.0
11	8.3	15.1	0.29	-2.25	0.030	49.2
13	8.4	15.2	0.22	-1.73	0.028	50.5
21	8.4	16.2	0.19	-1.51	0.006	76.7
23	8.3	15.7	0.33	-2.60	0.043	41.0
24	8.4	15.7	0.21	-1.60	0.018	59.5
25	8.4	16.2	0.24	-1.89	0.004	77.3
28	8.2	15.2	0.43	-3.33	0.010	68.3
31	8.3	16.3	0.29	-2.23	0.007	75.2
32	8.3	16.4	0.29	-2.29	0.003	81.8
33	8.3	17.0	0.28	-2.21	0.003	82.2
36	8.4	16.4	0.24	-1.85	0.003	83.3
38	8.3	15.6	0.29	-2.26	0.004	79.8
40	8.2	18.1	0.41	-3.19	0.017	61.1
43	8.4	17.0	0.21	-1.62	0.016	62.0
47	8.3	15.5	0.34	-2.64	0.017	59.0
52	8.3	16.5	0.29	-2.27	0.009	69.6
49	8.4	15.9	0.25	-1.92	0.005	78.5
54	8.4	16.5	0.24	-1.88	0.014	64.7
53	8.3	17.6	0.29	-2.25	0.004	79.5
58	8.2	16.6	0.48	-3.73	0.004	81.3
61	8.4	16.8	0.13	-1.05	0.004	79.1
62	8.3	16.4	0.30	-2.31	0.004	81.9

Table A6. Statistical results of RCP4.5 forcing scenario in Yap State.

GCMs	Mean (mm)	St Dev	NRMSE	RE (%)	BS	S_{score}
1	8.4	20.0	0.12	-0.95	0.017	64.6
2	8.3	19.1	0.36	-2.79	0.017	64.6
3	8.3	20.0	0.27	-2.10	0.016	62.2
4	8.3	17.2	0.31	-2.42	0.005	77.3
6	8.4	16.6	0.22	-1.74	0.003	82.9
7	8.4	16.0	0.25	-1.95	0.005	76.7
11	8.3	15.9	0.30	-2.34	0.004	79.6
12	8.5	16.0	0.03	-0.20	0.004	79.5
13	8.4	15.6	0.18	-1.42	0.009	71.7
19	8.3	18.3	0.34	-2.67	0.012	69.9
20	8.4	17.6	0.17	-1.31	0.006	77.8
21	8.4	16.6	0.23	-1.82	0.004	79.1
23	8.2	15.9	0.52	-4.02	0.005	76.9
24	8.4	15.8	0.16	-1.22	0.008	71.1
25	8.2	17.1	0.44	-3.41	0.003	83.4
28	8.3	16.9	0.34	-2.68	0.003	80.6
31	8.5	16.9	0.08	-0.64	0.005	77.7
32	8.2	16.2	0.47	-3.68	0.003	82.1
33	8.7	17.5	0.23	1.79	0.003	84.3
36a	8.3	16.9	0.29	-2.26	0.002	84.4
36b	8.4	16.6	0.14	-1.10	0.003	81.4
36c	8.4	15.9	0.18	-1.41	0.004	81.4
37	8.5	17.1	0.04	0.28	0.003	82.8
38a	8.5	16.5	0.01	-0.10	0.004	79.9
38b	8.3	16.1	0.36	-2.79	0.003	82.4

Table A7. Statistical results of RCP6.0 forcing scenario in Yap State.

GCMs	Mean (mm)	St Dev	NRMSE	RE (%)	BS	S_{score}
3	8.3	18.4	0.34	-2.67	0.014	67.5
4	8.3	15.9	0.38	-3.00	0.005	76.6
11	8.3	15.3	0.30	-2.32	0.028	49.8
23	8.3	16.1	0.30	-2.30	0.025	46.4
28	8.3	15.1	0.39	-3.07	0.007	72.1
31	8.3	16.4	0.32	-2.51	0.007	75.5
32	8.2	15.9	0.45	-3.51	0.005	77.6
33	8.3	16.8	0.31	-2.42	0.004	79.3
36	8.3	16.2	0.39	-3.08	0.007	71.8
38	8.4	16.0	0.19	-1.46	0.005	77.7
40	8.4	17.6	0.23	-1.76	0.010	69.9
43	8.4	16.7	0.24	-1.88	0.007	73.7
46	8.4	16.1	0.17	-1.31	0.020	56.9
47	8.4	16.4	0.24	-1.85	0.021	54.9
52	8.4	16.0	0.16	-1.26	0.021	56.4
49	8.4	15.3	0.24	-1.86	0.009	72.2
50	8.4	15.4	0.18	-1.39	0.009	72.9
58	8.3	16.1	0.34	-2.66	0.003	80.2
61	8.3	16.4	0.28	-2.22	0.008	71.7
62	8.3	16.3	0.28	-2.16	0.007	72.8

Table A8. Statistical results of RCP8.5 forcing scenario in Yap State. 39 GCMs were analyzed for this forcing, which represents a high emissions scenario driven by emissions

GCMs	Mean (mm)	St Dev	NRMSE	RE (%)	BS	S_{score}
1	8.4	17.9	0.24	-1.89	0.010	71.5
2	8.3	17.6	0.41	-3.17	0.014	69.6
3	8.5	18.8	0.09	-0.70	0.013	65.4
6	8.4	16.4	0.25	-1.97	0.004	81.7
7	8.3	15.4	0.26	-2.00	0.013	64.4
11	8.3	15.2	0.28	-2.15	0.024	53.6
12	8.5	16.4	0.08	-0.62	0.005	78.2
13	8.4	15.1	0.24	-1.87	0.027	49.1
19	8.3	17.5	0.26	-2.05	0.007	75.6
20	8.4	17.5	0.21	-1.61	0.004	80.4
21	8.3	15.2	0.28	-2.19	0.017	57.6
23	8.3	15.4	0.37	-2.90	0.039	42.1
24	8.4	15.6	0.17	-1.32	0.027	51.0
25	8.3	16.0	0.28	-2.17	0.004	79.8
28	8.2	15.3	0.42	-3.30	0.008	70.9
31	8.3	16.4	0.26	-2.06	0.006	76.2
32	8.2	16.3	0.47	-3.63	0.003	81.9
33	8.3	17.0	0.33	-2.60	0.003	82.5
36a	8.4	16.6	0.23	-1.82	0.003	80.7
36b	8.5	17.1	0.01	-0.07	0.002	83.9
36c	8.4	16.2	0.12	-0.94	0.005	78.1
38a	8.3	16.3	0.26	-2.03	0.004	79.3
38b	8.3	15.8	0.32	-2.50	0.003	80.8
38c	8.3	15.6	0.29	-2.24	0.006	74.1
40	8.3	18.5	0.33	-2.60	0.019	58.6
42	8.1	17.4	0.57	-4.43	0.013	67.3
43	8.4	17.4	0.15	-1.20	0.014	66.1
45	8.4	15.5	0.12	-0.95	0.008	70.6
46	8.4	15.4	0.15	-1.15	0.031	48.4
47	8.4	16.0	0.19	-1.52	0.018	56.5
48	8.2	18.5	0.41	-3.20	0.007	74.9
52	8.3	16.8	0.28	-2.19	0.008	71.1
49	8.4	15.7	0.17	-1.34	0.005	78.7
50	8.4	15.6	0.15	-1.16	0.004	80.2
54	8.4	16.3	0.21	-1.61	0.011	67.9
53	8.4	17.9	0.11	-0.88	0.004	79.9
58	8.1	16.2	0.57	-4.48	0.003	82.2
61	8.4	16.5	0.25	-1.93	0.003	81.8
62	8.3	16.6	0.33	-2.58	0.004	79.3

Table A9. Sensitivity analysis results showing the changes in lens thickness and volume for increasing depths to contact between the upper Holocene and lower Pleistocene aquifers.

Contact Depth (m)	10	15	20	30	40	50
Mangejang	6.19 80781.0	9.21 128364.4	8.50 127714.2	8.50 128199.2	8.29 122444.7	7.60 116475.1
Fassarai	2.09 12114.1	2.74 17770.6	3.24 18473.9	3.24 19214.7	2.24 16265.8	2.24 15326.4
Nikahlap	7.26 356914.5	12.26 895431.1	12.60 1076833.7	11.40 1078121.7	13.16 1138946.4	13.86 1155051.3
Pingelap	7.26 380837.3	12.27 961247.4	14.54 1263371.2	12.75 1318441.4	13.17 1385961.9	13.95 1414834.0
Deke	7.25 312547.4	11.53 617003.1	12.43 807582.0	11.36 759096.8	12.27 775642.7	12.65 798962.6

Table A10. Sensitivity analysis results showing the reaction of the lens thickness (top) and volume (bottom) to changes in the depth of annual lens recharge.

Annual Recharge (m/yr)	0.5	1	1.5	2	2.5	3	3.5	4
Mangejang	3.66 44682.3	5.19 80029.0	6.98 103640.1	7.75 120892.6	8.42 133331.3	9.33 144231.5	9.42 153635.7	11.39 165976.3
Fassarai	0.77 11723.7	1.70 15158.6	1.23 14615.5	3.24 18812.9	3.59 29125.3	3.60 38079.3	4.15 56142.5	4.67 71238.9
Nikahlap	7.00 539302.9	9.48 801908.2	13.45 991742.6	15.40 1155193.2	17.37 1318209.8	19.30 1440752.5	19.43 1507914.3	19.49 1533249.4
Pingelap	7.75 700694.2	11.38 1003446.3	13.60 1253290.6	15.55 1453367.4	17.49 1631517.6	19.45 1757468.4	19.51 1790259.2	19.56 1788907.6
Deke	5.68 366834.0	9.27 584803.7	11.51 663178.3	12.22 628365.5	12.26 638536.1	12.27 630897.9	12.27 601571.3	12.28 578731.3

Table A11. Sensitivity analysis results showing the fluctuations in lens thickness (top) and volume (bottom) with varying depths of annual coconut root extraction

Coconut Root Extraction (mm/yr)	400	500	600	700	800
Mangejang	8.45 138670.1	8.45 138518.3	8.45 138309.9	8.45 138105.4	8.45 137841.5
Fassarai	0.72 5359.5	0.30 5079.5	0.28 4693.2	0.28 4655.7	0.28 4664.2
Nikahlap	15.56 1241854.8	15.45 1192644.3	15.40 1152732.2	15.37 1117124.3	13.65 1075101.5
Pingelap	19.27 1645233.5	17.49 1603529.4	17.48 1558223.0	17.42 1509767.0	17.36 1462252.1
Deke	4.68 239134.5	4.19 217094.9	4.18 208987.9	3.72 199755.8	3.69 182611.8

APPENDIX II

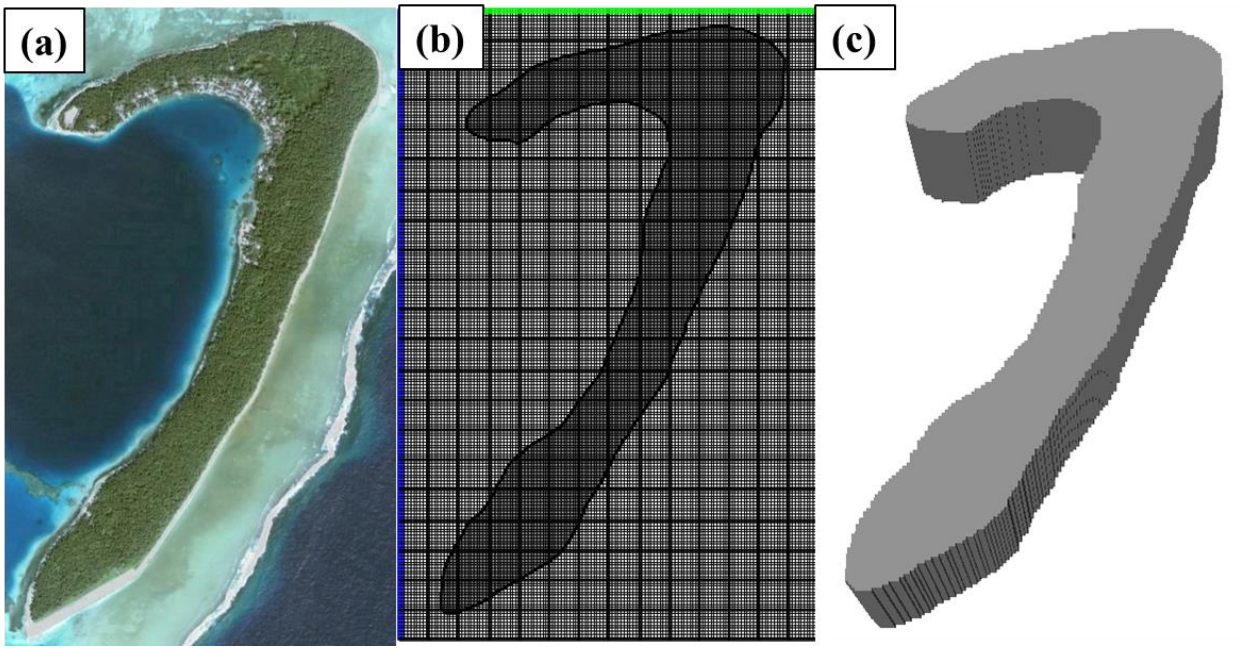

Figure B1. Model development for Kahlap Island in Pohnpei State. (a) Google Earth screen capture, (b) two-dimensional view of model grid, (c) three-dimensional representation of model

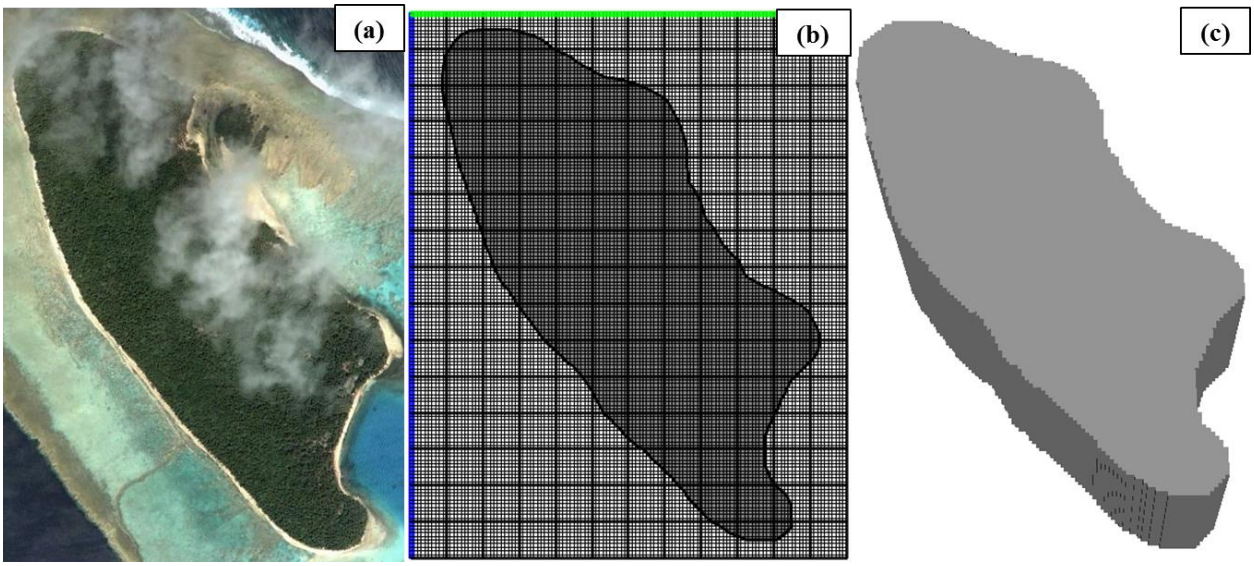

Figure B2. Model development for Nikahlap Island in Pohnpei State. (a) Google Earth screen capture, (b) two-dimensional view of model grid, (c) three-dimensional representation of model

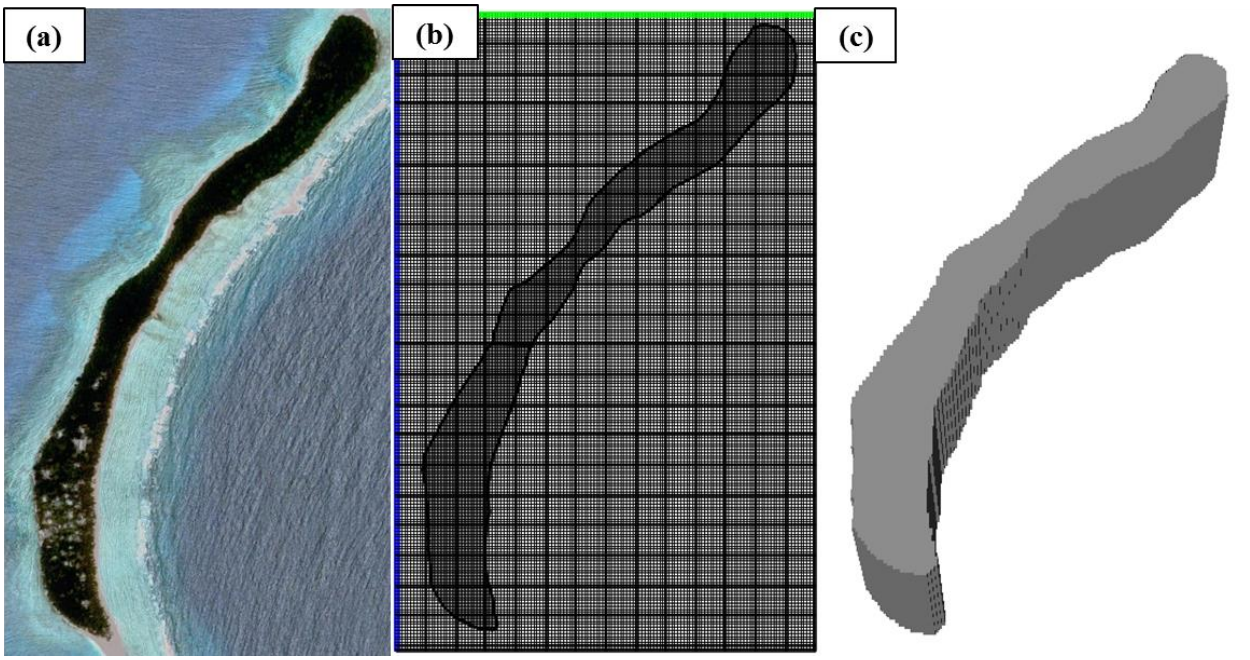

Figure B3. Model development for Fassarai Island in Yap State. (a) Google Earth screen capture, (b) two-dimensional view of model grid, (c) three-dimensional representation of model

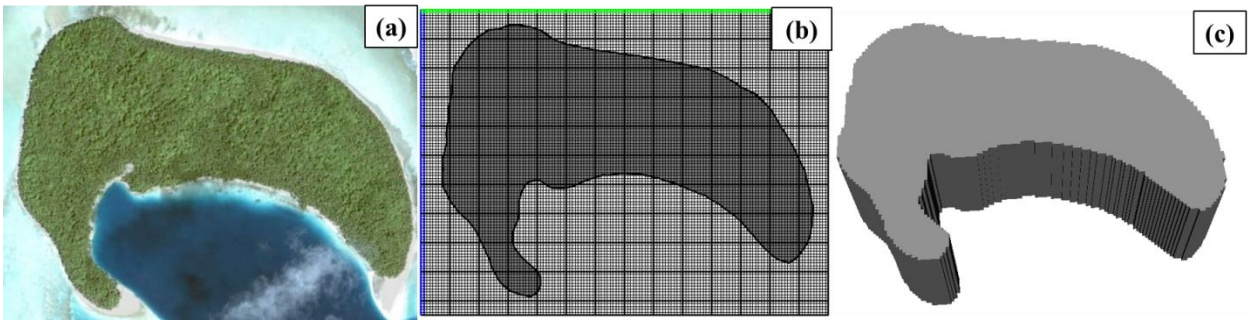

Figure B4. Model development for Deke Island in Pohnpei State. (a) Google Earth screen capture, (b) two-dimensional view of model grid, (c) three-dimensional representation of model

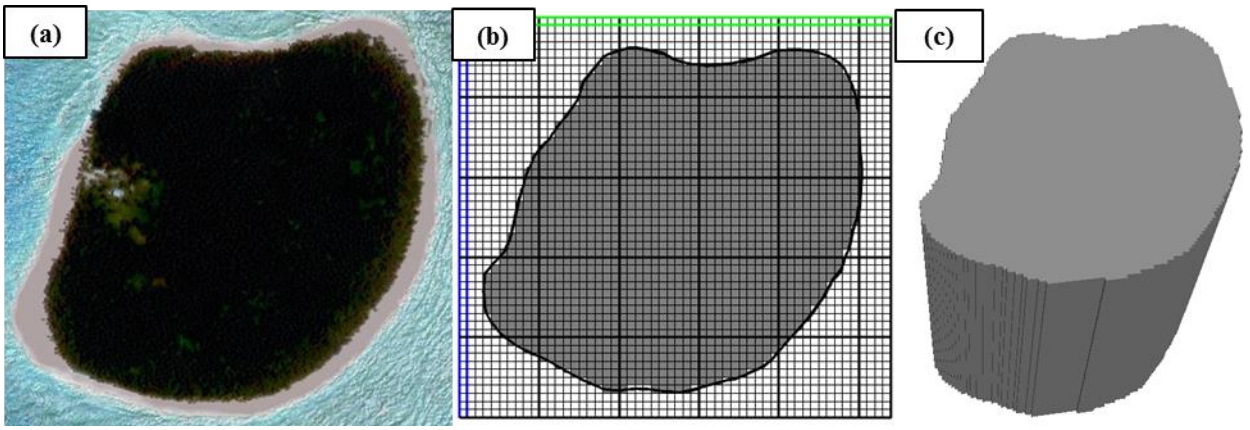

Figure B5. Model development for Mangejang Island in Yap State. (a) Google Earth screen capture, (b) two-dimensional view of model grid, (c) three-dimensional representation of model

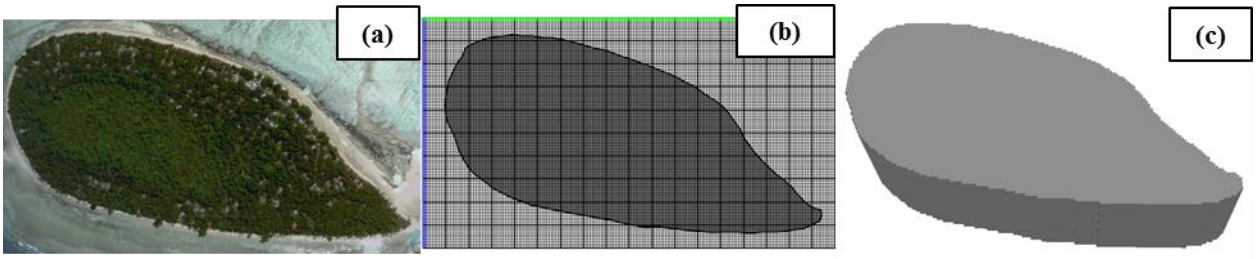

Figure B6. Model development for Ngatik Island in Pohnpei State. (a) Google Earth screen capture, (b) two-dimensional view of model grid, (c) three-dimensional representation of model

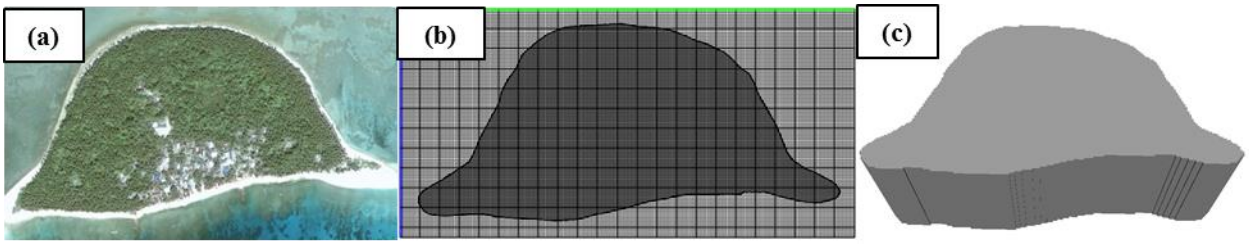

Figure B7. Model development for Mogmog Island in Yap State. (a) Google Earth screen capture, (b) two-dimensional view of model grid, (c) three-dimensional representation of model

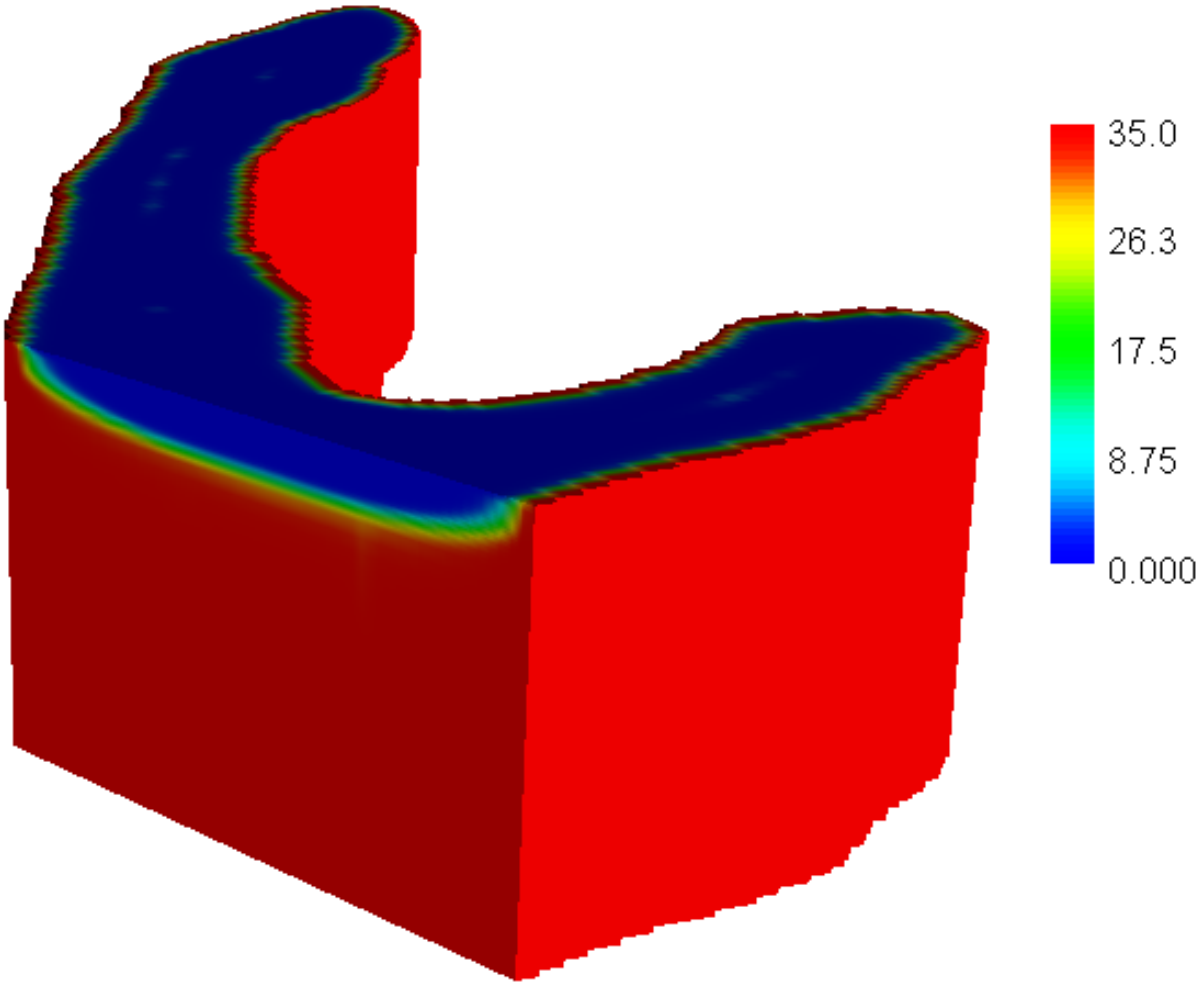

Figure B8. Cross-sectional view of three-dimensional model of Kahlap Island showing calibrated lens volume. Red indicates seawater salt concentration of 35 g/kg and blue indicates freshwater concentration of salt near 0 g/kg. A transitional zone is seen between the freshwater and seawater regions

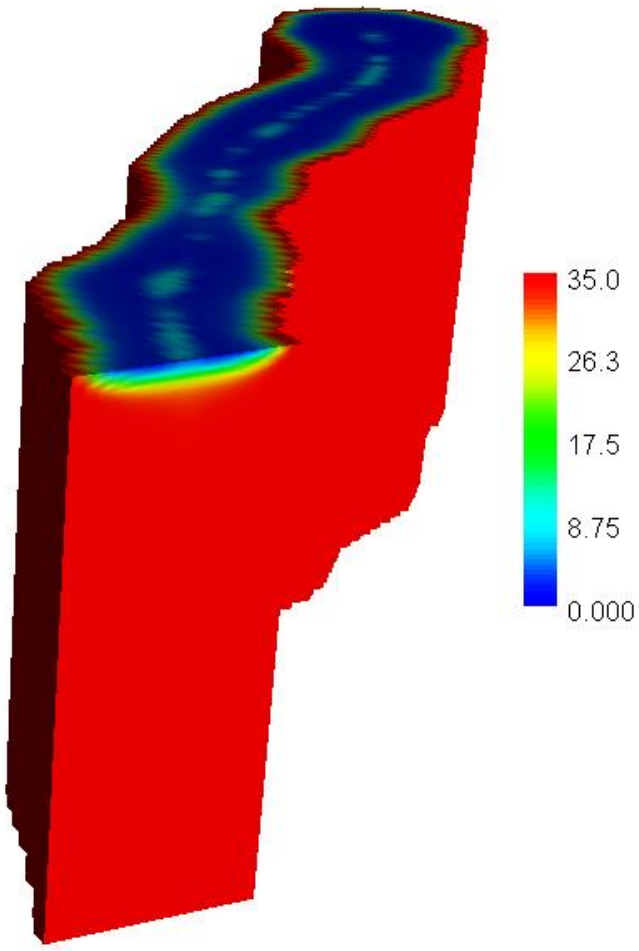

Figure B9. Cross-sectional view of three-dimensional model of Fassarai Island showing calibrated lens volume. Red indicates seawater salt concentration of 35 g/kg and blue indicates freshwater concentration of salt near 0 g/kg. A transitional zone is seen between the freshwater and seawater regions

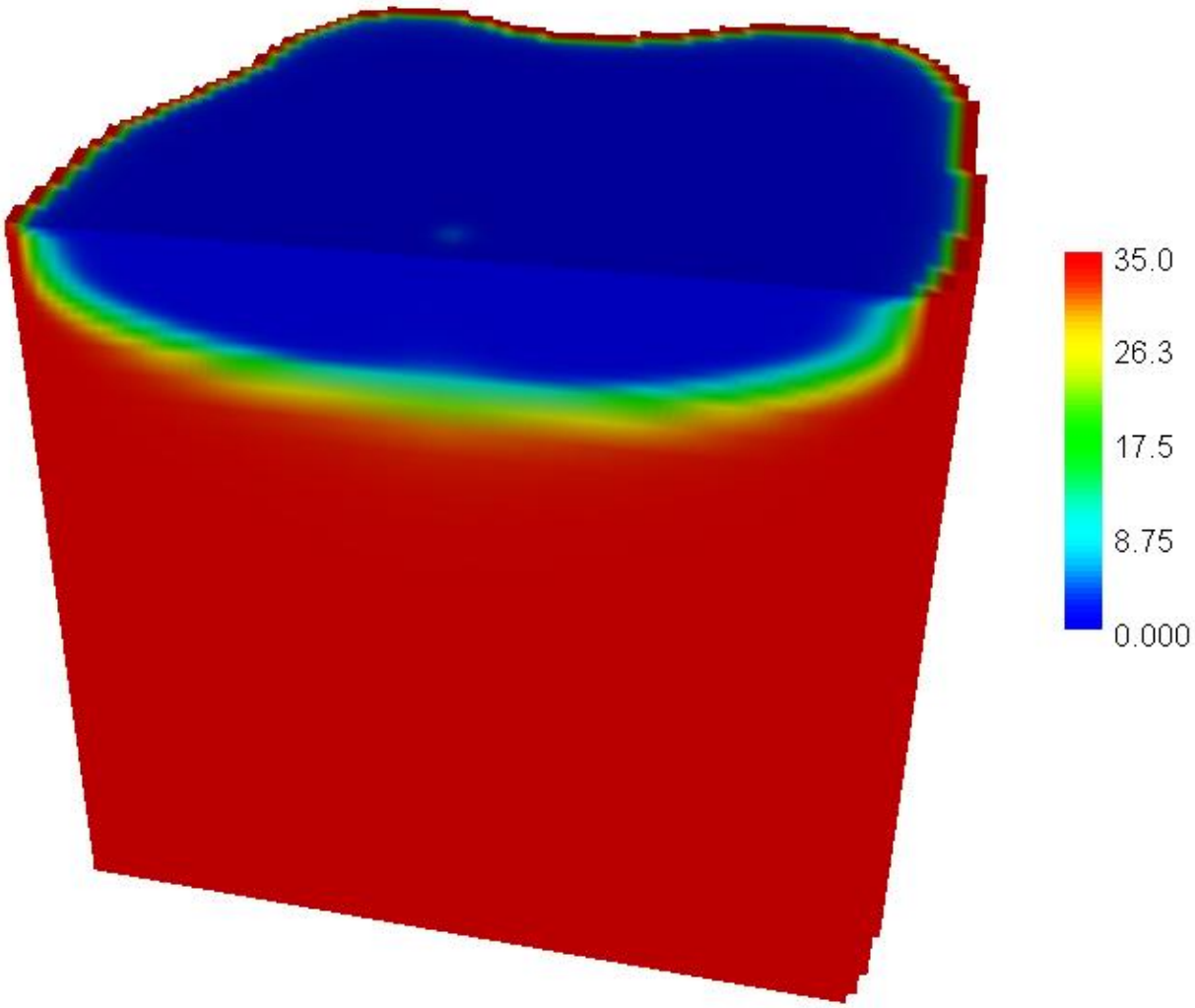

Figure B10. Cross-sectional view of three-dimensional model of Mangejang Island showing calibrated lens volume. Red indicates seawater salt concentration of 35 g/kg and blue indicates freshwater concentration of salt near 0 g/kg. A transitional zone is seen between the freshwater and seawater regions

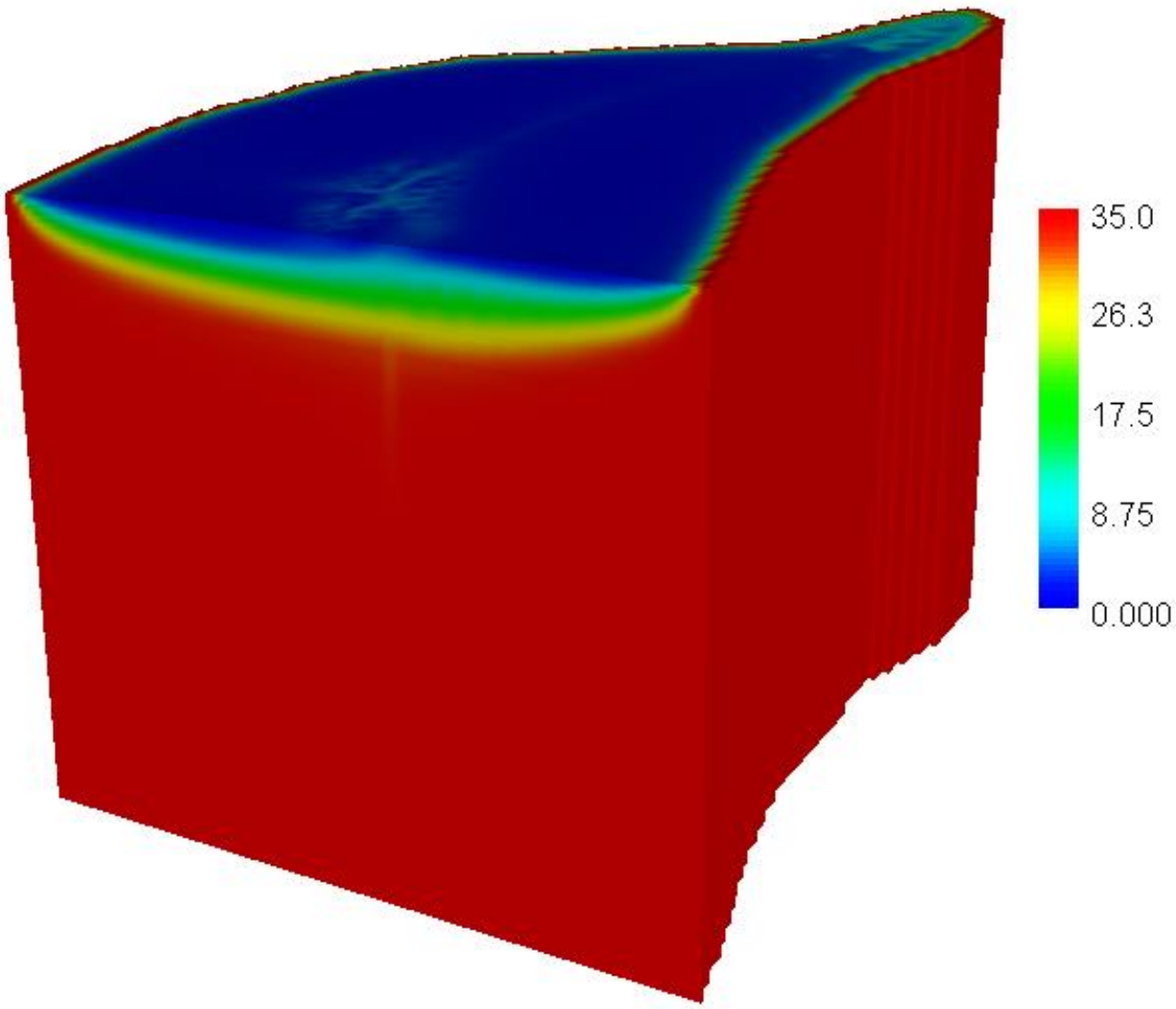

Figure B11. Cross-sectional view of three-dimensional model of Mogmog Island showing calibrated lens volume. Red indicates seawater salt concentration of 35 g/kg and blue indicates freshwater concentration of salt near 0 g/kg. A transitional zone is seen between the freshwater and seawater regions

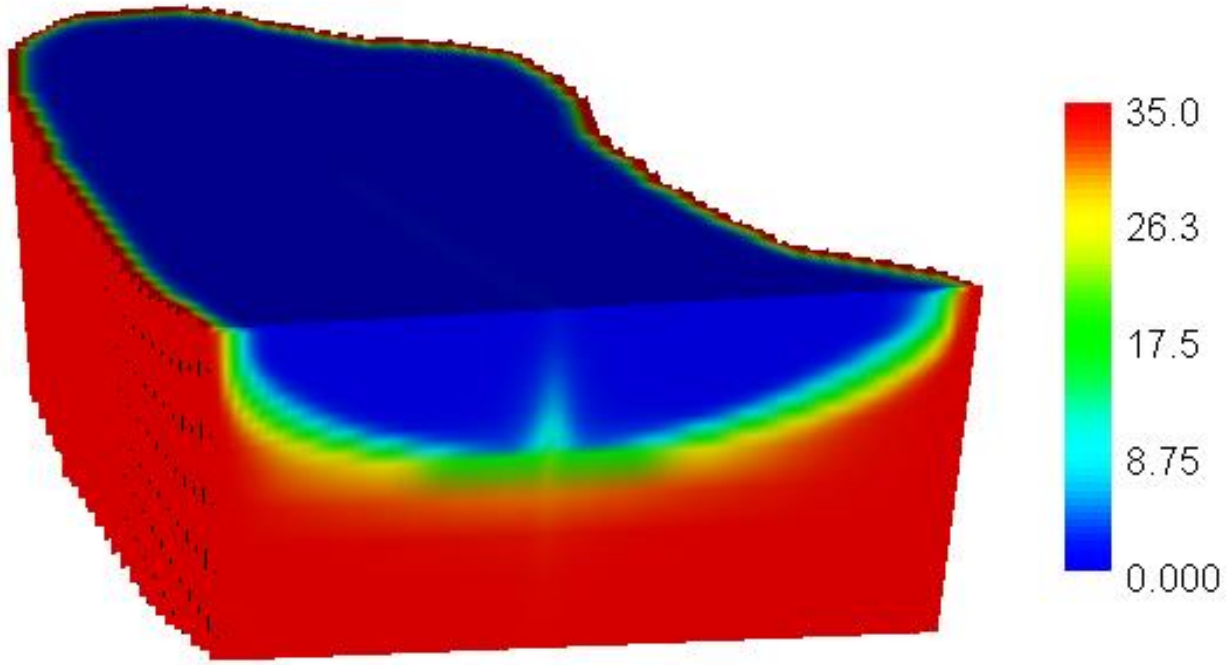

Figure B 12. Cross-sectional view of three-dimensional model of Nikahlap Island showing calibrated lens volume. Red indicates seawater salt concentration of 35 g/kg and blue indicates freshwater concentration of salt near 0 g/kg. A transitional zone is seen between the freshwater and seawater regions, with truncation occurring at a depth of 20 meters as the lens meets the contact between the Holocene and Pleistocene aquifers

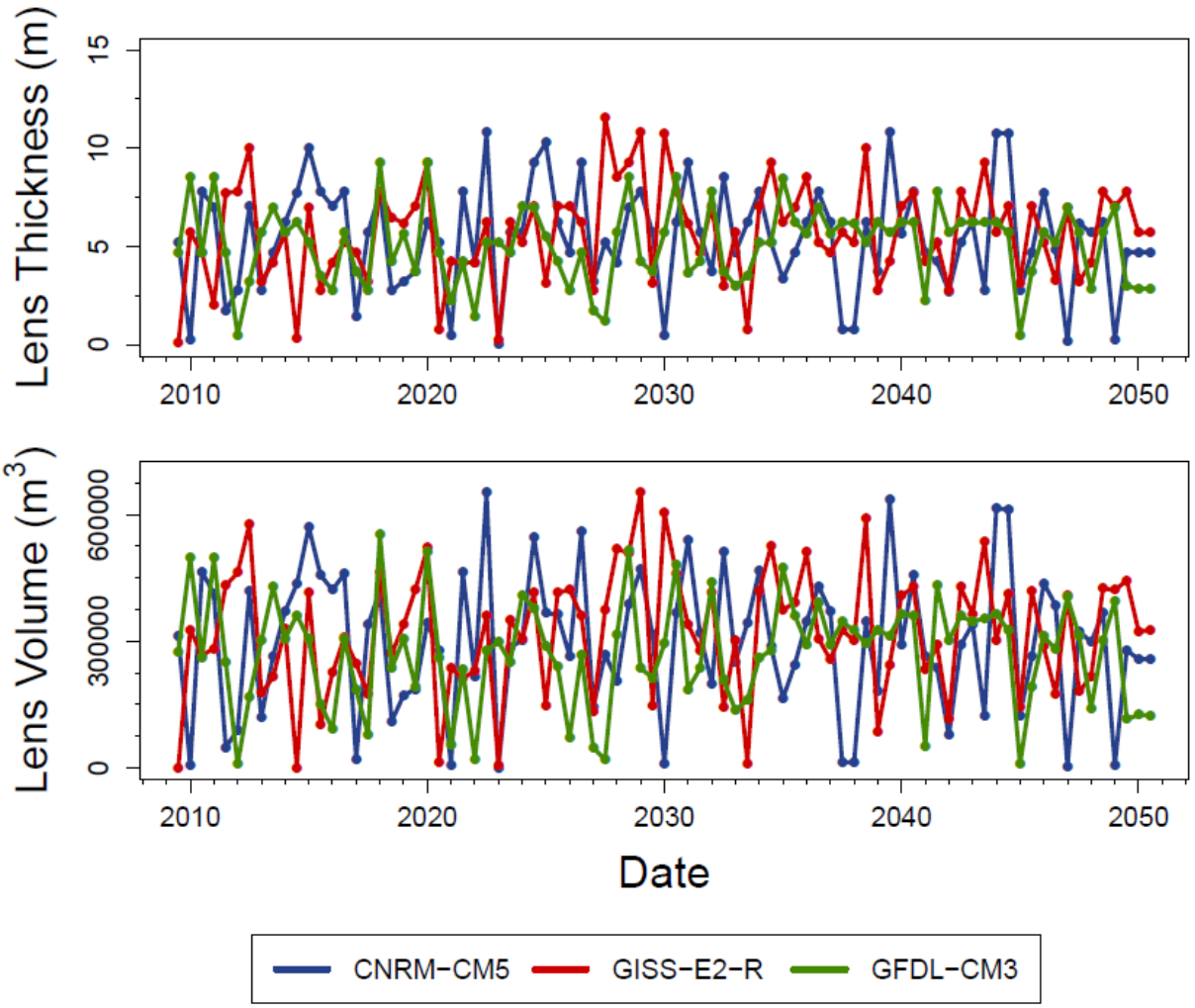

Figure B13. Time series of lens thickness and volume for the top three performing GCMs for Deke Island under the RCP2.6 forcing scenario

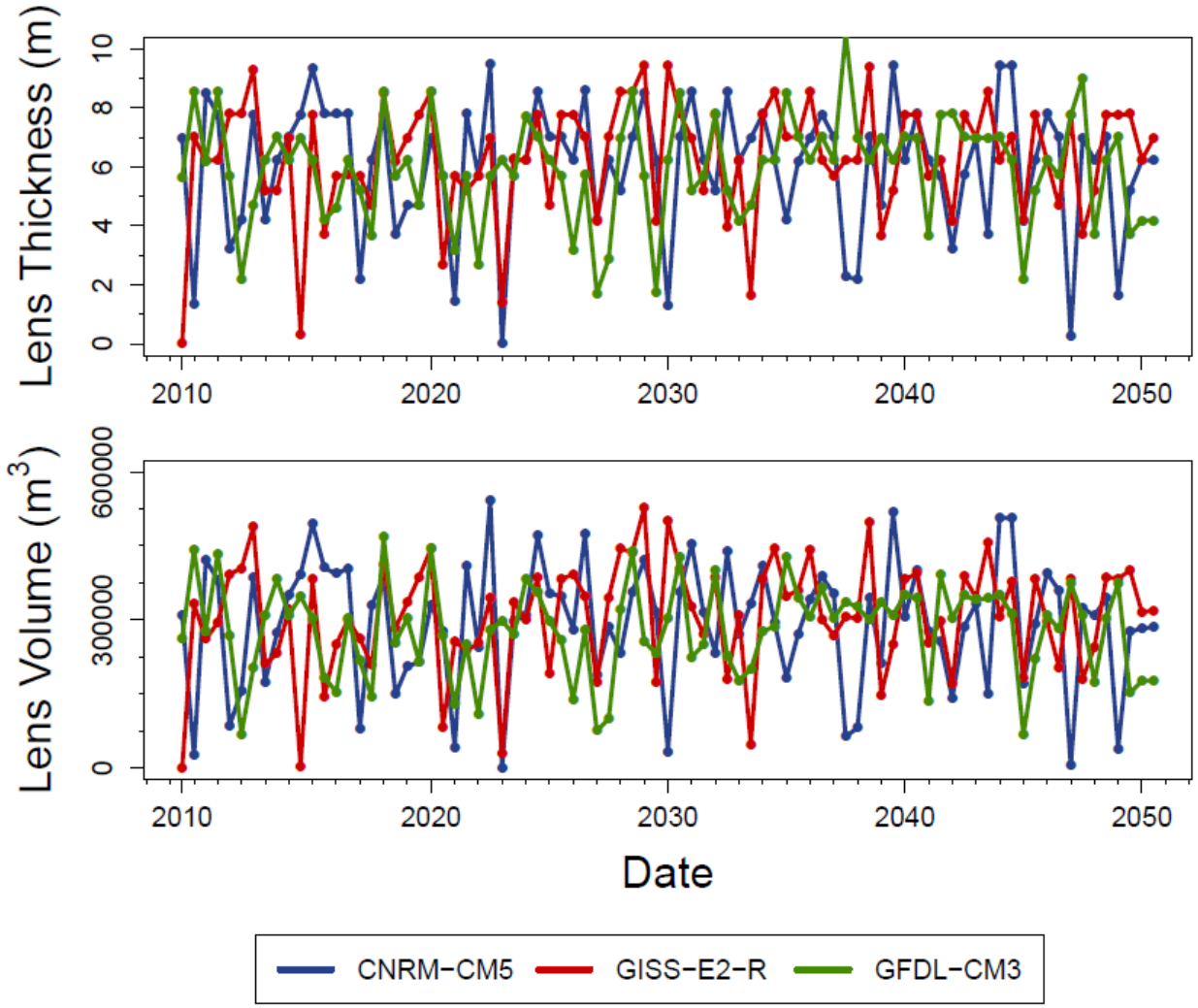

Figure B14. Time series of lens thickness and volume for the top three performing GCMs for Kahlap Island under the RCP2.6 forcing scenario

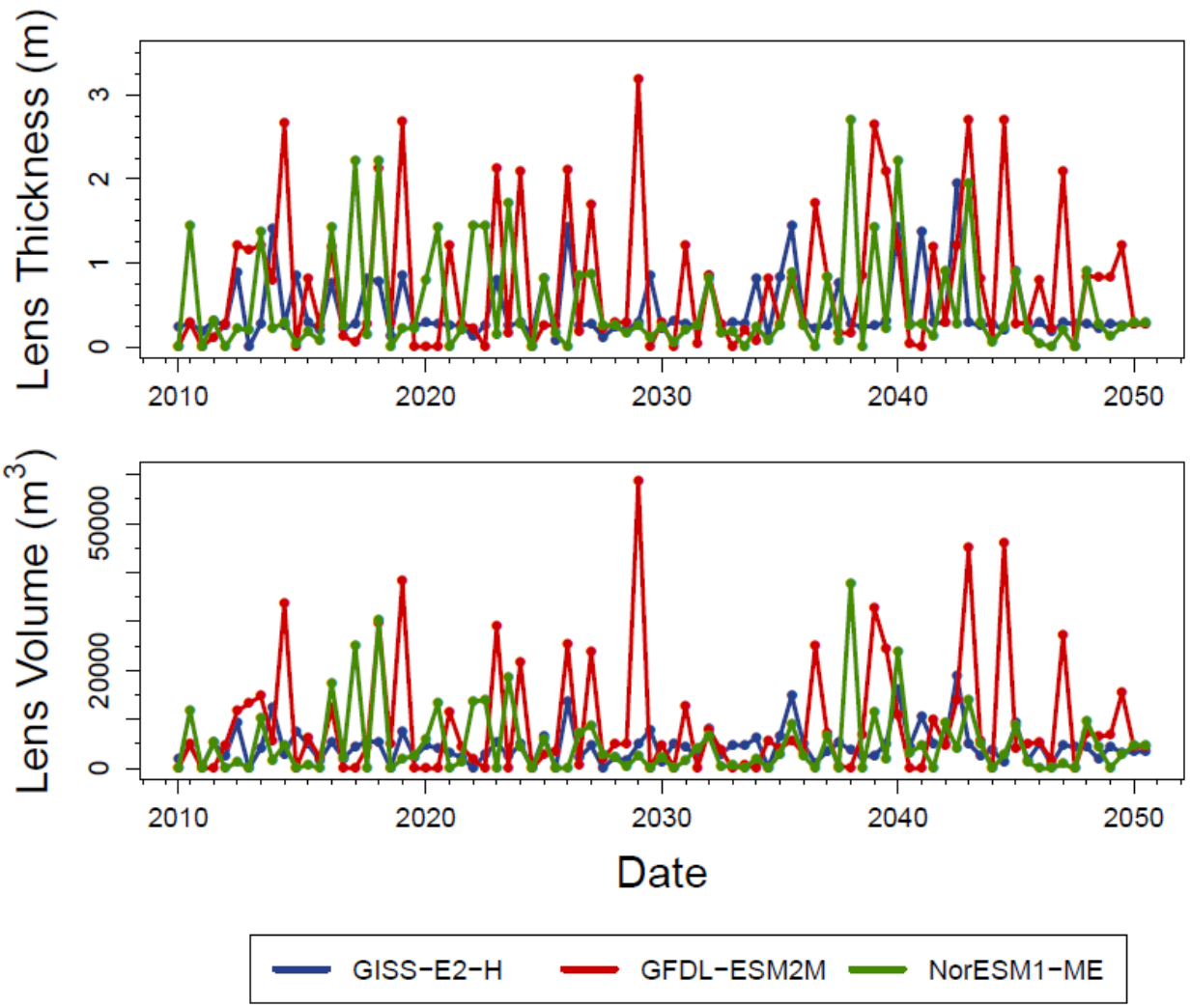

Figure B15. Time series of lens thickness and volume for Fassarai Island from 2010-2050 under the RCP2.6 forcing scenario

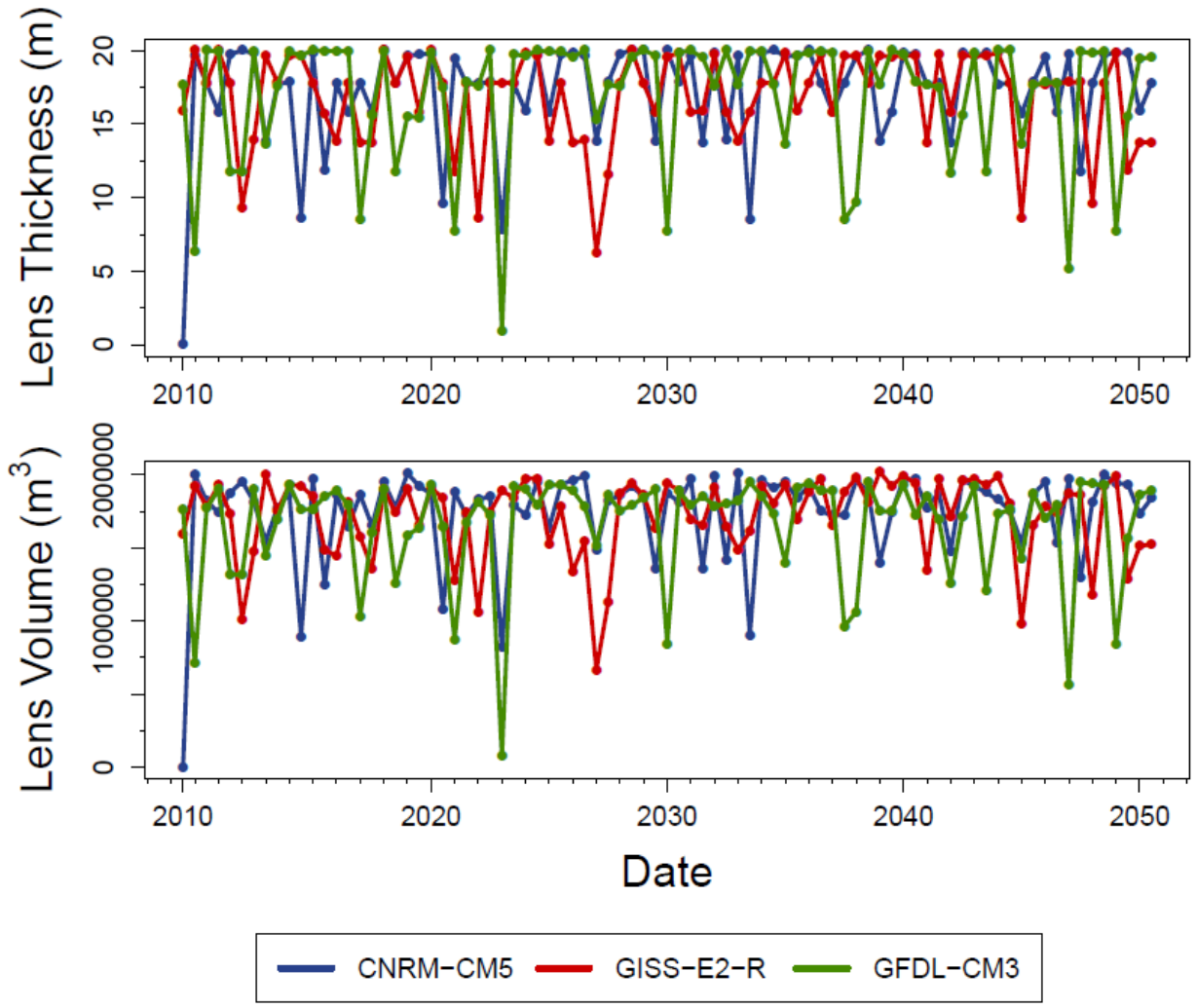

Figure B16. Time series of lens thickness and volume for the top three performing GCMs for Ngatik Island under the RCP2.6 forcing scenario

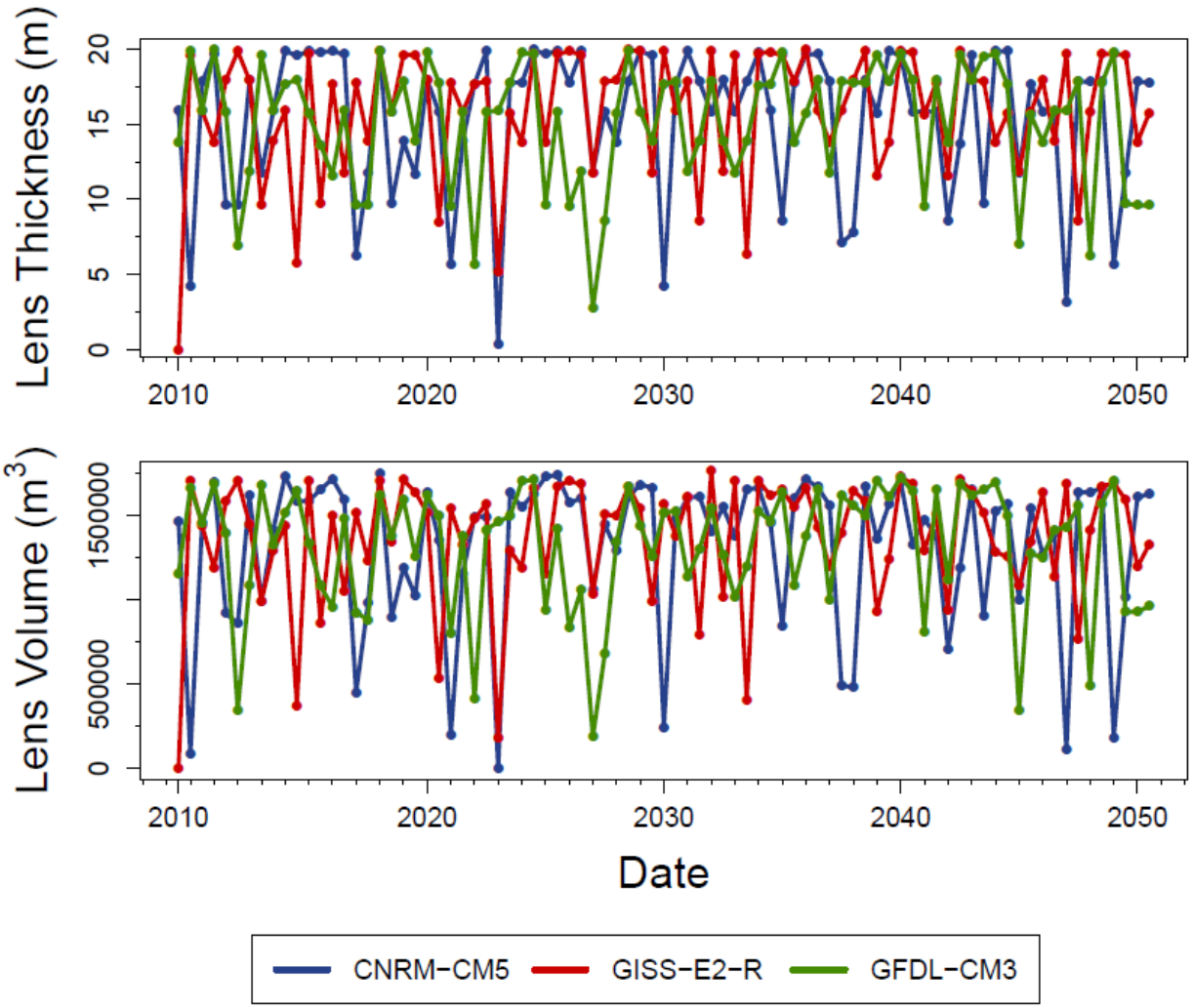

Figure B17. Time series of lens thickness and volume for the top three performing GCMs for Pingelap Island under the RCP2.6 forcing scenario

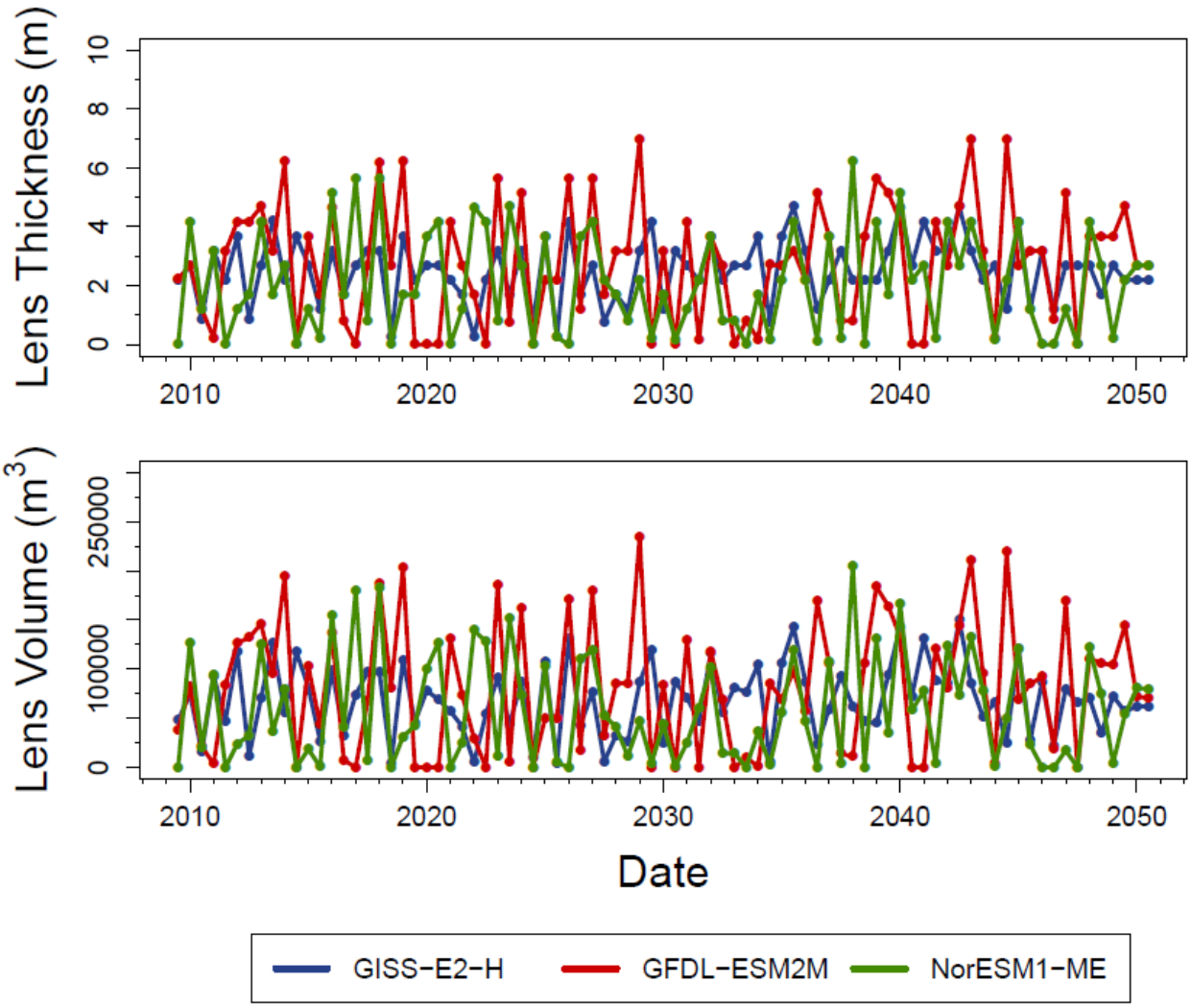

Figure B18. Time series of lens thickness and volume for the top three performing GCMs for Mogmog Island under the RCP2.6 forcing scenario

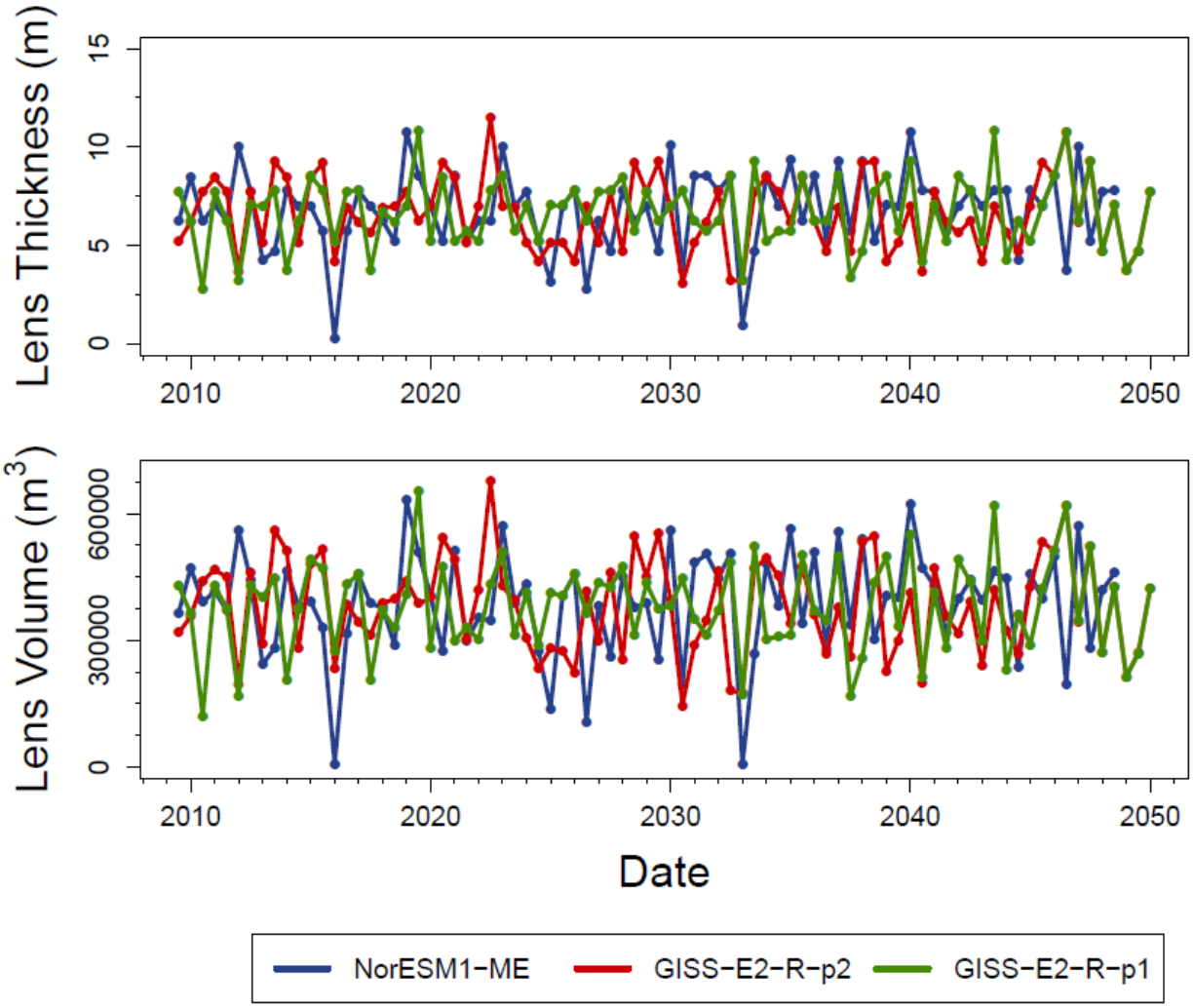

Figure B19. Time series of lens thickness and volume for the top three performing GCMs for Deke Island under the RCP8.5 forcing scenario

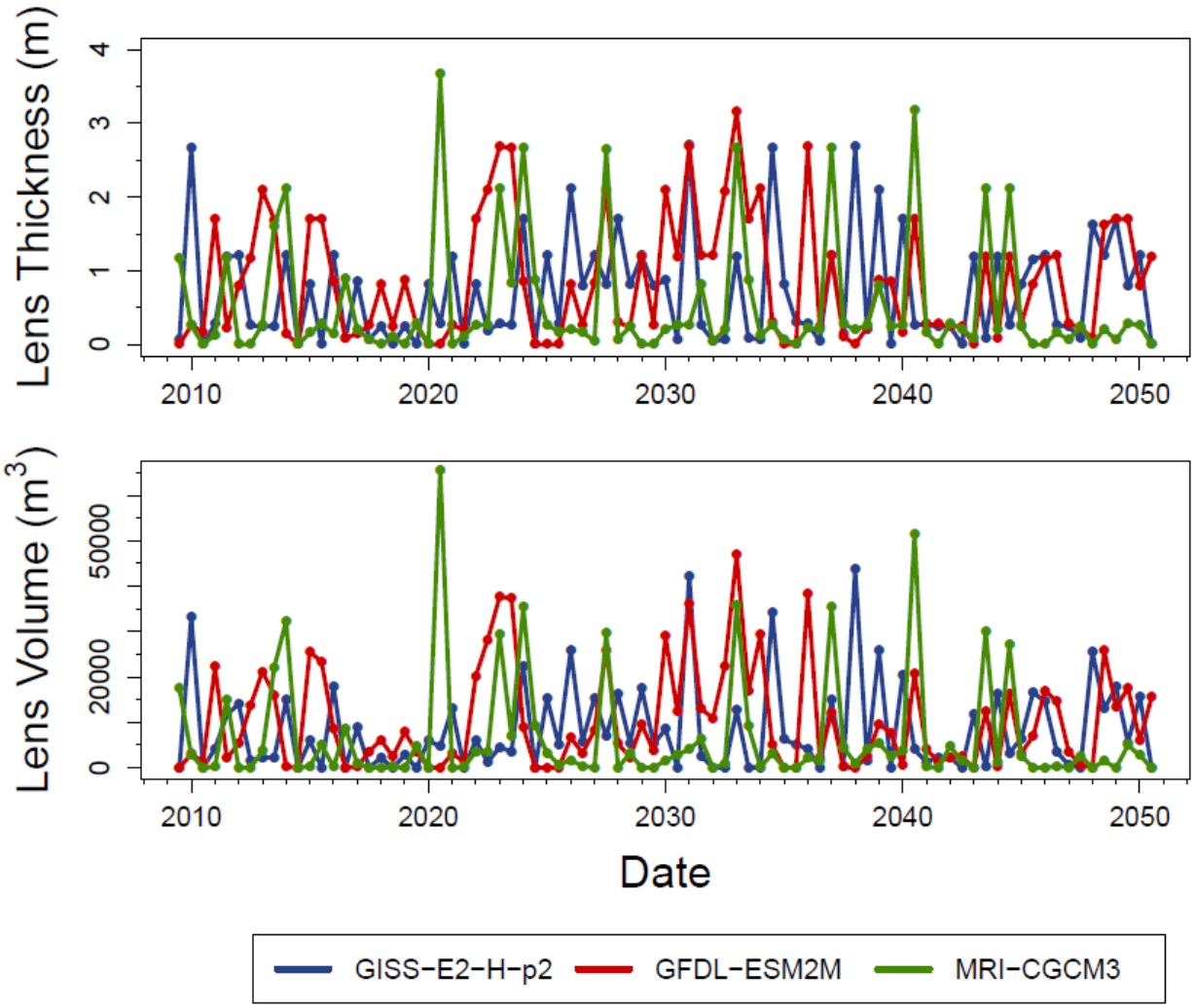

Figure B20. Time series of lens thickness and volume for the top three performing GCMs for Fassarai Island under the RCP8.5 forcing scenario

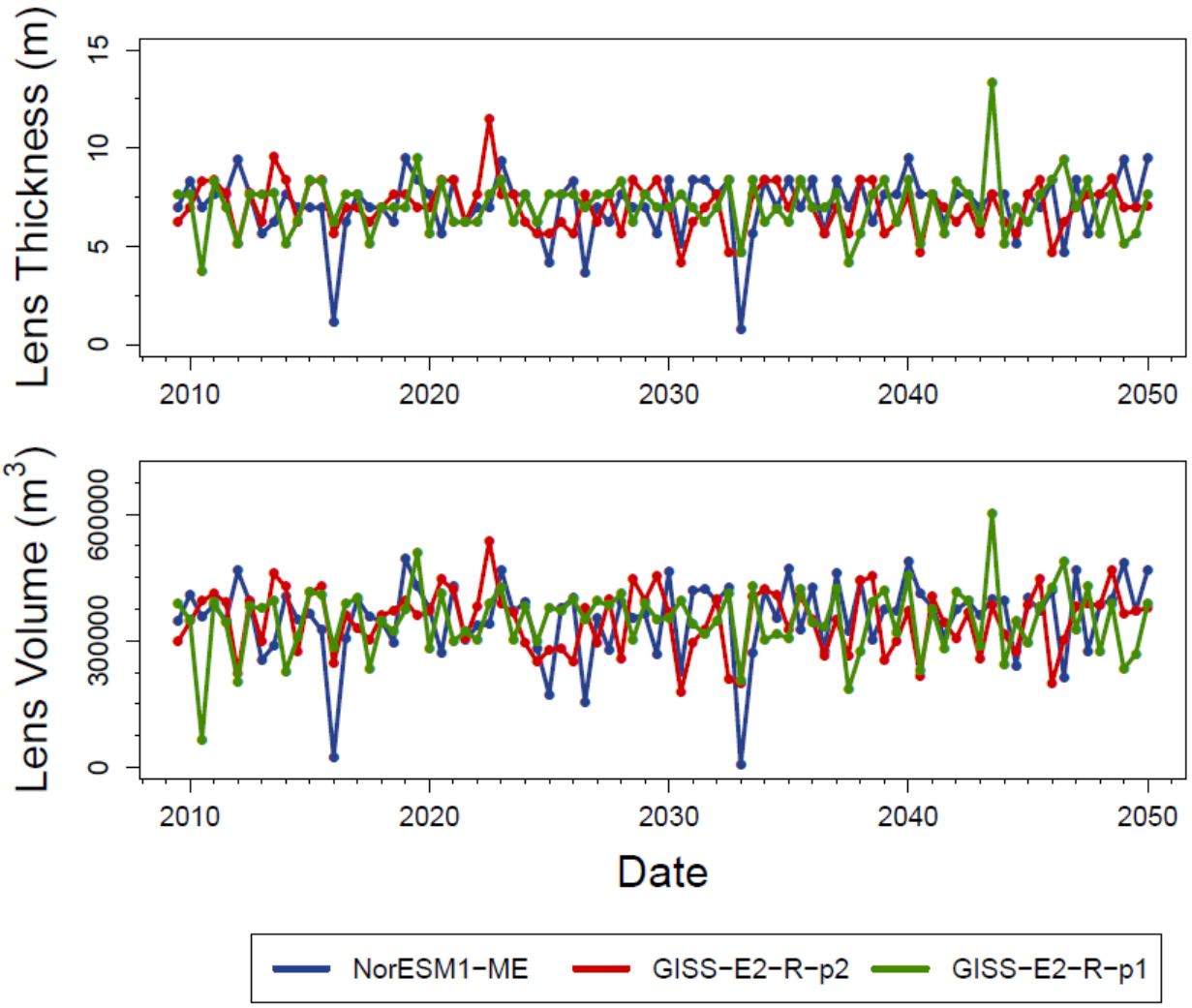

Figure B21. Time series of lens thickness and volume for the top three performing GCMs for Kahlap Island under the RCP8.5 forcing scenario

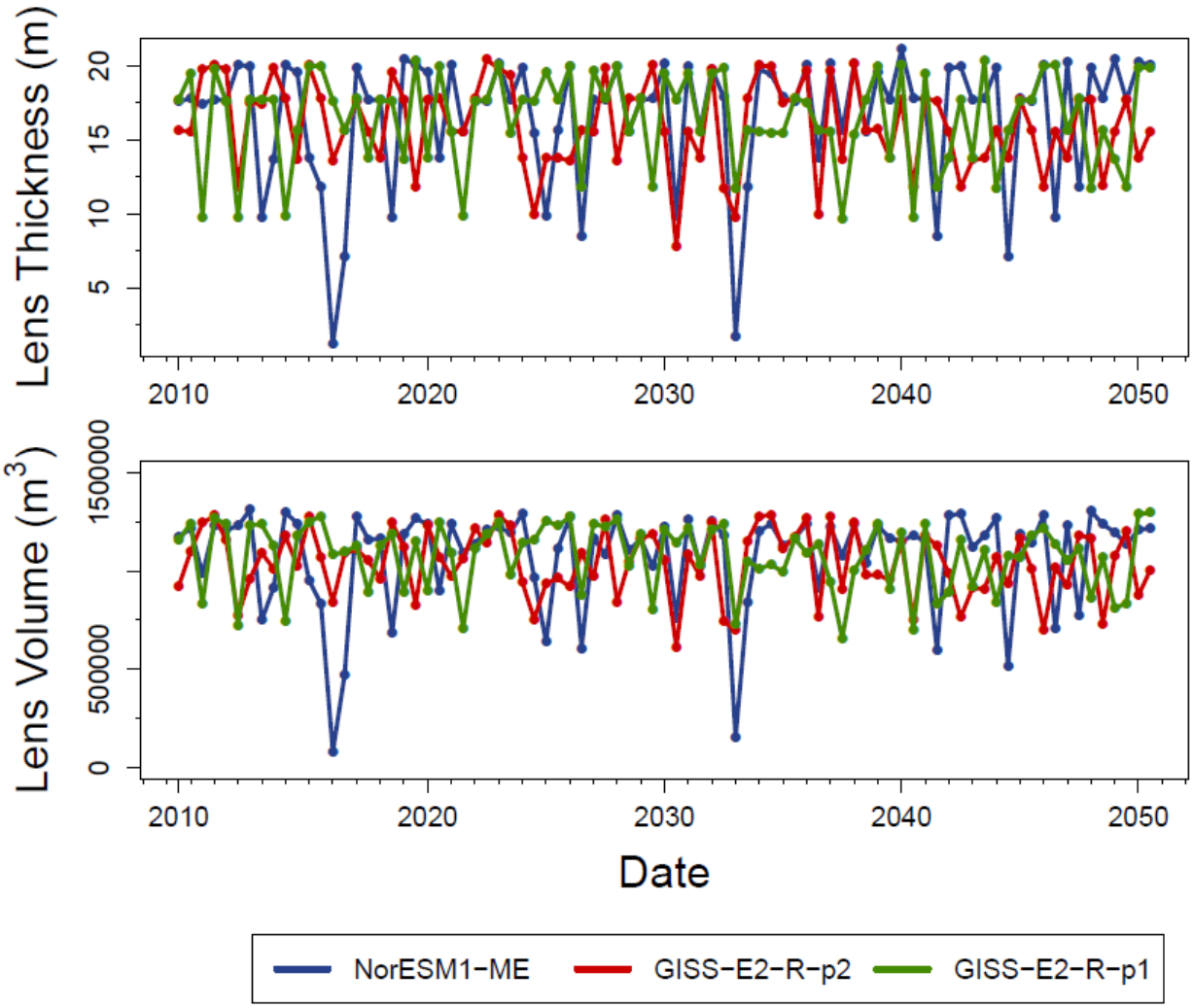

Figure B22. Time series of lens thickness and volume for the top three performing GCMs for Nikahlap Island under the RCP8.5 forcing scenario

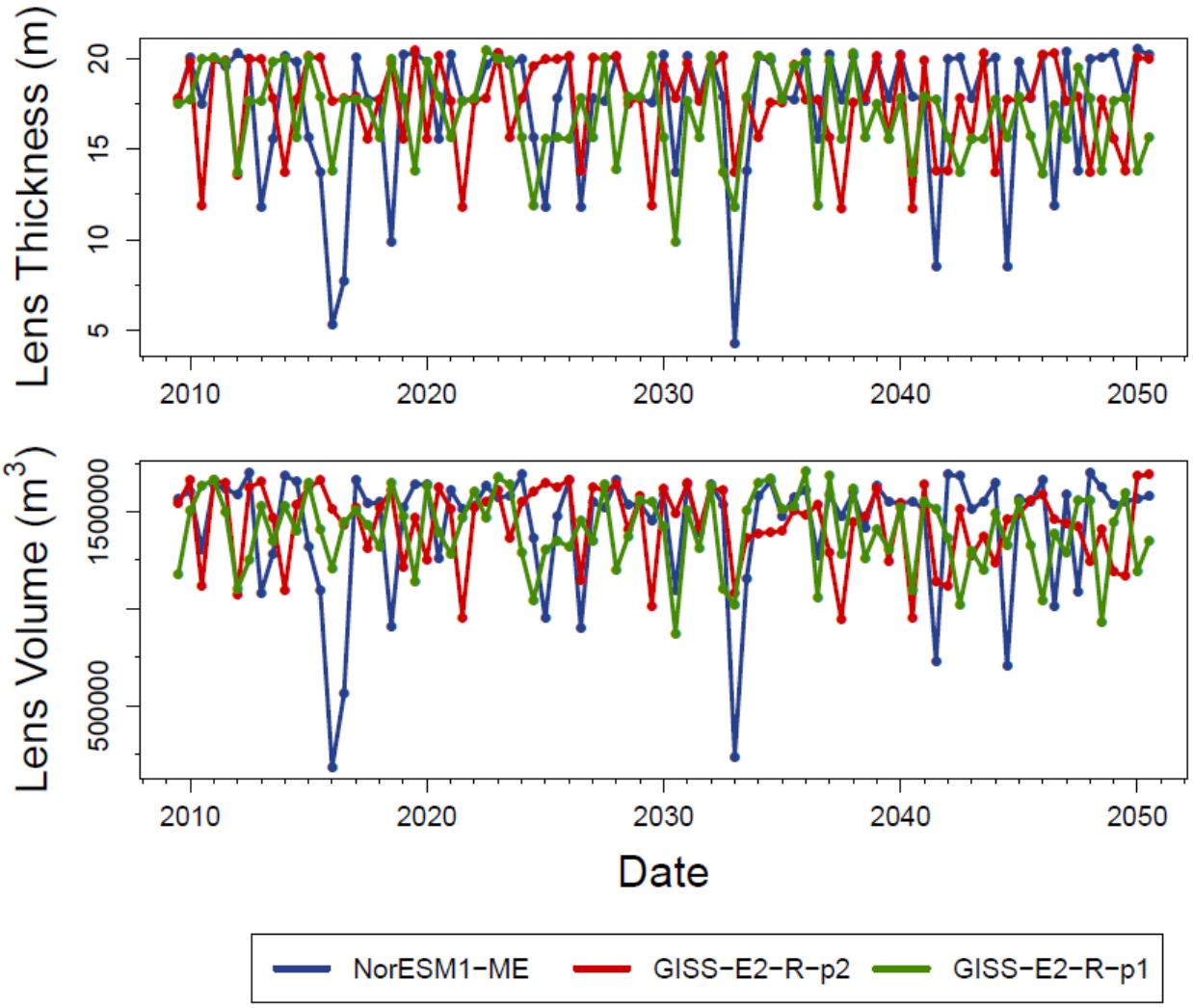

Figure B23. Time series of lens thickness and volume for the top three performing GCMs for Pingelap Island under the RCP8.5 forcing scenario

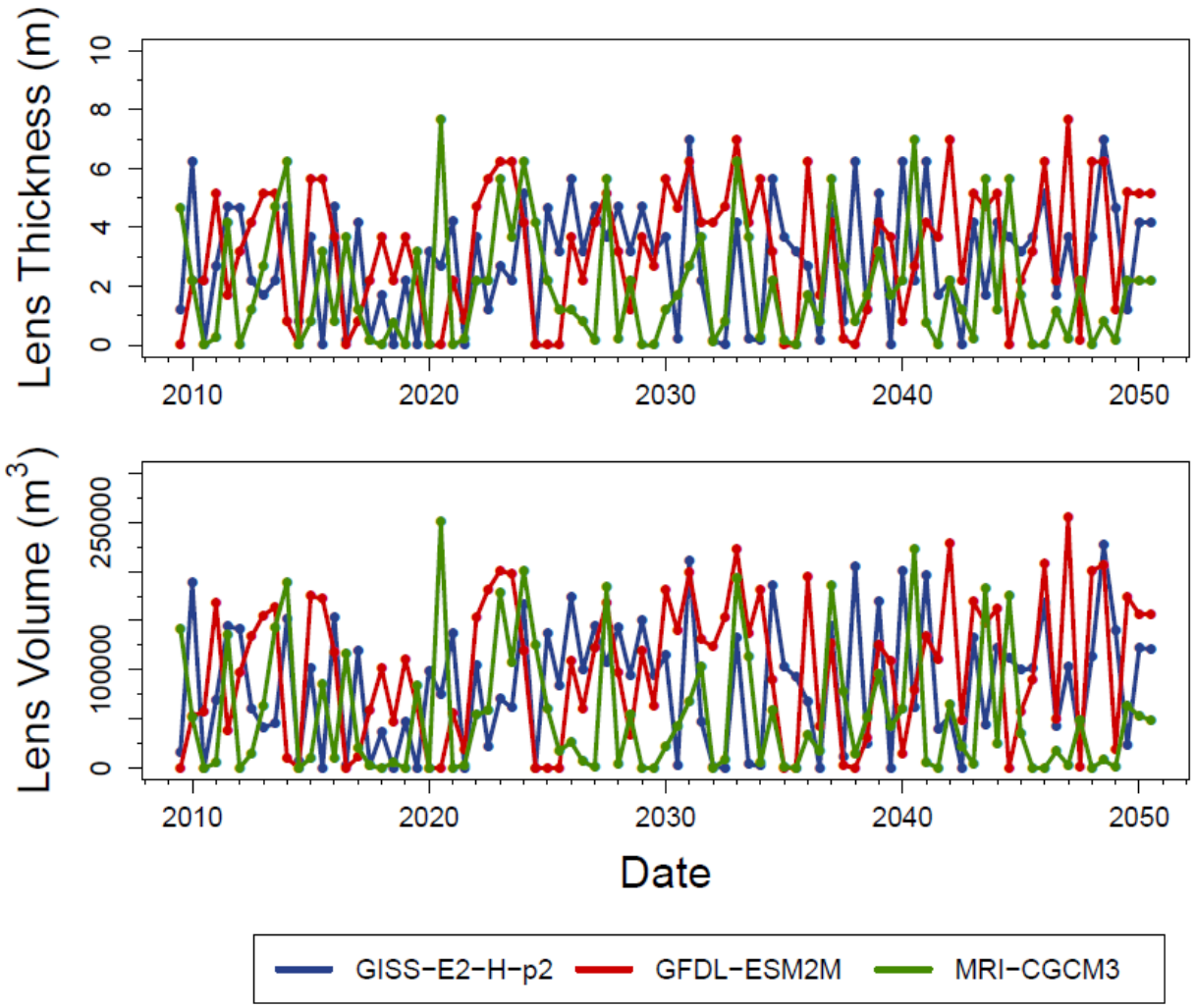

Figure B24. Time series of lens thickness and volume for the top three performing GCMs for Mogmog Island under the RCP8.5 forcing scenario

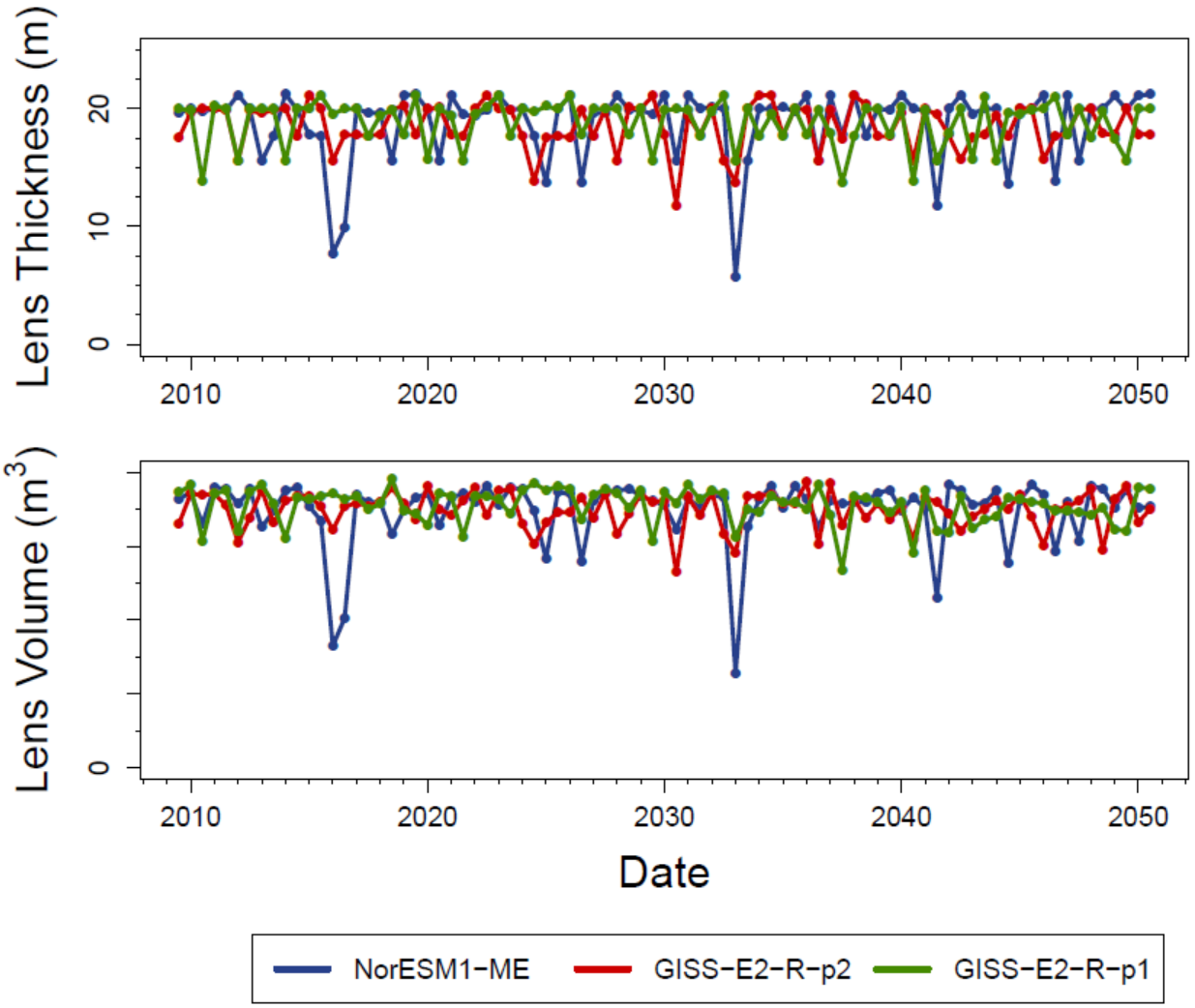

Figure B25. Time series of lens thickness and volume for the top three performing GCMs for Ngatik Island under the RCP8.5 forcing scenario